UNRAVELING THE ROLE OF HEMEOXYGENASE-1/CARBON MONOXIDE IN PULMONARY AND CARDIOVASCULAR DISEASES

by

Anuli Caroline Anyanwu

A dissertation submitted in partial fulfillment
of the requirements for the degree of
Doctor of Philosophy
(Molecular and Integrative Physiology)
in The University of Michigan
2013

Doctoral Committee:

Professor David J. Pinsky, Co – Chair
Professor Marc B. Hershenson, Co – Chair
Assistant Professor Carey N. Lumeng
Professor Bethany B. Moore
Professor Richard M. Mortensen

DEDICATION

Dedicated to my parents, Dr. Kane Chukwulozie & Margaret Iheoma Anyanwu, my brothers and sisters: Ngozi Jennifer Anyanwu, Akunna Elizabeth Anyanwu, Chima Patrick Anyanwu, Chinyere Juliet Anyanwu and Uchenna Kevin Anyanwu for providing the unwavered support and friendship that allowed me to smile throughout this process.

To my husband, Frank Nwachukwu Ofili, whose love, friendship and faith in my abilities have made me a better person and inspired my continual love for travel/adventure.

ACKNOWLEDGEMENTS

My graduate experience has been shaped most significantly by the guidance and support of my mentors, Dr. David J. Pinsky and Dr. Marc B. Hershenson. Marc and David's enthusiasm, intellect, passion, and scientific vision have been integral to my development as a scientist. I am honored to have worked for both of them and owe them a great debt of gratitude for the time and energy they have invested in my training and development.

Throughout these last five years I have become indebted to numerous people. Pursuing graduate degree has been a long and challenging road. If I've accomplished anything during this time, it is only because I've had the good fortune to be surrounded by great people who deserve my thanks. I have invested a lot of my heart and time in this thesis, but each of these people has given of themselves to help me throughout this process.

First and foremost, I would like to thank my mentor Dr. David Pinsky for being a great example for me and for always believing in my potential as a young scientist. I am really appreciative of his willingness and availability to answer complex scientific questions and all his valuable advice. Through his professional guidance, he always found a way to give me motivation to persevere, which helped move my research project forward and allowed me to grow as a young research investigator. I am glad I chose a mentor that always had a friendly smile to offer and was easily thrilled with new data, he definitely transmitted that excitement for science and discovery to me and I will always be grateful for that.

I would like to extend my deepest gratitude and appreciation to my second mentor, Dr. Marc Hershenson (aka Dr. H). Not only has he been an excellent advisor, but he has expanded the breadth of my knowledge by leaps and bounds over the course of the last five years. I am very

lucky to have had the opportunity of studying under his supervision, and learning from him, not only in science but also in my daily life. Dr. H's counsel, his knack of picking projects that hold the most promise, and his efforts in making every possible resource available to me to pursue my thesis objectives, have made my journey through research an exciting and fruitful venture. Dr. H's constant enthusiasm, unceasing dedication, and numerous brilliant ideas have made this dissertation fruitful and accomplished smoothly. Over the past five years, Dr. H has always supported me, encouraged me, and guided me through my entire graduate studies with his endless patience and passion. I cannot imagine any achievement without his tremendous help and encouragement. Besides, Dr. H is such a nice and approachable person that he makes me feel that five years' graduate study under his mentoring have taken only one day. Thank you for keeping me focused, for providing me with countless resources and all my inexperience with tireless feedback: you helped me discover how deep and far-reaching the field of BPD research can go, and you know that I can't say enough about how my writing has improved over the years. You've really made me stretch my thinking in ways I never knew possible and I will take that with me wherever I go in life.

I would like to thank my thesis committee members, Dr. Beth Moore, Dr. Carey Lumeng, Dr. Richard Mortensen. My committee has been an excellent sounding board for my scientific questions and has helped to guide the development of my dissertation projects. Moreover, they have continually been my champions and their support has opened many doors for my future career. There were several occasions when I was in need of their advice and technical know-how; their opinions undoubtedly gave my dissertation more structure and form. I know that what I have learned from these individuals will continue to help shape my science and my career well beyond graduate school, and for that I am truly grateful.

I want to acknowledge all the members of the Pinsky Lab, both past and present, especially Hui Liao, Diane Bouis and Keigo Fukase. These individuals have provided invaluable help with my projects and have made the lab an enjoyable place to be. I thank the Pinsky lab members for their enthusiasm, dedication, and friendship throughout our time as colleagues. I thank Takanori Hayaski for this initial help and contributions to my projects, and for being my sounding board for new ideas.

I would like to mention the member of my "army" (my amazing undergraduate

students). All 15 of you have impacted me more than I can describe. Whether it be socially or scientifically as an invaluable repository of scientific knowledge and techniques, I am not quite sure where this thesis would be without each of you. I was able to manage 3 major projects because of all your help and late night/weekend support. I wish you guys all the best in your future endeavors and always remember to "pay it forward".

I'd like to also thank all the members of the Hershenson lab especially, Dr. John Kelley Bentley for the wealth of information they provided me over the course of my studies. Kelley has helped me at crucial junctures in my thesis with his scientific expertise, and has shed light on insightful ways to tackle some of the road-blocks in my project. Kelley, thank you for believing in me and being patient when it took me a bit to understand a particular technique. I hope I will find such a great team of people wherever I work in the future.

I had the good fortune to work with excellent colleagues and collaborators whose effort and support were integral to successful completion of my dissertation. I thank all of my co-authors for their efforts on the studies described herein. My sincere thanks go out to, Shirley Wrobleski, Dan Myers and Jose Diaz and the entire Jobst Vascular Laboratory. I would also like to thank the Flow Cytometry and Bioinformatics core for their technical advice.

Finally, I have enjoyed working with all the members in the Lama lab, especially Takeshi Mimura. Thanks you for taking the time to help me with the deep venous thrombosis project. Without your support and precise surgical skills, we would not have been able to finish this project.

Lastly, I thank my family and friends for their unwavering support and encouragement, through this endeavor. I could not have completed this without you.

TABLE OF CONTENTS

LIST OF FIGURES

LIST OF TABLES

LIST OF ABBREVIATIONS

·OH – hydroxyl radical

ADP – adenosine diphosphate

AMP – adenosine monophosphate

ATP – adenosine triphosphate

BAL – bronchoalveolar lavage

BALF – bronchoalveolar lavage fluid

BPD – bronchopulmonary dysplasia

BVR – biliverdin reductase

cGMP – cyclic-guanosine-monophosphate

CO – carbon monoxide

CO-Hb – carboxyhemoglobin

COPD – chronic obstructive pulmonary disease

CPR – cytpchrome p450 reductase

DAB – diaminobenzidine

DVT – deep venous thrombosis

EC – endothelial cell

GP –glycoprotein

GSH – glutathione

HO – heme oxygenase

HPFs – high power fields

HRG – histidine-rich glycoprotein

IPA – Ingenuity Pathway Analysis

IPKB – Ingenuity Pathways Knowledge Base

IVC – inferior vena cava

MAPK – mitogen-activated protein kinase

MLI – mean linear intercept

NADPH – Nicotinamide adenine dinucleotide phosphate

NO – nitric oxide

O_2 – molecular oxygen

PAI-1 – plasminogen activator inhibitor

PCA – principal component analysis

PE – pulmonary embolism

PMN – polymononucleated

PSGL-1 – P-selectin glycoprotein ligand-1

RMA – robust multi-array average

ROS – reactive oxygen species

TF – tissue factor

TLR – Toll-like receptor

UDPGT – UDP-glucuronyl transferasea

VTE – venous thromboembolism

vWF – von Willebrand factor

WPB – Weibel-palade bodies

ABSTRACT

Unraveling the role of heme oxygenase-1/ carbon monoxide in pulmonary and cardiovascular disease

By

Anuli Caroline Anyanwu

Chair: David J. Pinsky and Co-Chair: Marc B. Hershenson

Heme oxygenase (HO) is an enzyme found in many cell types, and is expressed in multiple isoforms, each of which is responsible for the breakdown of heme into biliverdin and iron. In the process of catabolizing heme, CO gas is liberated as a byproduct. HO-1 is also known in the literature as heat shock protein 32 because of its molecular weight and its inducibility by cellular stress. Though it is well established that HO-1 possesses anti-inflammatory properties, which had initially been presumed to occur through antioxidant actions of biliverdin. Recent reports suggests that CO itself triggers potent cellular protective mechanisms, via its ability to suppress key regulatory transcription factors responsible for induction of many gene targets which lead to inflammation and coagulation. This led to the hypothesis that HO-1 is a critical regulator of inflammation through the catabolism of carbon monoxide. Studies of macrophage and neutrophil flux

into perinatal hyperoxia-induced lung tissue and of thrombosed vascular tissue reveal a novel role for HO-1/CO in the regulation of leukocyte activation. In the setting of hyperoxia-induced lung injury in the neonatal lung, inhalation of low dose CO mitigates the effect of neonatal hyperoxia on alveolar development and the developing lung by an anti-inflammatory mechanism. In the setting of deep venous thrombosis, HO-1/CO mediated-reduction of key inflammatory mediators manifests a profound suppression of leukocyte trafficking into the vascular milieu, and a concordant decrease in platelet aggregation. Further exploration of the role of HO-1/CO in other disease models reveal CO has emerged as a potently protective, homeostatic molecule that prevents the development of vascular and alveolar disorders when administered prophylactically. Accumulating evidence suggests that CO exerts key physiological functions in pulmonary and cardiovascular biology and more recently, has been demonstrated to have anti-apoptotic, anti-inflammatory and anti-proliferative effects. In total, this thesis will elucidate the signaling pathway involved in the anti-inflammatory effects of HO-1/CO as important not only for our basic understanding of mechanisms of action of HO-1/CO, but also for the consideration of novel therapeutic for acute and chronic inflammation with implications for a variety of pulmonary and cardiovascular diseases.

CHAPTER I

PUTTING IT ALL TOGETHER: HEME OXYGENASE-1/CARBON MONOXIDE SIGNALING PATHWAYS, HYPEROXIA-INDUCED BRONCHOPULMONARY DYSPLASIA AND DEEP VENOUS THROMBOSIS

INTRODUCTION

HO-1/CO Structure and Function

Heme degradation catalyzed by heme oxygenase

Heme is a prosthetic group that consists of an iron atom that is contained in the center of a porphyrin ring. There are several major types of heme in cells, including heme A, heme B, heme C, and heme O. The heme in heme oxygenase (HO) is a b-type heme with the iron coordinated to the four nitrogen atoms of the porphyrin and has a chemical formula of $C_{34}H_{32}FeN_4O_4$. In the presence of NADPH - cytochrome P450 reductase (CPR), heme oxygenase (HO, EC 1:14:99:3) catalyzes the degradation of heme into iron, CO and biliverdin, which is quickly reduced to bilirubin by biliverdin reductase (**Figure 1**).[1,2] The degradation of one molecule of heme to biliverdin requires seven electrons to be transferred and three molecules of oxygen to be consumed (**Equation 1**). Subsequently, biliverdin reductase (BVR) catalyzes the two-electron reduction of biliverdin to bilirubin using NADPH as an electron donor (**Equation 2**). A distinct color change occurs in this process: from purple (heme) to green (biliverdin), then finally to

yellow (bilirubin).

HO is present in organisms ranging from bacteria to eukaryotes, and is the only known enzyme that can degrade heme. In mammals, the electrons are provided by NADPH–cytochrome P450 reductase.[3] In HO, heme acts as not only a cofactor but also as a substrate that catalyzes its own destruction (**Figure 2**). The HO-bound heme is first oxidized to α-*meso*-hydroxyheme through a peroxy intermediate. The deprotonated state of α-*meso*-hydroxyheme has free radical character, which can react with oxygen to produce α-verdoheme and eliminate the α carbon atom from the porphyrin ring as CO. The α-verdoheme is subsequently converted to biliverdin and free iron in a reaction that requires NADPH–cytochrome P450 reductase and O_2. Recent studies indicated that product release involves sequential reduction of the ferric to the ferrous biliverdin complex, release of the ferrous iron, and finally dissociation of the biliverdin from the protein.[4]

Physiological functions of heme oxygenase

Heme and iron homeostasis

Iron is an essential element for all living organisms. It acts as a cofactor for many heme-containing proteins such as CPR and HO, forms iron-sulfur clusters in many non-heme-containing proteins such as ferredoxins and CODH, and provides oxygen transport and storage for hemoglobin and myoglobin, respectively. However, excess iron can be toxic,[5] since it can produce large amounts of highly reactive hydroxyl radical (·OH) by the Fenton reaction in cells.[6] An efficient way to maintain iron balance in cells is through regulation of its uptake. Dietary iron mainly exists as iron salts and heme iron. Uptake of

inorganic iron is mainly mediated by the iron transporters located in the brush border membrane, including DMT1 (divalent metal transporter-1)[7] and Dcytb (duodenal cytochrome b).[8] In comparison to inorganic iron uptake, heme uptake is very different and its transport mechanism has not been fully elucidated. A very recent report indicated that the HRG (histidine-rich glycoprotein) family proteins are potential heme transporters in *Caenorhabditis elegans*. [9] However, the heme transport pathway in mammals remains mysterious. After heme is transported into cells, the iron is released by heme degradation in a reaction that is catalyzed by HO. In addition to playing a role as an iron reservoir, heme has other critical physiological functions in cells. Heme is a common prosthetic group that is structurally associated with many electron transfer and redox enzymes and regulates genes involved in oxygen utilization in lower eukaryotes and prokaryotes. [10,11,12] Although heme plays crucial roles in various physiological processes, free heme can be toxic at concentrations greater than 1 μM,[13] causing oxidative stress induced by reactive oxygen species (ROS), hemolytic effects, and abnormal inflammation.[14] Because of the contradictory biological functions for heme and iron, their metabolism in mammals needs to be tightly and delicately regulated.

HO is the only known enzyme that can degrade heme in cells, playing a critical role in heme and iron homeostasis. Although the precise molecular mechanisms by which HO confers tissue protection are not clearly defined, it is believed that HO-dependent protection is mediated by the reaction products of heme degradation, including biliverdin, CO, and iron (**Figure 3**). Each product could contribute alone or in concert to the restoration of cellular homeostasis under inducing conditions. One potential mechanism of the HO-mediated cytoprotective effect is that HO may provide a possible antioxidative

function by accelerating the removal of heme to limit oxidative stress sustained through heme-dependent mechanisms. It has recently been reported that free iron, at physiological levels, has crucial effects on cytoprotection.[15,16] Furthermore, iron can also promote the ferritin-mediated cytoprotective process against mitochondrial dysfunction and oxidative stress.[17] In contrast, evidence showed that iron released from the HO reaction may potentially act as a catalyst of deleterious pro-oxidant reactions, such as the metal-catalyzed Haber-Weiss cycle, or iron-dependent lipid peroxidation.[18] In addition, HO-derived iron may also stimulate ferritin synthesis, sequestering reactive iron.[19]

CO signaling in cells

Historically, CO has been regarded as a lethal gas and is toxic at high levels (>500 ppm). The first identified molecular target of CO was the heme iron center of hemoproteins, such as hemoglobin. Carbon monoxide is a colorless, tasteless and odorless gas that, when inhaled, enters the bloodstream and replaces the oxygen on hemoglobin to form carboxyhemoglobin. High CO concentrations cause hypoxemia by competitive binding to the oxygen-binding sites of hemoglobin to form carboxyhemoglobin (CO-Hb), with an affinity that is > 200-fold higher than that of oxygen[13]. In humans, prolonged or elevated CO exposure can cause a number of acute clinical effects, including nausea, dizziness, and loss of consciousness.[13] Symptoms of

CO poisoning begin to appear at 20% CO-Hb, while death occurs between 50 and 80% CO-Hb.[13] However, when CO is applied at low concentrations (typically within the 15 to 20% CO-Hb) range, it can influence a number of signaling pathways in cells to confer various cytoprotective effects, including anti-inflammation, anti-apoptosis, and

anti- proliferation (**Figure 1.3**).[20,21] The CO signaling pathway is still not clearly elucidated. At a physiological level, CO can trigger the production of cyclic-guanosine-monophosphate (cGMP) to stimulate neuronal signaling processes and regulate vascular functions, including vessel tone, smooth muscle proliferation and platelet aggregation.[22,23] Furthermore, recent studies indicate that the activation of MAPK pathways, particularly the p38 MAPK signaling pathway, can be modulated by CO treatment.[24] MAPK pathways have been demonstrated to be critical for cellular response to inflammatory, apoptotic and proliferative stress.[24,25,26,27] The activation of p38 MAPK by CO has been reported to be dependent or independent of soluble guanylate cyclase (sGC), depending on the cell type. In addition, modulation of cellular ROS production, inhibition of cellular O_2 production, membrane NADPH-oxidase, and Toll-like receptor (TLR) trafficking and activation have also been implicated in CO dependent signaling.[28,29,30] Thus, CO can confer tissue protection in various models of acute lung injury, vascular injury, pulmonary hypertension, liver injury, organ I/R injury, organ transplantation, and numerous other condition.[23,31] Observations of CO-mediated tissue protection have also been described in transplantation of heart, lung, kidney, liver, and intestinal allografts or xenografts, whereby application of CO to the recipient or to the graft reduced inflammation and apoptosis associated with I/R injury, thus reducing the probability of graft, rejection.[32,33] In fact, CO-based inhalation therapies have been applied in the clinic. A recently reported clinical trial demonstrates that reduction of sputum eosinophils and improvement of methacholine responsiveness through inhalation of CO was observed in patients with stable chronic obstructive pulmonary disease (COPD).[34]

In cells, HO-catalyzed heme degradation is the major source of CO, especially in neurons and in the carotid body.[35] HO-derived CO is usually produced locally within tissues, serving as an endogenous physiological mediator. In the early 1990s, HO-derived CO was discovered as a neurotransmitter in olfactory neurotransmission.[36] Since then increasing evidence has been presented that HO-derived CO, instead of being a waste product of heme oxidation, actually plays critical roles in various physiological phenomena, including circadian modulation of heme biosynthesis, regulation of T cell function, modulation of caveolin-1 status in growth control,[37] activation of guanylate cyclase,[38] and mediation of O_2 sensing and the hypoxic response.[39] It is now believed that CO acts as a signaling molecule like another diatomic molecule, nitric oxide (NO), possessing anti-apoptotic, anti-inflammatory, and anti-proliferative properties.[26,37,40,41] Although the toxicity of CO has been studied extensively, it is now being explore for its physiological effects and potential therapeutic benefits.[42] Since the realization that the poisonous gas nitric oxide (NO) has a significant biological role in physiology and pathophysiology, CO, which is structurally similar gas, has gained a lot of attention as a molecule with many analogous chemical and biological properties. Like NO, CO is produced endogenously during cellular metabolism, primarily from the degradation of heme by the HO enzyme.[43] CO differs from NO in that CO is a highly stable diatomic gas, which lacks unpaired electron of NO and hence is unreactive with superoxide or other radicals produced during cellular or vascular injury. Endogenous CO formation has been measured in several biological systems, and normal human adults have been shown to exhale ~12mL of CO per day.[44] However, the major exogenous source for CO is generated from the incomplete burning of carbon from solid, liquid, and gaseous fuels.

Biliverdin and bilirubin homeostasis

Bilirubin, the final product of heme metabolism, is rapidly derived from biliverdin by biliverdin reductase (BVR) in mammals. Bilirubin can revert to biliverdin via oxidation, although the mechanism is unclear. The function of the BVR pathway in cells is not clearly understood because bilirubin is toxic and insoluble, while biliverdin is more water soluble. Bilirubin must be glucuronidated before its excretion in bile, which is primarily catalyzed by UDP-glucuronyl transferase (UDPGT) in liver.[45] Compared to bilirubin, biliverdin is more easily excreted. Bilirubin was first reported to mainly exist in the plasma and can cause brain damage.[46] However, it has been recently reported that biliverdin and bilirubin can act as chain-breaking antioxidants *in vitro*, which may provide cytoprotection (**Figure 1.3**).[47]

The cytotoxicity associated with deletion of HO appears to reflect a loss of bilirubin. Mice with targeted deletion of either HO-1 or HO-2 have reduced bilirubin levels and are more susceptible to neurotoxic damage, seizures, stroke damage, and traumatic brain injury.[48,49] The antioxidant actions of bilirubin are dramatically amplified by BVR in a biliverdin–bilirubin cycle. Depletion of BVR by RNA interference markedly diminishes the cytoprotective effects of exogenous bilirubin and leads to increased cellular levels of oxygen free radicals and cell death.[50,51] A recent study suggested that water-soluble glutathione (GSH) primarily protects water soluble proteins, whereas lipophilic bilirubin protects against lipid peroxidation of cell membranes.[51] Mice with deletion of HO-2, which generates biliverdin, display more oxidation of lipid than that of protein, while the reverse holds for GSH depletion. Pharmacologic application of

biliverdin and bilirubin can protect cultured cells against injury by oxidative or nitrosative stress.[52] One possible mechanism is that bilirubin can surpass α-tocopherol as the most potent protector against lipid peroxidation and acts as an antioxidant that is involved in resistance to oxidative stress.[47,53,54]

Differences between HO-1 and HO-2

There are two forms of HO (HO-1 and HO-2), which share similar physical and kinetic properties, but are differentially regulated and exhibit dissimilar physiological roles and tissue distributions.[55,43] Another isoform, HO-3, was recently reported in rat;[56] however, no activity was detected for this isoform and it is considered to be a pseudogene. Phylogenetic analysis of heme oxygenase indicates that HO-1 and HO-2 have a very high degree of evolutionary conservation among mammals.[57] Bacterial heme oxygenases have a closer evolutionary relationship with those in plants. However, the bacterial, plant and mammalian HOs have high structural similarity in their catalytic domains. A bacterial HO-2 crystal structure has been reported recently, which shows a high similarity at the core domain region with human HO-1 and HO-2 structures.[58] Plants contain several HOs, including one named HO-2, but these lack the C-terminal membrane spanning region seen in mammalian HOs [59] and are more closely related to the bacterial and insect HO-1 than to the mammalian HOs.[57] In higher plants, ferredoxin is utilized instead of NADPH-cytochrome P450 reductase as the reducing partner in the HO reaction.[7] Many plants do not produce bilirubin since they lack biliverdin reductase.[9]

HO-1, considered to be the inducible HO, is also known as heat-shock protein 32 and is found in most tissues, with particularly high levels in spleen and liver.[60,61]

Expression of HO-1 is regulated by heat shock and various oxidative stress conditions such as ischemia, hypoxia, hyperoxia, and alterations in glutathione levels.[43,62] On the other hand, HO-2 appears to be constitutively expressed, but exhibits a narrow tissue distribution, with high levels in the brain and in testes.[56,63,64] HO-2 has been implicated in oxygen sensing by the carotid body,[39,57] mediating oxidative stress in neurons,[65] and regulating cerebral blood flow and vascular tone in certain tissues.[66]

HO-1/CO and Bronchoplumonary Dysplasia (BPD)

Premature birth and Bronchoplumonary Dysplasia (BPD)

The incidence of human premature delivery, i.e. birth at gestational age of less than 37 weeks, is approximately 13% in the United States.[67] Due to lung immaturity, preterm infants are at risk of developing respiratory distress syndrome (RDS or hyaline-membrane disease). An estimated 30% of infants with a birth weight between 500g and 1,500g will develop RDS. RDS is a risk factor for the development of bronchoplumonary dysplasia (BPD). BPD is a significant global health problem with 65 to 75% patients having high risk for morbidity and mortality during the first years of life and respiratory problems throughout childhood and young adulthood.[68] Infants with BPD are more likely to need prolonged hospitalization and readmission in the first years of life than preterm infants without BPD[69]. Some infants with BPD continue to show lung function abnormalities into childhood and even early adulthood.[69, 70, 71] The patho-physiology of BPD is multifactorial and not completely clear. However, the main pathological hallmarks of BPD is marked inflammation and an arrest of alveolar development, characterized by large and simplified distal airspaces.[72, 73] (**Figure 4)** In addition, lungs of

ventilated premature infants with early stage BPD show increased levels of alveolar endothelial and epithelial cell death.[74, 75, 76] Even though, the number of endothelial cells has not been quantified in human BPD, decreased endothelial cells and microvascular dysmorphogenesis are characteristics of experimental BPD in perinatal mice.[77]

Lung development

During the saccular stage of lung development, the segments distal to the terminal bronchioles dilate and expand resulting in the formation of alveolar saccules and ducts, with associated reduction of interstitial tissue. Peripheral epithelial cells continue to differentiate into type I and type II pneumocyte epithelial cells, and the capillaries become more closely associated with type I epithelial cells. Elastin is deposited in areas where the future alveolar septa will form to create alveoli from the terminal alveolar saccules.[78, 79] During the alveolar stage, the saccules subdivide into smaller alveoli and a single capillary is formed to enable efficient gas exchange after birth.[78] In human lung, alveoli begin to form during the weeks preceding birth but the large majority of alveoli are formed postnatally.[78] Since the mouse is born during the saccular stage, its alveolarization takes place postnatally beginning around postnatal day 3 (PN-3) (**Table 1)**. Murine alveolar development begins on postnatal day 3, and saccular division is completed by the 14th postnatal day. This sequence and relative timing of alveolarization resembles human lung development. Murine models have several advantages compared to rats or primates, including ease of maintenance, amenable to genetic alteration or manipulation of specific gene products, and the ability to use multiple animals in one study.

Inflammation and BPD

Mechanical ventilation and oxygen supplemention of preterm infants can cause an inflammatory response, interrupting the alveolar and vascular development of the lung [79, 80, 81], and may possibly accelerate the development of injury and BPD in the already inflamed lung. This loss of compartmentalization results in increased fluid influx to the alveoli from the capillaries, causing pulmonary edema. The injured or ruptured cells attract neutrophil leukocytes and activate alveolar macrophages, causing inflammation in the lung.[82] In the lung, resident alveolar macrophages are important in the clearance of foreign material by phagocytosis.[83] When activated, alveolar macrophages secrete cytokines and chemokines that attract neutrophils and monocytes from the circulation.[84] Neutophils are often the first inflammatory cells to infiltrate the site of inflammatory response.[85] Neutrophils are critical for subsequent increase in lung monocytes/macrophages,[86] regulate their activation through an autocrine loop, perpetuating the inflammatory signal in lung injury. Neutrophil influx into the airways was observed immediately after initiation of ventilation and was associated with a decrease in the number of circulating neutrophils. This phenomenon was shown to correlate with the extent of pulmonary edema formation and an increased risk of developing BPD.

The development of BPD is associated with increased levels of pro-inflammtory and chemotatic factors IL-1β, IL-6, IL-8, tumor necrosis factor α, CC chemokines and transforming growth factor (TGF)-β1 in the lung of preterm infants.[87, 88, 89] However, the increase levels and enhanced mRNA expression of pro-inflammatory cytokines present in pulmonary tissue of premature infants may reflect an inability to regulate inflammation

through sufficient expression of anti-inflammatory cytokines (IL-10, IL-4, IL-12 and IL-13 or IL-1) receptor antagonist.[88, 90, 91] An imbalance between expression of pro-inflammatory and anti-inflammatory cytokines can be considered an important feature of lung injury. Prior to neutrophil migration, cellular attachment to endothelial cells is mediated through complex interaction of adhesion molecules. Infants developing BPD have increased levels of endothelial cell intracellular adhesion molecules (ICAM)-1 and selectin, which enable circulating inflammatory cells to transmigrate into the tissue.[92] Previous studies suggest these adhesion receptors are upregulated and accumulate into the alveolar septae during hyperoxic insult.[93] In newborn animals, hyperoxia has been shown to be a strong and independent inducer of various proinflammatory cytokines in airway cells and pulmonary tissue.[94, 95]

When organisms are faced with hyperoxic stress, they have evolved sophisticated and redundant mechanisms to ensure survival. Accumulating data exist in the literature supporting the paradigm that the stress-inducible heme-oxygenase-1, or its catalytic product, carbon monoxide, can confer potent cytoprotective effects in various models of tissue and cellular injury. [24, 32, 96, 97]One possible mechanism which HO-1/CO mediates cytoprotective effect is via anti-inflammatory properties.[97] CO has been shown to downregulate some these pro-inflammatory molecules, namely TNFα and IL1β in mouse models.[98] CO suppresses the pro-inflammatory response (TNFα) and promotes the anti-inflammatory (IL-10) response of macrophage, a cell that probably controls the balance of inflammation in many conditions through activation of p38 mitogen-activated protein kinase and the activation of guanylyl cyclase with the generation of cGMP.[49]

HO-1/CO and Hyperoxia-induced lung injury

Heme oxygenase is an enzyme found in many cell types, and is expressed in multiple isoforms, each of which is responsible for the breakdown of heme into biliverdin and iron. In the process of catabolizing heme, CO gas is liberated as a byproduct. HO-1, initially described as heat shock protein 32, has been found to have an important role in hyperoxia injury. HO-1 is an enzyme that degrades heme to bilirubin, is markedly induced by hyperoxia in multiple cell types including the lungs, and had been found to have profound cyoprotective effects. Overexpression of HO-1 in human epithelial cells conferred resistance to hyperoxia.[99] This effect was strengthened in vivo when exogenous HO-1 by gene transfer attenuated hyperoxic lung injury in rats.[100] Findings from human HO-1 deficiency indicate that the activity of this enzyme is essential for modulating the inflammatory response, apoptosis and cellular proliferation.[49]

One of the most interesting facets of HO-1 biology is that the reaction products of HO-1 catalysis also have intrinsic antioxidant, anti-inflammatory, and antiapoptotic properties that can collaboratively impose significant cytoprotective effects. My proposal focuses on the anti-inflammatory properties of HO-1.[101, 102] Unpublished data collected from our laboratory, suggests that CO itself triggers potent cellular protective mechanisms, acting as a signaling moiety in inflammation and coagulation, whether it is exogenously administered or produced by HO-1. This data is further supported by other reports that CO provides potent cytoprotection in model of ventilated-associated lung injury,[20] ischemia/reperfusion,[103] hyperoxia-induced lung injury[100] and many other clinically relevant research models. Despite the recognized cytoprotective effects of HO-1 and CO, the molecular pathways mediating the protective effects in neonatal hyperoxia-

induced lung injury are still not well defined and will thus be determined through the aims outlined in this proposal.

Significance

Bronchopulmonary dysplasia is a major crippling disease characterized by impairment of lung vascular and alveolar development. BPD is one of the most devastating complications of prematurity. Clinical studies have identified numerous risk factors for the development of BPD in premature infants, including hyperoxia, ventilator-induced pulmonary injury, and prenatal and antenatal infection. Despite attempts to avoid excessive oxygen supplementation, restrict fluids, prevent infection, and use "gentle" ventilation techniques, the incidence of BPD has not changed significantly. Carbon monoxide has emerged as a potently protective, homeostatic molecule that prevents the development of vascular and alveolar disorders when administered prophylactically.[96, 103] Accumulating evidence suggests that CO exerts key physiological functions in neuronal and cardiovascular biology and more recently, has been demonstrated to have anti-apoptotic, anti-inflammatory and anti-proliferative effects.[104] Studies here will elucidate the signaling pathway involved in the anti-inflammatory effects of CO as important not only for our basic understanding of the mechanisms of action of CO, but also for the consideration of novel therapeutic to overcome BPD, a life-threatening chronic disease.

HO-1/CO and Deep Venous Thrombosis

Venous Thrombogenesis

Venous thromboembolism (VTE) is a leading cause of morbidity and mortality worldwide. Thrombus, which develops in great veins of the legs and pelvis, represent an enormous public health burden, particularly when it embolizes to the lungs in a third of all cases. VTE, is a disease that manifested either by the development of deep venous thrombosis (DVT) or pulmonary embolism (PE). Studies have estimated, that approximately 2 million Americans will suffer from DVT annually, and more than 600,000 patients will develop PE.[105] Although anticoagulant therapy represents the mainstay of thromboprophylaxis and treatment, refractory VTE is not at all uncommon and the long term consequences, such as chronic venous insufficiency, remains a major burden to the health of an individual and to society at large. VTE is a multifactorial disease that can be influences by genetic factors, acquired factors and environmental factors. In spite of the enormous disease burden, surprisingly little is known about the pathophysiology of DVT. This is contrary to arterial thrombosis, in which the general outline of its mechanism is well defined, even at a molecular level.[106]

One of the most important advances in our understanding of venous thrombosis was proposed in the late 1870s by Rudolph Virchow. He deduced the major pathogenic determinants for DVT and PE. The triad of vessel wall injury, venous stasis, and blood hypercoagulability have historically been considered the major factors responsible for the development of venous thrombosis [107] **(Figure 5)**. Veins are particularly susceptible loci as blood flow is generally lower than on the arterial side of the circulation, there exist venous valve cusps on whose surfaces thrombi are known to form,[108] and local hypoxemia prevails as oxygen has been extracted from

blood in transit through the capillary plexus. The hemostatic system is faced with the complex task of maintaining the blood in a fluid state so that it can circulate, while simultaneously being able to convert the blood into an insoluble gel at sites of vascular injury. The hemostatic system is made up of two distinct but interlocking systems: platelets and the coagulation proteins. In normal blood flow or absence of vascular injury or inflammation, platelets do not adhere to the endothelium primarily because unstimulated endothelium has no receptors for unactivated platelets and the endothelium produces substances such as nitric oxide, proinflammatory mediators and prostacyclin that maintain the platelets in the unactivated state and impairs their adhesion. During vessel wall injury (such as hypoxia or loss of endothelium layer), platelets are exposed to subendothelial ligands for which they have specific receptors. Our work[109,110,111] as well as that of others, has shown that hypoxia alone is sufficient to trigger thrombosis at the blood wall interface, by mechanisms which include *de novo* expression of tissue factor and plasminogen activator inhibitor-1 (PAI-1) in local mononuclear phagocytes, as well as triggered release of von Willebrand Factor (vWF) and P-selectin from endothelium.

How platelets invite leukocytes to dance

For many years it has been known that platelets play an important role in thrombosis and hemostasis. Recently, it has become evident that platelets also have relevant functions in inflammation. It has been shown that thrombosis and inflammation share two intrinsically linked molecular and cellular mechanisms in the endothelium. The primary molecules responsible for initiation of platelet and leukocyte adhesion are von Willebrand factor (vWF) and P-selectin, respectively. These two molecules are stored in the same storage granules called Weibel-palade bodies (WPBs).[112,113,114,115] Endothelial cells fuse to endothelial surface and release there WPB content in response to vascular injury, releasing vWF, which triggeres platelet rolling and externalizing P-selectin, which in turn activates leukocytes trafficking.[112]

Endothelial exocytosis is one of the earliest responses to vascular damage and plays a pivotal role in thrombosis and inflammation. vWF is essential for WPBs formation,[116] and therefore mice with vWF deficiency cannot store P-selectin in endothelium leading to its partial degradation. This makes the mice less responsive to inflammatory stimuli.[117] P-selectin, an adhesion receptor that triggers leukocyte rolling along vessel wall, is externalized to the plasma membrane during vascular injury. P-selectin glycoprotein ligand-1(PSGL-1), the main ligand of P-selectin, expressed on leukocytes interacts with P-selectin and mediates leukocyte rolling along blood vessels. Mice lacking P-selectin have decreased leukocyte recruitment to sites of vascular injury.[118] Recent evidence even implicates both vWF and P-selectin freshly secreted from activated endothelium, mediate platelet interaction with the endothelial surface. Shear rates in the vessel wall determined which vascular modulator is activated. In stimulated veins under low shear rates, a large number of resting platelets translocate on vWF that is transiently bound to the endothelial.[119] However, higher venus shear rates, activated and non activated platelets are able to roll on endothelial cells (similar to leukocyte transmigration) a process mediated by P-selectin and E-selectin.[120,121] (**Figure 6)** Platelet glycoprotein (GP) GPIbα is another ligand of P-selectin and may therefore also support platelet rolling on activated endothelium.[122] The precise mechanism by which P-selectin promotes platelets rolling still remains unclear, however, they may include direct interactions between platelets and endothelial cells or involve the formation of microparticles.[123,121,122] Exocytosis of both vWF and P-selectin promotes thrombosis by distinct and complementary mechanisms. By externalizing P-selectin, exocytosis of WPBs is thus both procoagulant and proinflammatory.

Bidirectional relationship between thrombosis and inflammation

Inflammation can beget local thrombosis and thrombosis can amplify inflammation. Inflammation leads to an imbalance between procoagulant and anticoagulant properties of the endothelium that can lead to a local stimulation of the coagulant cascade. In order to preserve the smooth flow of blood under quiescent conditions, endothelium has evolved a powerful arsenal of anticoagulant forces, which can be arrayed against the forces of thrombosis, to keep them at bay. TNF- α (a pleiotropic cytokine), the first proinflammatory cytokine released at the site of infection, is a potent inducer of immune defense mechanism and a mediator of leukocyte recruitment.[124] The endothelium expresses thrombomodulin and promotes procoagulant state by inhibiting synthesis of the anticoagulant protein C[125] and eliciting tissue factor (TF) production on the endothelium and monocytes, thereby stimulating thrombin and fibrin formation.[126]

Increased expression of glycoprotein adhesion receptors on vascular endothelium, by hypoxia-triggered transcriptional cascades beginning with early growth response gene-1[127] leads to induction of ICAM-1, and consequent recruitment of activated leukocytes particularly mononuclear phagocytes which contribute to the local procoagulant milieu. Recent evidence even implicates the local formation of tissue factor-bearing microparticles[128] in the processes leading to venous thrombogenesis. Circulating TF, in the form of microparticles released by activated leukocytes, accumulate in areas of stasis, such as the vein valve pockets.[129] Leukocyte microparticles that express PSGL-1 bind to P-selectin both on platelets and activated endothelial cells[130,131,] and this source of TF could sustain the production of thrombin on the forming thrombus, promoting its

propagation.[132] Although there is a consensus that tissue factor plays a prominent role in driving early coagulant cascades leading to venous thrombosis,[132,133] conventional notions of just where this tissue factor resides and how it is expressed are changing. Classically, tissue factor is known to reside and be enriched in the subendothelial stroma. Following vascular injury, when subendothelial material is placed in direct contact with blood, this can rapidly act with Factor VIIa to trigger thrombosis. We now know however that macrophages recruited to sites of hypoxemia or vascular injury are rich sources of tissue factor,[109] and substantially can contribute to the initiation or propagation of thrombus. The relative contribution of leukocyte microparticles to venous thrombogenesis is not clear, however, several studies have shown that the vessel wall is the most important source of TF that promotes thrombogenesis,[134] and therefore activation of the endothelium may be pivotal in the inflammatory processes that lead to thrombosis.

As all or nearly all biological triggers have countervailing measures to dampen cascade reactions, so too the cascade of events initiating with the activation of red blood cells (RBCs) must be terminated rather than run unchecked in an inflammatory / coagulant maelstrom. The contribution of RBCs to venous thrombosis remains poorly understood, despite their abundance in the early venous thrombus and their contribution to platelet rich arterial thrombi.[135] The cytoplasm of RBCs is rich in iron, which when released into circulation is highly inflammatory because of its oxidative effects on the endothelium. Natural antioxidant, such as heme oxygenase -1 (HO-1)-derived carbon monoxide (CO) and superoxide dismutase, produced by cells within the vessel wall and thrombus, may limit these proinflammatory effects produced during thrombogenesis. This putative mechanism by which RBCs may influence the development of venous

thrombi is supported by the finding that propagation of venous thrombosis is enhanced in HO-1$^{-/-}$ mice[136] and genetic variants (long GT-repeat alleles) in the HO-1 gene appear to confer increased risk of recurrent venous thromboembolism in humans.[137] One of the primary focuses of this thesis is to explore the role of HO-1/CO in luekosequestration during thrombogensis.

Crosstalk between HO-1/CO, thrombosis and inflammation:

HO-1 has been implicated in maintaining cellular homeostasis and providing cellular defense by virtue of the anti-apoptotic, anti-inflammatory and anti-oxidative properties mediated by HO-reaction products.[138] Previous studies have indicated that products of HO-1 activity possess antithrombotic properties, and impairment of HO-1 activity may contribute to thrombus formation.[137,136] Elucidating the intrinsic mechanism involved in thrombus formation is critical to understanding the pathophysiology of DVT. Stewart et al demonstrated leukocyte migration into the vein wall with an intact layer of endothelial cells during DVT[139], linking inflammation and thrombosis. Recent studies also highlight the role of HO-1 expression and/or CO in modulation of vascular endothelial cell damage, which is a key factor in thrombus formation following hypoxia or oxidant injury,[140,141] irradiation-induced apoptosis,[142] and interleukin-18-dependent inflammation.[143]

HO-1 expression or endogenously generated CO inhibits production of proinflammatory cytokines such as tumor necrosis factor-α, interleukin-1, and monocyte chemoattractant protein-1, most likely through inhibition of NF-κB activation.[144,145] These same mechanisms also limit the expression of adhesion molecules such as E- and

P-selectin, and the expression of tissue factor von Willebrand factor and plasminogen activator inhibitor-1, which can facilitate intravascular thrombus formation.[146] Part of this thesis tests the hypothesis that heme oxygenase-1 and carbon monoxide play a critical role to mitigate venous thrombogenesis by squelching inflammatory reactions and key thrombotic mediators at the blood/vessel interface.

FIGURES

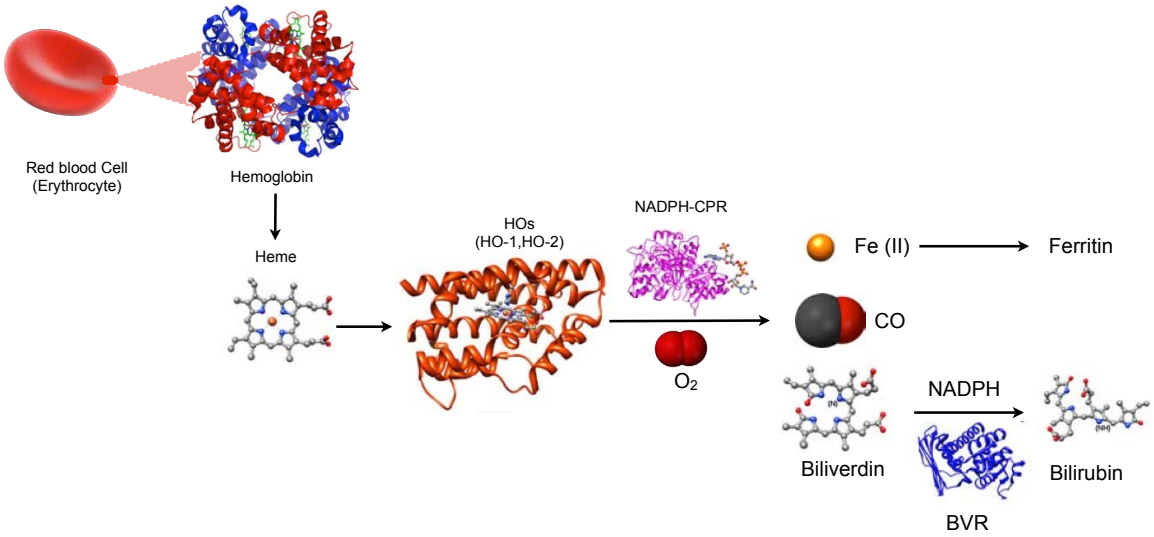

EQUATION 1

$$\text{Heme} + 7\ e^{-} + 3\ O_2 \rightarrow \text{Biliverdin} + CO + Fe\ (II) + 3\ H_2O \quad \text{(Eq.1)}$$

EQUATION 2

$$\text{Biliverdin} + 2\ e^{-} \rightarrow \text{Bilirubin} \quad \text{(Eq.2)}$$

FIGURE I.1: HEME-DEGRADATION CATALYZED BY HEME OXYGENASE.

Heme oxygenase (HO-1, HO-2) catalyzes the NADPH-cytochrome P450 reductase (CPR)-dependent degradation of heme into iron, CO and biliverdin, which is quickly reduced to bilirubin. Seven electrons are transferred and three molecules of O2 are consumed when one molecule of heme is oxidized to generate one molecule of biliverdin, one molecule of CO, one molecule of Fe (II), and three molecules of H2O. Two electrons are required for the reduction of one molecule of biliverdin.

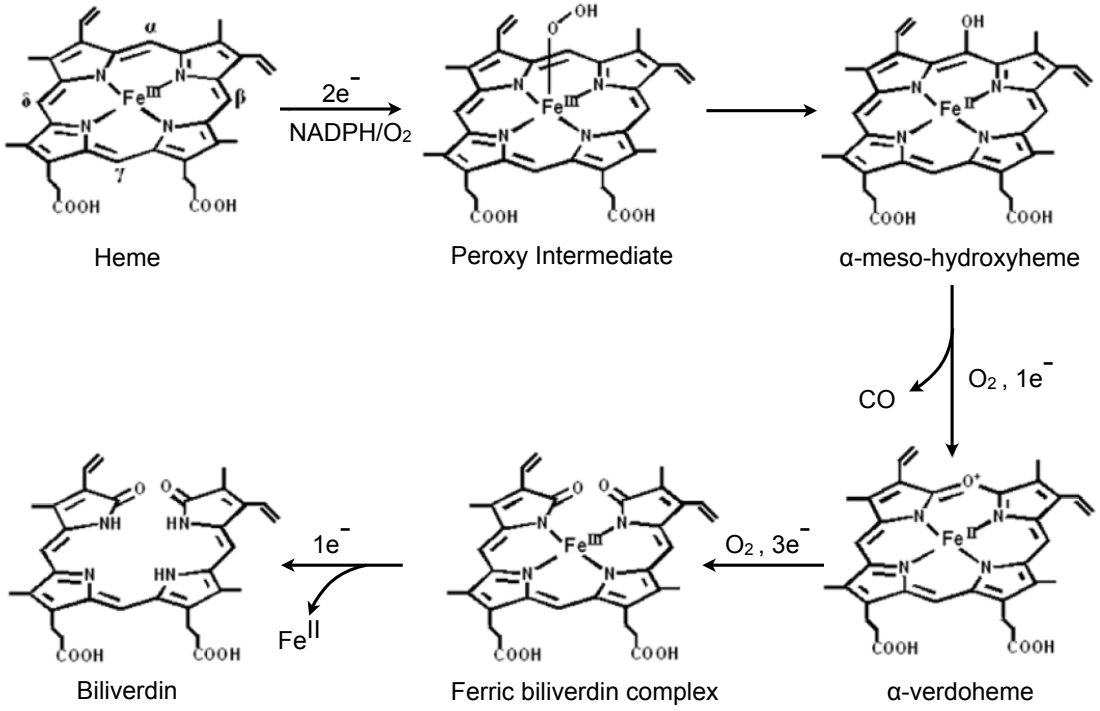

FIGURE I.2: HEME DEGRADATION PATHWAY

Heme is degraded to biliverdin through several key intermediates, including a peroxy intermediate, α-*meso*-hydroxyheme, α- verdoheme, and a ferric biliverdin complex.

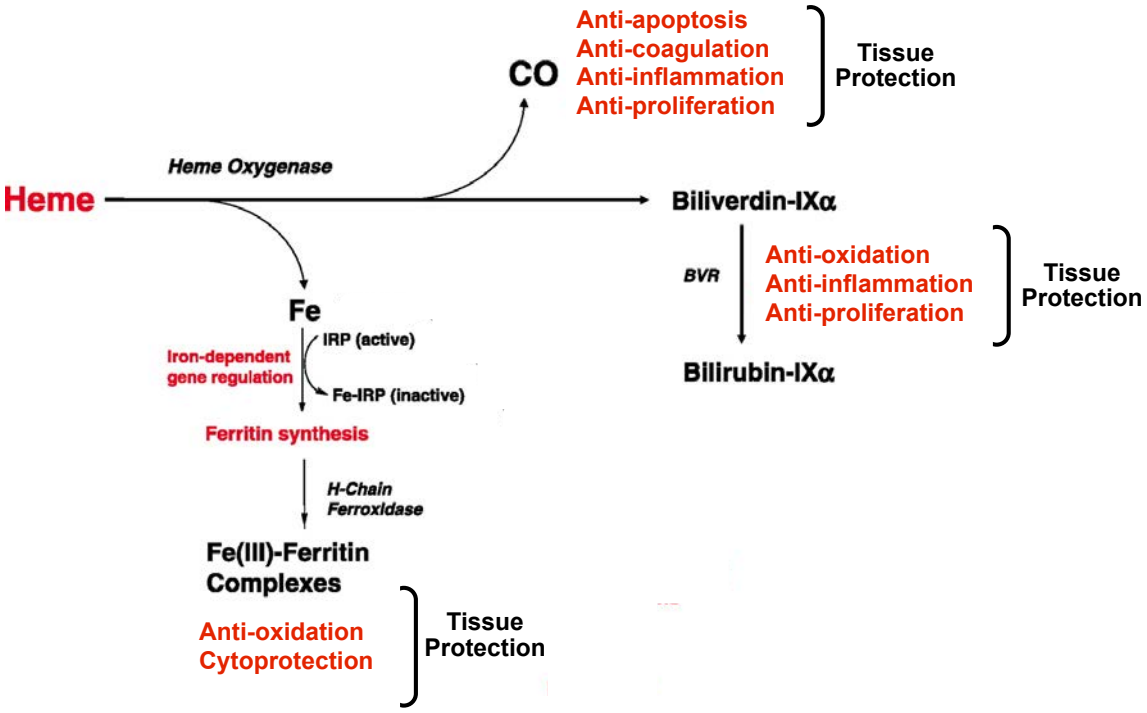

FIGURE I.3 TISSUE PROTECTION CONFERRED BY HO END PRODUCTS

All three end-products of heme degradation, including Fe, CO, and bilverdin/bilirubin, can contribute to the cytoprotective process. Iron released by HO activity stimulates a cytoprotective pathway involving the synthesis of ferritin. CO has been implicated in anti-inflammatory, anti-apoptotic, and anti-proliferative pathways. Biliverdin and bilirubin, potent lipid antioxidants, can exert anti-inflammatory and anti-proliferative effects.

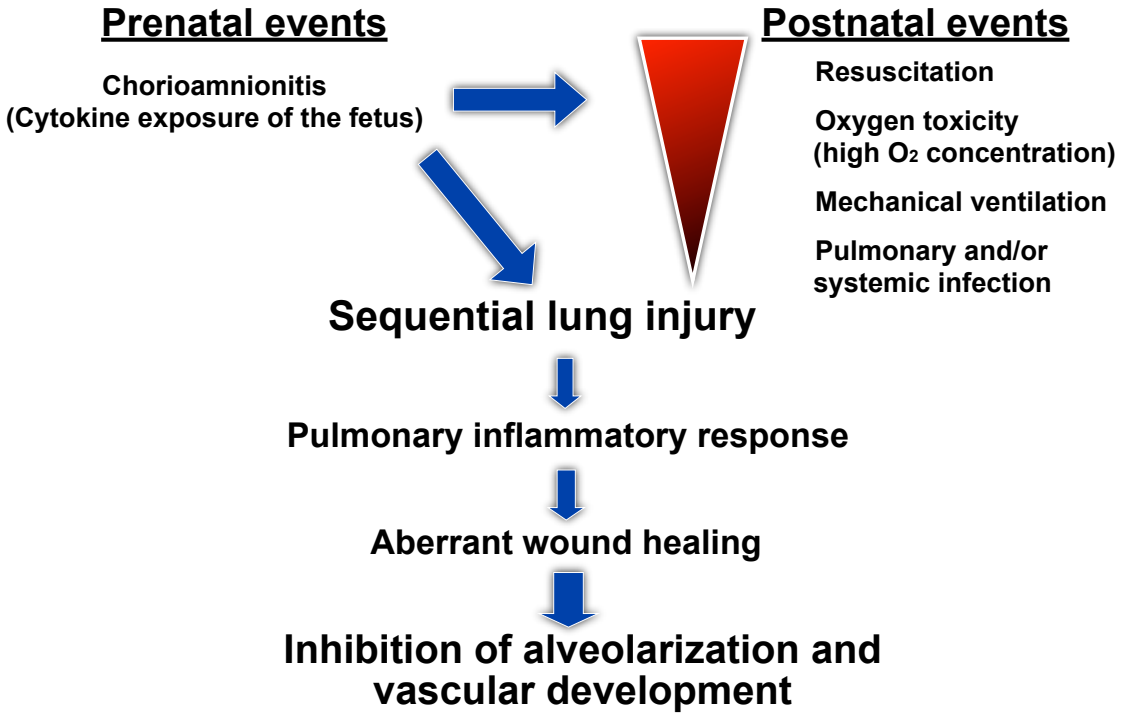

FIGURE I.4: THEORY ON THE PATHOGENESIS OF BPD.

There are two major events in the pathogenesis of BPD the prenatal and postnatal events. Prenatal event, which occurs when there is an increased expression of cytokines exposure in the fetus and postnatal event, which can occur due to improper resuscitation, oxygen toxicity, mechanical ventilation and pulmonary and/or systemic infection. Ultimately both events lead to the sequential lung Injury, pulmonary inflammatory response, aberrant wound healing and the inhibition of alveolarization and vascular development.

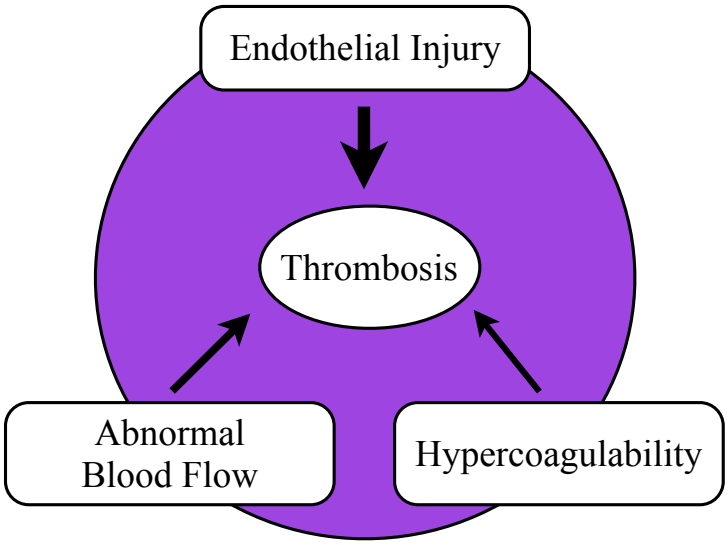

FIGURE I.5: VIRCHOW TRIAD

This schematic diagram describes the three categories of factors that are though to contribute to thrombosis. Hypercoagulability, hemodynamic changes (stasis, turbulence) and endothelial injury/dysfunction.

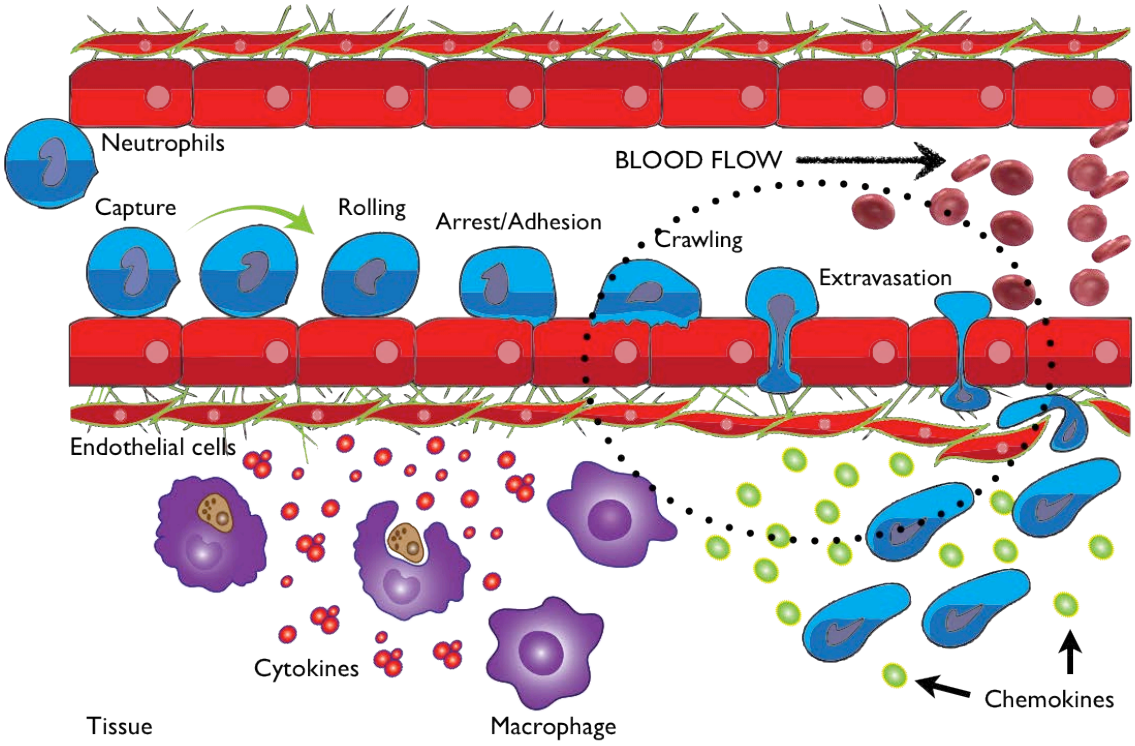

FIGURE I.6: LEUKOCYTE EXTRAVASATION

The diagram depicts the movement of leukocytes out of the circulatory system, towards the site of tissue damage or infection. This process forms part of the innate immune response, involving the recruitment of non-specific leukocytes. Monocytes also use this process in the absence of infection or tissue damage during their development into macrophages.

TABLE I.1: TIMING OF THE DEVELOPMENTAL STAGES IN HUMAN AND MOUSE.

Stage	Human (weeks) Term 40 weeks	Mouse (days) Term 19 days
Embryonic	3-7	9-12
Pseudoglandular	5-17	12-16
Canalicular	16-26	16-17
Saccular	24-38	17-PN 4
Alveolar	36-(1-2 years)	PN 4 -28

PN = Postnatal day

In human lung, alveoli begin to form during the weeks preceding birth but the large majority of alveoli are formed PN. Since the mouse is born during the saccular stage, its alveolarization takes place postnatally beginning around day 4, but in humans the alveoli continue to develop beyond the neonatal period.

REFERENCES

1. Maines, M.D. The heme oxygenase system: past, present, and future. *Antioxid Redox Signal.* **6**, 797-801. (2004).

2. Maines, M.D. New Insights into Biliverdin Reductase Functions: Linking Heme Metabolism to Cell Signaling. *Physiology* **20**, 382-389 (2005).

3. Schacter, B.A., Nelson, E.B., Marver, H.S. & Masters, B.S.S. Immunochemical Evidence for an Association of Heme Oxygenase with the Microsomal Electron Transport System. *Journal of Biological Chemistry* **247**, 3601-3607 (1972).

4. Montellano, P. The mechanism of heme oxygenase. *Current Opinion in Chemical Biology* **4**, 221-7 (2000).

5. Baker, H.M., Anderson, B.F. & Baker, E.N. Dealing with iron: Common structural principles in proteins that transport iron and heme. *Proceedings of the National Academy of Sciences* **100**, 3579-3583 (2003).

6. Papanikolaou, G. & Pantopoulos, K. Iron metabolism and toxicity. *Toxicology and Applied Pharmacology* **202**, 199-211 (2005).

7. Garrick MD, D.K., Horbinski C, Ghio AJ, Higgins D, Porubcin M, Moore EG, Hainsworth LN, Umbreit JN, Conrad ME, Feng L, Lis A, Roth JA, Singleton S, Garrick LM. DMT1: a mammalian transporter for multiple metals. *Biometals* **16**, 41-54 (2003).

8. Sargent PJ, F.S., Evans RW. Structure/function overview of proteins involved in iron storage and transport. *Current Medicinal Chemisty* **12**, 2683-93 (2005).

9. Rajagopal, A. et al. Haem homeostasis is regulated by the conserved and concerted functions of HRG-1 proteins. *Nature* **453**, 1127-1131 (2008).

10. Qi, Z., Hamza, I. & O'Brian, M.R. Heme is an effector molecule for iron-dependent degradation of the bacterial iron response regulator (Irr) protein. *Proceedings of the National Academy of Sciences* **96**, 13056-13061 (1999).

11. Ogawa, K. et al. Heme mediates derepression of Maf recognition element through direct binding to transcription repressor Bach1. *EMBO J* **20**, 2835-2843 (2001).

12. Dioum, E.M. et al. NPAS2: A Gas-Responsive Transcription Factor. *Science* **298**, 2385-2387 (2002).

13. Von Burg, D.R. Toxicology Update. *Journal of Applied Toxicology* **19**, 379-386 (1999).

14. Kumar, S. & Bandyopadhyay, U. Free heme toxicity and its detoxification systems in human. *Toxicology Letters* **157**, 175-188 (2005).

15. Grosser, N. et al. Antioxidant action of l-alanine: heme oxygenase-1 and ferritin as possible mediators. *Biochemical and Biophysical Research Communications* **314**, 351-355 (2004).

16. Ragsdale, S.W. Metals and Their Scaffolds To Promote Difficult Enzymatic Reactions. *Chemical Reviews* **106**, 3317-3337 (2006).

17. MacKenzie, E.L., Ray, P.D. & Tsuji, Y. Role and regulation of ferritin H in rotenone-mediated mitochondrial oxidative stress. *Free Radical Biology and Medicine* **44**, 1762-1771 (2008).

18. Ryter, S.W. & Tyrrell, R.M. The heme synthesis and degradation pathways: role in oxidant sensitivity: Heme oxygenase has both pro- and antioxidant properties. *Free Radical Biology and Medicine* **28**, 289-309 (2000).

19. Beale SI, Y.J. Deconstructing heme. *Nat Struct Biol* **6**, 903-5 (1999).

20. Dolinay, T., Szilasi, M., Liu, M. & Choi, A.M.K. Inhaled Carbon Monoxide Confers Antiinflammatory Effects against Ventilator-induced Lung Injury. *Am. J. Respir. Crit. Care Med.* **170**, 613-620 (2004).

21. Hoetzel, A. et al. Carbon Monoxide Protects against Ventilator-induced Lung Injury via PPAR-γ and Inhibition of Egr-1. *American Journal of Respiratory and Critical Care Medicine* **177**, 1223-1232 (2008).

22. Morita, T., Perrella, M.A., Lee, M.E. & Kourembanas, S. Smooth muscle cell-derived carbon monoxide is a regulator of vascular cGMP. *Proceedings of the National Academy of Sciences* **92**, 1475-1479 (1995).

23. Ryter, S.W., Alam, J. & Choi, A.M.K. Heme Oxygenase-1/Carbon Monoxide: From Basic Science to Therapeutic Applications. *Physiological Reviews* **86**, 583-650 (2006).

24. Otterbein, L. et al. Carbon monoxide has anti-inflammatory effects involving the mitogen-activated protein kinase pathway. *Nat Med* **6**, 422 - 428 (2000).

25. Otterbein, L.E. et al. Carbon monoxide suppresses arteriosclerotic lesions associated with chronic graft rejection and with balloon injury. *Nat Med* **9**, 183-190 (2003).

26. Otterbein, L.E. et al. MKK3 Mitogen-Activated Protein Kinase Pathway Mediates Carbon Monoxide-Induced Protection Against Oxidant-Induced Lung Injury. *The American Journal of Pathology* **163**, 2555-2563 (2003).

27. Brouard, S. et al. Carbon Monoxide Generated by Heme Oxygenase 1 Suppresses Endothelial Cell Apoptosis. *The Journal of Experimental Medicine* **192**, 1015-1026 (2000).

28. Wang, X.M., Kim, H.P., Nakahira, K., Ryter, S.W. & Choi, A.M.K. The Heme Oxygenase-1/Carbon Monoxide Pathway Suppresses TLR4 Signaling by Regulating the Interaction of TLR4 with Caveolin-1. *The Journal of Immunology* **182**, 3809-3818 (2009).

29. Nakahira, K. et al. Carbon monoxide differentially inhibits TLR signaling pathways by regulating ROS-induced trafficking of TLRs to lipid rafts. *The Journal of Experimental Medicine* **203**, 2377-2389 (2006).

30. Kim, H.P. et al. Caveolin-1 expression by means of p38β mitogen-activated protein kinase mediates the antiproliferative effect of carbon monoxide. *Proceedings of the National Academy of Sciences of the United States of America* **102**, 11319-11324 (2005).

31. Ryter, S.W. & Choi, A.M.K. Heme Oxygenase-1/Carbon Monoxide. *American Journal of Respiratory Cell and Molecular Biology* **41**, 251-260 (2009).

32. Song, R. et al. Carbon Monoxide Induces Cytoprotection in Rat Orthotopic Lung Transplantation via Anti-Inflammatory and Anti-Apoptotic Effects. *Am J Pathol* **163**, 231-242 (2003).

33. Kohmoto, J. et al. Low-dose carbon monoxide inhalation prevents ischemia/reperfusion injury of transplanted rat lung grafts. *Surgery* **140**, 179-185 (2006).

34. Bathoorn, E. et al. Anti-inflammatory effects of inhaled carbon monoxide in patients with COPD: a pilot study. *European Respiratory Journal* **30**, 1131-1137 (2007).

35. Boehning, D. & Snyder, S.H. Carbon Monoxide and Clocks. *Science* **298**, 2339-2340 (2002).

36. Verma A, H.D., Glatt CE, Ronnett GV, Snyder SH. Carbon monoxide: a putative neural messenger. *Science* **259**, 381-4 (1993).

37. Kim, H.P., Ryter, S.W. & Choi, A.M.K. CO AS A CELLULAR SIGNALING MOLECULE. *Annual Review of Pharmacology and Toxicology* **46**, 411-449 (2006).

38. Barañano, D.E. & Snyder, S.H. Neural roles for heme oxygenase: Contrasts to nitric oxide synthase. *Proceedings of the National Academy of Sciences* **98**, 10996-11002 (2001).

39. Williams, S.E.J. et al. Hemoxygenase-2 Is an Oxygen Sensor for a Calcium-Sensitive Potassium Channel. *Science* **306**, 2093-2097 (2004).

40. Moore, B.A. et al. Brief inhalation of low-dose carbon monoxide protects rodents and swine from postoperative ileus *. *Critical Care Medicine* **33**, 1317-1326 10.1097/01.CCM.0000166349.76514.40 (2005).

41. Ryter, S.W., Morse, D. & Choi, A.M.K. Carbon Monoxide: To Boldly Go Where NO Has Gone Before. *Sci. STKE* **2004**, re6- (2004).

42. Wu, L. & Wang, R. Carbon Monoxide: Endogenous Production, Physiological Functions, and Pharmacological Applications. *Pharmacological Reviews* **57**, 585-630 (2005).

43. Maines, M.D. The Heme Oxygenase System: A Regulator of Second Messenger Gases. *Annual Review of Pharmacology and Toxicology* **37**, 517-554 (1997).

44. Coburn, R.F., Williams, W.J. & Forster, R.E. Effect of Erythrocyte Destruction on Carbon Monoxide Production in Man*. *The Journal of Clinical Investigation* **43**, 1098-1103 (1964).

45. Childs B, S.J., Migeon CJ. Glucuronic acid conjugation by patients with familial nonhemolytic jaundice and their relatives. *Pediatrics* **23**, 903-13 (1959).

46. Vittorio Calabrese, D.A.B., Giovanni Scapagnini, A.M. Giuffrida Stella, and Professor Mahin D. Maines. Redox Regulation of Heat Shock Protein Expression by Signaling Involving Nitric Oxide and Carbon Monoxide: Relevance to Brain

Aging, Neurodegenerative Disorders, and Longevity *Antioxidants & Redox Signaling* **8**, 444-447 (2006).

47. Stocker, R., Yamamoto, Y., McDonagh, A., Glazer, A. & Ames, B. Bilirubin is an antioxidant of possible physiological importance. *Science* **235**, 1043 - 1046 (1987).

48. Chang EF, W.R., Vreman HJ, Igarashi T, Galo E, Sharp FR, Stevenson DK, Noble-Haeusslein LJ. Heme oxygenase-2 protects against lipid peroxidation-mediated cell loss and impaired motor recovery after traumatic brain injury. *J Neurosci* **23**, 3689-96 (2003).

49. Yachie, A. et al. Oxidative stress causes enhanced endothelial cell injury in human heme oxygenase-1 deficiency. *J Clin Invest* **103**, 129 - 135 (1999).

50. Sedlak, T.W. & Snyder, S.H. Bilirubin Benefits: Cellular Protection by a Biliverdin Reductase Antioxidant Cycle. *Pediatrics* **113**, 1776-1782 (2004).

51. Sedlak, T.W. et al. Bilirubin and glutathione have complementary antioxidant and cytoprotective roles. *Proceedings of the National Academy of Sciences* **106**, 5171-5176 (2009).

52. Foresti R, G.C., Motterlini R. Generation of bile pigments by haem oxygenase: a refined cellular strategy in response to stressful insults. *Biochem Soc Symp*, 177-92 (2004).

53. Barañano, D.E., Rao, M., Ferris, C.D. & Snyder, S.H. Biliverdin reductase: A major physiologic cytoprotectant. *Proceedings of the National Academy of Sciences* **99**, 16093-16098 (2002).

54. Fondevila, C. et al. Biliverdin therapy protects rat livers from ischemia and reperfusion injury. *Hepatology* **40**, 1333-1341 (2004).

55. Maines, M.D. The heme oxygenase system: update 2005. *Antioxid Redox Signal.* **7**, 1761-6 (2005).

56. McCoubrey, W.K., Huang, T.J. & Maines, M.D. Isolation and Characterization of a cDNA from the Rat Brain that Encodes Hemoprotein Heme Oxygenase-3. *European Journal of Biochemistry* **247**, 725-732 (1997).

57. Hoshi, T. & Lahiri, S. Oxygen Sensing: It's a Gas! *Science* **306**, 2050-2051 (2004).

58. Sugishima, M. et al. Crystal Structure of Dimeric Heme Oxygenase-2 from Synechocystis sp. PCC 6803 in Complex with Heme†,‡. *Biochemistry* **44**, 4257-4266 (2005).

59. Davis SJ, B.S., Durski AM, Walker JM, Vierstra RD. The heme-oxygenase family required for phytochrome chromophore biosynthesis is necessary for proper photomorphogenesis in higher plants. *Plant Physiology* **126**, 656-69 (2001).

60. Pimstone, N.R. et al. Inducible heme oxygenase in the kidney: a model for the homeostatic control of hemoglobin catabolism. *The Journal of Clinical Investigation* **50**, 2042-2050 (1971).

61. Adlercreutz H, T.R. Some aspects of the interaction between natural and synthetic female sex hormones and the liver. *Am J Med* **49**, 630-48 (1970).

62. Maines, M. Heme Oxygenase: Clinical Applications and Functions. (1992).

63. Maines, M.D., Eke, B.C. & Zhao, X. Corticosterone promotes increased heme oxygenase-2 protein and transcript expression in the newborn rat brain. *Brain Research* **722**, 83-94 (1996).

64. Trakshel, G.M., Kutty, R.K. & Maines, M.D. Purification and characterization of the major constitutive form of testicular heme oxygenase. The noninducible isoform. *Journal of Biological Chemistry* **261**, 11131-11137 (1986).

65. Regan, R., Chen, J. & Benvenisti-Zarom, L. Heme oxygenase-2 gene deletion attenuates oxidative stress in neurons exposed to extracellular hemin. *BMC Neuroscience* **5**, 34 (2004).

66. Galbraith, R. Heme oxygenase: who needs it? *Proc Soc Exp Biol Med.* **222**, 299-305 (1999).

67. Martin JA, H.B., Sutton PD, Ventura SJ, Menacker F, Kirmeyer S, Munsun ML: Centers for Disease Control and Prevention National Center for Health Statustics National Vital Statistics System. Births: final data for 2005. *Natl Vital Stat Rep* **56**, 1-103 (Dec 5 2007).

68. Lemons, J.A. et al. Very Low Birth Weight Outcomes of the National Institute of Child Health and Human Development Neonatal Research Network, January 1995 Through December 1996. *Pediatrics* **107**, e1- (2001).

69. Vrijlandt, E.J.L.E., Boezen, H.M., Gerritsen, J., Stremmelaar, E.F. & Duiverman, E.J. Respiratory Health in Prematurely Born Preschool Children with and without Bronchopulmonary Dysplasia. *The Journal of Pediatrics* **150**, 256-261 (2007).

70. Doyle, L.W. et al. Respiratory function at age 8-9 years in extremely low birthweight/very preterm children born in Victoria in 1991-1992. *Pediatric Pulmonology* **41**, 570-576 (2006).

71. Wong, P.M. et al. Emphysema in young adult survivors of moderate-to-severe bronchopulmonary dysplasia. *Eur Respir J* **32**, 321-328 (2008).

72. Jobe, A.J. The New BPD: An Arrest of Lung Development. *Pediatric Research* **46**, 641 (1999).

73. Husain AN, S.N.a.s.J. Pathology of arrested acinar development in postsurfactant bronchopulmonary dysplasia. *Hum Pathol* **29**, 710-7 (1998).

74. Hargitai, B. et al. Apoptosis in Various Organs of Preterm Infants: Histopathologic Study of Lung, Kidney, Liver, and Brain of Ventilated Infants. *Pediatric Research* **50**, 110-114 (2001).

75. Lukkarinen, H.P., Laine, J. & Kaapa, P.O. Lung Epithelial Cells Undergo Apoptosis in Neonatal Respiratory Distress Syndrome. *Pediatric Research* **53**, 254-259 (2003).

76. May, M. et al. Apoptosis and proliferation in lungs of ventilated and oxygen-treated preterm infants. *Eur Respir J* **23**, 113-121 (2004).

77. Coalson, J.J., Winter, V.T., Siler-Khodr, T. & Yoder, B.A. Neonatal Chronic Lung Disease in Extremely Immature Baboons. *Am. J. Respir. Crit. Care Med.* **160**, 1333-1346 (1999).

78. Burri, P.H. Structural Aspects of Postnatal Lung Development â€“ Alveolar Formation and Growth. *Neonatology* **89**, 313-322 (2006).

79. Jobe, A.H. Neonatal -perinatal medicine. Disease of the fetus and infant. (ed. R, F.A.a.M.) 973-991 (Mosby Inc St. Louis, MO, 2002).

80. Coalson, J.J. Experimental models of bronchopulmonary dysplasia. *Biol Neonate* **77**, 35-8 (1997).

81. Deng, H., Nicholas Mason, S. & Auten, R.L., Jr. Lung Inflammation in Hyperoxia Can Be Prevented By Antichemokine Treatment in Newborn Rats. *Am. J. Respir. Crit. Care Med.* **162**, 2316-2323 (2000).

82. Dreyfuss, D. & Saumon, G. Ventilator-induced Lung Injury . Lessons from Experimental Studies. *Am. J. Respir. Crit. Care Med.* **157**, 294-323 (1998).

83. E, M. The respiratory system. . in *Human anatomy and Physiology* 834-886 (Addison Wesley Longman Inc., , San Francisco 2001).

84. Maus, U.A. et al. Role of resident alveolar macrophages in leukocyte traffic into the alveolar air space of intact mice. *Am J Physiol Lung Cell Mol Physiol* **282**, L1245-1252 (2002).

85. Kaplanski, G., Marin, V., Montero-Julian, F., Mantovani, A. & Farnarier, C. IL-6: a regulator of the transition from neutrophil to monocyte recruitment during inflammation. *Trends in Immunology* **24**, 25-29 (2003).

86. Janardhan KS, S.S., Singh B Neutrophil depletion inhibits early and late monocyte/macrophage increase in lung inflammation. *Front Bioscience* **1**, 1569-76 (2006).

87. Baier, R.J., Majid, A., Parupia, H., Loggins, J. & Kruger, T.E. CC chemokine concentrations increase in respiratory distress syndrome and correlate with development of bronchopulmonary dysplasia. *Pediatric Pulmonology* **37**, 137-148 (2004).

88. Kakkera, D.K., Siddiq, M.M. & Parton, L.A. Interleukin-1 Balance in the Lungs of Preterm Infants Who Develop Bronchopulmonary Dysplasia. *Neonatology* **87**, 82-90 (2005).

89. Kotecha, S., Wilson, L., Wangoo, A., Silverman, M. & Shaw, R.J. Increase in Interleukin (IL)-1[beta] and IL-6 in Bronchoalveolar Lavage Fluid Obtained from Infants with Chronic Lung Disease of Prematurity. *Pediatric Research* **40**, 250-256 (1996).

90. Jones, C.A. et al. Undetectable Interleukin (IL)-10 and Persistent IL-8 Expression Early in Hyaline Membrane Disease: A Possible Developmental Basis for the Predisposition to Chronic Lung Inflammation in Preterm Newborns. *Pediatric Research* **39**, 966-975 (1996).

91. Baier, R.J., Loggins, J. & Kruger, T.E. Interleukin-4 and 13 concentrations in infants at risk to develop Bronchopulmonary Dysplasia. *BMC Pediatrics* **3**, 8 (2003).

92. Ramsay, P.L., O'Brian Smith, E., Hegemier, S. & Welty, S.E. Early Clinical Markers for the Development of Bronchopulmonary Dysplasia: Soluble E-Selectin and ICAM-1. *Pediatrics* **102**, 927-932 (1998).

93. Perkowski, S. et al. Dissociation between alveolar transmigration of neutrophils and lung injury in hyperoxia. *Am J Physiol Lung Cell Mol Physiol* **291**, L1050-1058 (2006).

94. Wagenaar, G.T.M. et al. Gene expression profile and histopathology of experimental bronchopulmonary dysplasia induced by prolonged oxidative stress. *Free Radical Biology and Medicine* **36**, 782-801 (2004).

95. Rozycki, H.J., Comber, P.G. & Huff, T.F. Cytokines and oxygen radicals after hyperoxia in preterm and term alveolar macrophages. *Am J Physiol Lung Cell Mol Physiol* **282**, L1222-1228 (2002).

96. Otterbein, L., Mantell, L. & Choi, A. Carbon monoxide provides protection against hyperoxic lung injury. *Am J Physiol* **276**, L688 - L694 (1999).

97. Otterbein, L.E., Soares, M.P., Yamashita, K. & Bach, F.H. Heme oxygenase-1: unleashing the protective properties of heme. *Trends in Immunology* **24**, 449-455 (2003).

98. Ghosh, S., Gal, J. & Marczin, N. Carbon monoxide: Endogenous mediator, potential diagnostic and therapeutic target. *Annals of Medicine* **42**, 1-12.

99. Lee, P., Alam, J., Wiegand, G. & Choi, A. Overexpression of heme oxygenase-1 in human pulmonary epithelial cells results in cell growth arrest and increased resistance to hyperoxia. *Proc Natl Acad Sci USA* **93**, 10393 - 10398 (1996).

100. Otterbein, L. et al. Exogenous administration of heme oxygenase-1 by gene transfer provides protection against hyperoxia-induced lung injury. *J Clin Invest* **103**, 1047 - 1054 (1999).

101. Morse, D. & Choi, A. Heme oxygenase-1. The "emerging molecule" has arrived. *Am J Respir Cell Mol Biol* **27**, 8 - 16 (2002).

102. Ryter, S., Otterbein, L., Morse, D. & Choi, A. Heme oxygenase/ carbon monoxide signaling pathways: regulation and functional significance. *Mol Cell Biochem* **234-235**, 249 - 263 (2002).

103. Fujita, T. et al. Paradoxical rescue from ischemic lung injury by inhaled carbon monoxide driven by derepression of fibrinolysis. *Nat Med* **7**, 598 - 604 (2001).

104. Song, R. et al. Carbon Monoxide Inhibits Human Airway Smooth Muscle Cell Proliferation via Mitogen-Activated Protein Kinase Pathway. *Am. J. Respir. Cell Mol. Biol.* **27**, 603-610 (2002).

105. Hirsh, J. & Hoak, J. Management of Deep Vein Thrombosis and Pulmonary Embolism: A Statement for Healthcare Professionals From the Council on Thrombosis (in Consultation With the Council on Cardiovascular Radiology), American Heart Association. *Circulation* **93**, 2212-2245 (1996).

106. Andrews RK, B.M. Adhesion-dependent signalling and the initiation of haemostasis and thrombosis. *Histol Histopathol* **13**, 837-44 (1998).

107. Wakefield, T.W., Myers, D.D. & Henke, P.K. Mechanisms of Venous Thrombosis and Resolution. *Arteriosclerosis, Thrombosis, and Vascular Biology* **28**, 387-391 (2008).

108. Aird, W.C. Vascular bed-specific thrombosis. *Journal of Thrombosis and Haemostasis* **5**, 283-291 (2007).

109. Lawson, C.A. et al. Monocytes and tissue factor promote thrombosis in a murine model of oxygen deprivation. *The Journal of Clinical Investigation* **99**, 1729-1738 (1997).

110. Pinsky, D.J. et al. Coordinated induction of plasminogen activator inhibitor-1 (PAI-1) and inhibition of plasminogen activator gene expression by hypoxia promotes pulmonary vascular fibrin deposition. *The Journal of Clinical Investigation* **102**, 919-928 (1998).

111. Pinsky, D.J. et al. Hypoxia-induced exocytosis of endothelial cell Weibel-Palade bodies. A mechanism for rapid neutrophil recruitment after cardiac preservation. *The Journal of Clinical Investigation* **97**, 493-500 (1996).

112. Weibel, E.R. & Palade, G.E. New Cytoplasmic Components In Arterial Endothelia. *The Journal of Cell Biology* **23**, 101-112 (1964).

113. Wagner, D.D., Olmsted, J.B. & Marder, V.J. Immunolocalization of von Willebrand protein in Weibel-Palade bodies of human endothelial cells. *The Journal of Cell Biology* **95**, 355-360 (1982).

114. Bonfanti, R., Furie, B., Furie, B. & Wagner, D. PADGEM (GMP140) is a component of Weibel-Palade bodies of human endothelial cells. *Blood* **73**, 1109-1112 (1989).

115. McEver, R.P., Beckstead, J.H., Moore, K.L., Marshall-Carlson, L. & Bainton, D.F. GMP-140, a platelet alpha-granule membrane protein, is also synthesized by vascular endothelial cells and is localized in Weibel-Palade bodies. *The Journal of Clinical Investigation* **84**, 92-99 (1989).

116. Wagner, D.D. et al. Induction of specific storage organelles by von Willebrand factor propolypeptide. *Cell* **64**, 403-413 (1991).

117. Denis, C.V. et al. Interleukin 11 significantly increases plasma von Willebrand factor and factor VIII in wild type and von Willebrand disease mouse models. *Blood* **97**, 465-472 (2001).

118. Mayadas, T.N., Johnson, R.C., Rayburn, H., Hynes, R.O. & Wagner, D.D. Leukocyte rolling and extravasation are severely compromised in P selectin-deficient mice. *Cell* **74**, 541-554 (1993).

119. André, P. et al. Platelets adhere to and translocate on von Willebrand factor presented by endothelium in stimulated veins. *Blood* **96**, 3322-3328 (2000).

120. Frenette, P.S., Johnson, R.C., Hynes, R.O. & Wagner, D.D. Platelets roll on stimulated endothelium in vivo: an interaction mediated by endothelial P-selectin. *Proceedings of the National Academy of Sciences* **92**, 7450-7454 (1995).

121. Frenette, P.S. et al. P-Selectin Glycoprotein Ligand 1 (Psgl-1) Is Expressed on Platelets and Can Mediate Platelet–Endothelial Interactions in Vivo. *The Journal of Experimental Medicine* **191**, 1413-1422 (2000).

122. Romo, G.M. et al. The Glycoprotein Ib-IX-V Complex Is a Platelet Counterreceptor for P-Selectin. *The Journal of Experimental Medicine* **190**, 803-814 (1999).

123. Cambien, B. & Wagner, D.D. A new role in hemostasis for the adhesion receptor P-selectin. *Trends in Molecular Medicine* **10**, 179-186 (2004).

124. Nathan, C. Points of control in inflammation. *Nature* **420**, 846-52 (2002).

125. Yamamoto K, S.T., Kojima T, Loskutoff DJ, Saito H. Regulation of murine protein C gene expression in vivo: effects of tumor necrosis factor-alpha, interleukin-1, and transforming growth factor-beta. *Thrombosis and Haemostasis* **82**, 1297-1301 (1999).

126. Kirchhofer, D. et al. Endothelial cells stimulated with tumor necrosis factor-alpha express varying amounts of tissue factor resulting in inhomogenous fibrin

deposition in a native blood flow system. Effects of thrombin inhibitors. *The Journal of Clinical Investigation* **93**, 2073-2083 (1994).

127. Yan SF, F.T., Lu J, Okada K, Shan Zou Y, Mackman N, Pinsky DJ, Stern DM. Egr-1, a master switch coordinating upregulation of divergent gene families underlying ischemic stress. *Nature Medicine* **6**, 1355-61 (2000).

128. Myers, D.D. et al. P-selectin and leukocyte microparticles are associated with venous thrombogenesis. *Journal of Vascular Surgery* **38**, 1075-1089 (2003).

129. Manly, D.A., Boles, J. & Mackman, N. Role of Tissue Factor in Venous Thrombosis. *Annual Review of Physiology* **73**, 515-525 (2011).

130. Furie, B. & Furie, B.C. Mechanisms of Thrombus Formation. *New England Journal of Medicine* **359**, 938-949 (2008).

131. Falati, S. et al. Accumulation of Tissue Factor into Developing Thrombi In Vivo Is Dependent upon Microparticle P-Selectin Glycoprotein Ligand 1 and Platelet P-Selectin. *The Journal of Experimental Medicine* **197**, 1585-1598 (2003).

132. Giesen, P.L.A. et al. Blood-borne tissue factor: Another view of thrombosis. *Proceedings of the National Academy of Sciences* **96**, 2311-2315 (1999).

133. Owens AP 3rd, M.N. Tissue factor and thrombosis: The clot starts here. *Thrombosis and Haemostasis* **104**, 432-9 (2010).

134. Sharlene M. Day, J.L.R., Brian Pedersen, Diana M Farris, Daniel D. Myers, Michael Im, Thomas W. Wakefield, Nigel Mackman, and William P. Fay.

Macrovascular thrombosis is driven by tissue factor derived primarily from the blood vessel wall. *Journal of The American Society of Hematology* **105**, 192-198 (2005).

135. Turitto VT, W.H. Red blood cells: their dual role in thrombus formation. *Science* **207**, 541-3 (1980).

136. Tracz, M.J. et al. Induction of Heme Oxygenase-1 is a Beneficial Response in a Murine Model of Venous Thrombosis. *The American Journal of Pathology* **173**, 1882-1890 (2008).

137. Mustafa, S. et al. Genetic variation in heme oxygenase 1 (HMOX1) and the risk of recurrent venous thromboembolism. *Journal of Vascular Surgery* **47**, 566-570 (2008).

138. Otterbein, L.E. & Choi, A.M.K. Heme oxygenase: colors of defense against cellular stress. *Am J Physiol Lung Cell Mol Physiol* **279**, L1029-1037 (2000).

139. Stewart GJ, R.W., Lynch PR. Venous endothelial damage produced by massive sticking and emigration of leukocytes. *American Journal of Pathology* **74**, 507-32 (1974).

140. Lindenblatt, N., Bordel, R., Schareck, W., Menger, M.D. & Vollmar, B. Vascular Heme Oxygenase-1 Induction Suppresses Microvascular Thrombus Formation In Vivo. *Arteriosclerosis, Thrombosis, and Vascular Biology* **24**, 601-606 (2004).

141. Yet, S. et al. Hypoxia induces severe right ventricular dilatation and infarction in heme oxygenase-1 null mice. *J Clin Invest* **103**, R23 - R29 (1999).

142. Ewing P, W.A., Eissner G, Holler E, Andreesen R, Gerbitz A. Expression of heme oxygenase-1 protects endothelial cells from irradiation-induced apoptosis. *Endothelium* **12**, 113-9 (2005).

143. Zabalgoitia, M. et al. Carbon monoxide donors or heme oxygenase-1 (HO-1) overexpression blocks interleukin-18-mediated NF-κB–PTEN-dependent human cardiac endothelial cell death. *Free Radical Biology and Medicine* **44**, 284-298 (2008).

144. Bilban, M. et al. Heme oxygenase and carbon monoxide initiate homeostatic signaling. *Journal of Molecular Medicine* **86**, 267-279 (2008).

145. Ryan, M.J. et al. Renal vascular responses to CORM-A1 in the mouse. *Pharmacological Research* **54**, 24-29 (2006).

146. True, A.L. et al. Heme Oxygenase-1 Deficiency Accelerates Formation of Arterial Thrombosis Through Oxidative Damage to the Endothelium, Which Is Rescued by Inhaled Carbon Monoxide. *Circulation Research* **101**, 893-901 (2007).

CHAPTER II

SUPPRESSION OF CCL2-DEPENDENT INFLAMMATORY CELL TRAFFICKING AND ALVEOLAR SIMPLIFICATION BY THE HEME OXYGENASE-1 PRODUCT CARBON MONOXIDE

ABSTRACT

Bronchopulmonary dysplasia (BPD), a lung disease of prematurely-born infants, is characterized in part by arrested development of pulmonary alveolae. We hypothesized that heme oxygenase (HO-1) and its byproduct carbon monoxide (CO), which are thought to be cytoprotective against redox stress, mitigate lung injury and alveolar simplification in hyperoxia-exposed neonatal mice, a model of BPD. Three-day old C57BL/6J mice were exposed to air or hyperoxia (FiO_2 = 75%) in the presence or absence of inhaled CO (250 ppm for 1 h twice daily) for 21 days. Hyperoxic exposure increased mean linear intercept, a measure of alveolar simplification, whereas CO treatment attenuated hypoalveolarization, yielding a normal-appearing lung. Conversely, HO-1 null mice showed exaggerated hyperoxia-induced hypoalveolarization. CO also inhibited hyperoxia-induced pulmonary accumulation of $F4/80^+$, $CD11c^+$ and $CD11b^+$ monocytes and $Gr\text{-}1^+$ neutrophils. Further, CO attenuated lung mRNA and protein expression of pro-inflammatory cytokines including the monocyte chemoattractant CCL2 *in vivo,* and decreased hyperoxia-induced lung epithelial cell CCL2 production *in vitro*. Accordingly, we tested the requirement of CCL2 for hyperoxia-induced lung injury.

Hyperoxia-exposed CCL2 null mice, like CO-treated mice, showed attenuated alveolar simplification and lung infiltration of $CD11b^{+}$ monocytes. We conclude that, in hyperoxia-exposed neonatal mice, inhalation of CO suppresses CCL2-dependent inflammation and alveolar simplification.

INTRODUCTION

An estimated 30% of premature infants with a birth weight between 500-1500 g will develop respiratory distress syndrome, with many proceeding to develop bronchopulmonary dysplasia (BPD). Pathological features of BPD include interstitial fibrosis and abnormal cellular proliferation, as well as arrested alveolar development. Infants with BPD are at high risk for morbidity and mortality during the first years of life including increased medication use, hospital readmissions [1] and lung function abnormalities which persist into childhood and even early adulthood. [2, 3]

The pathophysiological mechanisms underlying BPD are likely multifactorial and not completely clear. Recent studies implicate lung inflammation as a potential contributor to the development of BPD. Infiltrates of leukocytes and inflammatory mediators have been detected in the lungs of patients with BPD [4, 5]. Neutrophils and cells of the monocyte/macrophage lineage appear to play a particularly important role in chronic lung disease in preterm infants The development of BPD has been associated with increased lung levels of pro-inflammatory cytokines, including IL-1β, IL-6, tumor necrosis factor-α, as well as CXC and CC-chemokines [6, 7, 8]. Treatment of hyperoxia-exposed neonatal lungs with antibodies or antagonists against the neutrophil chemokines CXCL1 or CXCL2 prevents lung inflammation and alveolar simplification [9, 10, 11].

Oxidative stress has also been implicated as one of the major causes of pulmonary injury leading to the development of BPD. Prolonged exposure to sublethal hyperoxia in animal models recapitulates some of the processes observed in BPD, such as arrested

alveolar development, marked by a paucity of α-actin-positive myofibroblasts at the alveolar septal tips, and a corresponding increase in the number of interstitial myofibroblasts [12, 13, 14, 15]. Importantly, rodents exhibit at birth a saccular stage of lung development that is completed after 2 weeks of postnatal alveolarization, thus closely resembling the stage of lung development in premature infants between 26 and 28 wk gestation requiring intensive care [16]. In newborn animals, hyperoxia has been shown to be a strong inducer of various proinflammatory cytokines in airway cells and pulmonary tissue [17]. Reactive oxygen species may be produced by resident lung epithelial cells under hyperoxic conditions, or from neutrophils and macrophages invading the lungs as part of the inflammatory process induced by hyperoxia [18].

Organisms faced with hyperoxic stress have evolved sophisticated and redundant mechanisms to ensure survival. Emerging evidence has highlighted a crucial role for stress-inducible heme oxygenase (HO)-1 and its catalytic byproducts, carbon monoxide (CO) and biliverdin, in cytoprotection against hyperoxic and ischemic forms of tissue and cellular injury [16, 19, 20, 21, 22, 23, 24, 25, 26, 27]. Although the precise mechanisms whereby CO modulates the inflammatory milieu remain under study, there is some evidence that it does so by tilting the milieu towards the production of the anti-inflammatory cytokine IL-10 [21, 25, 26], while at the same time blunting expression of TNF-α and IL-1β [27]. In immature rodents, HO-1 expression is induced during lung maturation and following exposure to hyperoxia, consistent with adaptation to extrauterine conditions of increased oxidative stress and inflammation [28, 29]. It has recently been shown that HO-1 and CO mitigate hyperoxia-induced pulmonary inflammation in neonatal mice [16]. However, arrested alveolar development was minimally affected by CO administration, and the

mechanisms by which CO reduced pulmonary inflammation were not explored.

We hypothesized that inhalation of low dose episodic CO mitigates the effect of neonatal hyperoxia on alveolar development and the developing lung by an anti-inflammatory mechanism. We report here that inhalation of CO suppresses CCL2-dependent inflammatory cell trafficking, pro-inflammatory cytokine expression and alveolar simplification in hyperoxia-exposed mice.

METHODS

Experimental animals. All animal experiments were performed accordingly to protocols approved by and carried out in accordance with the University of Michigan Institutional Animal Care and Use Committee. Timed pregnant C57BL/6J mice were either purchased from Jackson Laboratories (Bar Harbor, ME) or bred at the University of Michigan animal facility. Murine alveolar development begins on postnatal day 3, and saccular division is completed by the 14th postnatal day [30]. This sequence and relative timing of alveolarization resembles human lung development [31]. After birth, three day-old (P3) newborn pups from six different litters were subdivided into four groups within 24 h of birth: normoxia (21% O_2); hyperoxia (75% O_2); carbon monoxide (CO 250 ppm) + normoxia; and CO (250 ppm) + hyperoxia. Selected experiments also employed B6.129S4-*Scya2*^{tm1Rol} CCL2 null mice (Jackson Laboratories, Bar Harbor, ME). In addition, we obtained HO-1 null mice (C57BL/6J background) from Dr. Mu-En Lee (Harvard School of Public Health) [32]. Colonies of HO-1 gene null mice were maintained by breeding HO-1$^{-/-}$ males with HO-1$^{+/-}$ females. Offspring were genotyped at the time of birth using PCR to amplify the wildtype and mutant alleles of genomic DNA from tail biopsies [33]. For all experiments, HO-1$^{+/+}$ and HO-1$^{-/-}$ mice were age-matched at postnatal (PN) day 3. Each litter consisted of 8-10 pups per group to control for the effects of litter size on nutrition and growth. All animals were either exposed to room air or various gas mixtures, for up to three weeks.

To achieve 75% O_2, 100% O_2 was delivered at a flow rate of 0.5 L/min into a custom-made 1.5 m^3 plastic chamber. Oxygen concentrations were monitored continuously with an oxygen analyzer (Neutronics, Exton, PA), gas lines were filtered

with activated charcoal to remove excess ammonia and calcium chloride was used to maintain CO_2 levels below 0.05%. Animals were exposed to 250 ppm CO at a flow rate of 10 L/min into the same custom-made plexiglass chamber. A CO analyzer (Ntron model 1100, Neutronics, Exton, PA) was used to measure CO levels continuously in the chamber. CO was administered at a concentration of 250 ppm for 1 h twice daily. CO levels were monitored and recorded daily. Dams were rotated between normoxia and hyperoxia conditions, or CO + normoxia and CO + hyperoxia conditions daily to minimize oxygen toxicity to the dams and to remove potential confounders of milk production induced in the various environments. Relative humidity in the chamber was measured using a standard humidity and temperature monitor and was maintained at 45-50%. Dams and pups were given food and water *ad libitum* and maintained on a 12 h dark:light cycle. For measurement of body weight, mice pups were weighed at 24 and 48 h intervals until completion of time course. Mice were euthanized with an overdose of ketamine and xylazine followed by thoracotomy after exposure for the indicated time periods and experimental conditions.

Histological analysis. Lungs were perfused with phosphate buffered saline (PBS) with 20 mM EDTA through the right ventricle at a constant pressure of 20 cm H_2O for 3-5 min. Lungs were then intratracheally inflated with 10% formalin, fixed overnight at 4^oC, then stored in 70% ethanol prior to embedding in paraffin. Five μm sections were stained with hematoxylin and eosin. Stained sections were visualized under light microscopy and images were captured using MetaMorph version 7.0r3 software (Molecular Devices, Sunnyvale, CA) on an Eclipse TE2000-E microscope (Nikon Instruments, Melville, NY).

Morphometric analysis. To assess alveolarization, mean alveolar diameter was

determined by measurement of mean linear intercept (MLI). MLI, equal to the mean interalveolar distance, was measured by dividing the total length of a line drawn across the lung section by the number of intercepts encountered, as described [34]. Briefly, three representative lung sections for each animal were photographed at 200x magnification. A grid with parallel lines spaced at 60 μm was overlaid onto the image and the length of each cord was defined by the intercept with the alveolar walls. Fifteen non-overlapping fields for each section were examined. Metamorph image analysis software was used for morphometric analysis.

Cytospin preparation and lung inflammation. To quantify inflammatory cells, lung cells were obtained by mincing the tissue, subjecting it to proteolysis in collagenase type IV (Invitrogen, Carlsbad, CA), and straining it through a 70 μm nylon mesh (BD Falcon, San Jose, CA). The resulting pellet was treated with RBC lysis buffer (BD Biosciences, San Diego, CA), and leukocytes were enriched by spinning the cells through 40% Percoll (Sigma-Aldrich). The cell suspension was cytocentrifuged at 500 g for 5 min using a Cytospin 4 (Thermo Fisher Scientific, Waltham, MA). Lung leukocytes were stained with Diff-Quick (Dade Behring, Newark, DE) and differential counts were determined from 10,000 cells.

Bronchoalveolar inflammatory and differential cell counts. Bronchoalveolar lavage fluid (BAL) fluid was obtained through intratracheal instillation of 3 x 1 mL ice-cold PBS and filtered via a 70 μm cell strainer to exclude contamination from clustered epithelial cells. Erythrocyte contaminants were lysed using RBC Lyse (BD Biosciences, San Diego, CA). BAL fluid was centrifuged at 2000 rpm for 15 min, and supernatants

were removed and stored in -80^{o}C until further analysis. The cell pellet was resuspended in PBS, and total infiltrating cells (neutrophils and macrophages) were counted using a HEMAVET 950FS cell hemocytometer (Drew Scientific, Dallas, TX).

Immunohistochemistry and fluorescence microscopy. Paraffin blocks were sectioned at 500 μm intervals at a thickness of 5 μm. After deparaffinization, rehydration and antigen retrieval, endogenous peroxidase was blocked using a rodent serum block. Serial sections were probed with fluorophore-labeled mouse anti-α-smooth muscle actin (clone 1A4, Sigma-Aldrich), Alexa Fluor (AF)-conjugated donkey anti-goat IgG (Molecular Probes, Portland OR), rat anti-mouse F4/80 (AbD Serotec, Raleigh, NC), anti-CD11b (R&D systems, Minneapolis, MN) and rat anti-mouse Gr-1 (R&D systems, Minneapolis, MN). Slides were subsequently incubated with secondary antibody, ABC reagent (Vector Laboratories, Burlingame, CA) and diaminobenzidine (DAB). Nuclei were counterstained with 4',6-diamidino-2-phenylindole-DAPI (Molecular Probes, Portland OR) and immunofluorescence (DAPI). In addition, sections were incubated with Alexa Flour (AF)-555-conjugated goat anti-mouse JE/MCP-1 (R&D), AF633-rat anti-mouse CD68 (AbD Serotec, Raleigh, NC) or AF conjugated isotype control IgGs. To examine endogenous HO-1 staining, we used a rabbit polycolonal to rat HO-1 (StressGen; Vicoria, British Columbia, Canada). Images were visualized using an Axiovert 100M inverted fluorescent microscope (Carl Zeiss, Thornwood, NY).

Focused gene array analysis of neonatal mouse lung lysates. Lung RNA from mice exposed to normoxia, hyperoxia or episodic low-dose CO in the presence of hyperoxia were subjected to a targeted PCR array examining 84 mouse inflammatory cytokines (SA

Biosciences, Frederick, MD). Total RNA extraction was performed using the Qiagen Animal Spin protocol (Valencia, CA). Total RNA was quantified using the Nanodrop N-1000 (Agilent Biosystems, Santa Clara, CA). After verification of RNA quality and integrity, first-strand cDNA synthesis was performed on an Eppendorf Mastercycler using a Reaction Ready First-Strand cDNA Synthesis kit (SA Biosciences). The cDNA template was combined with RT^2 Real-Time SYBR Green/Rox Master Mix (SA Bioscience) and RNAse-free water. A final reaction volume of 25 μL was added to each well of PCR array. Finally, pathway-focused mRNA was amplified on a 7300 Fast Real-Time PCR system (Applied Biosystems, Foster City, CA) following the manufacturer's protocol. Genes were plotted as heat maps by hierarchical clustering using the correlation coefficient as a distance measure and the average of each cluster for cluster formation of the genes using Amap software (Bioconductor, Fred Hutchinson Cancer Research Center, Seattle, WA). Expression values are visualized with color ranging from red (high expression) over white (intermediate expression) to blue (low expression).

RNA isolation and real-time reverse transcriptase-polymerase chain reaction (RT-PCR). Quantitative RT-PCR was performed on 8 genes with increased or decreased expression following the different exposure conditions in C57BL/6J (n=10-18 samples/condition). Lung total RNA was extracted using an RNAeasy Mini kit (Qiagen, Gaithersburg, MD). First strand cDNA (500 ng) was reverse-transcribed with a High Capacity cDNA Reverse Transcription Kit (Applied Biosystems, Foster City, CA). Real time PCR was performed with an ABI PRISM 7000 sequence detection system with TaqMan Universal PCR Master Mix and Assay-on-Demand gene expression probes (Applied Biosystems). The following primers were used in the PCR reaction: IL-1β,

TNF-α, IL-10, IL-13, IL-6, CCL-2, CxCL-2 and CxCL-1. β-actin served as housekeeping gene. All primers and probe sets were purchased from Applied Biosystems. All samples were analyzed in quadruplicate. mRNA expression was normalized to β-actin level by the $2^{-\Delta\Delta Ct}$ method.

Protein extraction and cytokine expression. Whole lung samples were homogenized with lysis buffer containing 1 mM Tris-HCl, pH 7.4, 0.5M EDTA, 5M NaCl, 1% TritonX-100, 1% sodium deoxycholate and 10% SDS supplemented with protease inhibitors (Complete Protease Inhibitor Cocktail, Roche, Indianapolis, IN). Supernatants were analyzed for IL-1β, IL-6, IL-10, IL-13, KC/CXCL1, MCP-1/CCL2, TNF-α, MIP-2/CXCL2, MCP-1 protein abundance using a multiplex mouse immunoassay kit (BioRad, Hercules, CA) using the Luminex 200 System (Luminex Corporation, Autsin TX), following the manufacturer's instructions. Supernatants were analyzed in triplicate.

Flow-cytometric analysis of infiltrating leukocyte populations. Lung tissues were harvested and single cell suspensions were obtained by digestion with collagenase IV (Gibco Life Technology, Grand Island, NY) for 1 h at 25^{o}C while shaking. FACSlyse buffer (BD Bioscience, Franklin Lake, NJ) was used to lyse erythrocyte contaminants. Total lung cell counts were assessed by Hemavet hemocytometer (Drew Scientific) and reconfirmed by flow cytometry analysis using FITC-anti mouse CD45 antibody (BD Bioscience, Franklin Lakes, NJ) and flow cytometry absolute count standard beads (BD Bioscience). Viable cells were identified by the absence of DAPI (Molecular Probes, Portland OR) staining. Nonspecific antibody staining was inhibited using Fc Block (BD Bioscience). Analysis of whole lung total alveolar leukocytes was performed using APC-

anti-mouse CD11b and PE-anti-mouse Ly6G/Ly-6C (Gr-1) (both from BD Bioscience). In order to detect infiltrating alveolar macrophages, cells were purified and identified in four stages. First, the leukocyte population was gated using FITC-conjugated anti-mouse CD45. Second, infiltrating monocyte/macrophages, double positive for staining with APC-Cy7-conjugated anti-mouse F4/80^{high} and PE-conjugated anti-mouse CD11c were then positively gated. Third, cells were gated using PerCPCy5.5-conjugated anti-mouse CD11b (all from BD Bioscience). For calculation of total cell numbers in tissue, normalization to weight of tissue was performed. Data were acquired on a BD FACS Canto^{TM} flow cytometer and analyzed with FlowJo v.9.4.11 (Tree Star, Ashland, OR).

In vitro **cell culture and CO exposure.** A549 human respiratory epithelial cells were obtained from ATCC (Manassas VA). The cells were maintained in Ham's F-12K Nutrient Mixture Medium (Invitrogen, Carlsbad, CA) supplemented with 10% fetal bovine serum (HyClone, Thermo Fisher Scientific, Waltham, MA), 10 mM L-glutamine, 100 IU/mL penicillin and 100 μg/mL streptomycin. Cell culture was maintained in humidified incubators (5% CO_2, 95% air) at 37^{o}C. Cells were grown to 60-80% confluence and rendered quiescent in medium containing serum-free medium. Selected cultures were exposed to 95% O_2 or 250 ppm CO + 95% O_2 in an incubator chamber (Biospherix, Lacona, NY). Control cells were cultured in standard tissue culture conditions (95% air, 5% CO_2).

Statistical analysis. All results were expressed as mean ± SEM, with the number of experiments performed provided in the figure legends. Comparison of results between different groups with more than 2 conditions were compared using a one-way analysis of

variance (ANOVA) or Mann-Whitney U test, as appropriate, using GraphPad Prism software (LaJolla, CA). To pinpoint differences between specific groups, Newman-Keuls test was used. Values were considered significantly different when $P \leq 0.05$.

RESULTS

CO partially mitigates the effects of hyperoxia-induced lung injury on body weight and survival.

Prolonged neonatal exposure to hyperoxia adversely affected somatic growth **(Figure 1A)**. Hyperoxic exposure resulted in a significantly decreased weight at the end of the exposure period compared to air-exposed littermates. Hyperoxic mice weighed an average of 6% less at day 7, 10% less at day 10, 13% less at 2 week and 21% less at 3 week compared with normoxic mice; $p<0.05$). This was true for all experiments under hyperoxic conditions despite rotation of dams. Intermittent exposure to CO at 250 ppm during hyperoxic exposure tended to increase body weight, with the difference reaching statistical significance on day 21 ($p <0.05$). We constructed survival curves for the four groups **(Figure 1B)**. In this set of experiments, 72% of neonatal mice exposed to hyperoxia survived, with the majority of deaths occurring between 3 and 7 days of life. Administration of 250 ppm CO with 75% O_2 treatment increased survival to 89%, with the results approaching statistical significance ($p=0.07$, Log-rank Mantel Cox test). Normoxia-exposed pups did not show signs of illness and all survived the first 3 weeks after birth.

CO mitigates hypoalveolarization in hyperoxia exposed neonatal mice.

Premature mice are born at the saccular stage of lung development. Sacculi are transformed into alveoli within the first 2 weeks after birth by septal thinning and secondary septation. Histological analysis in untreated postnatal 3-day (p3) hyperoxia-

exposed mice revealed markedly underdeveloped lungs at the saccular stage of development **(Figure 1C)**. After 7-21 days of exposure, hyperoxic mice exhibited a significant structural delay in alveolar development compared to age-matched normoxia-exposed counterparts. Alveolar simplification in hyperoxia-exposed mice was accompanied by increased collagen deposition in the alveolar walls (not shown). Lungs of mice intermittently exposed to 250 ppm CO for 1 hr twice daily were structurally similar to normoxic control mice**.** Mice exposed to 75% oxygen and CO showed partial mitigation of hypoalveolarization compared with mice exposed to hyperoxia alone. To quantitate these differences, morphometric measurements of the mean linear intercept (MLI) were compared between study groups **(Figure 1D)**. Compared to air-exposed mice, mean MLI for hyperoxia-exposed mice was significantly increased at 10, 14 and 21 days of exposure. When neonatal pups were exposed to 250 ppm CO in the setting of hyperoxia, we observed a significant decrease in MLI on day 10 of exposure in comparison with hyperoxia-exposed mice ($P < 0.001$). Similar decreases in MLI were observed at other timepoints, though the differences were not statistically significant. Together, these data demonstrate that chronic neonatal hyperoxic exposure results in markedly decreased alveolarization, which is mitigated by intermittent CO treatment.

CO suppresses hyperoxia-induced lung leukocyte recruitment.

We hypothesize that CO mitigates the effect of hyperoxia on the developing lung via an anti-inflammatory mechanism. To quantify inflammatory cells, cells were obtained from minced lung tissue, enriched for leukocytes using a 40% Percoll gradient, cytocentrifuged and stained with Diff-Quick. Hyerpoxic exposure increased the number of monocyte/macrophages on days 7, 10 and 14 of exposure, and these changes were

mitigated by CO treatment **(Supplemental Figure S1A; data for day for 14 are shown in Figure 2A)**. Similar effects were observed for lung neutrophils **(Figures 2A, S1A).**

We also examined the inflammatory cell response in the BAL fluid **(Figures 2B, S1B)**. The number of BAL polymorphonuclear cells and monocyte/macrophages was significantly increased in hyperoxia-exposed pups at 7 days, reaching a peak at 14 days of hyperoxia exposure. Macrophages from hyperoxia-exposed mice showed a larger, foamy appearance, indicative of activation (data not shown), concordant with their previously reported apperance [19]. CO treatment decreased the number of neutrophils and monocyte/macrophages in the BAL fluid. Together, the above findings indicate that CO treatment may confer significant protection against hyperoxia-induced pulmonary inflammation in developing lungs.

Using flow cytometry to quantify leukocyte infiltration, we isolated whole lungs from neonatal pups after 7-21 days of exposure to air, air + CO, hyperoxia and hyperoxia + CO, as described in the Materials and Methods. We employed antibodies against Gr-1 (Ly6C/G) and CD45 to identify infiltrating neutrophils ($CD45^{high}$ $Gr\text{-}1^{+}$) **(Figures, S1C, D)**. Following hyperoxic exposure, the number of $CD45^{high}$ $Gr\text{-}1^{+}$ cells increased compared to normoxic littermates (P <0.001). Exogenous CO decreased infiltrating neutrophils at all time points compared to hyperoxia-exposed mice.

Immunofluorescent staining confirmed the localization of CD11b-positive (red), F4/80-positive (green; colocalization, yellow) macrophages in the alveolar septae and alveolar spaces of lungs from hyperoxia-exposed mice **(Figure 2C)**. Intermittent CO exposure during hyperoxia significantly decreased macrophage infiltration into the

alveolar space. Hyperoxic exposure also induced a significant increase in infiltrating Gr-1-positive neutrophils compared with normoxic control littermates. Exogenous application of CO to hyperoxic neonatal mice attenuated the infiltration of neutrophils, as it did for macrophages.

To further understand the role of HO-1/CO in neonatal lung injury, we measured lung HO-1 mRNA expression in hyperoxia-exposed mice. Hyperoxia significantly increases HO-1 expression **(Figure 3A)**. HO-1 null mice exposed to hyperoxia showed exaggerated alveolar simplification compared to wild-ype mice **(Figure 3B)**. Exaggerated hypoalveolarization was confirmed by mean linear intercept measurements **(Figure 3C)**. Immunohistochemistry showed that hyperoxia increases HO-1 expression in alveolar macrophages **(Figure 3D)**. As expected, HO-1 expression was not detectable in hyperoxia-exposed HO-1 null mice. Finally, compared to wild-type hyperoxia-exposed mice, HO-1 null mice showed a significant increase in BAL macrophages. Together, these data demonstrate that HO-1 deficiency is sufficient to exacerbate the effects of hyperoxia on the newborn lung.

To characterize the inflammatory (monocyte/macrophage) response to hyperoxic exposure and CO treatment, neonatal pups were exposed hyperoxia and treated with intermittent CO for up to 21 days. More than 90% of the isolated whole lung inflammatory cells were CD45-positive cells. By day 7, the percentage of cells expressing the monocyte/macrophage cell surface markers $F4/80^+$ and $CD11c^+$ [19] significantly increased under hyperoxic exposure. The total number of $F4/80^+$ and $CD11c^+$ double positive cells peaked at 10-14 days of hyperoxic exposure **(Figures 4A, 4C S2A)**. CO treatment tended to decrease the accumulation of cells infiltrating in the

hyperoxic exposed lungs. On the other hand, hyperoxia-exposed HO-1 null mice showed increased F4/80+ and CD11c+ double positive macrophages.

Recent studies suggest that, unlike resident alveolar macrophages, freshly recruited macrophages express low levels of CD11c and high levels of CD11b, which is required for their successful migration to inflamed tissues [35, 36]. We therefore analyzed CD45-positive lung cells for both CD11c and CD11b **(Figure 4B, 4C)**. We found three distinct subpopulations of cells. $CD11c^{+}$ $CD11b^{low}$ cells (population A) increased early during hyperoxic exposure. Backgating of these cells showed them to be small, low complexity cells, probably lymphocytes **(Figure S2B)**. $CD11c^{high}$ $CD11b^{high}$ cells, presumably representing exudative macrophages (population B), increased significantly early during hyperoxic exposure. $CD11c^{low}$ $CD11b^{high}$ cells (population C), which presumably represent a transitional population of inflammatory monocytes, were also increased throughout the hyperoxic exposure period. Both $CD11b^{high}$ populations backgated to the large, high complexity region typical of macrophages **(Figure S2C)**. Administration of CO dramatically reduced the number of cells in populations A, B and C **(Figure 4B, 4C).** Interestingly, lungs of air/CO-exposed mice also showed smaller but significant increases in population C cells. Finally, compared to hyperoxia-exposed wild-type mice, lungs from HO-1 null mice showed increased lung macrophages, in particular $CD11c^{low}$ $CD11b^{high}$ cells.

Exogenous CO administration regulates the expression of pro- and anti-inflammatory cytokines/chemokine under hyperoxic conditions.

To determine the cytokines responsible for hyperoxia-induced macrophage/monocyte

lung infiltration, we performed a gene array focusing inflammatory markers. Lung mRNA from day 3 normoxia-exposed mice, day 14 normoxia-exposed mice, day 14 normoxia-exposed mice, day 14 hyperoxia-exposed mice and day 14 hyperoxia + CO exposed mice was subjected to a targeted PCR array examining mouse inflammatory cytokines **(Figure 5).** Hierarchical clustering revealed a group of 12 genes, which were downregulated during normal development, increased by hyperoxic exposure, and decreased by concomitant CO exposure. This group of genes included *Ccl2, Cxcl1* and *Il1b*. We therefore examined the mRNA and protein levels of these and other cytokines by qPCR and multiplex immune assay, respectively. Lung samples from 14 days post-exposure were studied **(Figure 6A-H)**. Expression of mRNAs encoding the pro-inflammatory cytokines IL-1β, TNF-α, IL-6, the monocyte chemoattractant CCL-2, and the neutrophil chemoattractants CXCL1 and CXCL2 were significantly greater in the lungs of hyperoxia-treated mice compared with lungs from air-exposed mice**.** Similar increases were observed on the protein level. CO treatment under hyperoxia effectively suppressed all pro-inflammatory markers measured.

In addition to examining pro-inflammatory cytokines/chemokines, experiments were also performed to determine the expression levels of two "anti-inflammatory" cytokines, IL-10 and IL-13 **(Figure 6G, H)**. IL-10 and IL-13 were decreased in the lungs of hyperoxia-treated mice. Concordantly, the protein levels of both cytokines were also decreased after hyperoxic exposure. CO tended to increase IL-10 and significantly increased IL-13 mRNA and protein levels during both air and hyperoxic exposure.

CCL2 is required for hyperoxia-induced macrophage/monocyte infiltration and hypoalveolarization.

Based on the strong induction of CCL2 demonstrated by our microarray data, we chose to evaluate in depth the functional consequences of its expression in the development of BPD. CCL2 is a critical monocyte chemoattractant protein, also called MCP-1 (or JE in humans), which binds to its cognate ligand CCR2 expressed on monophagocytes, recruiting them to sites of inflammation. To further characterize hyperoxia-induced CCL2 expression, we performed immunofluorescence staining of lung sections for CCL2 and CD68, a macrophage marker **(Figure 7A).** Hyperoxia increased the number of CD68-positive cells, indicating macrophage infiltration. CCL2 expression was also increased, primarily in CD68-negative cells of the airway and alveolar epithelium. CO administration decreased hyperoxia-induced CCL2 expression. We tested whether hyperoxia increases respiratory epithelial CCL2 expression *in vitro*. A549 cells were cultured in an incubator chamber containing a normoxic or hyperoxic atmosphere in the absence or presence of 250 ppm CO **(Figure 7B)**. Hyperoxia caused a rapid increase in CCL2 mRNA expression, which was attenuated by CO treatment. Taken together, these data suggest that CO attenuates hyperoxia-induced lung inflammation by decreasing respiratory epithelial cell CCL2 expression.

To test the hypothesis that CCL2 is required for hyperoxia-induced macrophage/monocyte infiltration and hypoalveolarization, wild-type and CCL2 null mice were exposed to air or hyperoxia, as described above. As shown previously, hyperoxia blocked alveolar development, as evidenced by an increase in mean linear intercept **(Figure 8A, 8B).** In contrast, CCL2 null mice showed no increase in mean chord length. CCL2 null mice showed reduced BAL neutrophils and a trend toward reduced BAL monocytes **(Figure 8C, 8D).** In CCL2 null mice exposed to hyperoxia,

flow cytometry showed a reduction in $F4/80^{+}$ $CD11c^{+}$ macrophages, $CD11c^{high}$ $CD11b^{high}$ (population B) exudative macrophages, and $CD11c^{low}$ $CD11b^{high}$ (population C) inflammatory monocytes **(Figure 9A-D).**

DISCUSSION

In this report, we show for the first time that: 1) brief episodic exposure to low-dose CO significantly mitigates the deleterious effects of hyperoxia on alveolar development; 2) HO-1 deficiency exacerbates hyperoxia-induced lung injury; and 3) CCL2 is required for hyperoxia-induced alveolar simplification. Taken together, these studies indicate that, in hyperoxia-exposed neonatal mice, inhalation of the HO-1 product CO suppresses CCL2-dependent inflammatory cell trafficking, pro-inflammatory cytokine expression, and alveolar simplification.

Previous studies have examined the role of neutrophils and macrophages in the pathogenesis of neonatal hyperoxic lung injury. In neonatal rats, hyperoxia induces neutrophil influx and hypoalveolarization, which is attenuated by neutralizing antibodies against the neutrophil chemoattractants CXCL1[9] or CXCL2 [10]. Neutrophilic inflammation in hyperoxia is also prevented by a selective chemical antagonist of CXCR2 [11]. Neutralizing antibodies against MCP-1/CCL2, a monocyte chemoattractant, also decrease lung hypoalveolarization, as well as lung macrophage and neutrophil counts, in hyperoxia-exposed rats [37].

In our study, we extend these observations by demonstrating that hyperoxia induces the accumulation of different F4/80-positive macrophage subsets into the lung, specifically $CD11c^{low}$ $CD11b^{high}$ and $CD11c^{high}$ $CD11b^{high}$ cells. Previously, it was shown that, during influenza infection [38] and bleomycin exposure [39], $CD11c^{-}$ $CD11b^{+}$ inflammatory monocytes are recruited to the lung and develop into a $CD11c^{high}$ $CD11b^{+}$

activated macrophage population known as exudative macrophages. On this basis, we speculate that the $CD11c^{low}$ $CD11b^{high}$ cells (our population C) represent inflammatory monocytes, and that $CD11c^{high}$ $CD11b^{high}$ cells (our population B) represent exudative macrophages, a major source of inflammatory cytokines and chemokines in the lung.

In addition to lung inflammation, hyperoxia increased the size of airspaces in the lung, indicating hypoalveolarization of the developing lung. Murine alveolar development begins on postnatal day 3, and saccular division is completed by the 14^{th} postnatal day [30]. This result is in agreement with previous work showing that exposure of the perinatal lung to supraphysiological levels of oxygen confers profound hypoalveolarization [40, 41], and are consistent with the notion that oxygen exposure may be a contributing factor in the pathogenesis of BPD. .

Next, we examined the effects of one-hour, twice per day CO treatment on lung development and inflammation. CO treatment during hyperoxia significantly reduced hyperoxia-induced hypoalveolarization. In addition, CO decreased the number of exudative macrophages and inflammatory monocytes in the lung. Conversely, compared to wild-type mice, HO-1 null mice exposed to hyperoxia showed increased alveolar simplification and lung infiltration with CD11b(+) cells. Overall, these data are concordant with the hypothesis that CO protects against lung injury, and is facilitative for alveolar development, even under hyperoxic stress conditions. Unexpectedly, we found that CO treatment tended to increase the number of lung inflammatory cells in normoxia-treated mice. This may relate to CO's anti-apoptotic effects [42, 43], which may prevent normal clearance of leukocytes from the lung.

In our previous work, we demonstrated that HO-1-deficient mice have significantly decreased survival upon ischemic lung injury, and that CO can rescue these mice [44]. Recent reports have demonstrated the cytoprotective role of HO-1/CO in *in vivo* models of acute lung injury. Intravenous hemoglobin, a potent inducer of HO-1 (a major heme degradative enzyme), prevented lung injury in a rat model of sepsis [45]. In a separate report, intratracheal administration of hemoglobin protected rats from hyperoxia-induced lung injury[46]. It was subsequently shown that adenoviral gene transfer of HO-1 conferred protection against hyperoxic-induced lung injury[47]. Inhaled CO at low concentrations (50-500 ppm) protected against hyperoxia-induced lung injury in adult rats [22]. Recently, the effects of HO-1 overexpression and CO administration (250 ppm for 1 h daily) were examined in a model of neonatal hyperoxic lung injury [16]. HO-1 overexpression and CO each attenuated hyperoxia-induced arterial remodeling, right ventricular hypertrophy pulmonary edema and hemosiderosis, while increasing blood vessel number. HO-1 overexpression and CO administration had modest effects on alveolar architecture and BAL , but the mechanisms driving inflammatory changes were not further explored.

To determine the mechanism of hyperoxia- and CO-mediated changes in lung inflammation, we examined the mRNA and protein levels of candidate cytokines by gene array, followed by qPCR and multiplex immune assay. Increases in lung leukocyte subpopulations with hyperoxia and mitigation of this response by CO were reflected in lung cytokine mRNA and protein levels. Lungs of hyperoxia-exposed mice showed increased levels of CCL2 mRNA and protein, which were reduced by CO treatment. We found a similar pattern for the type I cytokines IL-1β, TNF-α, CXCL1, and CXCL2. CCL2 is a chemoattractant for exudative macrophages [38]. We therefore tested the hypothesis that respiratory epithelial cells produce CCL2 in response to hyperoxic

exposure, leading to monocyte and macrophage infiltration of the lung. First, we found that hyperoxia increased epithelial CCL2 protein expression *in vivo*, and that CO attenuated this response. Second, we exposed A549 cells to hyperoxia *in vitro*. We found that hyperoxia increased A549 cell CCL2 mRNA expression, and that expression was inhibited by CO treatment. Finally, we exposed CCL2 null mice to hyperoxia *in vivo,* and found that these mice were protected from alveolar simplification. In addition, the lungs of hyperoxia-exposed CCL2 null mice showed significantly reduced exudative macrophages and inflammatory monocytes, reproducing the effects of exogenous CO. Taken together, these data are consistent with the notion that inhalation of the HO-1 product CO suppresses CCL2-dependent inflammatory cell trafficking, pro-inflammatory cytokine expression and alveolar simplification.

The precise mechanisms by which inflammation inhibits alveolar development are not completely known. Using a fetal lung explant model, it was recently shown that IL-1β-producing tissue macrophages mediate the inflammatory response to lipopolysaccharide and that macrophage activation inhibits airway morphogenesis [48]. Conversely, macrophage depletion protected airway branching. Further, tissue-specific macrophage activation induced by overexpression of IκB kinase inhibited lung development *in vivo.* We propose that CO protects against hyperoxia-induced alveolar simplification by blocking macrophage infiltration and activation. It is also conceivable that hyperoxia retards the growth of blood vessels in the lung needed for alveolar development [13, 49, 50], and that CO promotes angiogenesis [51, 52].

In summary, we have provided a detailed *in vivo* analysis of lung inflammation and development after hyperoxic exposure in neonatal mice. Our studies demonstrate a direct link between CO, the CCL2-dependent control of leukocyte migration into

hyperoxic lung tissue, and alveolar growth. Inhibition of inflammatory cell infiltration by either CO or CCL2 gene deletion was associated with the attenuated alveolar simplification. Improved understanding of the mechanisms regulating macrophage recruitment into the developing lung could lead to new insights into the pathogenesis of BPD. Finally, these data suggest that additional studies exploring low dose CO as a possible therapeutic option in neonatal lung injury are warranted.

FIGURES

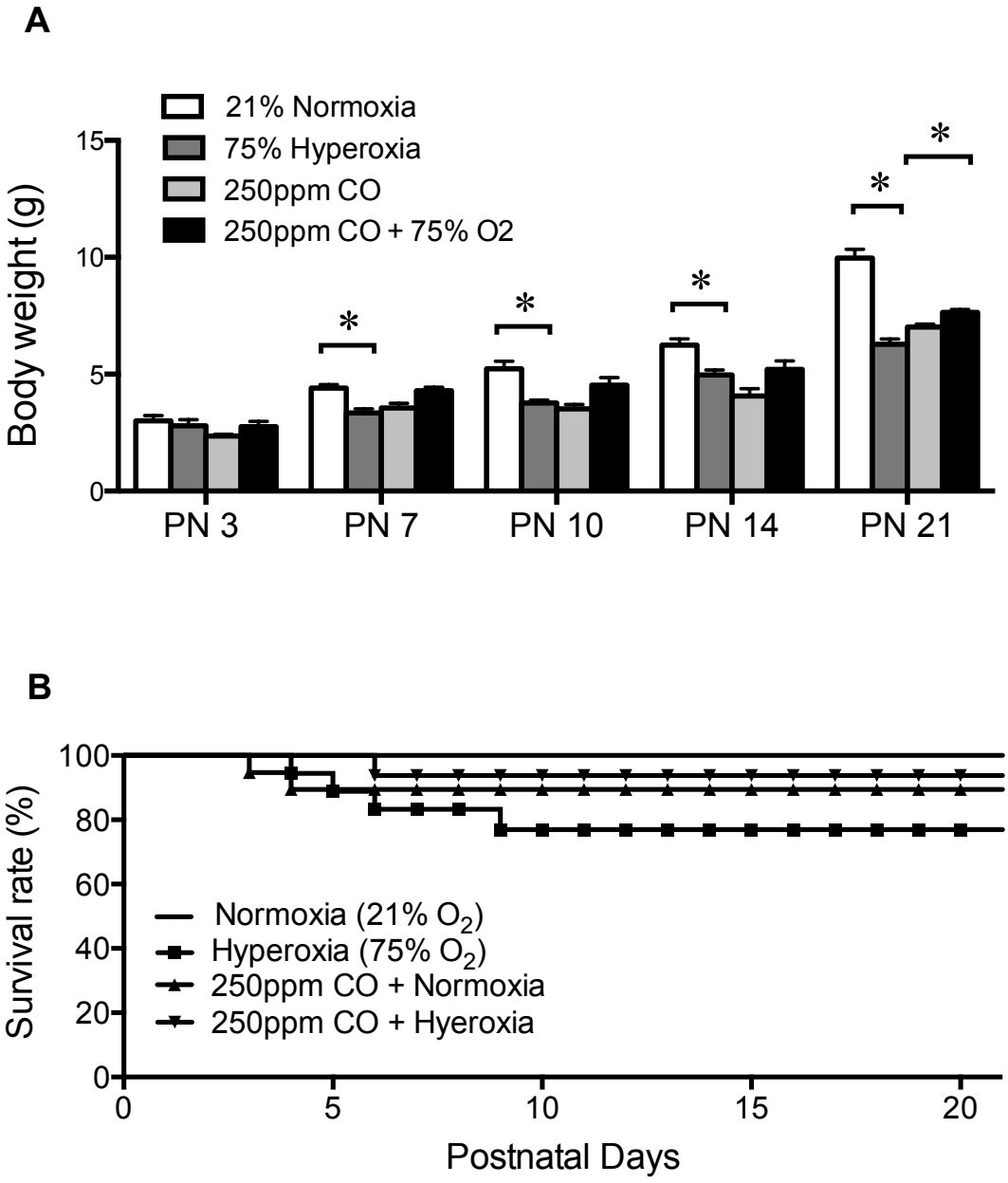
A
21% Normoxia
75% Hyperoxia
250ppm CO
250ppm CO + 75% O2
Body weight (g)
15
10
5
0
*
*
*
*
*
PN 3
PN 7
PN 10
PN 14
PN 21
B
Survival rate (%)
100
80
60
40
20
0
Normoxia (21% O2)
Hyperoxia (75% O2)
250ppm CO + Normoxia
250ppm CO + Hyeroxia
0
5
10
15
20
Postnatal Days

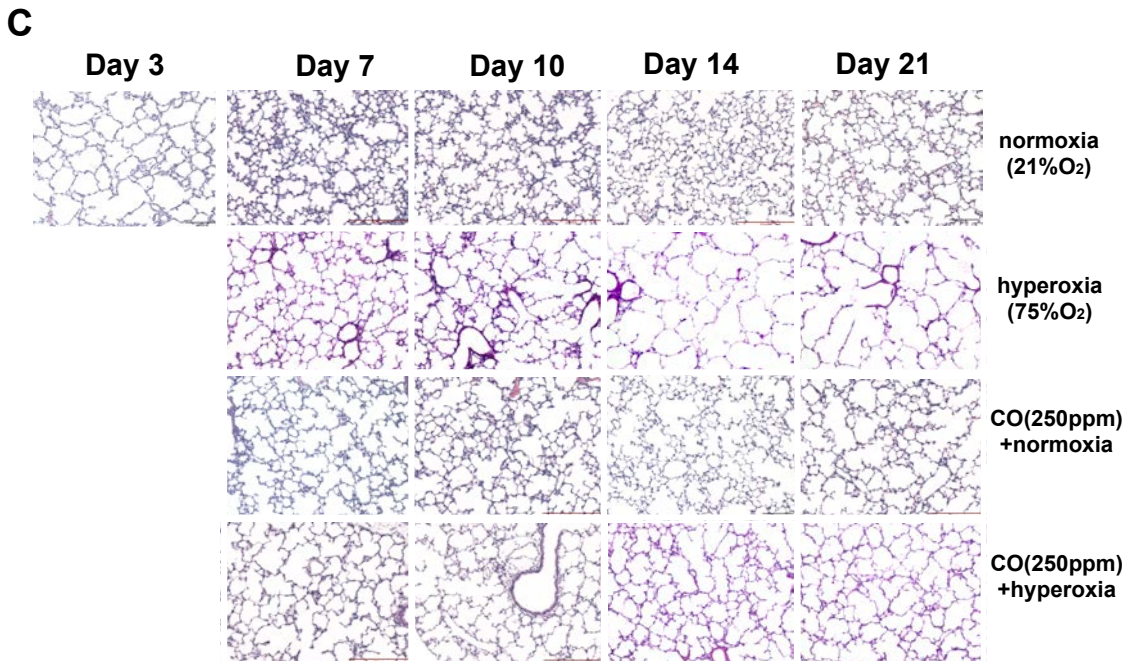
C
Day 3
Day 7
Day 10
Day 14
Day 21
normoxia (21%O2)
hyperoxia (75%O2)
CO(250ppm) +normoxia
CO(250ppm) +hyperoxia

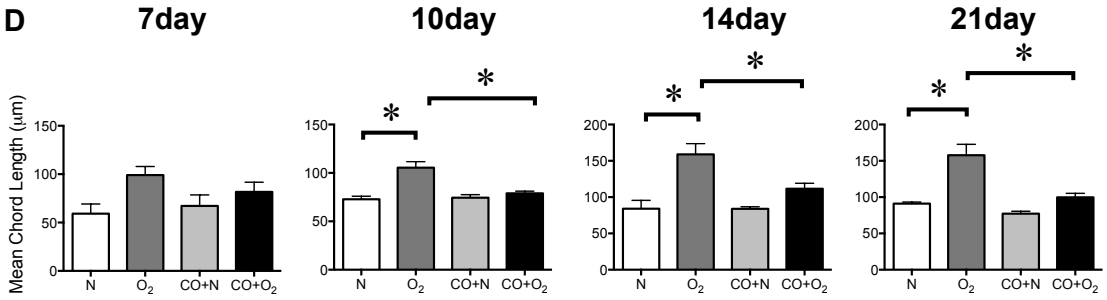
D
7day
10day
14day
21day
Mean Chord Length (μm)
N
O2
CO+N
CO+O2
*

FIGURE II.1: LOW INTERMITTENT DOSE CO PARTIALLY MITIGATES THE EFFECTS OF HYPEROXIA ON BODY WEIGHT, SURVIVAL AND ALVEOLAR ARREST IN NEONATAL MICE.

(A) Group mean body weight at 3, 7 10 14 and 21 days of life under conditions of normoxia (n=167), hyperoxia (n=106), CO+normoxia (n=52) and CO+hyperoxia (n=64). Hyperoxic exposure decreased body weight compared to normoxia. On day 21, mice of the hyperoxia+CO group were significantly larger than mice of the hyperoxia group (*$p<0.05$, ANOVA). (B) Survival curves are plotted for all experimental groups as determined using the Kaplan-Meyer method. Compared to the hyperoxia group, there was a trend towards increased survival in the CO+hyperoxia group (all groups n=21; hyperoxia survival, 76.9%; hyperoxia+CO survival, 93.7%, Log rank test p=0.072). (C) Representative images of hematoxylin and eosin stained lungs of neonatal mice exposed to normoxia (21% oxygen), hyperoxia (75% oxygen), intermittent exposure to 250 ppm carbon monoxide plus compressed air for 1 hr twice daily (normoxia+CO) or 75% oxygen and 250 ppm CO for 1 hr twice daily (hyperoxia+CO). Compared to air-exposed mice, hyperoxia-exposed mice demonstrated increased alveolar size indicative of alveolar development arrest. CO-treated mice exposed to hyperoxia showed attenuated alveolar simplification compared to hyperoxia-exposed mice. CO-treated mice exposed to normoxia showed similar alveolar architecture as normoxia-treated mice. Solid bar scale represents 200 μm and all panels are (200x). (D). Corresponding group mean linear intercepts (MLIs) of all groups. Data are reported as mean±SEM. N =17-24 per group, *different from hyperoxia, $P<0.05$. All data were assessed by one-way ANOVA.

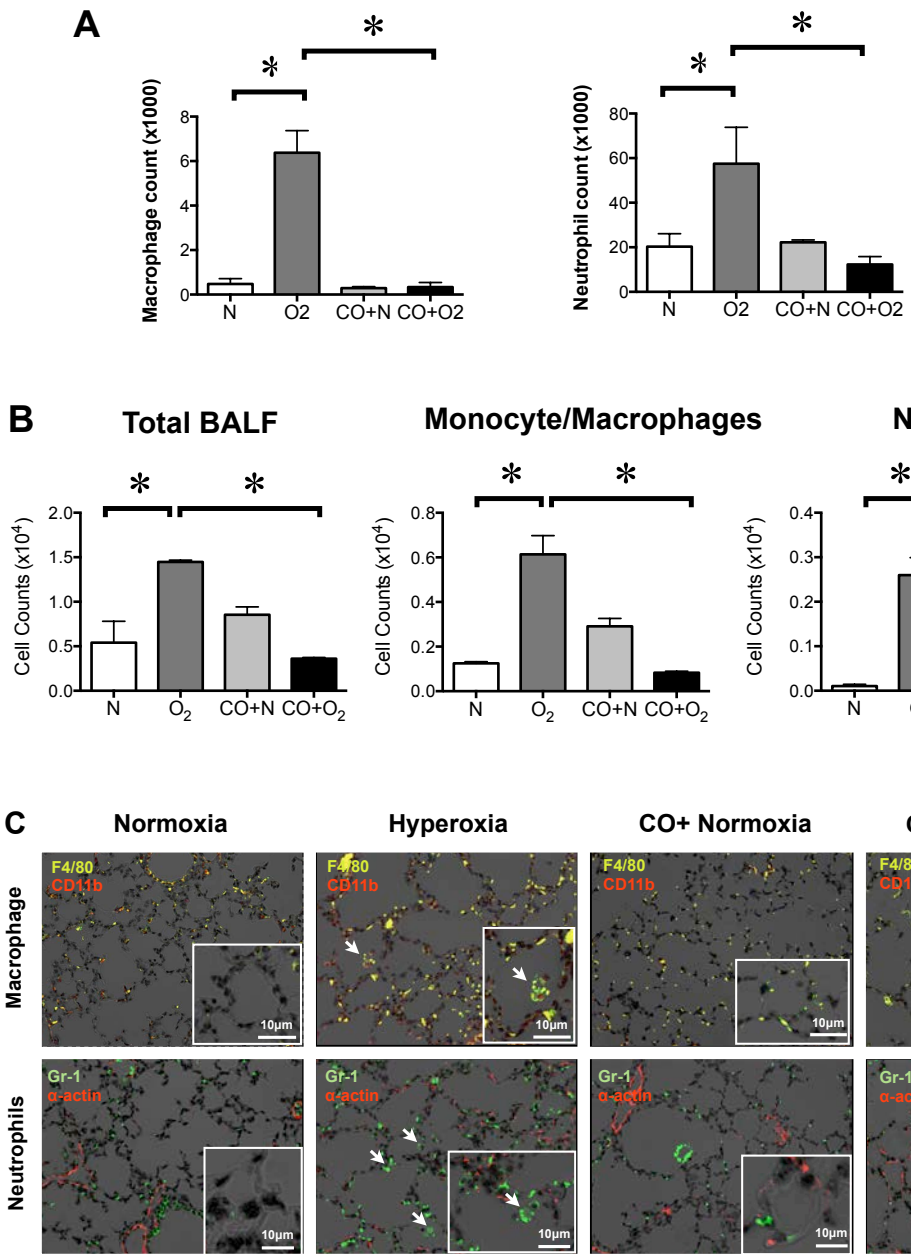
A
Macrophage count (x1000)
Neutrophil count (x1000)
N
O2
CO+N
CO+O2
B
Total BALF
Monocyte/Macrophages
Neutrophils
Cell Counts (x10⁴)
N
O2
CO+N
CO+O2
C
Normoxia
Hyperoxia
CO+ Normoxia
CO + Hyperoxia
Macrophage
Neutrophils
F4/80
CD11b
Gr-1
α-actin
10μm

FIGURE II.2: EPISODIC CO TREATMENT SUPPRESSES LEUKOCYTE TRAFFICKING TO THE LUNGS OF HYPEROXIA-EXPOSED NEONATAL MICE.

(A). Lungs were digested and cytospins were stained with Diff-Quik. Cell counts of monocyte/macrophages (left) and neutrophils (right) are shown (mean±SEM, n= 3-8 per group, *$p<0.05$, ANOVA). (B) Bronchoalveolar lavage fluid (BALF) from 17 day-old pups exposed to normoxia or hyperoxia in the absence or presence of CO for 14 days. Total BALF cells (left), monocyte/macrophages (middle) and neutrophils (right) were measured by Hemavet. N = 12-17 per group, *$p<0.05$, ANOVA). (C) Immunofluorescent stains of 14-day lung sections from normoxia- hyperoxia- CO+normoxia- and CO+hyperoxia-exposed mice. Macrophage staining panels include F4/80 (green) and CD11b (red). Colocalization (yellow) indicates CD11b-positive macrophages (arrows). Neutrophil panels show Gr-1 (green, arrows) and α-actin (red). Nuclei were counterstained with DAPI (black). Original magnification is 200X, scale bar = 10 μm. Insets show high magnification views (400x).

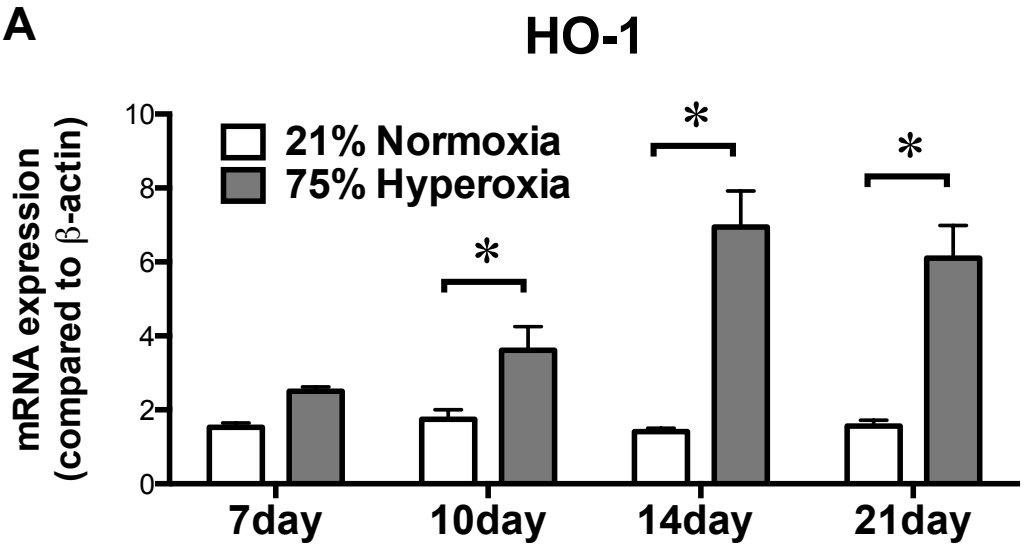
A
HO-1
mRNA expression
(compared to β-actin)
10
8
6
4
2
0
21% Normoxia
75% Hyperoxia
*
*
*
7day
10day
14day
21day

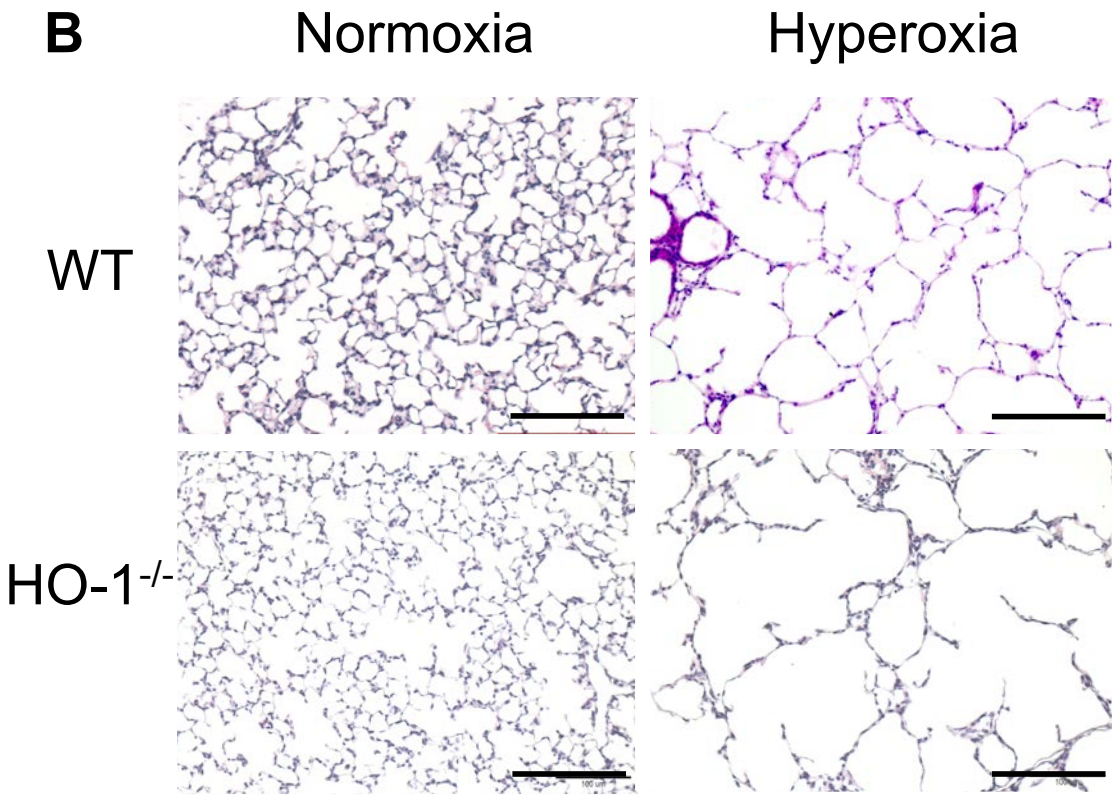
B
Normoxia
Hyperoxia
WT
HO-1-/-

c

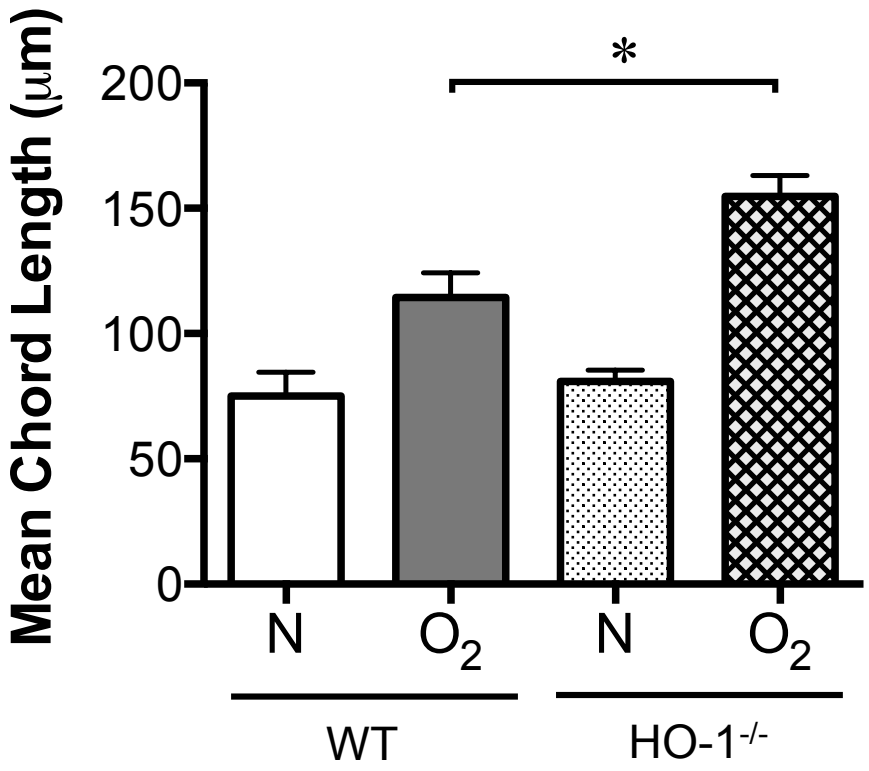

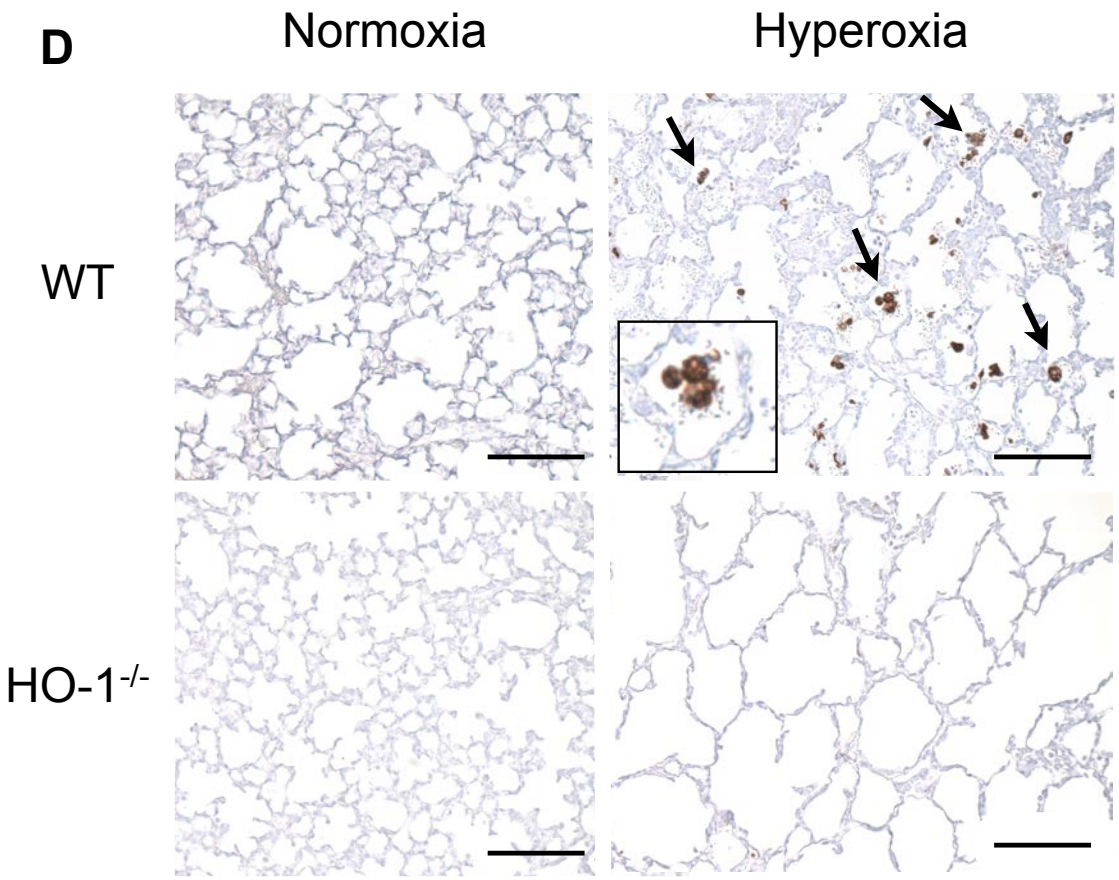
D
Normoxia
Hyperoxia
WT
HO-1-/-

E

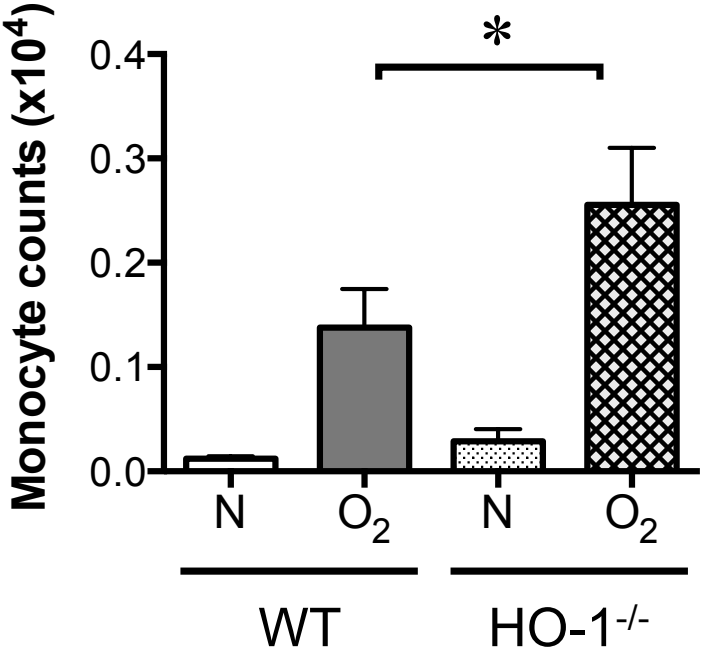
Monocyte counts (x10^4)
0.4
0.3
0.2
0.1
0.0
*
N
O2
N
O2
WT
HO-1-/-

F

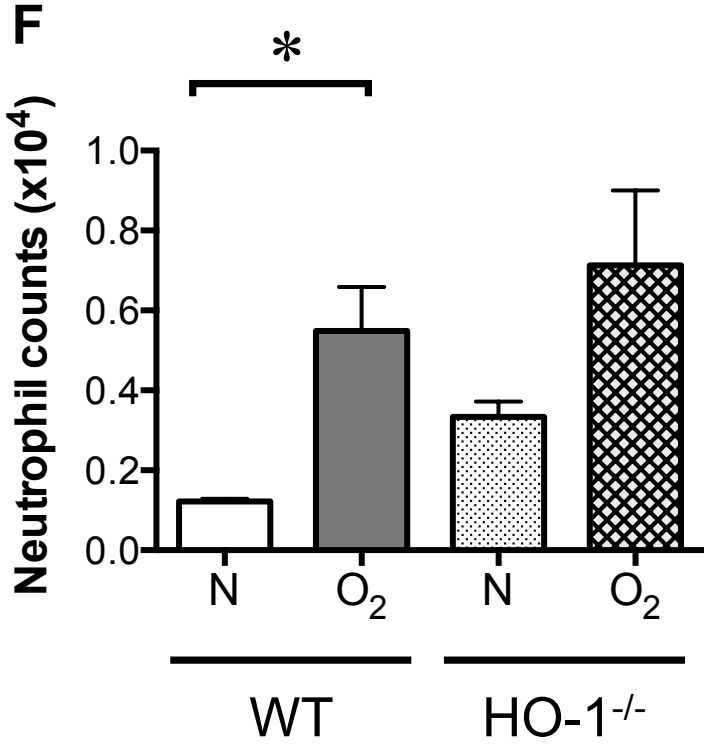
Neutrophil counts (x10^4)
1.0
0.8
0.6
0.4
0.2
0.0
*
N
O2
N
O2
WT
HO-1-/-

FIGURE II.3: HO-1 KNOCKOUT EXACERBATES HYPOALVEOLARIZATION AND INCREASES LEUKOCYTE INFILTRATION IN HYPEROXIA-EXPOSED NEONATAL MICE.

(A) Whole lung HO-1 mRNA expression from wild-type mice exposed to either normoxia (n= 20-26 mice per group) or hyperoxia (n = 19-23 mice per group) for up to 21 days. Hyperoxic exposure increased mRNA expression, as measured by qPCR (*p<0.05, ANOVA). (B) Three-day-old wild-type or heme oxygenase-1 null mice were exposed to air or 75% oxygen for 14 days. As previously, hyperoxia-exposed wild-type mice showed alveolar arrest with large airspaces. Hyperoxia-exposed HO-1 null mice showed exaggerated alveolar simplification compared to wild-type mice. (C) Group mean chord length data (n = 4-9 per group, *p<0.05, ANOVA). (D) Hyperoxia-induced HO-1 expression is observed in lung alveolar macrophages (arrows). Immunohistochemistry was performed with an antibody against murine HO-1 (scale bar = 100 μm). (E-F). Hyperoxia-induced inflammatory cell influx in neonatal mouse lungs is exacerbated by HO-1 deletion. BALF monocytes (E) and neutrophils (F) were counted 14 days after exposure to room air (21% O_2) or hyperoxia (75% O_2). Compared to wild-type mice, HO-1 null mice showed a significant increase in macrophages and a trend towards increased neutrophils (n = 4-7 mice per group, mean±SEM, *different from hyperoxia-exposed group, P <0.05, ANOVA).

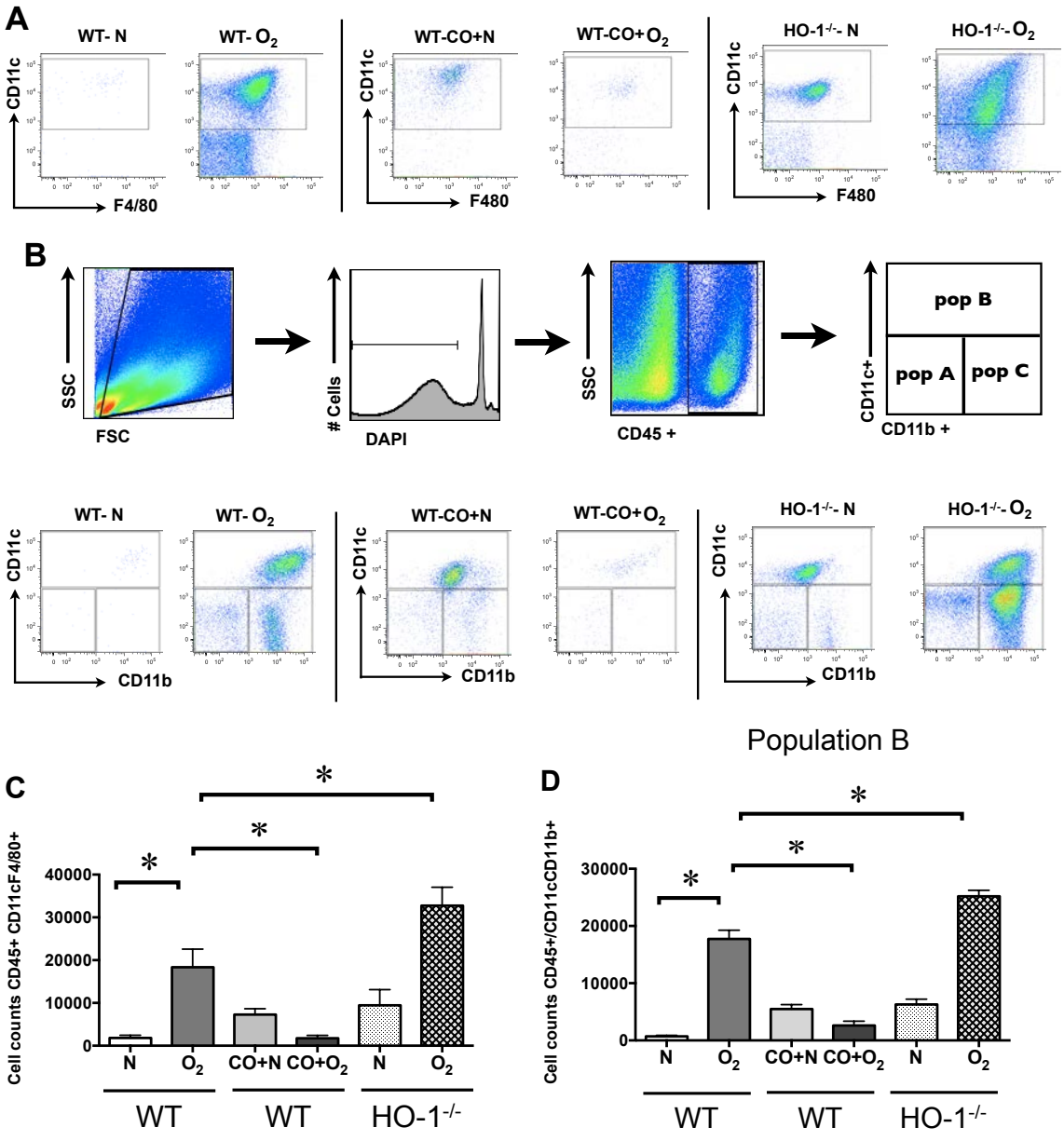
A
WT- N
WT- O2
WT-CO+N
WT-CO+O2
HO-1-/- N
HO-1-/- O2
CD11c
F4/80
F480
B
SSC
FSC
Cells
DAPI
CD45 +
pop B
pop A
pop C
CD11c+
CD11b +
CD11b
C
Cell counts CD45+ CD11cF4/80+
40000
30000
20000
10000
0
N
O2
CO+N
CO+O2
WT
HO-1-/-
Population B
D
Cell counts CD45+/CD11cCD11b+

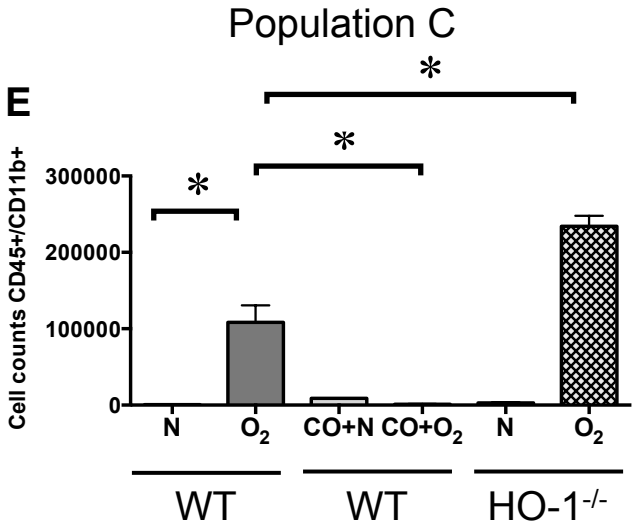

FIGURE II.4: HYPEROXIC EXPOSURE INDUCES ALVEOLAR MONOCYTE/MACROPHAGE INFILTRATION INTO NEONATAL LUNGS THAT IS AMELIORATED BY CO INDUCED TREATMENT.

Representative flow cytometric scattergrams of monocyte/macrophage subpopulations within the lungs of wild-type and HO-1 null mice exposed to normoxia and hyperoxia for 14 days. Wild-type mice were also exposed to normoxia+CO or hyperoxia+CO. Each dot plot is representative of four independent experiments). (A) CD45+, CD11c+, F4/80+ macrophages. (B) Gating scheme used in subsequent flow cytometric analysis. Whole lung live CD45+ cells were analyzed for expression of CD11c and CD11b. (C-E) Comparison of cell counts for F4/80 and CD11c double positive macrophages (panel C), $CD11c^{high}$ $CD11b^{high}$ exudative macrophages (subpopulation B, panel D) and $CD11c^{low}CD11b^{high}$ inflammatory monocytes (subpopulation C, panel E). Hyperoxia increased the trafficking of macrophage subpopulations into the neonatal lung and CO treatment attenuated macrophage recruitment. $HO\text{-}1^{-/-}$ mice showed increases lung macrophages. N = 4-10 per group, mean±SEM, *compared to hyperoxia alone, $P < 0.05$, ANOVA.

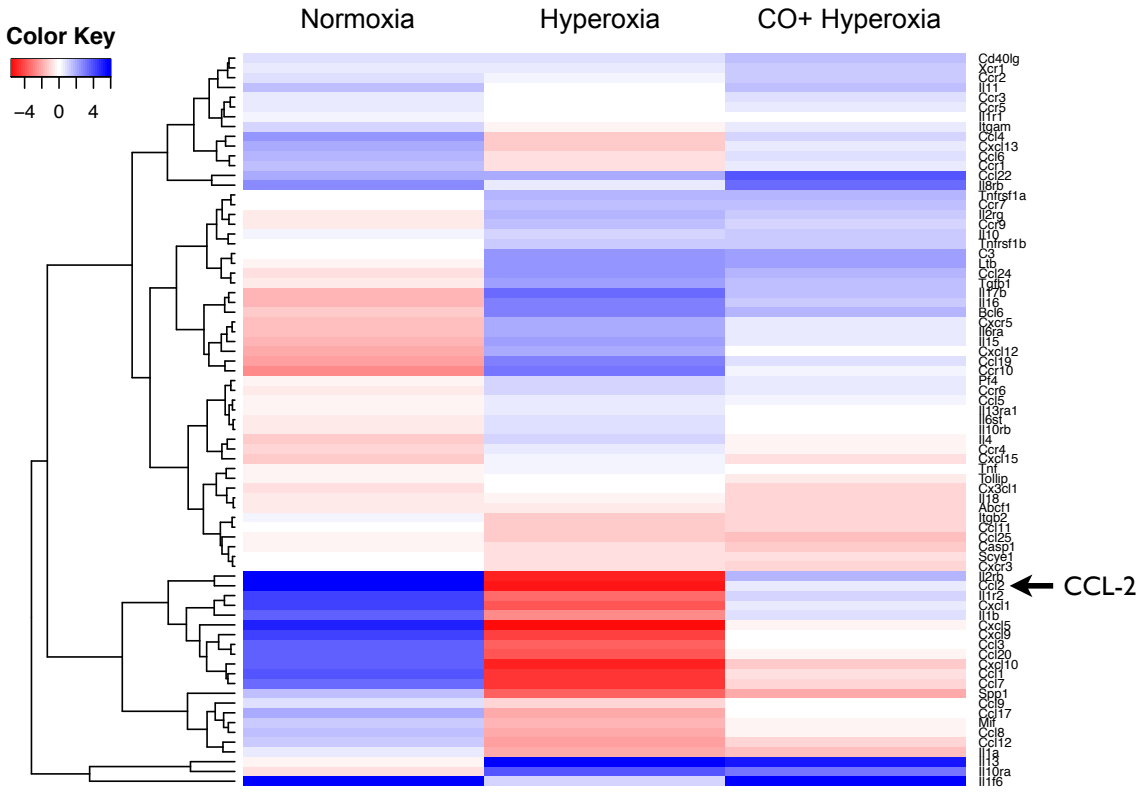

FIGURE II.5: HIERARCHICAL CLUSTERING DIAGRAM OF DIFFERENTIAL INFLAMMATORY GENE EXPRESSION IN NEONATAL MICE LUNGS ON 14DAYS POST HYPEROXIC-INDUCED LUNG INJURY.

Gene expression was measured by focused mRNA array and analyzed by hierarchical clustering and plotted on a heat map using R software. Each lane represents the expression profile of 84 unique probe sets. Lane 1 compares gene expression from two P3 normoxia and two 14 day normoxia-exposed mice. Lane 2 compares gene expression from two P3 normoxia and two P17 hyperoxia-exposed mice. Lane 3 compares two P3 normoxia and two P17 hyperoxia+CO mice. Red and blue colors indicate up- and downregulated expression levels, respectively. White color indicates no change in

expression level. The bracket indicates a group of genes that were downregulated with development (lane 1), increased with hyperoxic exposure (lane 2) and suppressed by CO treatment (lane 3).

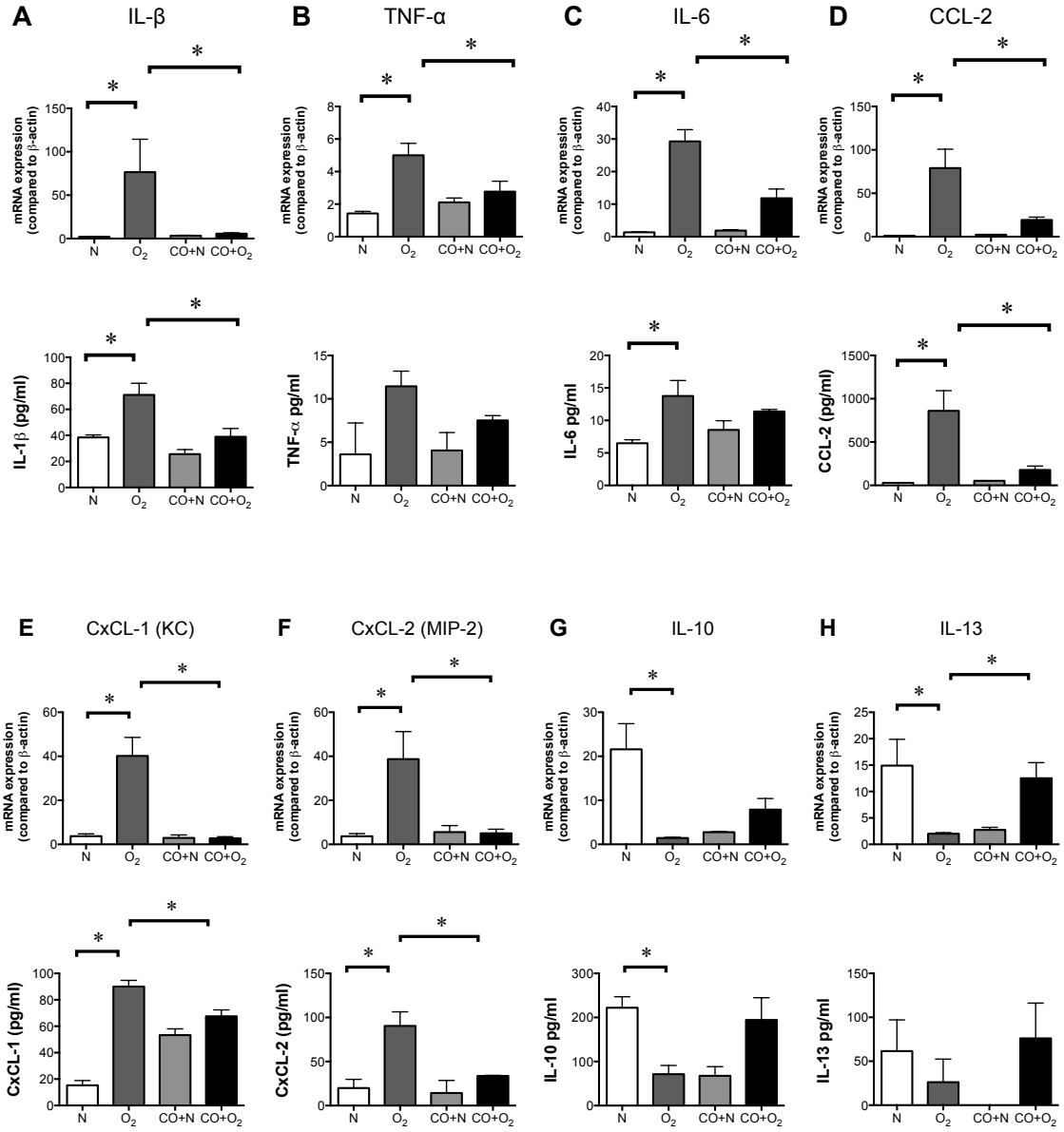

FIGURE II.6 EXOGENOUS CO ADMINISTRATION REGULATES THE EXPRESSION OF PRO- AND ANTI- INFLAMMATORY CYTOKINES UNDER HYPEROXIC CONDITIONS.

mRNA and protein levels were measured by quantitative PCR and multiplex immune assay at 14 day post-exposure. (A-F) Hyperoxia increased the mRNA and protein expression of IL-1β, TNF-α, IL-6, CCL-2, IL-10, IL-13, CxCL-1 and CxCL-2 (A-F). .CO administration significantly reduced IL-1β, TNF-α, IL-6, CCL-2, CxCL-1 and

CxCL-2 mRNA expression as well as IL-1β, CCL-2, CxCL-1 and CxCL-2 protein expression. (G, H). IL-10 and IL-13 were downregulated by hyperoxic treatment and increased with CO exposure. The data pool at least three independent experiments (mean±SEM, n=10-18 animals per group for mRNA analysis, n = 4 per group for protein analysis, *P <0.05, ANOVA).

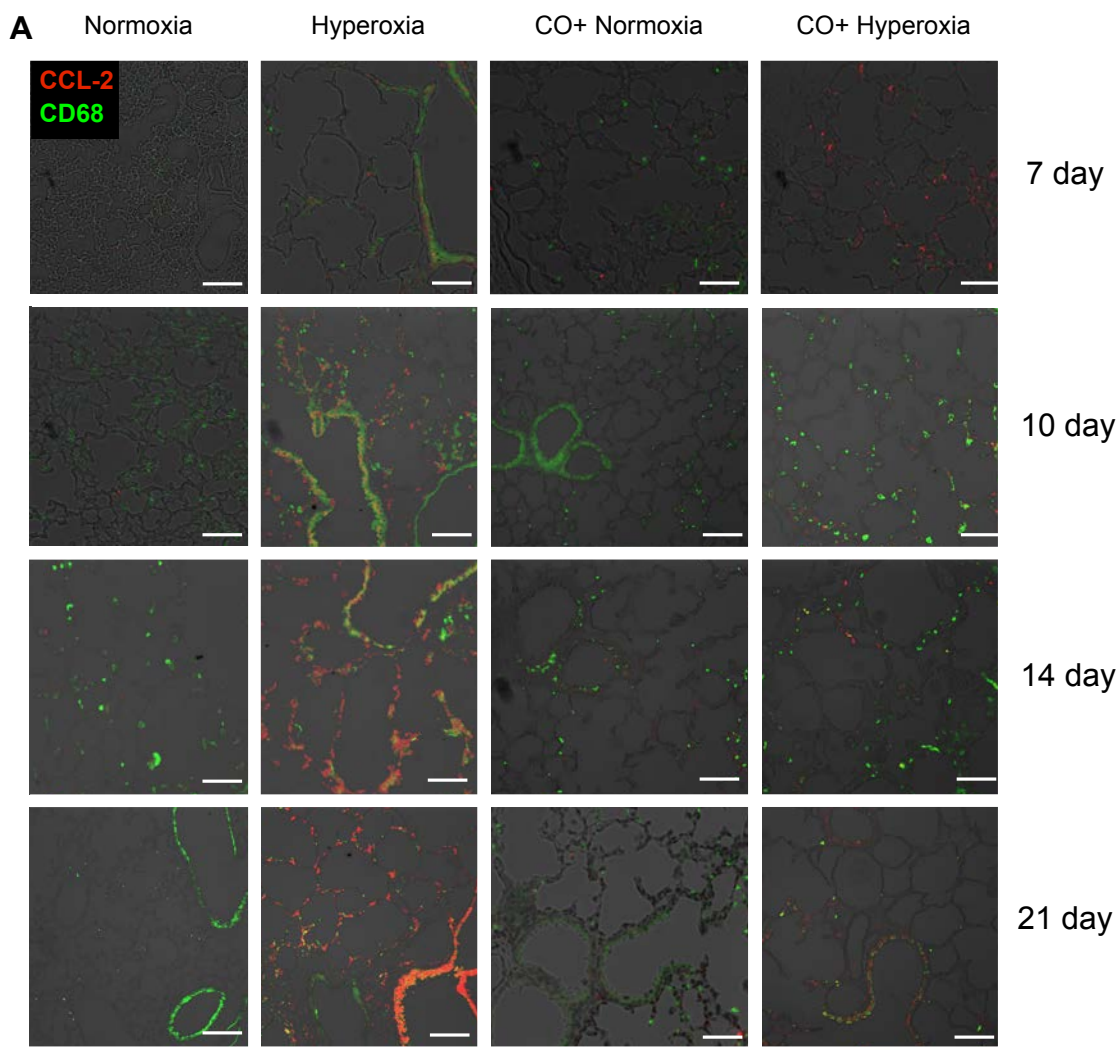
A
Normoxia
Hyperoxia
CO+ Normoxia
CO+ Hyperoxia
CCL-2
CD68
7 day
10 day
14 day
21 day

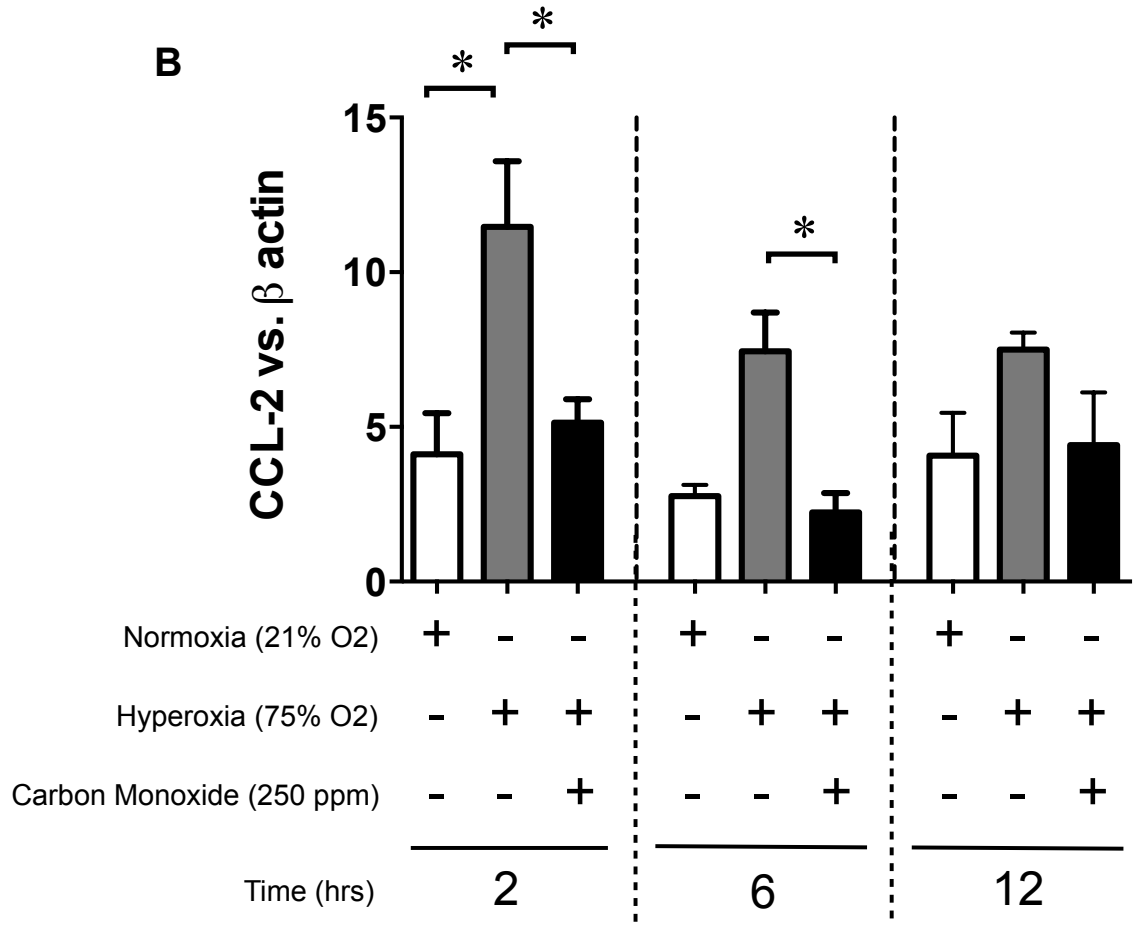

FIGURE II.7: HYPEROXIA EXPOSURE IS ASSOCIATED WITH AN INCREASE IN RESPIRATORY EPITHELIAL CELL CCL2 EXPRESSION.

Lung sections were stained for CCL2 (red) or CD68 (green); colocalization appears yellow. Compared to normoxia-exposed mice, hyperoxia-exposed mice show an increase in CCL2 expression primarily in the epithelium as well as an increase in CD68-positive macrophages. Episodic CO treatment the presence of hyperoxic exposure suppressed CCL2 expression (line segment = 50 μm, results are typical of three individual experiments). (B) A549 respiratory epithelial cells were exposed to 250 ppm CO or room air in the absence or presence of high oxygen tension (>95% O_2) for a duration of 2, 6 or 12 hrs. CCL2 mRNA expression was increased by hyperoxia and attenuated by CO.

Group mean data for CCL2 mRNA expression are presented (mean±SEM, n=3, *P<0.05, ANOVA).

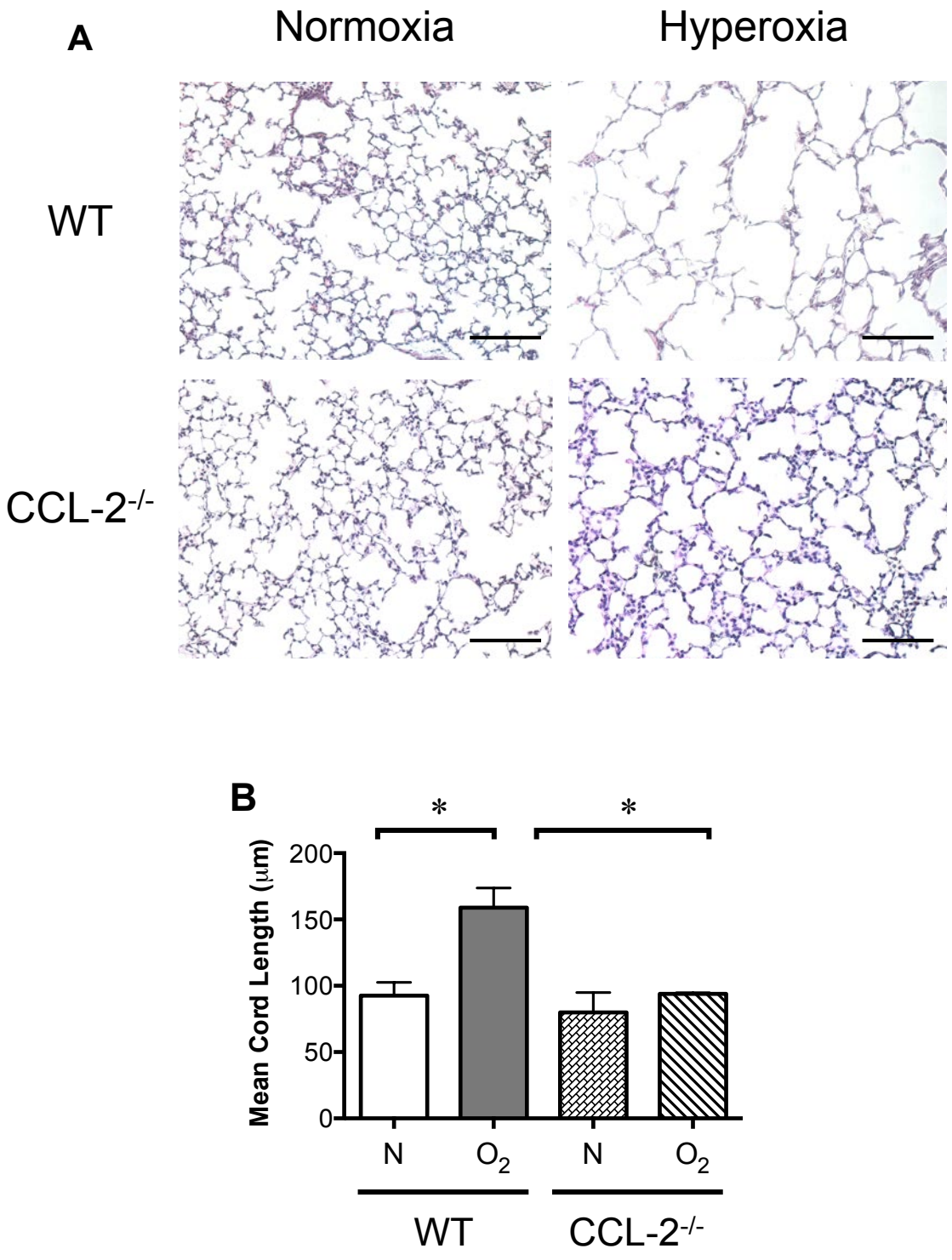
A
Normoxia
Hyperoxia
WT
CCL-2-/-
B
*
*
Mean Cord Length (μm)
200
150
100
50
0
N
O2
N
O2
WT
CCL-2-/-

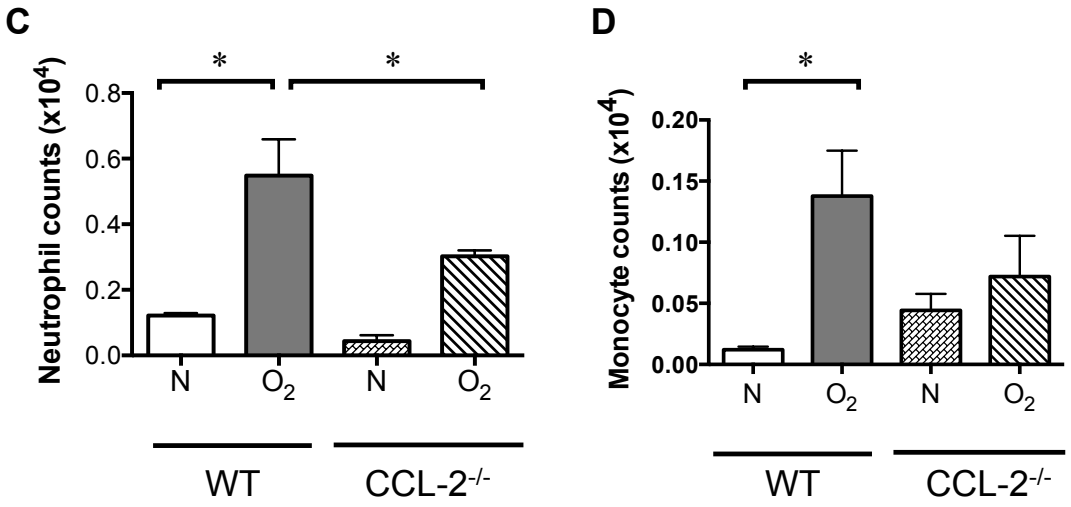

FIGURE II.8: CCL2 DELETION DECREASES HYPEROXIA-INDUCED ALVEOLAR SIMPLIFICATION AND INFLAMMATORY CELL TRAFFICKING.

(A) Representative lung sections from wild-type and CCL2 null mice exposed to normoxia or hyperoxia for 14 days were stained with hematoxylin and eosin. (B). Alveolar size, as measured by mean chord length, confirmed features noted on lung histology (n= 15-18 mice per group, **P* <0.05, ANOVA). (B). Bronchoalveolar lavage cells were measured Hemavet. Compared to hyperoxia-exposed wild-type mice, CCL2 null mice tended to show decreased neutrophils (C) and macrophages (D). (N = 5-8 mice per group, mean ±SEM, *different from hyperoxia-exposed group, **P* <0.05, ANOVA).

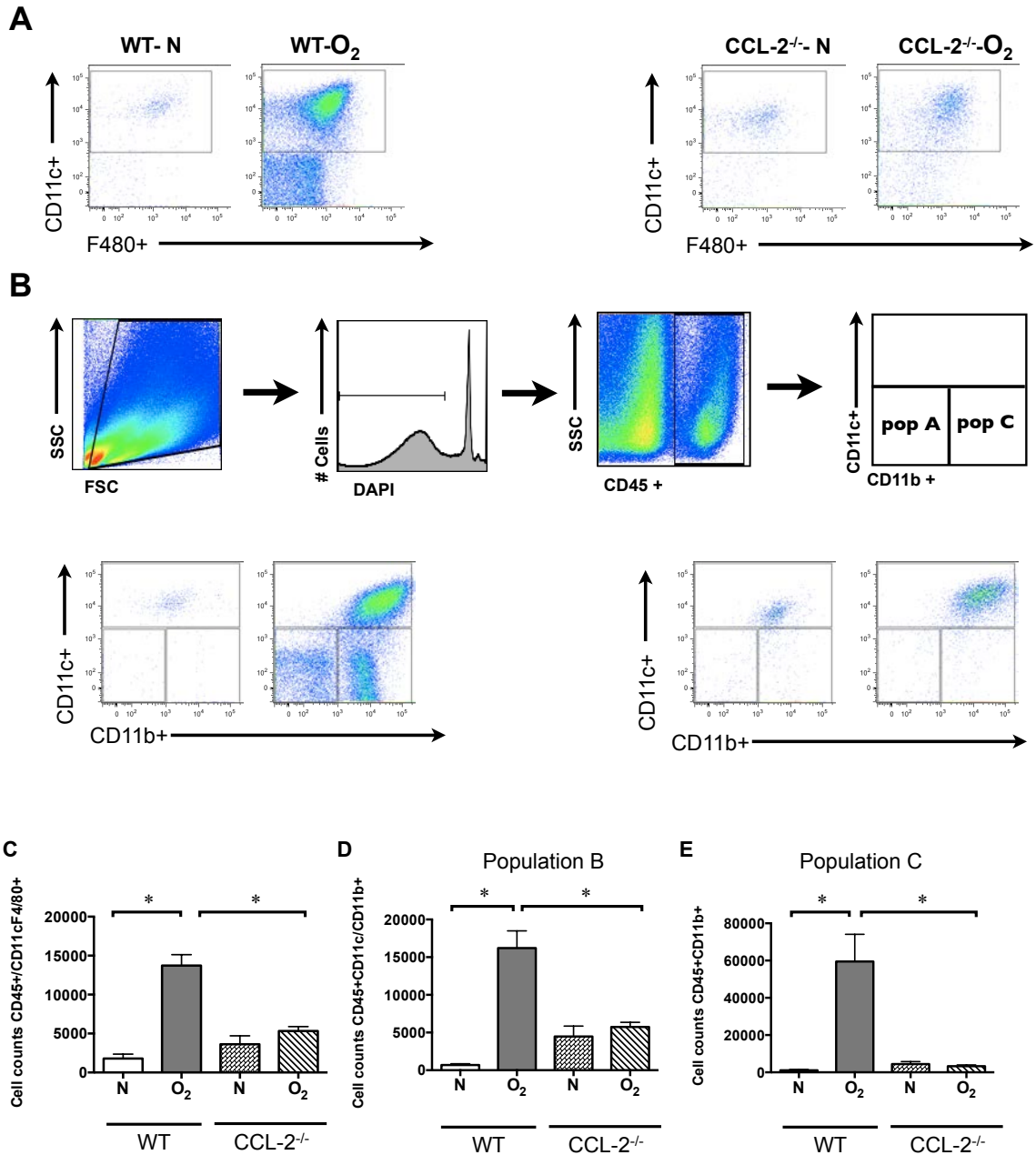

FIGURE II.9: CCL2 DELETION DECREASES ALVEOLAR MONOCYTE/MACROPHAGE INFILTRATION INTO HYPEROXIA-EXPOSED NEONATAL LUNGS.

Representative flow cytometric scattergrams of monocyte/macrophage subpopulations within the lungs of wild-type and CCL2 null mice exposed to normoxia and hyperoxia for

14 days. Each dot plot is representative of four independent experiments. (A) CD45+, CD11c+, F4/80+ macrophages. (B) The gating scheme used for CD11c and CD11c staining was explained in Figure 4 and is briefly shown here. Each dot plot is again representative of four independent experiments. Comparison of cell counts for F4/80 and CD11c double positive macrophages (panel C), $CD11c^{high}$ $CD11b^{high}$ exudative macrophages (subpopulation B, panel D) and $CD11c^{low}CD11b^{high}$ inflammatory monocytes (subpopulation C, panel E). Hyperoxia increased the trafficking of macrophage subpopulations into the neonatal lung and CCL2 deletion attenuated macrophage recruitment.(n = 8-14 mice per group, mean±SEM, *different from hyperoxic exposed group, $P < 0.05$, ANOVA).

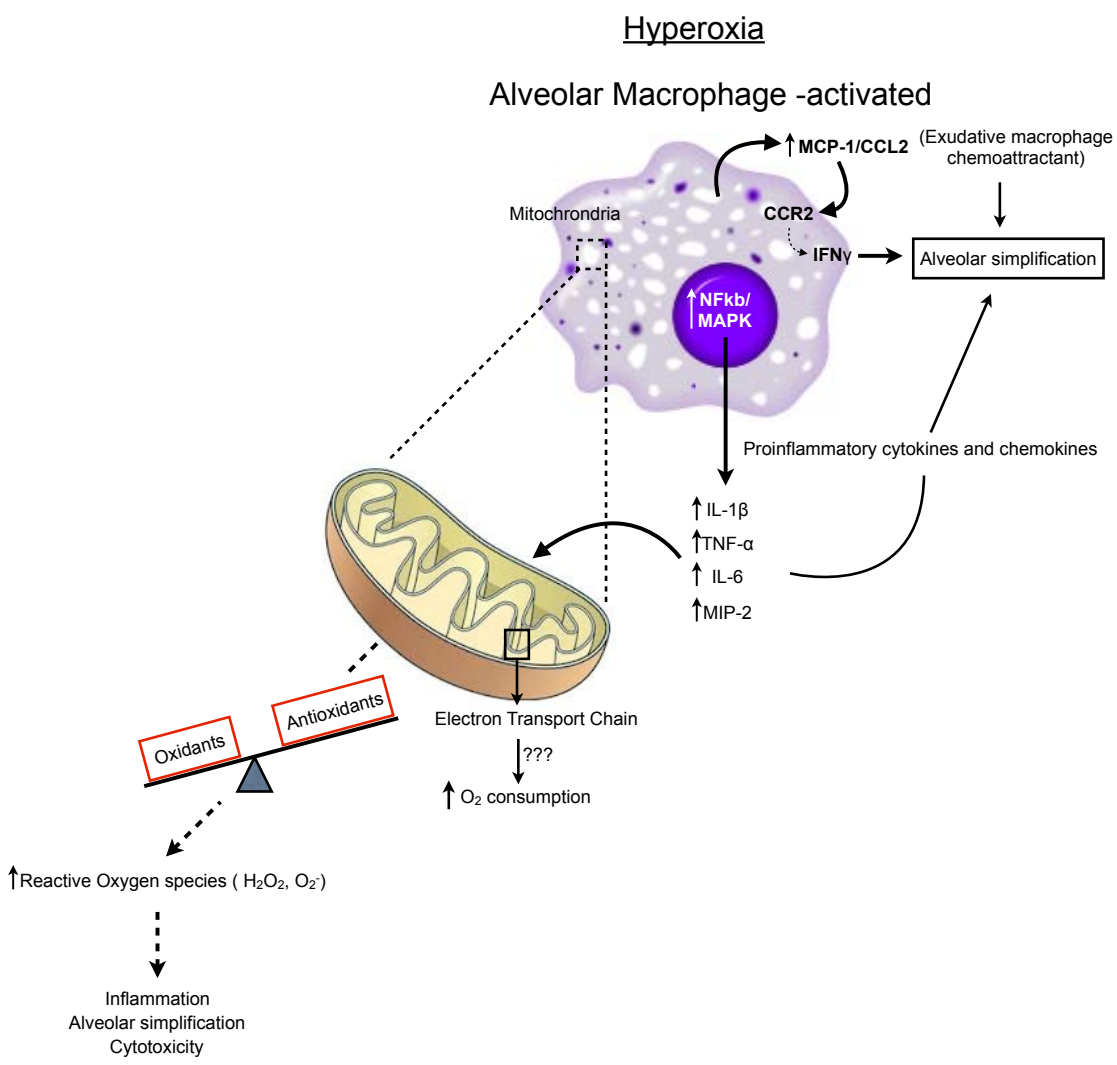
Hyperoxia
Alveolar Macrophage -activated
MCP-1/CCL2
(Exudative macrophage chemoattractant)
Mitochrondria
CCR2
IFNγ
Alveolar simplification
NFkb/ MAPK
Proinflammatory cytokines and chemokines
IL-1β
TNF-α
IL-6
MIP-2
Oxidants
Antioxidants
Electron Transport Chain
???
O2 consumption
Reactive Oxygen species (H2O2, O2-)
Inflammation
Alveolar simplification
Cytotoxicity

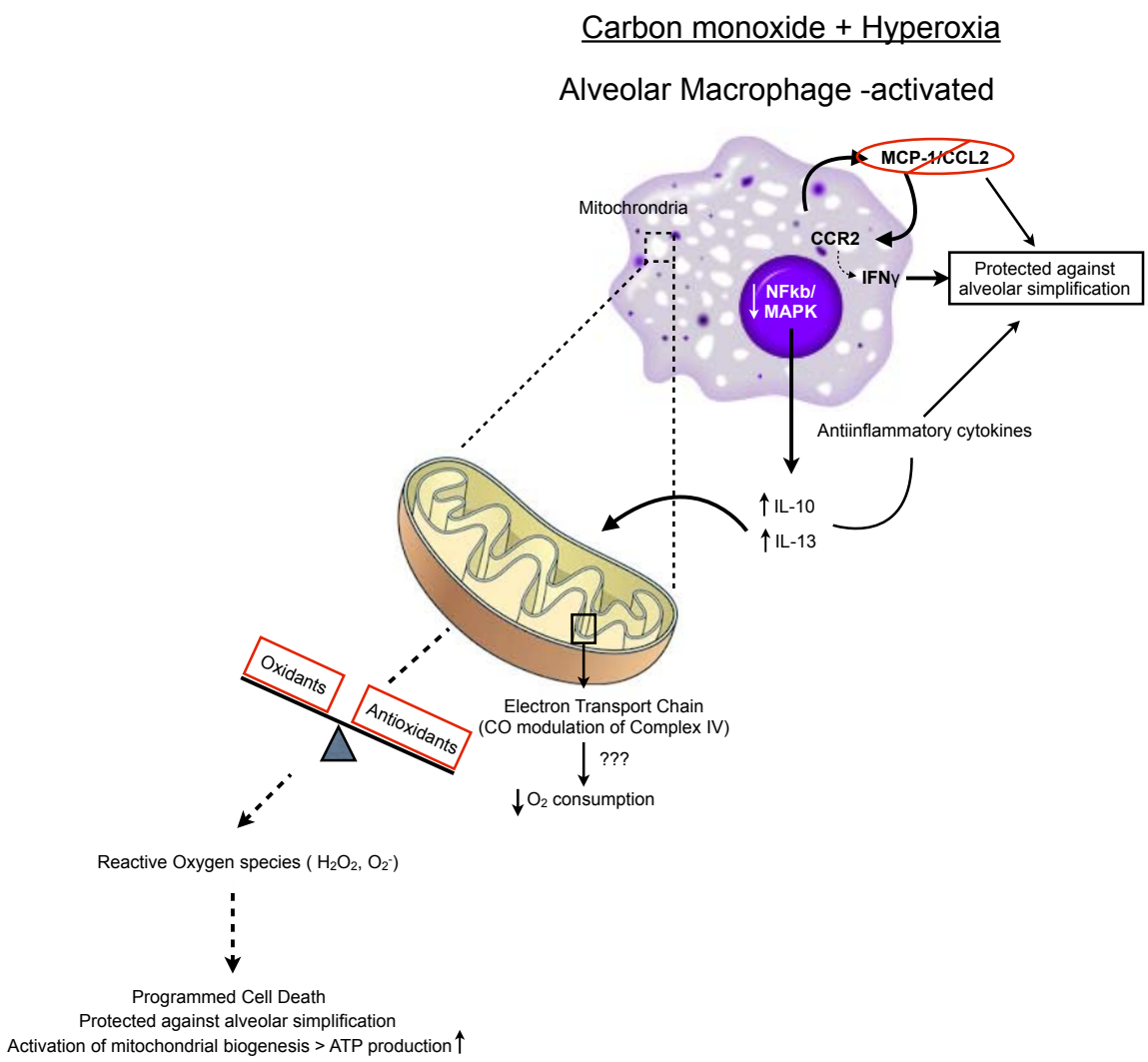

FIGURE II.10 GRAPHICAL REPRESENTATION SUMMARIZING THE MECHANISM(S) POTENTIALLY INVOLVED IN THE ANTI-INFLAMMATORY ACTIVITIES OF HO-1/CO VIA SUPRESSION OF MCP-1/CCL-2 IN HYPEROXIA INDUCED BRONCHOPULMONARY DYSPLASIA

The precise mechanisms by which inflammation inhibits alveolar development are not completely known. In our current study we used a neonatal hyperoxic induced mouse model to depicted our proposed mechanism of an activated alveolar macrophage during hyperoxia induce bronchoplumonary dysplasia and CO treatment. During hyperoxia exposure and in the absence of HO-1, exudative and activated macrophages secrete

proinflammatory cytokine and chemokines, which ultimately lead to mitochondrial dysfunction and an increase in reactive oxygen species. However, when these cells are treated with low dose of pulsatile carbon monoxide and in the absence of CCL-2, there is an increase in anti-inflammatory cytokine IL-10 and IL-13 and a subsequent increase in anti oxidants, which lead to protection of alveolar damage. Our studies demonstrate a direct link between CO, the CCl-2-dependent control of leukocyte migration into hyperoxic lung tissue, and alveolar growth. Inhibition of inflammatory cell infiltration by either CO or CCL-2 gene deletion was associated with the attenuated alveolar simplification.

SUPPLEMENTAL FIGURES

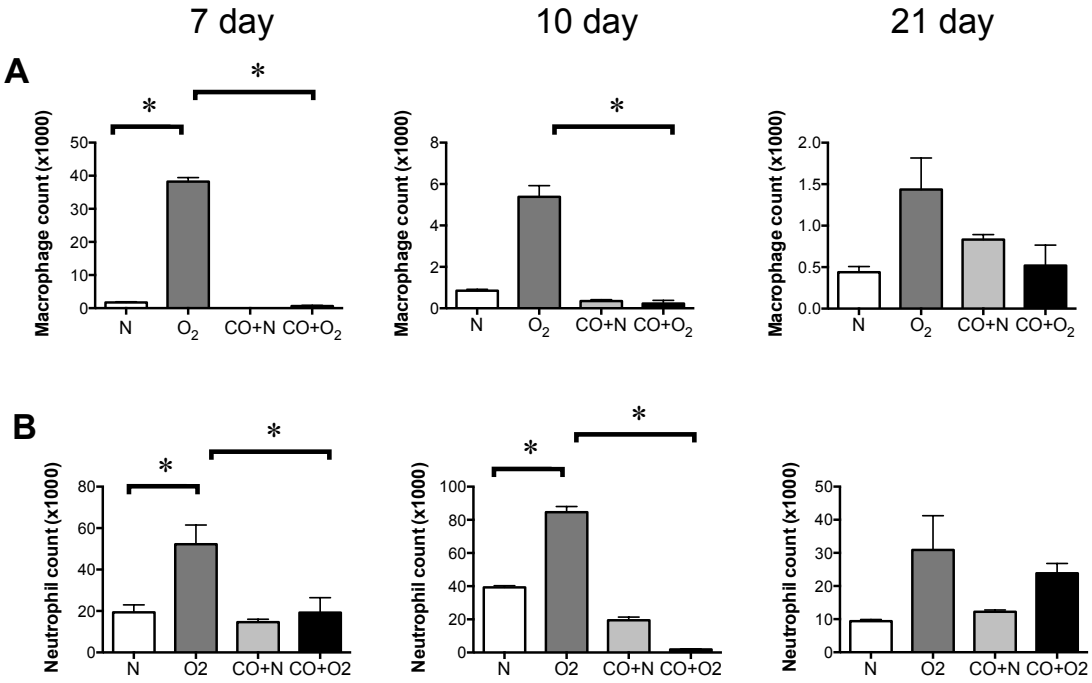

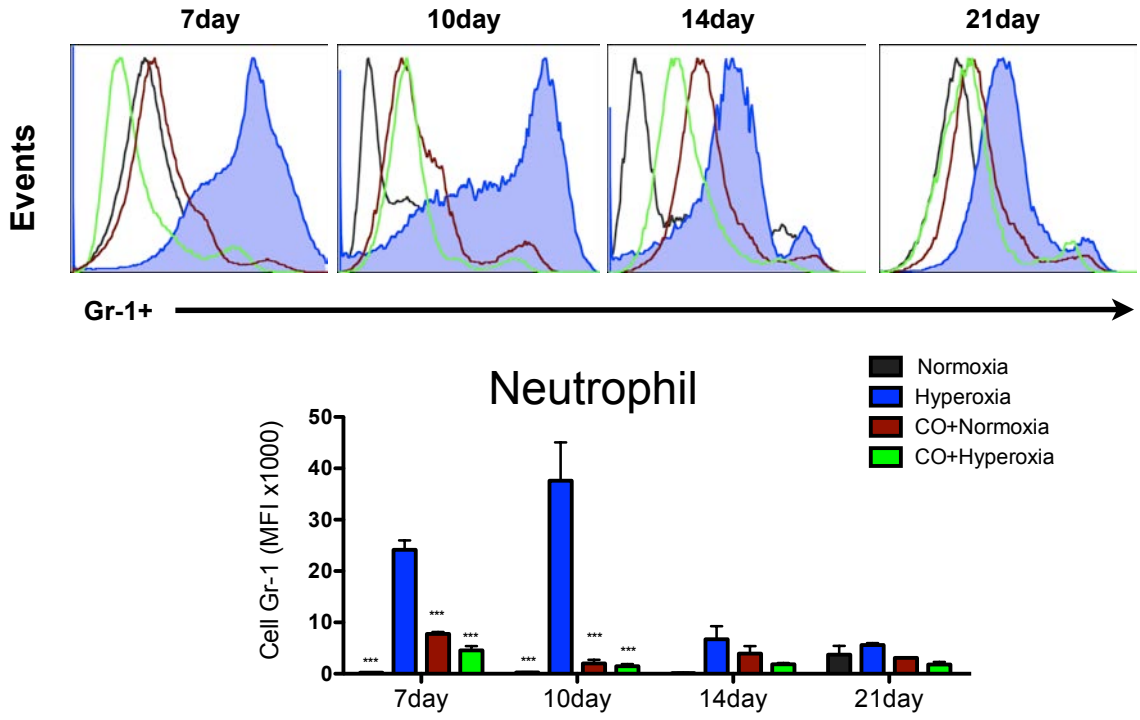

SUPPLEMENTAL FIGURE II.1: TIME COURSE FOR CO-INDUCED SUPPRESSION OF LEUKOCYTE MIGRATION TO THE LUNGS OF HYPEROXIA-EXPOSED NEONATAL MICE.

The effect of CO on lung infiltration by leukocytes was assessed using cytospins from PN days 7, 10 and 21 days. Cell counts of monocyte/macrophages (A) and neutrophils (B) are depicted (y-axis indicates cell number x 1000). Data represent mean±SEM, n = 12-17 per group, *different from hyperoxia-exposed group, P <0.05, ANOVA. (C) Hyperoxia-induced neutrophil inflammation in neonatal mouse lungs is attenuated by exogenous CO exposure. DAPI-negative (live), CD45-positive, Gr-1+ neutrophils were identified by flow cytometric analysis. Representative histogram showing Gr-1^{+} staining from 7, 10 and 21 days of hyperoxic exposure in the presence and absence of CO. Effects of the various treatments on Gr-1 mean fluorescent intensity (MFI, y-axis indicates MFI x 1000). Numbers represent mean±SEM, n = 12-17 per group; *different from hyperoxia-exposed group, $P < 0.05$, ANOVA

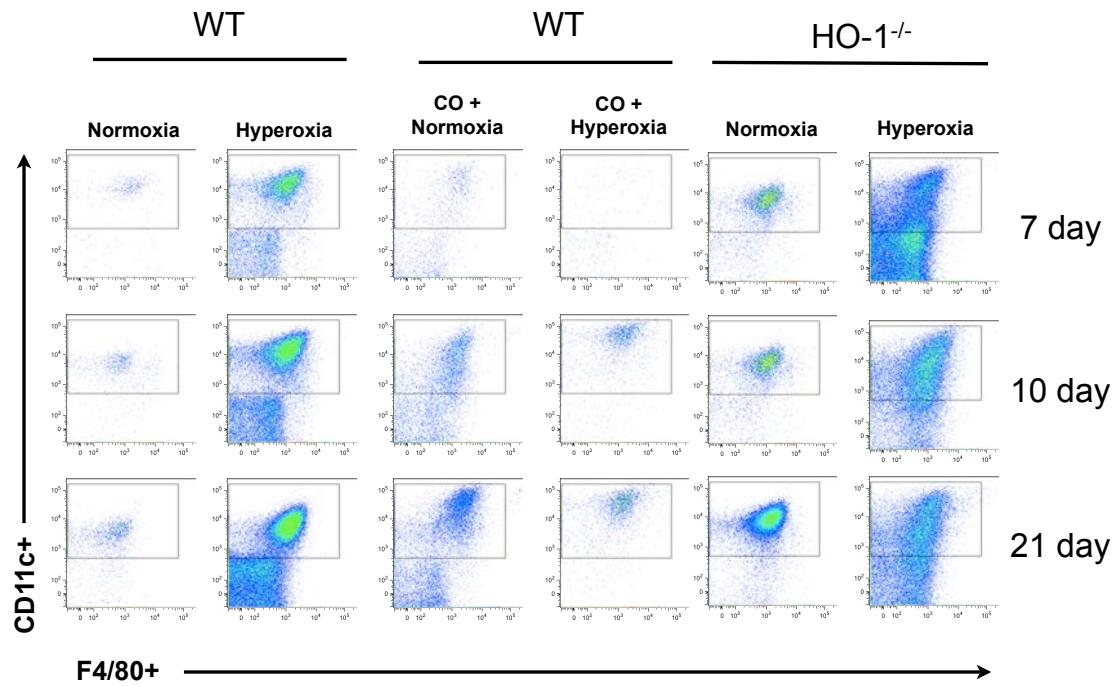
WT
WT
HO-1-/-
Normoxia
Hyperoxia
CO + Normoxia
CO + Hyperoxia
Normoxia
Hyperoxia
7 day
10 day
21 day
CD11c+
F4/80+

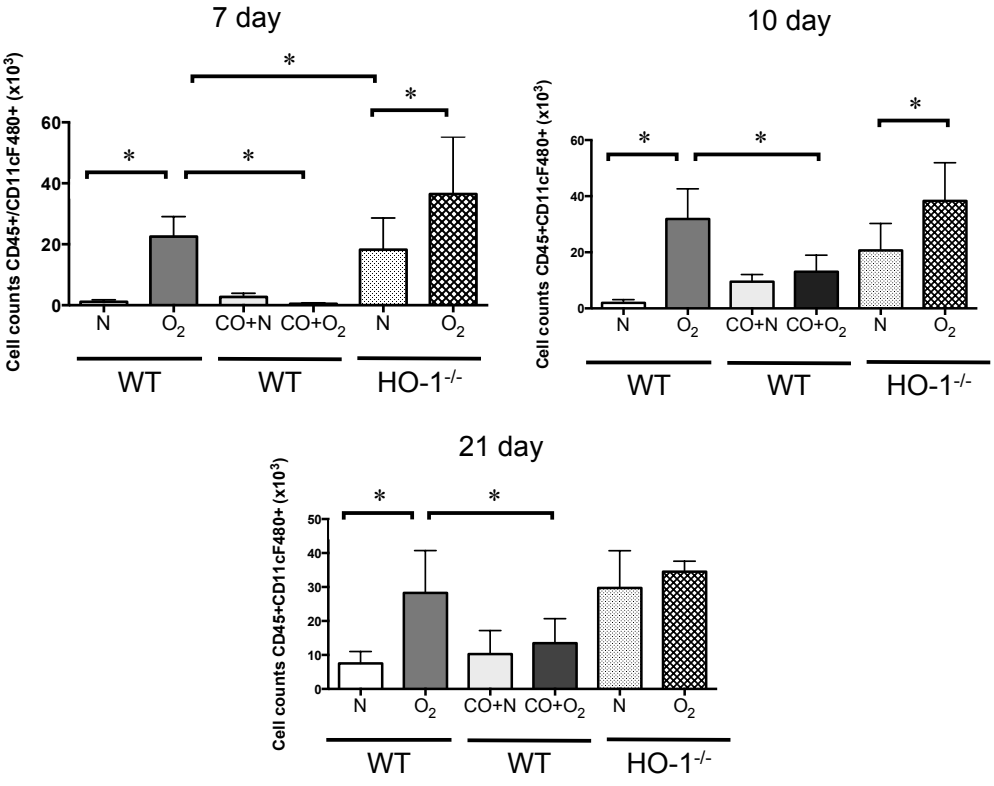
7 day
10 day
21 day
Cell counts CD45+/CD11cF480+ (x10³)
Cell counts CD45+CD11cF480+ (x10³)
N
O2
CO+N
CO+O2
WT
WT
HO-1-/-

Population-A

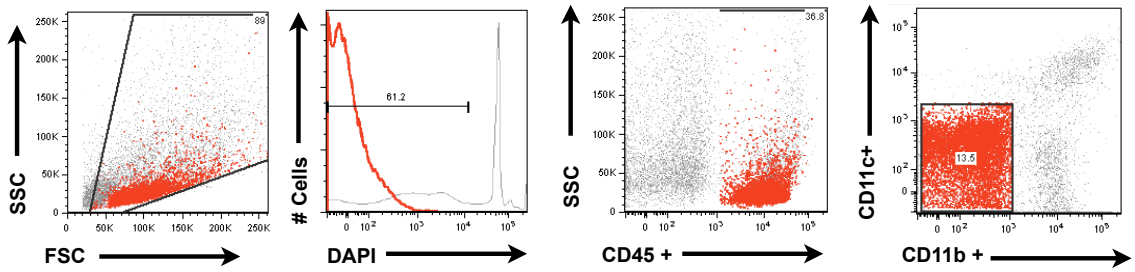

Population-B

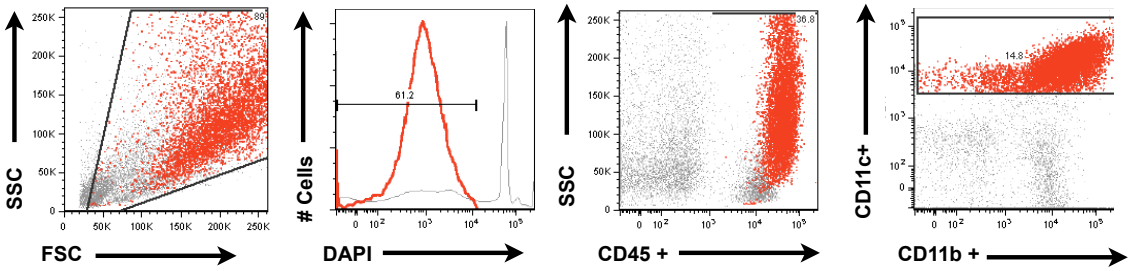

Population-C

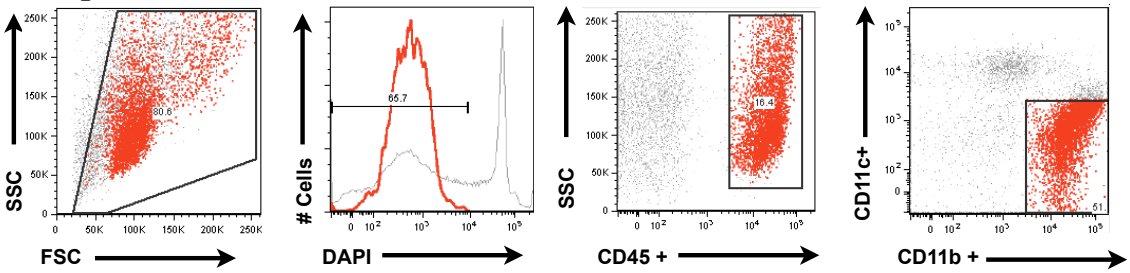

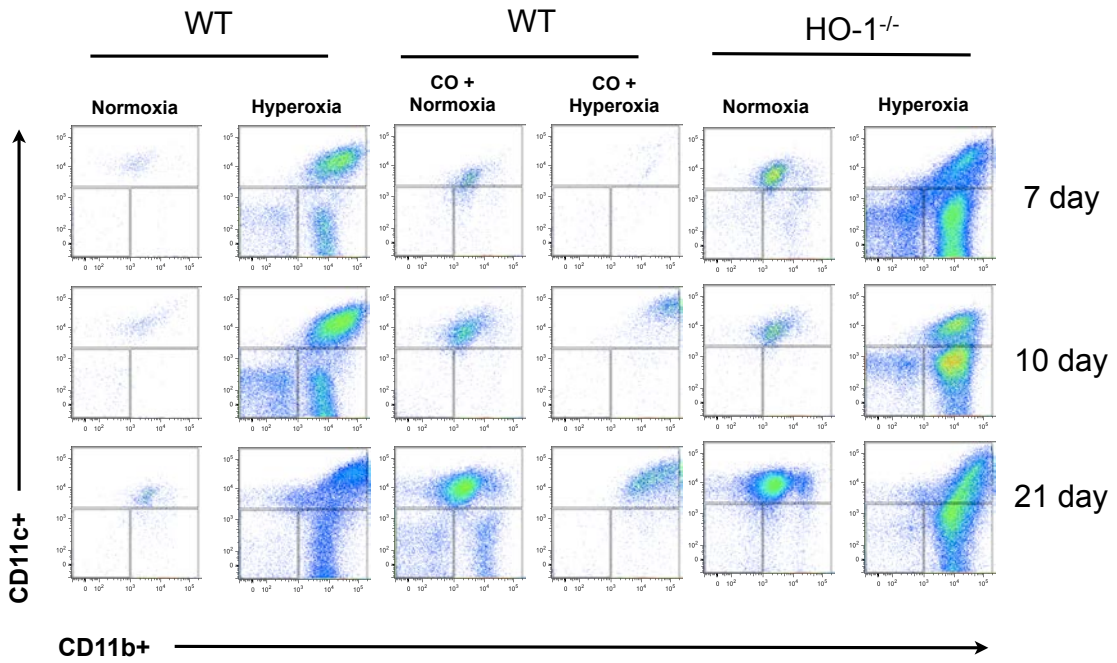

Population B

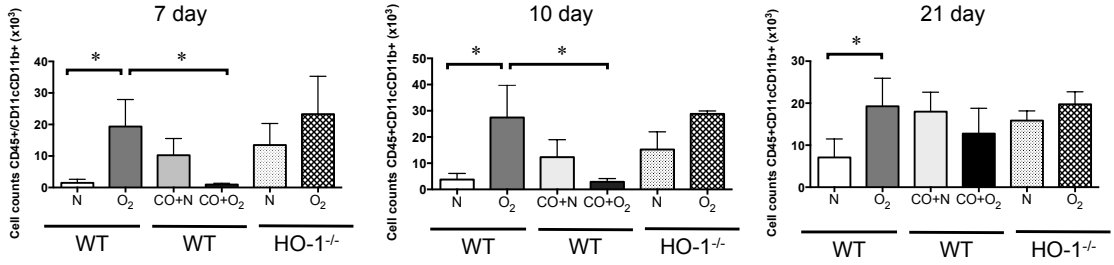

Population C

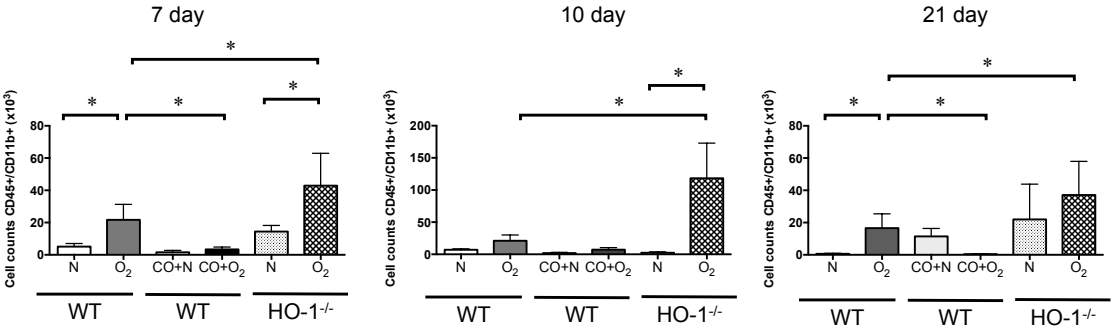

SUPPLEMENTAL FIGURE II.2: TIME COURSE OF MONOCYTE/MACROPHAGE INFILTRATION INTO NEONATAL LUNGS EXPOSED TO HYPEROXIA IN THE PRESENCE OR ABSENCE OF EPISODIC CO TREATMENT.

(A) Flow cytometric analysis of viable (negative for DAPI) alveolar monocyte/macrophages from neonatal mouse lungs of wild-type or HO-1 null mice after 7, 10 or 21 days of normoxic or hyperoxic exposure, in the presence and absence of CO. Flow cytometry plots show the expression of $CD45^+$, $CD11c^+/F4/80^+$ macrophages. CO treatment tended to decrease percentage and total number of $F4/80^+/CD11c^+$ double positive cells. HO-1 deletion tended to increase in $F4/80^+/CD11c^+$ double positive cells. Group mean data are also shown. Results are depicted as mean±SEM, n = 4-10 per group, *different from hyperoxia alone, P <0.05, ANOVA. (B). Back-gating analysis of CD11c and CD11b cells in hyperoxic exposed mice. Back gating analysis showed that cells isolated from population A were located in the lymphocytic region based on side and forward scatter. Population B $CD11c^{high}$ $CD11b^{high}$ cells tended to be large cells with varying granularity. Population C $CD11c^{low}$ $CD11b^{high}$ were smaller with moderate granularity, reflecting recruited monocytes. C. Time course of alveolar monocyte/macrophage subpopulations after exposure to hyperoxia or CO treatment. More than 85% of the viable live cells isolated (gated for side and forward scatter) were CD45+ cells. More than 65-75% of $CD45^+$ cells expressed varying levels of cell surface antigens CD11c and CD11b. Dot plot analysis showed three distinct subpopulations of monocyte/macrophages under conditions of normoxia, hyperoxia, CO+normoxia and CO+hyperoxia. Data for 7, 10 and 21 day time points are shown; these plots are representative of four independent experiments. Plots of group mean data for subpopulations B ($CD11c^{high}$ $CD11b^{high}$) and C ($CD11c^{low}CD11b^{high}$) are shown. HO-1

null mice exposed to hyperoxia had significantly more infiltrating cells compared to wild-type hyperoxia-exposed mice. Hyperoxia increased the amount of $CD11c^{high}$ $CD11b^{high}$ macrophages infiltrating into the neonatal lung in both hyperoxia-exposed wild-type and hyperoxia-exposed $HO\text{-}1^{-/-}$ mice. CO treatment attenuated macrophage recruitment starting at day 7 of exposure. These data are from three independent time course experiments, n=5-10 per group at each time point. Results are depicted as mean±SEM; *different from hyperoxia alone, $*P < 0.05$, ANOVA.

DISCLOSURES

Dr. Pinsky has an equity interest in Proterris, which is developing inhaled CO for clinical use, and potential patent-related royalties from Columbia University.

ACKNOWLEDGEMENTS

This work was supported by: Systems in Integrative Biology predoctoral training grant T32GM008322 (to A.C. Anyanwu); NIH grants HL086676 (to D.J. Pinsky), and HL079339 (to M.B. Hershenson), the J. Griswold Ruth MD & Margery Hopkins Ruth Professorship (to D.J. Pinsky); and the A. Alfred Taubman Medical Research Institute at the University of Michigan.

Special thanks to Joanna D. Solarewicz, Julia Solarewicz, Martin Gruca and Joy Tsai for technical assistance.

NOTES

This manuscript is currently under review.

REFERENCES

1. Ehrenkranz, R.A., Walsh, M.C., Vohr, B.R., Jobe, A.H., Wright, L.L., Fanaroff, A.A., Wrage, L.A., Poole, K., Health, f.t.N.I.o.C., and Human Development Neonatal Research Network. 2005. Validation of the National Institutes of Health Consensus Definition of Bronchopulmonary Dysplasia. *Pediatrics* 116:1353-1360.

2. Kennedy, J.D. 1999. Lung function outcome in children of premature birth. *Journal of Paediatrics and Child Health* 35:516-521.

3. Eber, E., and Zach, M.S. 2001. Paediatric origins of adult lung disease 8: Long term sequelae of bronchopulmonary dysplasia (chronic lung disease of infancy). *Thorax* 56:317-323.

4. Merritt, T.A., Stuard, I.D., Puccia, J., Wood, B., Edwards, D.K., Finkelstein, J., and Shapiro, D.L. 1981. Newborn tracheal aspirate cytology: Classification during respiratory distress syndrome and bronchopulmonary dysplasia. *Journal of Pediatrics* 98:949-956.

5. Munshi, U.K., Niu, J.O., Siddiq, M.M., and Parton, L.A. 1997. Elevation of interleukin-8 and interleukin-6 precedes the influx of neutrophils in tracheal aspirates from preterm infants who develop bronchopulmonary dysplasia. *Pediatric Pulmonology* 24:331-336.

6. Baier, R.J., Majid, A., Parupia, H., Loggins, J., and Kruger, T.E. 2004. CC chemokine concentrations increase in respiratory distress syndrome and correlate with development of bronchopulmonary dysplasia. . *Pediatr. Pulmonol.* 37:137-148.

7. Kakkera, D.K., Siddiq, M.M., and Parton, L.A. 2005. Interleukin-1 balance in the lungs of preterm infants who develop bronchopulmonary dysplasia. *Neonatology* 87:82-90.

8. Kotecha, S., Wilson, L., Wangoo, A., Silverman, M., and Shaw, J.R. 1996. Increase in Interleukin (IL)-1b and IL-6 in bronchoalveolar lavage fluid obtained from infants with chronic lung disease of prematurity. *Pediatr. Res.* 40:250-256.

9. Auten, R.L., Mason, S.N., Tanaka, D.T., Welty-Wolf, K., and Whorton, M.H. 2001. Anti-neutrophil chemokine preserves alveolar development in hyperoxia-exposed newborn rats. *Am J Physiol: Lung Cell. Mol. Physiol.* 281:L336-L344.

10. Deng, H., Nicholas M.S., and Auten R.L., Jr. 2000. Lung inflammation in hyperoxia can be prevented by antichemokine treatment in newborn rats. *Am. J. Respir. Crit. Care Med.* 162:2316-2323.

11. Yi, M., Jankov, R.P., Belcastro, R., Humes, D., Copland, I., Shek, S., Sweezey, N.B., Post, M., Albertine, K.H., Auten, R.L., et al. 2004. Opposing effects of 60% oxygen and neutrophil influx on alveologenesis in the neonatal rat. *Am. J. Respir. Crit. Care Med.* 170:1188-1196.

12. Toti, P., Buonocore, G., Tanganelli, P., Catella, A.M., Palmeri, M.L., Vatti, R., and Seemayer, T.A. 1997. Bronchopulmonary dysplasia of the premature baby: an immunohistochemical study. *Pediatr. Pulmonol.* 24:22-28.

13. Bhatt, A.J., Pryhuber, G.S., Huyck, H., Watkins, R.H., Metlay, L.A., and Maniscalco, W.M. 2001. Disrupted pulmonary vasculature and decreased vascular endothelial growth factor, Flt-1, and TIE-2 in human infants dying with bronchopulmonary dysplasia. *Am. J. Respir. Crit. Care Med.* 164:1971-1980.

14. Kaarteenaho-Wiik, R., Kinnula, V.L., Herva, R., Soini, Y., Pollanen, R., and Paakko, P. 2002. Tenascin-C is highly expressed in respiratory distress syndrome and bronchopulmonary dysplasia. *J. Histochem. Cytochem.* 50:423-431.

15. Kaarteenaho-Wiik, R., Pääkkö, P., Herva, R., Risteli, J., and Soini, Y. 2004. Type I and III collagen protein precursors and mRNA in the developing human lung. *J. Pathol.* 203:567-574.

16. Fernandez-Gonzalez, A., Alex M.S., Liu, X., and Kourembanas, S. 2012. Vasculoprotective effects of heme oxygenase-1 in a murine model of hyperoxia-induced bronchopulmonary dysplasia. *Am J Physiol: Lung Cell. Mol. Physiol.* 302:L775-L784.

17. Wagenaar, G.T.M., ter Horst, S.A.J., van Gastelen, M.A., Leijser, L.M., Mauad, T., van der Velden, P.A., de Heer, E., Hiemstra, P.S., Poorthuis, B.J.H.M., and Walther, F.J. 2004. Gene expression profile and histopathology of experimental

bronchopulmonary dysplasia induced by prolonged oxidative stress. *Free Rad. Biol. Med.* 36:782-801.

18. Rozycki, H.J., Comber, P.G., and Huff, T.F. 2002. Cytokines and oxygen radicals after hyperoxia in preterm and term alveolar macrophages. *Am J Physiol: Lung Cell. Mol. Physiol.* 282:L1222-1228.

19. Vergadi, E., Chang, M.S., Lee, C., Liang, O.D., Liu, X., Fernandez-Gonzalez, A., Mitsialis, S.A., and Kourembanas, S. 2011. Early macrophage recruitment and alternative activation are critical for the later development of hypoxia-induced pulmonary hypertension. *Circulation* 123:1986-1995.

20. Song, R., Kubo, M., Morse, D., Zhou, Z., Zhang, X., Dauber, J.H., Fabisiak, J., Alber, S.M., Watkins, S.C., Zuckerbraun, B.S., et al. 2003. Carbon monoxide induces cytoprotection in rat orthotopic lung transplantation via anti-inflammatory and anti-apoptotic effects. *Am. J. Pathol.* 163:231-242.

21. Otterbein, L., Bach, F., Alam, J., Soares, M., Tao Lu, H., Wysk, M., Davis, R., Flavell, R., and Choi, A. 2000. Carbon monoxide has anti-inflammatory effects involving the mitogen-activated protein kinase pathway. *Nat. Med.* 6:422 - 428.

22. Otterbein, L., Mantell, L., and Choi, A. 1999. Carbon monoxide provides protection against hyperoxic lung injury. *Am. J. Physiol.* 276:L688 - L694.

23. Minamoto, K., Harada, H., Lama, V.N., Fedarau, M.A., and Pinsky, D.J. 2005. Reciprocal regulation of airway rejection by the inducible gas-forming enzymes heme oxygenase and nitric oxide synthase. *J. Exp. Med.* 202:283-294.

24. Mishra, S., Fujita, T., Lama, V.N., Nam, D., Liao, H., Okada, M., Minamoto, K., Yoshikawa, Y., Harada, H., and Pinsky, D.J. 2006. Carbon monoxide rescues ischemic lungs by interrupting MAPK-driven expression of early growth response 1 gene and its downstream target genes. *Proc. Natl. Acad. Sci. USA* 103:5191-5196.

25. Otterbein, L.E., Soares, M.P., Yamashita, K., and Bach, F.H. 2003. Heme oxygenase-1: unleashing the protective properties of heme. *Trends Immunol.* 24:449-455.

26. Drechsler, Y., Dolganiuc, A., Norkina, O., Romics, L., Li, W., Kodys, K., Bach, F.H., Mandrekar, P., and Szabo, G. 2006. Heme oxygenase-1 mediates the anti-inflammatory effects of acute alcohol on IL-10 induction involving p38 MAPK activation in monocytes. *J. Immunol.* 177:2592-2600.

27. Ghosh, S., Gal, J., and Marczin, N. Carbon monoxide: Endogenous mediator, potential diagnostic and therapeutic target. *Ann. Med.* 42:1-12.

28. Dennery, P.A., Lee, C.S., Ford, B.S., Weng, Y.-H., Yang, G., and Rodgers, P.A. 2003. Developmental expression of heme oxygenase in the rat lung. *Pediatr. Res.* 53:42-47.

29. Stanford, S.J., Hislop, A.A., Oltmanns, U., Nabel, E.G., Sang, H., Haworth, S.G., and Mitchell, J.A. 2005. Transition from placental to air breathing stimulates haem-oxygenase-1 expression without functional consequence for pulmonary vascular adaptation in pigs and mice. *Br. J. Pharmacol.* 144:467-476.

30. Amy, R.W., Bowes, D., Burri, P.H., Haines, J., and Thurlbeck, W.M. 1977. Postnatal growth of the mouse lung. *J. Anat.* 124:131-151.

31. Jobe, A.H., and Ikegami, M. 1998. Mechanisms initiating lung injury in the preterm. *Early Human Devel.* 53:81-94.

32. Yet, S.-F., Perrella, M.A., Layne, M.D., Hsieh, C.-M., Maemura, K., Kobzik, L., Wiesel, P., Christou, H., Kourembanas, S., and Lee, M.-E. 1999. Hypoxia induces severe right ventricular dilatation and infarction in heme oxygenase-1 null mice. *J. Clin. Invest.* 103:R23-R29.

33. Fujita, T., Toda, K., Karimova, A., Yan, S.-F., Naka, Y., Yet, S.-F., and Pinsky, D.J. 2001. Paradoxical rescue from ischemic lung injury by inhaled carbon monoxide driven by derepression of fibrinolysis. *Nat. Med.* 7:598-604.

34. Cooney, W.M. and Thurlbeck, T.P. 1982. The radial alveolar count method of Emery and Mithal: a reappraisal 2 -- intrauterine and early postnatal lung growth. *Thorax* 37:580-3.

35. Janssen, W.J., Barthel, L., Muldrow, A., Oberley-Deegan, R.E., Kearns, M.T., Jakubzick, C., and Henson, P.M. 2011. Fas determines differential fates of resident and recruited macrophages during resolution of acute lung injury. *Am. J. Respir. Crit. Care Med.* 184:547-560.

36. Silva, M.F.d., Napimoga, M.H., Rodrigues, D.B.R., Pereira, S.A.L., and Silva, C.L. 2011. Phenotypic and functional characterization of pulmonary macrophages

subpopulations after intratracheal injection of Paracoccidioides brasiliensis cell wall components. *Immunobiol.* 216:821-831.

37. Vozzelli, M.A., Mason, S.N., Whorton, M.H., and Auten, R.L. 2004. Antimacrophage chemokine treatment prevents neutrophil and macrophage influx in hyperoxia-exposed newborn rat lung. *Am. J. Physiol. Lung Cell. Mol. Physiol.* 286:L488-L493.

38. Lin, K.L., Suzuki, Y., Nakano, H., Ramsburg, E., and Gunn, M.D. 2008. CCR2+ monocyte-derived dendritic cells and exudate macrophages produce influenza-induced pulmonary immune pathology and mortality. *J. Immunol.* 180:2562-2572.

39. Tighe, R.M., Liang, J., Liu, N., Jung, Y., Jiang, D., Gunn, M.D., and Noble, P.W. 2011. Recruited exudative macrophages selectively produce CXCL10 after noninfectious lung injury. *Am. J. Respir. Cell Mol. Biol.* 45:781-788.

40. Bozyk, P.D., Popova, A.P., Bentley, J.K., Anyanwu, A.C., Linn, M.D., Pryhuber, G.S., Moore, B.B., and Hershenson, M.B. 2012. Neonatal periostin knockout mice are protected from hyperoxia-induced alveolar simplification. *PLoS One* 7:e31336.

41. Ratner, V., Starkov, A., Matsiukevich, D., Polin, R.A., and Ten, V.S. 2009. Mitochondrial dysfunction contributes to alveolar developmental arrest in hyperoxia-exposed mice. *Am. J. Respir. Cell Mol. Biol.* 40:511-518.

42. Wang, X., Wang, Y., Kim, H.P., Nakahira, K., Ryter, S.W., and Choi, A.M.K. 2007. Carbon monoxide protects against hyperoxia-induced endothelial cell

apoptosis by inhibiting reactive oxygen species formation. *J. Biol. Chem.* 282:1718-1726.

43. Lee, S.-J., Ryter, S.W., Xu, J.-F., Nakahira, K., Kim, H.P., Choi, A.M.K., and Kim, Y.S. 2011. Carbon monoxide activates autophagy via mitochondrial reactive oxygen species formation. *Am. J. Respir. Cell Mol. Biol.* 45:867-873.

44. Fujita, T., Toda, K., Karimova, A., Yan, S., Naka, Y., Yet, S., and Pinsky, D. 2001. Paradoxical rescue from ischemic lung injury by inhaled carbon monoxide driven by derepression of fibrinolysis. *Nat. Med.* 7:598 - 604.

45. Otterbein L , S.S., Choi AM. 1995. Hemoglobin provides protection against lethal endotoxemia in rats: the role of heme oxygenase-1. *Am. J. Respir. Cell Mol. Biol.* 13:595-601.

46. Taylor, J., Carraway, M., and Piantadosi, C. 1998. Lung-specific induction of heme oxygenase-1 and hyperoxic lung injury. *Am. J. Physiol.* 274:L582 - L590.

47. Otterbein, L., Kolls, J., Mantell, L., Cook, J., Alam, J., and Choi, A. 1999. Exogenous administration of heme oxygenase-1 by gene transfer provides protection against hyperoxia-induced lung injury. *J. Clin. Invest.* 103:1047 - 1054.

48. Blackwell, T.S., Hipps, A.N., Yamamoto, Y., Han, W., Barham, W.J., Ostrowski, M.C., Yull, F.E., and Prince, L.S. 2011. NF-κB signaling in fetal lung macrophages disrupts airway morphogenesis. *J. Immunol.* 187:2740-2747.

49. Thébaud, B., Ladha, F., Michelakis, E.D., Sawicka, M., Thurston, G., Eaton, F., Hashimoto, K., Harry, G., Haromy, A., Korbutt, G., et al. 2005. Vascular endothelial growth factor gene therapy increases survival, promotes lung angiogenesis, and prevents alveolar damage in hyperoxia-induced lung injury. *Circulation* 112:2477-2486.

50. Kunig, A.M., Balasubramaniam, V., Markham, N.E., Seedorf, G., Gien, J., and Abman, S.H. 2006. Recombinant human VEGF treatment transiently increases lung edema but enhances lung structure after neonatal hyperoxia. *Am. J. Physiol. Lung Cell. Mol. Physiol.* 291:L1068-L1078.

51. Li Volti G.S.D., Sangras B, Vanella A, Mezentsev A, Scapagnini G, Falck J.R., Abraham N.G., 2005 May-Jun. Carbon monoxide signaling in promoting angiogenesis in human microvessel endothelial cells. *Antioxid. Redox. Signal.* 7:704-710.

52. Choi, Y.K., Kim, C.-K., Lee, H., Jeoung, D., Ha, K.-S., Kwon, Y.-G., Kim, K.-W., and Kim, Y.-M. 2010. Carbon monoxide promotes VEGF Expression by increasing HIF-1α protein level via two distinct mechanisms, translational activation and stabilization of HIF-1α protein. *J. Biol. Chem.* 285:32116-32125.

CHAPTER III

HEME OXYGENASE-1/CARBON MONOXIDE (HO-1/CO) SUPPRESSES THROMBUS MASS AND PLATELET-LEUKOCYTE AGGREGATION IN A MOUSE MODEL OF VENOUS THROMBOSIS

ABSTRACT

Deep venous thrombosis (DVT) formation instigates an inflammatory response, resulting in vessel wall damage and an increase leukocyte infiltration. The objective of this study was to understanding venous thrombosis and the relationship between thrombosis and inflammation during acute verses chronic venous thrombosis. Heme oxygenase-1 (HO-1) and its byproduct carbon monoxide (CO) are strongly induced in injured tissues are thought to have anti-inflammatory and anticoagulant properties by augmenting fibrinolysis and inhibiting platelet aggregation. Vascular injury activates endothelial cells and promotes expression of P-selectin (P-sel), von Willebrand factor (vWF) on vein wall of endothelial cells during stasis-induced DVT. However, whether HO-1/CO, P-sel and vWF plays a role in platelet recruitment in DVT remains elusive. We hypothesize that HO-1/CO modulates venous thrombosis through a combination of anti-inflammatory and anti-thrombotic effects in part through mitigating the expression of vWF and P-sel. We employed an inferior vena cava (IVC) ligation mouse model of venous thrombosis. HO-

$1^{+/+}$ and HO-$1^{-/-}$ mice underwent IVC-ligation for 48 hrs. WT animals were also exposed to 250ppm of CO for 7 days post-IVC ligation. Mouse blood was drawn via cardiac puncture and the infra-hepatic thrombus containing IVC was removed *in toto*. We examined serum levels of a soluble form of vWF and P-sel. vWF, P-selectin and inflammatory cytokine levels were measured in the venous wall by ELISA and qRT-PCR. Flow cytometry was used to measure expression of platelet and leukocyte surface markers, in order to determine the relative activation and binding of platelets and leukocytes in whole blood. Compared to HO-$1^{+/+}$, thrombus weights increased significantly in HO-$1^{-/-}$ mice and episodic low dose of CO treatment had a modest inhibitory effect on thrombus weight. We also showed P-sel and vWF levels in HO-$1^{-/-}$ IVC ligated mice plasma was significant increase compared to IVC-ligated HO-$1^{+/+}$ mice. Additionally, compared to IVC-ligated HO-$1^{+/+}$ mice, platelet-leukocyte aggregates were significantly increased in IVC-ligated HO-$1^{-/-}$ null mice. Furthermore, pro-inflammatory cytokines and chemokine (IL-6, CCL-2, CxCL-1 and CxCL-2) mRNA levels increased in IVC ligated HO-1 null mice. The application of low-dose CO for 7 days after IVC ligation decreased expression of these proinflammatory modulators in the venous wall and thrombus as well as leukocyte infiltration into the clot. These findings suggest that platelets binding to activate leukocytes contribute to the inflammatory milieu in thrombi of IVC-ligated mice. DVT strongly induce vascular-protective enzyme HO-1, the actions of which may mitigate inflammatory upregulation of leukocyte adhesion receptors such as P-sel and vascular modulator, vWF. Exogenous CO may also mitigate thrombosis by attenuating the accompanying inflammatory response.

INTRODUCTION

Venous thromboembolism (VTE), which comprises deep vein thrombosis (DVT) and pulmonary embolism (PE), is the third most common cardiovascular disease in the United States.[1] Current therapy primarily involves anticoagulation with heprin, followed by a vitamin K antagonist.[2] Although anticoagulant therapy is efficacious when used prophylactically, it carries a significant major bleeding when used for long-term therapy.[3] There is increasing evidence that inflammatory process and DVT are closely interrelated.[4] It is known that during vascular injury, the endothelium is activated and promotes Weibel-Palade body (WPB) release and facilitates blood coagulation.[5,6] WPB stores P-selectin, von Willebrand factor (vWF) and other vascular modulators. vWF, a multimeric protein that mediates platelet adhesion to the vessel wall and platelet recruitment to the growing thrombus.[7] In arterial thrombosis, the role of vWF in the developing thrombus has been repeatedly demonstrated, and more recently the role of vWF in platelet recruitment in a mouse model of venous thrombosis was reported.[8] Research in various animal models suggests an integral association between inflammation and thrombosis. Specifically, a proinflammatory environment, which is mediated by cell adhesion molecules such as P-selectin and E-selectin.[9,10,11,12] The expression of P-selectin on the endothelial and platelet surface plays an important role in perithrombothic inflammation.[12] P-selectin allows for the interaction and recruitment of leukocytes and monocyte to thrombotic sites with fibrin deposition for thrombus stabilization and mediates leukocyte influx into areas of inflammation.[13,11]

Recent clinical and basic science studies have revealed that heme oxygenase-1 (HO) is involved in modulating a number of disease processes.[14,15] Heme oxygenases are the rate-limiting enzymes in the catabolism of heme into bilirubin, free iron, and carbon monoxide (CO), and exist in different isoforms.[16] HO-2 is thought to be constitutive, whereas HO-1 is inducible by various stimuli, such as cytokines and oxidants.[16] HO-3 is also involved in heme degredation, but is a less efficient heme catalyst than the other isozymes. Recently, compelling studies have shown that products of HO-1 activity possess antithrombotic properties, and impairment of HO-1 activity may contribute to thrombus formation.[17] Although the beneficial roles of HO-1 are not completely understood, these cytoprotective and anti-inflammatory effects of HO-1 are related to the formation of its end-products. CO, an odorless gas that is commonly viewed as an environmental poison, is produced endogenously by mammalian cells as a product of heme degradation by HO enzyme, of which HO-1 plays a homeostatic role in host defense and inflammation.[18] Several, experimental studies have also shown that non-toxic, low doses of CO exert anti-coagulant effects by affecting fibrinolysis[19], platelet aggregation[20,21] and by maintaining the integrity of the vessel wall.[22,23] Exogenous CO might prove beneficial in deep venous thrombosis by attenuating pro-inflammatory cytokines and chemokine production as well as neutrophil recruitment. However, the progression and time course of endothelial injury by stasis-induced venous thrombosis are not well represented by the models previously used in experimental studies evaluating CO and HO-1's cytoprotective effects. Therefore, the aim of this study was to examine the effects of pulsatile low-dose exogenous CO on stasis-induced venous thrombosis and delineate the role of HO-1 in leukocyte recruitment during acute and chronic thrombus

formation. In addition, we examined the effects of HO-1/CO on key inflammatory modulators (p-selectin and vWF), cytokine and chemokine levels and peripheral whole-blood leukocyte-platelet aggregation. The results demonstrated that pulsatile CO treatment acutely reduced leukocyte recruitment to the vessel wall post-IVC ligation and endogenous CO production attenuates the inflammatory response and leukocyte-platelet aggregates. These studies provide a basis for further investigation of HO-1/CO treatment after stasis-induced venous thrombosis.

METHODS

Animals

A colony of homoxygous male HO-1–deficient mice ($HO\text{-}1^{-/-}$) bred on a C57BL/6 background for more than fifteen backcrosses was established at the University of Michigan.[24] Age- and sex-matched specific pathogen-free 8–10-wk-old male C57BL/6 mice were purchased from The Jackson Laboratory (Bar Harbor, ME). $HO\text{-}1^{-/-}$ generated by targeted disruption of the HO-1 gene was used[25] with $HO\text{-}1^{+/+}$ progeny serving as littermate controls. Colonies of mice were maintained by breeding $HO\text{-}1^{-/-}$ males with $HO\text{-}1^{+/-}$ females and genotype was confirmed by genomic PCR analysis of DNA extracted from tail clippings. All animals were housed in specific pathogen-free conditions within the University of Michigan Animal Care Facility. All animal experiments preceded in accordance with National Institutes of Health policies on the human care and use of laboratory animals and were approved by the University Committee on Use and Care of Animals at the University of Michigan.

Inferior vena cava stasis model of deep venous thrombosis

Experiments were performed in a recently described IVC ligated stasis mouse model for studying deep venous thrombosis.[26,27] In brief, animals were anesthetized using continuous flow of 5% isoflurane gas and 100% oxygen and placed on a temperature-

regulated heatpad to maintain body temperature at 37°C. Following a midline laparotomy to access the IVC and exteriorize the bowel and intestines, anesthesia was maintained using an inhalation mixture of 2% isoflurane and 100% oxygen. All dorsal branches were cauterized and venous side branches caudal to the left renal vein were ligated using 7–0 Prolene suture (Ethicon, Inc, Somerville, NJ). The abdominal wall was closed in a bilayer fashion with 5–0 Vicryl (Ethicon, Inc, Somerville, NJ) for abdominal muscles and Vetbond tissue adhesive (3 M Animal Care Products, St. Paul, MN) for the skin. Following euthanasia, the IVC containing the thrombus was carefully removed, weighed in miligrams (mg). The thrombus was then removed from the IVC and the vein wall and thrombus were weighed individually in miligrams (mg). All animals were euthanized at specific time points, post-thrombosis, for tissue harvest and blood collection.

Episodic administration carbon monoxide

Mice were intermittently treated with exogenous CO gas as follows. Cages were placed in a plexiglass exposure chamber immediately after competition of IVC ligation and exposed to 250ppm for 1 hour twice daily (balanced with air) or 21% oxygen and continuing for up to 7 days. This concentration of CO was based on previous reports of their use in different model systems.[24,28,29,30,31] Flow into the 5.70-ft^2 plexiglass chamber was maintained at rate of 12L/min. The final CO levels in the chambers (250 ppm) were monitored using a CO analyzer (Interscan Corporation). There were no fluctuations in the CO concentrations after the chamber had equilibrated. Ventilation was adjusted using an Oxycycler controller (Biospherix, Lacona, NY) to remove CO_2 so that it did not exceed

0.5%. Ammonia was removed by ventilation and activated charcoal filtration through an air purifier. At the end of the exposure period, mice were killed and IVC tissues were harvested for further analysis.

Thrombus containing Inferior vena cava weight measurement

After stasis induced IVC liagtion of HO-$1^{+/+}$ and HO-$1^{-/-}$ mice or empirically administered CO at 250ppm in air for 1 hour twice a day in breathing chamber, groups of mice were analyzed for different experimental conditions at each time point. This technique is an indirect measure of thrombus content. At sacrifice, IVC (including contents) was removed, weight and length were measured in milligrams (mg) and centimeter (cm), respectively, and then IVC was carefully stripped from the thrombus and both were weighed independently.

Histopathological evaluation, immunocytochemistry and morphometric analysis

Thrombus containing IVC were excised, fixed in 10% formalin for 2 hrs, then stored in 70% ethanol prior to embedding in paraffin. Five μm sections were cut and stained with hematoxylin and eosin, visualized under light microscopy and images were captured using MetaMorph version 7.0r3 software (Molecular Devices, Sunnyvale, CA) on an Eclipse TE2000-E microscope (Nikon Instruments, Melville, NY) at 400x magnification. Morphometric measurements of cross-sectional areas were performed to assess vein wall inflammatory cell infiltrate (total inflammatory cells, polymononucleated (PMNs),

monocte/macrophage, or lymphocytes). To ensure our result were unbias, a board-certified veterinary pathologist blinded to experimental conditions using a previously described thrombus surface organization scoring criteria[27] chose five representative high-powered fields (5HPFs) from a least three different sections from each experimental group were examined. Results from each 5HPF were added together for each section studied, and mean ± SEM was calculated for each experimental group. Immunocytochemistry for P-selectin and vWF was performed by immersion in 4% formalin, incubation with blocking serum, followed by incubation at 4^{o}C overnight with rabbit polyclonal stained for CD62P (Ab 59738 - Abcam, Cambridge, MA or vWF (A0082 – Dako, Carpinteria, CA) at as a primary antibody. A secondary antibody conjugated to a horseradish peroxidase-labeled polymer (EnVision+, HRP, Rabbit, catalog no. K4003, Dako, Carpinteria, CA) was further used. Slides were counterstained with hematoxylin, and images acquired with a 400x objective, and analyzed using MetaMorph image analysis software (Molecular Devices, Sunnyvale, CA) on an Eclipse TE2000-E microscope (Nikon instruments Inc).

Hematology

Blood was drawn from each experimental group via direct cardiocentesis into EDTA microtainer tubes (BD, Franklin Lakes, NJ). A complete hematological blood profile was run on 30μL using the CDC Technologies HEMAVET® Multispecies Hematology Analyzer (Drew Scientific, Inc. Oxford, CT). The hematologic parameter examined at outline on Table 1.

vWF and P-selectin analysis by enzyme-linked immunosorbent assay

Following IVC ligation and blood cell count analysis, EDTA (Becton Dickinson, and Co. Franklyn Lakes, NJ) treated whole blood samples were spun down and plasma was processed according to the manufacturer's instructions. Aliquots of plasma from varying experimental groups were measured for vWF (Perkin Elmer, Waltham, MA) and soluble P-selectin (R&D systems Minneapolis, MN) post-thrombus induction and exogenous carbon monoxide exposure. Plasma vWF antigen levels were determined by AlphaLISA custom designed kit, using a polyclonal anti-human vWF antibody (DAKO, Glostrup, Denmark) conjugated to Alphalisa acceptor beads and well as biotinylated anti-human VWF antibody (also DAKO) to interact with streptavidin coated donor beads. AlphaLISA signals were determined on an EnSpire 2300 Multimode Plate reader (Perkin Elmer), and VWF levels were calculated by comparing signals to a dilution series of C57BL/6J plasma. All vWF levels are reported as a percent of C57BL/6J plasma and samples were assayed at least 3 times.

Flow cytometry

To assess platelet-leukocyte aggregates a 6-color flow cytometry assay was used to measure the interdependence of both platelets and leukocytes in this model. Whole blood from each animal was collected from the retro-oribital plexus of each experimental group and assayed for flow cytometry by standard techniques. Total cell counts were assessed by Hemavet hemocytometer (Drew Scientific) and reconfirmed by flow cytometry analysis using PerCPCy5.5-anti mouse CD45 antibody (BD Bioscience, Franklin Lakes,

NJ) and absolute count standard beads (BD Bioscience). Neutrophils were stained using APC-Cy7-anti-mouse Ly6G/Ly-6C (Gr-1) and monocyte/macrophage were detected using APC-anti-mouse CD11b. Within the CD11b/CD45 and Gr-1/CD45 positive-double events, subpopulation was identified using rat anti-mouse CD41 (platelet glycoprotein (GP) IX)- PE antibody to label platelets; the activation of platelets bound to leukocytes was assessed by counting CD62P (P-selectin) – fluorescein isothiocyanate (FITC)-positive events. Activated platelet –monocyte (CD11b-APC/CD41-PE/CD62P-FITC) and activated platelet–neutrophil (GR-1-APC-Cy7/CD41-PE/CD62P-FITC) aggregates were calculated from CD41-PE/CD62P double positive gates. Antibody specificity was verified using an appropriate isotype-labeled antibody (anti–rat IgG2a or anti–rat IgG2b). Erythrocytes were depleted from the preparations with BD FACS lysing solution (BD). Flow cytometric measurement was performed on a FACSCanto (BD) using DIVA software. All antibodies were purchased from BD Bioscience. Dead cells were excluded with DAPI (Sigma-Aldrich, St. Louis, MO). Files were analyzed in FlowJo (Tree Star, San Carlos, CA).

Quantitative reverse-transcription PCR

RNA was isolated from the whole IVC using the RNEasy MicroKit (Qiagen, Valencia, CA) or TRIzol (Invitrogen, Carlsbad, CA) according to manufacturer's instructions. cDNA was prepared with Superscript II (Invitrogen). Quantitative PCR was performed with TaqMan (Applied Biosystems, Carlsbad, CA) per manufacturer's instructions, and the ABI Prisim 7500fast sequence detection system (Applied Biosystems, Carlsbad,CA).

Real-time PCR was run on the cDNA template according to the manufacturer's protocol for β-actin (house keeping gene). Relative expression was calculated using the ΔΔ threshold cycle method. All the primers used for qRT-PCR were purchased from Invitrogen.

Statistical analysis.

Representaive data was displayed as mean ± SEM, with the numbers of experiments performed provided in the figure legends. Comparison of results between different groups with more than 2 conditions were compared using a one-way analysis of variance (ANOVA) or a Mann-Whitney U test, as appropriate, using GraphPad Prism software (LaJolla, CA). To discern differences between specific groups, Newman-Keuls test was used. Values were considered significantly different when $P \leq 0.05$.

RESULTS

Pulsatile exposure of low dose carbon monoxide decrease thrombus mass and inflammatory cells in the vein wall post IVC-ligation.

We previously reported an essential role for CO during an orthotopic lung transplant model [32] and double-lumen airway transplant model for studying chronic airway rejection.[24] To assess if carbon monoxide decreases thrombus mass and mitigates inflammatory cell trafficking into the vein wall, we used C57BL/6 mice as wildtype control group and performed a time course and exposed mice to empirical low dose twice a day of 250ppm of CO in 21% oxygen to determine at which time point CO decrease thrombus weight. Thrombus size was smaller in the CO+N exposed wild type mice as compared with normoxia exposed wild type mice at 7day of exposure **(Fig 1A).** We then performed hematoxylin and eosin staining on the thrombus containing inferior vena cava sections 7-day post IVC-ligation and exposure of CO+N. In the 7-day CO+N exposed wildtype group, we observed decreased vein wall and inflammatory cells and compared to the 7day N exposed wild type **(Fig 1B,C).** Morphometric analysis revealed at day 7 in shams (N and CO+N) and IVC-ligated (N and CO+N) groups, CO treatment significantly decreased vein wall monocytes and lymphocytes post-IVC ligation compared to normoxic exposed mice. In contrast, vein wall polymorphonuclear cells (neutrophils) show a trend towards a decrease during CO+N treatment **(Fig 1D-G).** These data demonstrate that

exogenous CO shown to have a remarkable salutary effect on the thrombus formation, reduce expression of inflammatory cells especially leukocyte traffic, and thrombus mass.

Heme oxygenase -1 deficiency is affected by thrombogenesis and leukocyte infiltration into the vein wall

Since arterial thrombosis only occurred in HO-1-/- mice and CO, a product of HO-1, has been implicated in venous thrombosis[17], we further investigated the role of endogenous CO production via absence of HO-1 in acute venous thrombogenesis model in which HO-1 null mice subjected up to 7 day of IVC-liagtion and thrombus mass and inflammatory cell accumulation in the vessel wall was measured **(Fig 2).** Quantitative RT-PCR measurement show an increase in HO-1 mRNA and thrombus mass at 48hrs post-IVC ligation in wild type C57BL/6 mice **(Fig 2 A, B).** Our finding is in accordance with previous report that demonstrated HO-1 mRNA was strongly induced at 24hrs and 48hrs following IVC-ligation.[17] Using 48hrs IVC-ligated acute venous thrombosis model we performed all ligations in HO-1 null mice using 48hr model. **Fig 2C** depicts an enlarged thrombus containing IVC for HO-$1^{-/-}$ stasis-induced venous thrombosed mice compared to HO-$1^{+/+}$ IVC-ligated mice. In addition, thrombus mass was also markedly increased in HO-1 null mice compared to HO-$1^{+/+}$ IVC-ligated mice **Fig 2D**. Thus, ligation of the inferior vena cava at 48hrs promotes increase in thrombogenesis by increasing expression of HO-1, thereby causing an increase in thrombus mass in HO-1 deficient mice. To evaluate the inflammatory cells in the vein wall at 2day post IVC-

ligation, similar to **Fig 1B,C** we evaluated thrombus containing IVC histologic and morphometric profiles using H&E and selecting five high powered field around the vein wall to assess leukocyte accumulation, respectively (**Fig 3**). H&E analysis revealed significant thicker vessel wall and more prominent inflammatory cell infiltration in HO-$1^{-/-}$ compared to HO-$1^{+/+}$ 48hrs post IVC-ligation (**Fig 3A-D)**. Morphometric evaluation of vein wall showed statistically more neutrophils (12.8±.47 vs 6.2±.25 cells/5HPFs, $P<0.05$) and total inflammatory cell (14.7±.3 vs 9.8±.15 cells/5HPFs, $P<0.05$) in the vein walls of HO-$1^{-/-}$ 48hrs compared to HO-$1^{+/+}$ animals (**Fig 3 E, G).** In contrast, vein wall monocyte/macrophages and lymphocytes were not increased at 48hrs following IVC-ligation (**Fig 3 F, H).** These data indicate that heightened inflammatory response is primarily due to neutrophil influx not the monocytes macrophages. It is possible to conclude that monocytes may recruited to the vein wall/thrombus interface at a later time point following thrombus.

Peripheral whole-blood hematology profile following IVC-liagtion

To verify exaggerated inflammatory accumulation observed in HO-$1^{-/-}$ mice subjected to IVC-ligation, we examined hematological profile of all 4 groups. The normal reference range previously reported for mice for peripheral blood cell counts were normal between the sham-operated HO-$1^{+/+}$ and HO-$1^{-/-}$ animals. In contrast, peripheral neutrophil, monocyte, lymphocyte, and red blood cell were significantly different between IVC-ligated HO-$1^{+/+}$ and HO-$1^{-/-}$ mice (**Table 1**). Interestingly, HO-$1^{-/-}$ showed a trend towards an increase in circulating platelet counts (282±41 vs 195±37 K/μL p=ns, respectively)

and also showed significant increase in mean platelet volume (7.5± .35 vs 6.2±.29 fL $p<0.05$, respectively) compared to HO-$1^{+/+}$ IVC-ligated animals (**Fig 4A, B**).

Circulating and vein wall P-selectin and vWF following IVC-ligation are increased in HO-$1^{-/-}$ mice and decreased during treatment to low dose of carbon monoxide

To test wether P-selectin or vWF play a role in the development of DVT, we employed our model of venous thrombosis on HO-$1^{+/+}$ and HO-$1^{-/-}$ mice and treated wildtype mice with empirically low dose of CO to measure levels of these two inflammatory mediators. Immunocytochemical staining indicated P-selectin and vWF were both localized in vein wall of HO-$1^{+/+}$ and HO-$1^{-/-}$ IVC-ligated mice **(Fig 5A-D).** Interestingly, HO-$1^{-/-}$ IVC-ligated animals had larger vessel wall and slightly modest increase in localized staining of both P-selectin and vWF compared to HO-$1^{+/+}$ mice **(Fig 5B,D).** One of the major precursors during an inflammatory response is the release of vWF and P-selectin from weibel-Palade body (WPB). The interaction of P-selectin, its receptors PSGL-1 and vWF facilitate platelet rolling leukocytes and thrombus amplification. Therefore, we hypothesized that exogenous CO treatment or endogenous CO release from HO-1 null mice may reduce the release of these vascular mediators caused by IVC-ligation. We measured soluble levels of P-seletin and vWF using ELISA. We show that in HO-$1^{-/-}$ IVC-ligated mice had a modest increase in P-selectin (4.2±0.59 vs 3.7±0.7 ng/mg $p<0.05$) expression and as well as a significant increase in vWF (263±18.4 vs 151± 21.7 ng/mg $p<0.05$) compares to HO-$1^{+/+}$ IVC-ligated animals **(Fig 6A,B).** Concordantly, pulsatile dose of CO administered twice a day for up to 7days, resulted in significant

decrease in both P-selectin (0.42±.09 vs 0.72±0.14 ng/mg $p<0.05$) and vWF (102±13 vs 187±19.5 ng/mg $p<0.05$) levels compared to normoxic exposed wild type mice **(Fig 6C,D).** Taken together, our results demonstrate that absence of HO-1 or exogenous treatment of carbon monoxide plays a role in mitigating leukocyte infiltration into the vessel wall by regulating P-sel and vWF.

IVC-ligation enhances the accumulation of platelet-leukocyte aggregates following ligation of IVC in HO-$1^{+/+}$ and HO-$1^{-/-}$ mice.

Previous work in venous thrombosis has showed recruitment of inflammatory leukocytes also can involve thrombosis.[17] Animal studies utilizing rat and mouse thrombosis models have demonstrated the upregulation of P-selectin in the vein wall as early as six hours after thrombus induction.[26] P-selectin on activated platelets is a major mediator of adhesion to leukocytes.[33] Because the role of P-selectin in venous thrombosis was previously reported, we sought to investigate the role of platelet-leukocyte interactions in our model of venous thrombosis in the absence of HO-1 by using a 5-color flow cytometry. The percentage of monocyte/macrophage and neutrophils found aggregated with platelets in blood obtained from IVC-ligated HO-$1^{-/-}$ vs HO-$1^{+/+}$ mice was approximately 3.2 fold and 5 folds higher, respectively **(Fig 7A,B).** The number of P-selectin-positive platelets in the blood of thrombus induced HO-$1^{-/-}$ mice was not different from that of HO-$1^{+/+}$ mice (data not shown). However, the absolute cell counts for platelet-monocyte (595±13.7 vs 302±14.8, $P<0.05$) and Platelet-neutrophils (196±24.2 vs 92±15.7, $P<0.05$) was significantly greater in HO-$1^{-/-}$ vs HO-$1^{+/+}$ IVC-

ligated mice. These data indicates HO-1 null mice subjected to IVC-ligation had an increase in the number of leukocytes, particularly monocytes and neutrophils, and thrombosis resulted in accumulation of aggregation of leukocytes to platelets.

Effects of thrombogenesis on vein wall proinflammatory cytokines and chemokine mediators on IVC mRNA expression

We examined the effects of HO-1 knockout on IVC-ligation by isolating total IVC mRNA and measured levels of pro inflammatory cytokines and chemokine via quantitative RT-PCR. Following IVC-ligation HO-$1^{-/-}$ mice showed an increase in IL-6, CCL-2, CxCL-1 and CxCL-2 **(Fig 8A-D)**. Pulsitile treatment of CO twice a day to wild type mice, demonstrated no significant decrease in IL-6 and CxCL-2 **(Fig 8E,H)**. However, two genes related to macrophage and neutrophil recruitment to the vessel wall during injury (CCL-2 and CxCl-1), were significantly downregulated by CO treatment **(Fig 8F,G)**. As reported previously[17], in a chronic model of venous thrombosis in the absence of HO-1, thrombosis increased the expression of these key proinflammatory mediators that we examined, suggesting exogenous and endogenous CO production suppresses inflammation by regulating proinflammatory cytokines and chemokines.

DISCUSSION

The dynamic and complex balance that exists between thrombosis and inflammation during thrombogenesis plays a pivotal role in the pathogenesis of DVT. Using a well-established and widely employed model of stasis-induced venous thrombosis, the present study demonstrates that stress-induced enzyme HO-1 and its byproduct CO, attenuates thrombus formation and mitigates leukocyte influx into the vessel wall. Absence of HO-1 was associated with significantly increased thrombus size and leukocyte influx. The increase in thrombus cellularity with deletion of HO-1 is consistent with other experimental model of venous thrombosis.[34,17,35,8] Our findings also showed that platelets binding to activate leukocytes might contribute to the inflammatory milieu in thrombi of HO-1 deficient IVC-ligated mice. This increase of vascular wall thrombogenicity may directly result from the marked upregulation of leukocyte adhesion receptors P-selectin and the induction of prothrombotic modulator, von Willebrand factor.

Thrombus formation initiates a local inflammatory response.[36,37] During the acute stages of inflammation, neutrophils are the predominant cellular responder. Over time, monocytes increase at the site of thrombosis and are important in proteolytic digestion and resolution of the thrombus components.[38,39,40] The differential role of the monocytes in the vessel wall response and thrombus resolution after IVC-ligation has been previously reviewed.[41,36] Counterintuitively; a greater monocyte number is not necessarily associated with greater vein wall injury. In a rat model of stasis induced

venous thrombosis, P-selectin inhibition was associated with increased vein wall monocyte accumulation, but decreased stiffness and fibrosis.[42] Monocyte subtypes may confer a pro- or antiinflammatory state depending on the local environmental ques.[43] Using morphometric analysis of leukocyte cell migration through the vein wall during thrombosis, we demonstrated that acute and chronic inflammatory patterns in both HO-1 null mice and wildtype mice exposed to empirical low dose of CO for up to 7days in this study. In this study, HO-1 deficient mice increased the recruitment of PMN in the vessel wall 48hrs post-IVC ligation. In addition, neutrophil migration through the vein wall show a trend towards decrease during pulsatile CO administration. In contrast, in the absence of HO-1, monocytes showed a gradual but not significant increase in migration 48hrs post- IVC ligation, compared to HO-$1^{+/+}$ mice. The increase in vein wall monocyte extravasation occurred by day 7, surpassing neutrophil levels by 7days post-IVC ligation in HO-1 null mice (data not shown). These results demonstrate that induction of HO-1 can modulate the early, and acute inflammatory response to a direct vascular injury post venous thrombosis.

In previous studies, in which arterial thrombosis was induced in HO-1 deficient mice under conditions of oxidative stress, hemin administration resulted in arterial clot formation, which was hastened in HO-$1^{-/-}$ mice.[44] Similar to our results, one study demonstrated that genetic deficiency of HO-1 impaired thrombus resolution and exaggerated the inflammatory response to thrombus formation 10 day post stasis induced thrombosis and they also show that clot size at day 2 was not different in HO-$1^{+/+}$ and HO-$1^{-/-}$ mice.[17] The investigators also suggested that the exaggerated clot size that was

observed in the HO-1$^{-/-}$ mice following stasis induced venous thrombosis may not be ascribed to an inherent, pre-existing, hemostatic defects present in the mutant strain.[17] In acute stasis-induced venous thrombosis, IVC-ligated HO-1 deficient model used in our study demonstrated a significantly larger thrombus and increase neutrophil recruitment at 48hr post IVC-ligation. With this model, neutrophil, monocytes, lymphocytes and platelets count in hematologic profiles represented in Table 1, contributes significantly to the pro-thrombotic milieu 48hrs post- IVC ligation. The increase in mean platelet volume observed in HO-1 null mice post IVC-ligation provided a concordant increased supply of P-selectin, and vWF, which results in a pro-thrombotic environment within these mice. Mean platelet volume has been identified as a prognostic marker for inflammatory conditions and thrombosis.[45] Taken together, this finding suggests that increase in platelet number in the HO-1 IVC ligated animals may occur during inflammatory events where platelets are being consumed.

When HO-1 activity is suppressed, proinflammatory heme would accumulate and trigger endothelial cell activation and the expression of proinflammatory genes presumably involved in the pathogenesis of DVT.[46] One possible explanation for the requirement of HO-1 to suppress venous thrombosis is that HO-1 enzymatic function is necessary to eliminate proinflammatory free heme as it accumulates through release of oxidized hemoglobin post-IVC ligation. An alternative but not mutually exclusive explanation would be that HO enzymatic activity is needed to generate one or more of the end-products of heme catabolism, e.g. bilirubin, free iron that leads to ferritin expression, and/or CO. These antiinflammatory molecules would then abrogate the proinflammatory

responses that lead to DVT. Our study favored the second hypothesis and tested directly whether the exogenous treatment of CO would account for the protective effect of HO-1 in preventing thrombus formation and leukocyte accumulation. CO has been shown to be protective in multiple models of injury, including vascular injury[47], transplantation[48] and ischemia-reperfusion.[19]

Experimental studies have rarely addressed the effects of CO on the relatively acute and chronic development of injury in response to vascular insult to the vein wall during venous thrombosis. Leukocyte trafficking is dependent on a number of factors affecting activation, chemoattraction, and attachment of the cells. The specific mechanisms by which CO can affect neutrophil migration from the peripheral blood to the vein wall have not been fully characterized. Previous reports have documented that the expression of adhesion molecules including P-selectin[17] is modulated by HO-1 and that CO-releasing molecules mediated anti-thromboic effects *in vivo* by inhibition of platelet mediated thrombus formation.[49] The results of our studies suggested that exposure to pulsatile low dose of CO fully suppressed P-selectin and vWF plasma levels. This data suggests that CO can fully substitute for the protective effect of HO-1 in this model. This data also suggests that the major mechanism by which HO-1 prevents inflammatory cell infiltration may not involve elimination of free heme but rather the generation of one of the end products of heme catabolism by HO-1, e.g., CO. We do not exclude that other end products of HO-1 activity, e.g., iron/ferritin and bilirubin, may contribute to prevent venous thrombus formation as well. However, our present data shows that CO alone can fully substitute for HO-1.

To address the question weather HO-1 deficiency would affect platelet-leukocyte aggregation, we employed a 5-color flow cytometry system to define interdependence between circulating platelets and inflammatory cells in a stasis model of venous thrombosis. In our study, we were able to consistently show that platelet specific marker, CD41, binds to neutrophils and monocytes in the peripheral blood, which likely promote adhesion to endothelial cells and the induction of vascular injury in IVC-ligated HO-1 deficient mouse model. The analysis of platelet-leukocyte aggregates revealed more platelets bound to monocytes than neutrophils in the absence of HO-1 post IVC-ligation. These observations provide some evidence that P-selectin-positive platelet-leukocyte aggregates tether and roll on endothelial cells with higher avidity than single leukocytes, thereby exacerbating endothelial inflammation. Thus the binding of multiple platelets associated with the increased monocytes adhesive and oxidative activities may represent a newly recognized mechanism contributing to monocyte/macrophage activation in the peripheral blood in vivo.

To further distinguish the role of HO-1 and CO in this model, we studied key inflammatory cytokine and chemokine's post IVC ligation in HO-1 deficient mice and episodic CO administration in WT mice. One of the main inflammatory cytokines that we studied, IL-6 has been demonstrated to play a role in stasis induced venous thrombosis.[50] Systemic neutralization of IL-6 during early stages of venous thrombosis, using the IVC ligation mouse model, modulates CCL-2 (also known as monocyte chemotactic protein-1

(MCP-1)) expression and is responsible for monocyte recruitment and ultimately modulates thrombus resolution.[50] Based on this information, we hypothesized that HO-1 deficiency would upregulate IL-6, CCL-2 and other inflammatory chemokine's post venous thrombosis. Our study further substantiates, the absence of HO-1 regulates the expression of IL-6, CCL-2, CxCL-1 (KC) and CxCl-1 (MIP-2). In contrast, episodic low dose of CO decreased expression of these key inflammatory mediators. All together, our findings suggest that intermittent administration of CO over short exposure times would be beneficial and we also demonstrated that the degree of vascular injury also dictated the relative efficacy of CO treatment. However, it is important to note that inflammatory response may also vary with the age, gender, and genetic background of the mouse[51], suggested that a number of additional studies would be required to completely understand the effectiveness of CO treatment post IVC ligation. The present studies cannot rule out the possibility that CO would be even more effective in models producing less inflammation or more focal injury. In any case, it would appear important to examine the effects of CO treatment at early and later time points to fully evaluate HO-1/CO role in acute venous thrombosis.

In conclusion, vascular HO-1 with the release of CO attenuates thrombus formation, most probably via the modulation of P-selectin and vWF expression on endothelial cells. HO-1 and CO have differential roles in leukocyte infiltration post IVC-ligation and HO-1 deficiency appears to promote platelet-leukocyte aggregates by a CO-independent mechanism as HO-1 induces key adhesion molecules. These data suggest several possible mechanisms, including other byproduct of heme oxygenase. The

protective effects are likely to be multifactorial. Although new therapies are on the horizon for DVT treatment, these all primarily target the coagulation cascade, and the bleeding risk remains.[2] Indeed, a concern of those new agents is the lack of antidotes.[52] The next generation of DVT therapy should have rapid onset, require little monitoring, and have little bleeding risk. Further delineation of mechanisms associated in HO-1/CO anti-inflammatory and anti-thrombotic effects holds promise as a therapeutic adjunct in the treatment of venous thrombosis.

FIGURES

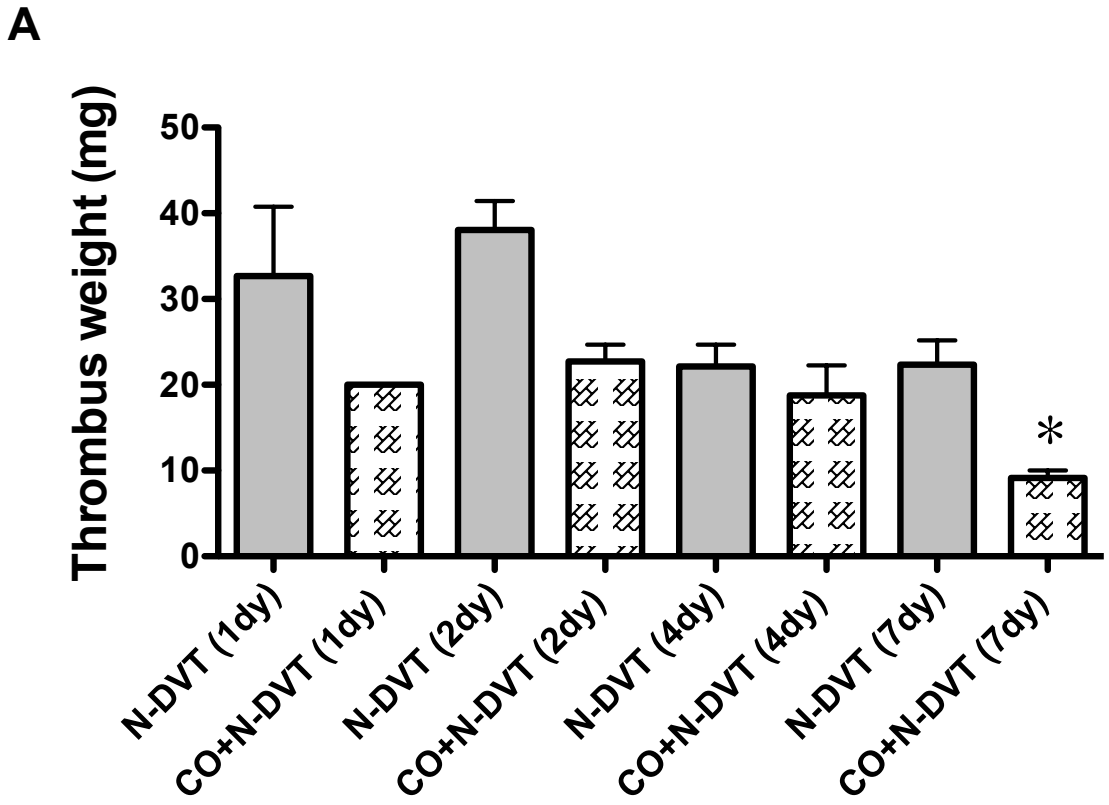
A
Thrombus weight (mg)
50
40
30
20
10
0
*
N-DVT (1dy)
CO+N-DVT (1dy)
N-DVT (2dy)
CO+N-DVT (2dy)
N-DVT (4dy)
CO+N-DVT (4dy)
N-DVT (7dy)
CO+N-DVT (7dy)

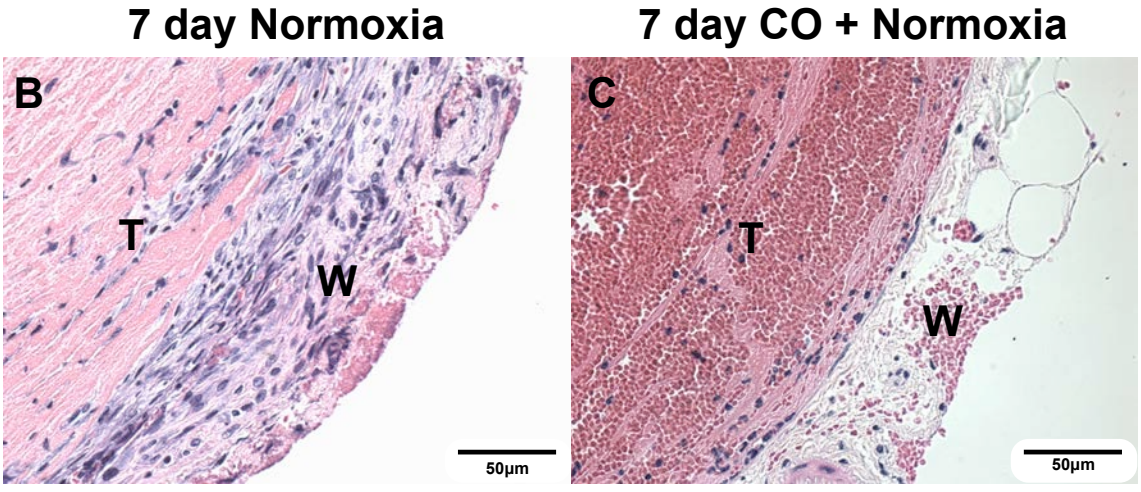
7 day Normoxia
7 day CO + Normoxia
B
T
W
50µm
C
T
W
50µm

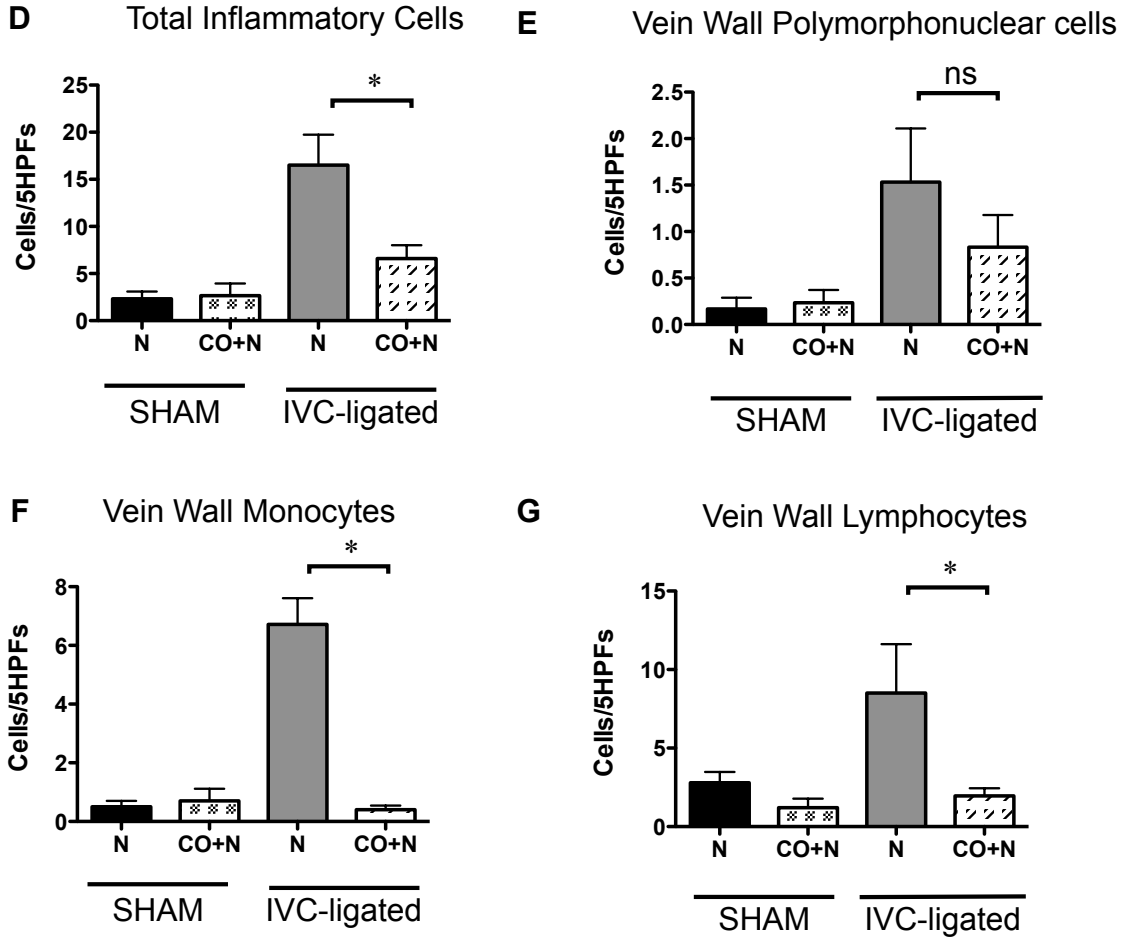
D
Total Inflammatory Cells
Cells/5HPFs
25
20
15
10
5
0
*
N
CO+N
N
CO+N
SHAM
IVC-ligated
E
Vein Wall Polymorphonuclear cells
Cells/5HPFs
2.5
2.0
1.5
1.0
0.5
0.0
ns
N
CO+N
N
CO+N
SHAM
IVC-ligated
F
Vein Wall Monocytes
Cells/5HPFs
8
6
4
2
0
*
N
CO+N
N
CO+N
SHAM
IVC-ligated
G
Vein Wall Lymphocytes
Cells/5HPFs
15
10
5
0
*
N
CO+N
N
CO+N
SHAM
IVC-ligated

FIGURE III.1: PULSATILE EXPOSURE OF LOW DOSE CARBON MONOXIDE DECREASE THROMBUS MASS AND INFLAMMATORY CELLS IN THE VEIN WALL POST IVC-LIGATION.

(A) Thrombus were harvested from C57BL/6 mice, exposed to normoxia (N - 21% Oxygen) or carbon monoxide (CO+N - 250ppm and 21% Oxygen) and thrombus weight were compared between days 1 to 7 post IVC-ligation. Thrombus size was smaller in the CO+N exposed wild type mice as compared with normoxia exposed wild type mice at 7day of exposure. All mice C57BLK6: 1d, n = 4-5; 2d, n = 11-20; 4d, n = 8-9; 7d, n = 8-11 per group. (B-C) Representative hematoxylin and eosin stained inferior vena cava sections of 7-day wild type samples exposed to either N or CO+N. Note the decreased vein wall and acellularity in the 7 day CO+N compared to the 7day N exposed wild type. Original magnification is 400X, scale bar = 50 μm. (T-Thrombus and W- vein wall). (D-G) Morphometric evaluation of inflammatory cells in the vein wall of five high-powered fields (5HPFs) at day 7 in Shams (N and CO+N) and IVC-ligated (N and CO+N). CO exposure significantly decreased vein wall inflammatory cells post-IVC ligation compared to normoxic exposed mice (N =17-25 per group). All results represents mean ± SEM of tissue harvested from indicated number of mice. *Different from normoxia, $P<0.05$. All data were assessed by one-way ANOVA.

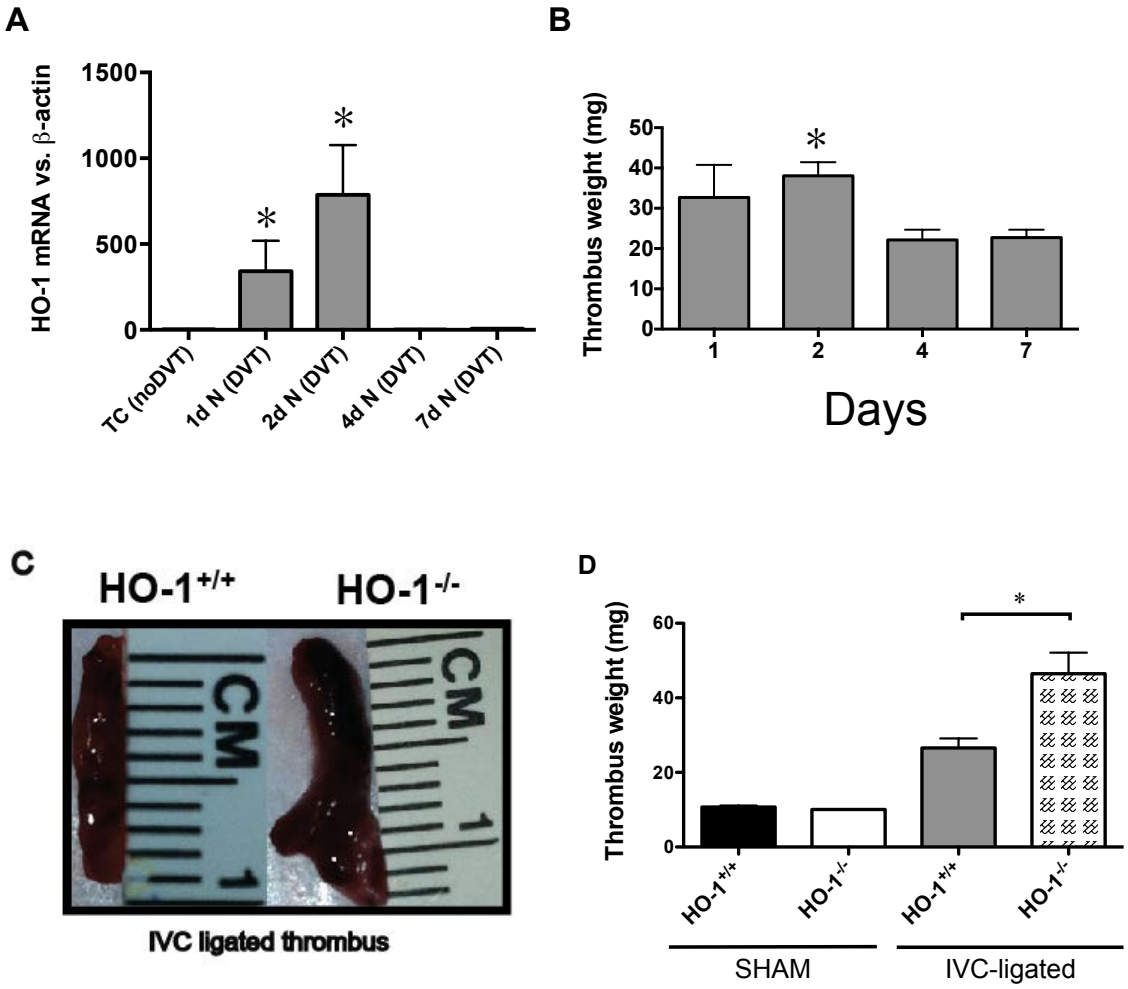

FIGURE III.2: HEME OXYGENASE -1 DEFICIENCY IS AFFECTED BY THROMBOGENESIS.

(A) Real-time reverse transcriptase polymerase chain reaction of HO-1 mRNA in WT mice exposed to normoxia from 1-7 days following IVC ligation. HO-1 mRNA is significantly increased at 2dy. (N =8-11 per group) TC, true controls (mice that did not receive ligation). *Different from WT 1 day IVC ligated $P<0.05$. (B) Thrombus weight in WT mice at 1-7 days following the thrombogensis was significantly different at 2dy post-IVC ligation. (N =11-20 per group) (C) Representative photograph of 48hr HO-$1^{+/+}$ IVC-

ligated thrombus (left) and HO-1$^{-/-}$ stasis-induced venous thrombosis (right). D, Weight, in miligrams of thrombus harvested from sham-operated and stasis-induced venous thrombosis in HO-1$^{+/+}$ and HO-1$^{-/-}$ mice at 48 hours (Sham: HO-1$^{+/+}$, n = 11; HO-1$^{-/-}$ n = 9. IVC-ligated: HO-1$^{+/+}$, n = 13; HO-1$^{-/-}$ n = 14). Bars represent mean ± SEM from tissue harvested from indicated number of mice. *Different from HO-1$^{+/+}$ IVC ligated $P<0.05$. All data were assessed by one-way ANOVA.

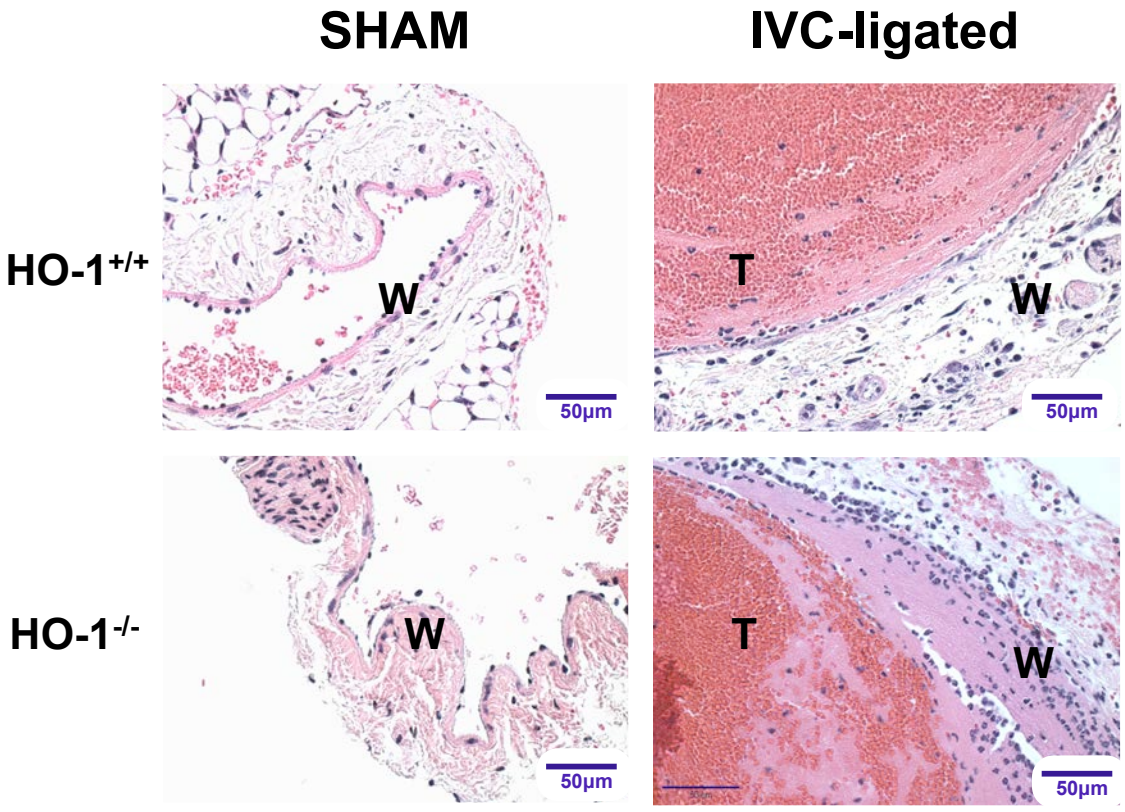
SHAM
IVC-ligated
HO-1+/+
HO-1-/-
W
T
50μm

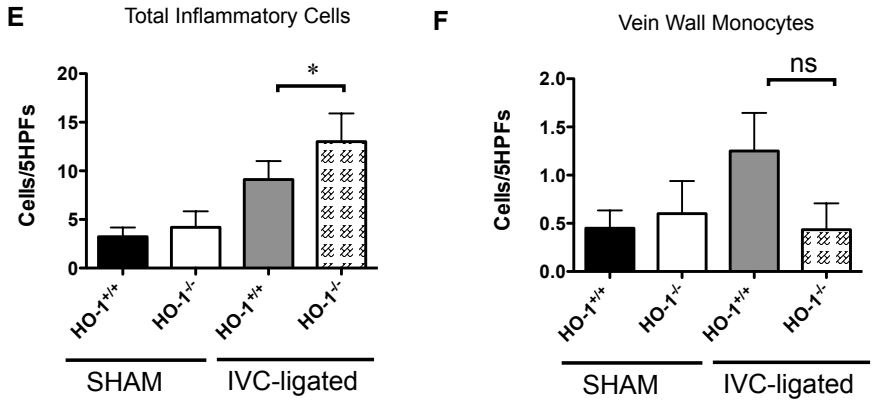
E
Total Inflammatory Cells
Cells/5HPFs
*
HO-1+/+
HO-1-/-
SHAM
IVC-ligated

F
Vein Wall Monocytes
Cells/5HPFs
ns
HO-1+/+
HO-1-/-
SHAM
IVC-ligated

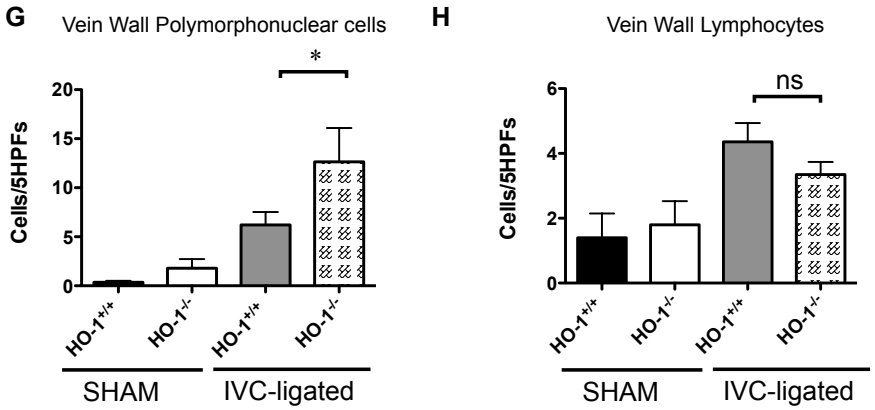
G
Vein Wall Polymorphonuclear cells
Cells/5HPFs
*
HO-1+/+
HO-1-/-
SHAM
IVC-ligated

H
Vein Wall Lymphocytes
Cells/5HPFs
ns
HO-1+/+
HO-1-/-
SHAM
IVC-ligated

FIGURE III.3: VEIN WALL HISTOLOGICAL EXAMINATION SHOWING THE AFFECT OF THROMBOGENESIS AND INFLAMMATORY CELL ACCUMULATION 48 HR POST-IVC LIGATION.

Representative hematoxylin and eosin stained inferior vena cava section of 48 hr sham operated (A and C) and thrombosed IVC (B and D) of HO-$1^{+/+}$ and HO-$1^{-/-}$ mice. (D) The venous wall of thrombus containing IVC of HO-$1^{-/-}$ mice show a markedly increase in leukocyte accumulation compared to HO-$1^{+/+}$ mice. (Magnification = original x400; scale bar = 50 μm. (T-Thrombus and W- vein wall). (E-H) Morphometric evaluation of inflammatory cell counts of five high-powered field in the vein wall of HO-$1^{+/+}$ and HO-$1^{-/-}$ mice 48h post IVC ligation and sham-operated controls. Total inflammatory cell (E), Monocyte/macrophage (F), Polymorphonuclear cells (neutrophils) (G), and lymphocytes (H) (n = 9-14 all groups). Bars represent mean ± SEM from tissue harvested from indicated number of mice. *Different from HO-$1^{+/+}$ IVC ligated $P<0.05$. All data were assessed by one-way ANOVA.

TABLE III.1: HEMATOLOGICAL PARAMETERS OBTAINED FROM HO-1$^{+/+}$ AND HO-1$^{-/-}$ MICE.

Animal Strains	WBC (K/uL)	NE(K/uL)	MO(K/uL)	LYM(K/uL)	RBC(K/uL)	HCT%	PLT(K/uL)
HO-1$^{+/+}$ SHAM	0.14-1.04 (0.41)	0.01-0.04 (0.02)	0.01-0.04 (0.02)	0.21-0.97 (0.43)	0.15-1.33 (0.60)	2.5-8.2 (3.8)	22-322 (135)
HO-1$^{-/-}$ SHAM	0.5-2.82 (1.39)	0.03-0.71 (0.17)	0.02-0.15 (0.07)	0.45-1.64 (1.08)	0.32-2.08 (0.88)	↑ **4.8-11.3 (7.13)**	164-363 (232)
HO-1$^{+/+}$ DVT	0.18-1.08 (0.49)	0.01-0.07 (0.03)	0.00-0.04 (0.02)	0.23-0.97 (0.49)	0.19-2.15 (0.84)	2.5-13.0 (5.56)	14-261 (132.5)
HO-1$^{-/-}$ DVT	↑ **1.15-3.6 (2.55)**	↑ **0.12-0.42 (0.27)**	↑ **0.09-0.3 (0.20)**	↑ **1.29-2.78 (2.04)**	0.75-0.89 (0.89)	3.5-4.1 (3.8)	↑ **162-421 (283)**

Blood samples from four mice were analyzed for each profile, and data are represented as mean ± SEM. Hematology values displayed as ranges and means. Bold numbers are arrows represent increase (upward arrow) seen in HO-1$^{+/+}$ and HO-1$^{-/-}$ 48 hrs post-IVC ligated mice.

WBC= White Blood Cells, NE = Neutrophils, MO = Monocytes, LYM = Lymphocytes, RBC = Red blood Cells, HCT = Hematocrit, PLT = Platelets.

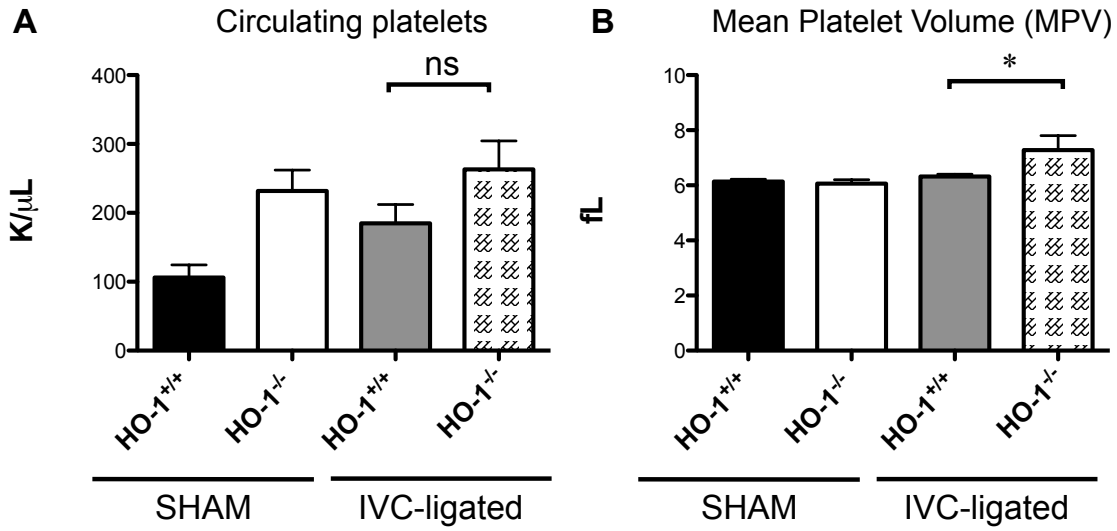

FIGURE III.4: CIRCULATING PLATELETS AND MEAN PLATELET VOLUME IN HO-1$^{+/+}$ AND HO-1$^{-/-}$ MICE 48 HR POST-IVC LIGATION.

(A-B) Circulating platelets and Mean platelet volume (MPV) levels at day 2 in sham-operated and IVC ligated HO-1$^{+/+}$ and HO-1$^{-/-}$ mice. HO-1$^{-/-}$ mice showed a trend towards increase in circulating platelet levels and MPV. (N = 5-8 per group) *Different from HO-1$^{+/+}$ IVC ligated $P<0.05$. All data were assessed by one-way ANOVA.

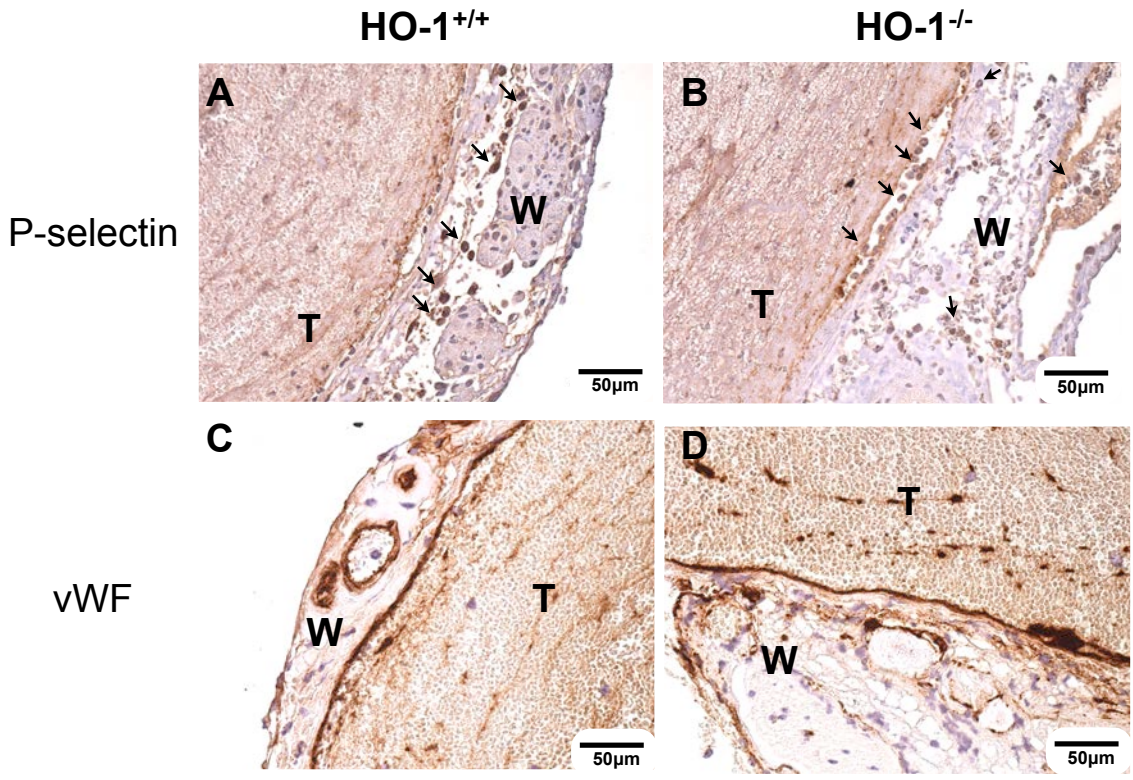

FIGURE III.5: IMMUNOHISTOCHEMISTRY IMAGES OF THROMBUS CONTAINING IVC STAINED WITH P-SELECTIN AND VWF 48HR POST-IVC LIGATION.

(A, B) IVC-ligated HO-$1^{+/+}$ and HO-$1^{-/-}$ mice stained with P-selectin (C, D) IVC-ligated HO-$1^{+/+}$ and HO-$1^{-/-}$ mice stained with vWF. Cells expressing P-selectin and VWF appear dark brown in color (indicated by dark arrows). Original Magnification x 200; scale bar = 50 μm. (T-Thrombus and W- vein wall).

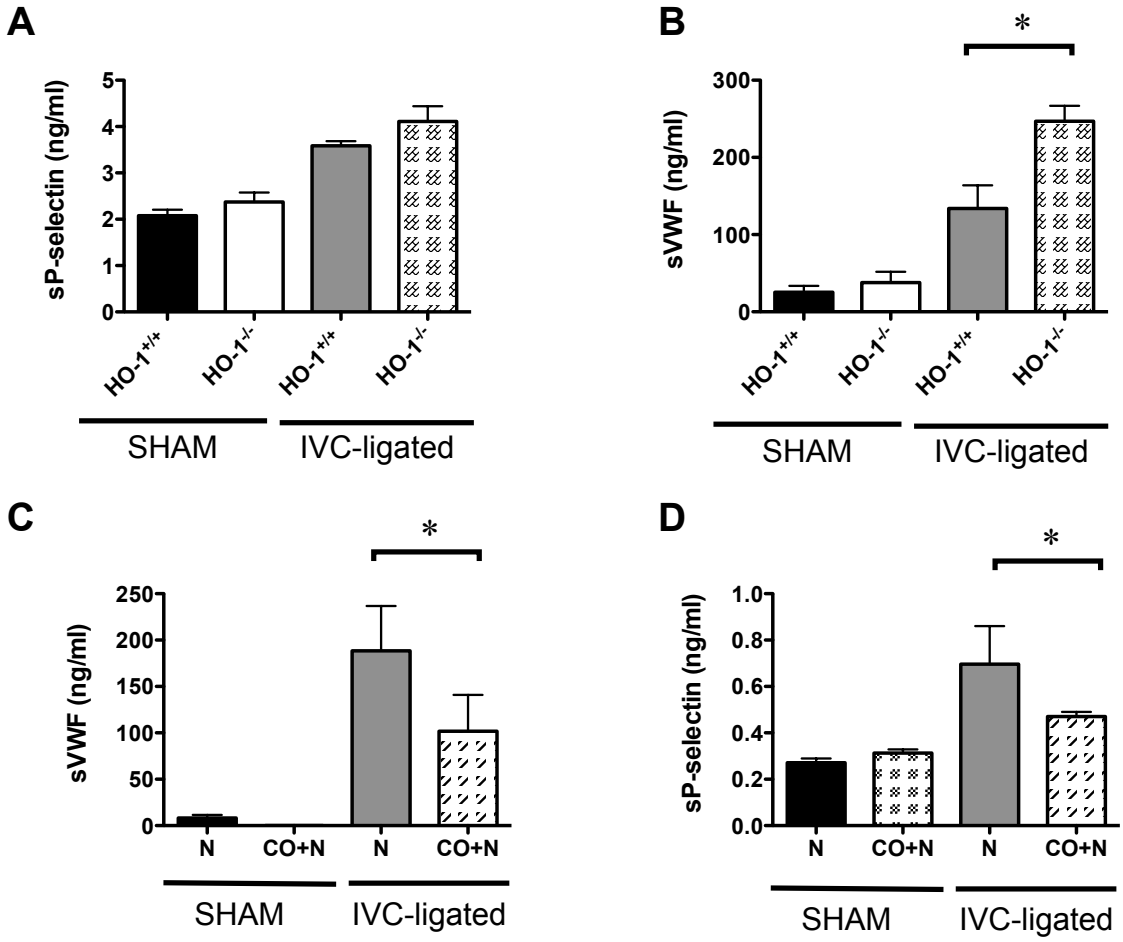

FIGURE III.6: ELISA MEASUREMENT OF SOLUBLE P-SELECTIN AND VWF FOLLOWING LIGATION OF THE INFERIOR VENA CAVA.

(A-D) Soluble P-selectin (sP-sel) and vWF was measure 48hrs post thrombogenesis in HO-$1^{+/+}$, HO-$1^{-/-}$ mice and wildtype mice exposed to normoxia (21% Oxygen) or episodic low dose of carbon monoxide (twice a day 1 hr exposure of 250ppm of CO and 21% normoxia) using ELISA based assay. (A) Sham – operated and IVC ligated HO-$1^{+/+}$ and HO-$1^{-/-}$ mice measuring sP-sel or vWF (B). (C) Sham – operated and IVC ligated wild type mice exposed to normoxia and carbon monoxide measuring sP-sel or vWF 7 days

post-IVC ligation and exposure. (D). The trends show increase levels of sP-sel and vWF in plasma of HO-$1^{-/-}$ mice 48hrs post-IVC ligation. Concordantly, plasma from thrombus containing IVC shows sP-sel and vWF was significantly decreased in CO+N compared to N exposed wildtype mice. HO-$1^{+/+}$ and HO-$1^{-/-}$ mice: N = 6-10 per group and Normoxia and CO+N: N = 3-5 per group. Bars represent mean ± SEM from tissue harvested from indicated number of mice. *Different from HO-$1^{+/+}$ IVC ligated or wildtype normoxia $P<0.05$. All data were assessed by one-way ANOVA.

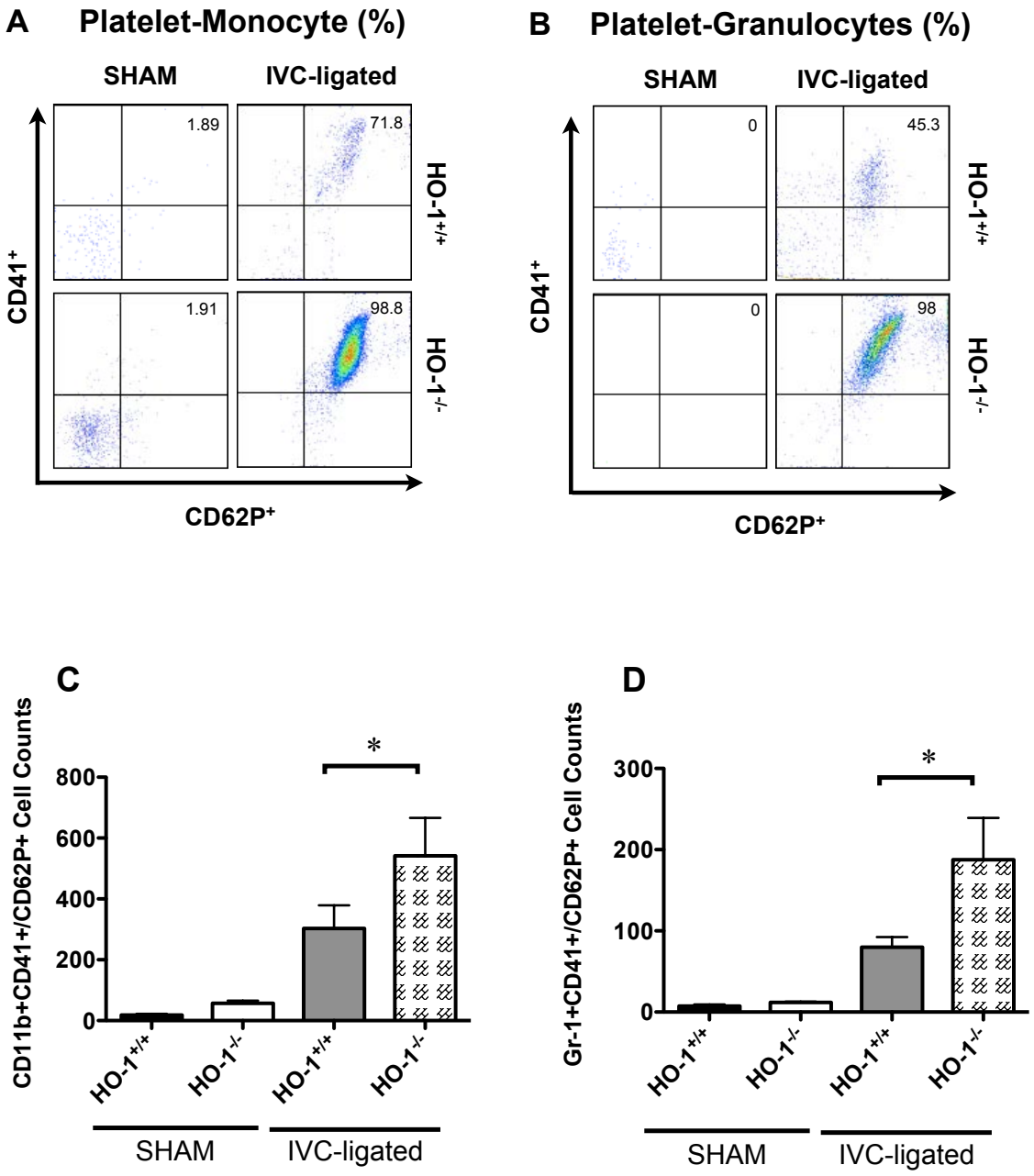

FIGURE III.7: THROMBOGENESIS ENHANCES THE ACCUMULATION OF PLATELET-LEUKOCYTE AGGREGATES FOLLOWING LIGATION OF IVC IN HO-1$^{+/+}$ AND HO-1$^{-/-}$ MICE.

Pre-gating strategy: forward and side scatter were used to identify ganulocyte and monocyte cell population, DAPI negative cells were subgated to CD45^{+} leukocytes. (A,

B) Representative dot plot of percentage of whole-blood platelet-granulocyte (neutrophils – Gr-1^{+}) (A) and platelet-monocyte ($CD11b^{+}$) (B) aggregates in HO-$1^{+/+}$ and HO-$1^{-/-}$ sham operated or IVC-ligated mice 48hrs following IVC ligation. The percentage of neutrophils and monocytes found in heteroaggregates with P-selectin ($CD62P^{+}$) and platelets ($CD41^{+}$) is greater in HO-$1^{-/-}$ compared to HO-$1^{+/+}$ IVC-ligated mice. (C, D) Quantitative cell count analysis of Gr-1 and CD11b-$CD41^{+/}CD62P^{+}$ cells in HO-$1^{+/+}$ and HO-$1^{-/-}$ sham operated or IVC-ligated mice. N = 3-5 per group. Bars represent mean ± SEM from tissue harvested from indicated number of mice. *Different from HO-$1^{+/+}$ IVC ligated $P<0.05$. All data were assessed by one-way ANOVA.

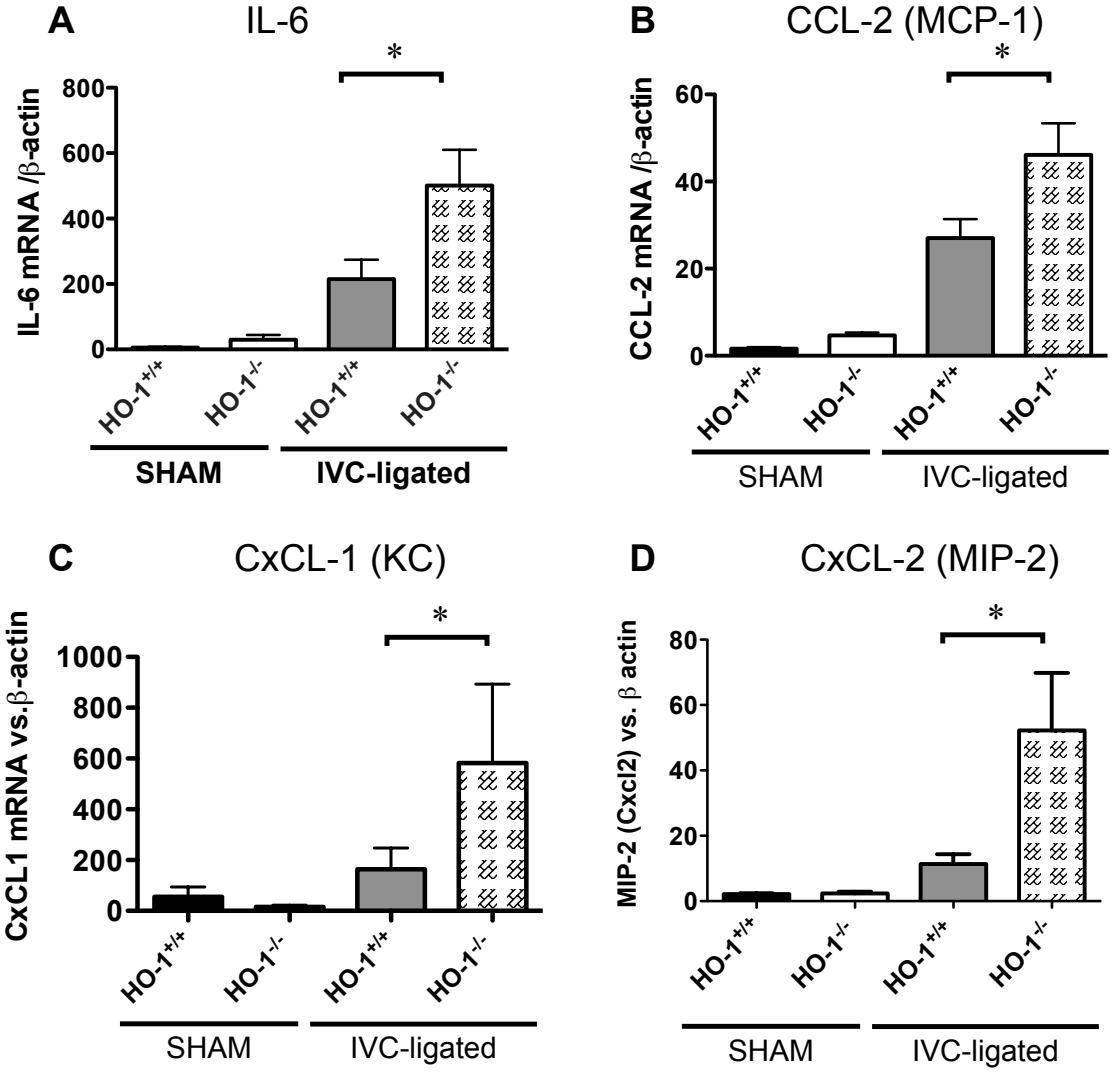
A
IL-6
IL-6 mRNA /β-actin
800
600
400
200
0
*
HO-1+/+
HO-1-/-
HO-1+/+
HO-1-/-
SHAM
IVC-ligated
B
CCL-2 (MCP-1)
CCL-2 mRNA /β-actin
60
40
20
0
*
HO-1+/+
HO-1-/-
HO-1+/+
HO-1-/-
SHAM
IVC-ligated
C
CxCL-1 (KC)
CxCL1 mRNA vs.β-actin
1000
800
600
400
200
0
*
HO-1+/+
HO-1-/-
HO-1+/+
HO-1-/-
SHAM
IVC-ligated
D
CxCL-2 (MIP-2)
MIP-2 (Cxcl2) vs. β actin
80
60
40
20
0
*
HO-1+/+
HO-1-/-
HO-1+/+
HO-1-/-
SHAM
IVC-ligated

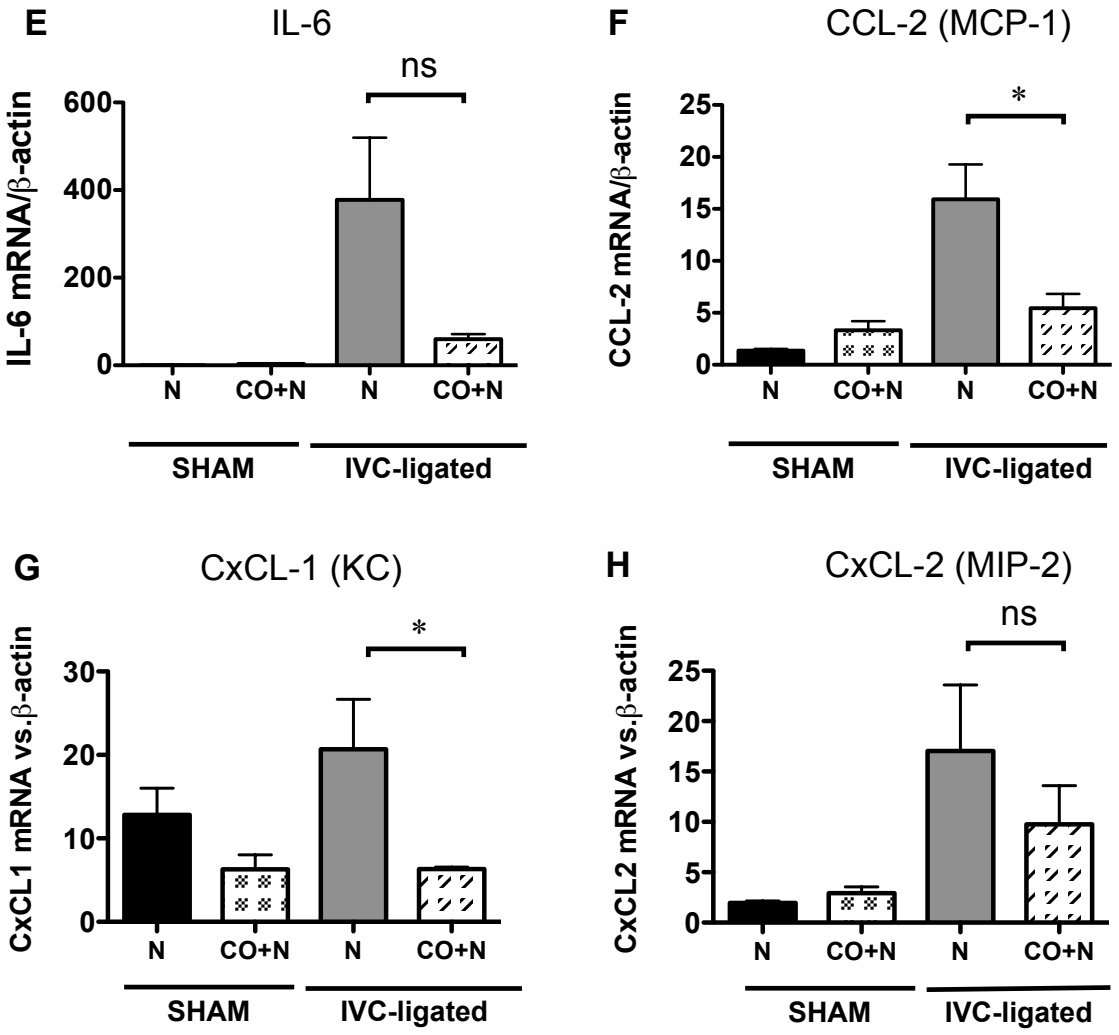

FIGURE III.8: EFFECTS OF THROMBOGENESIS ON VEIN WALL PROINFLAMMATORY CYTOKINES AND CHEMOKINE MEDIATORS IN HO-1$^{+/+}$ AND HO-1$^{-/-}$ MICE.

(A-D) mRNA from IVC was measured by quantitative PCR of sham-operated and IVC-ligated HO-1$^{+/+}$ and HO-1$^{-/-}$ mice 48 hr post thrombosis. (E-H) mRNA from IVC was measured by quantitative PCR of sham-operated and IVC-ligated of wildtype exposed to normoxia (21% Oxygen) or episodic low dose of carbon monoxide (twice a day 1 hr exposure of 250ppm of CO and 21% normoxia). We examined mRNA expression of IL-6, CCL-2 (MCP-1), CxCL-1 (KC), and CxCL-2 (MIP-2). (n = 5-11 per group). Fold

changes (y-axis) were normalized to β-actin. Results are shown as the mean ± SEM and *different from HO-$1^{+/+}$ IVC ligated or wild type normoxia $P<0.05$. All data were assessed by one-way ANOVA.

ACUTE DVT (HO-1 null mice)

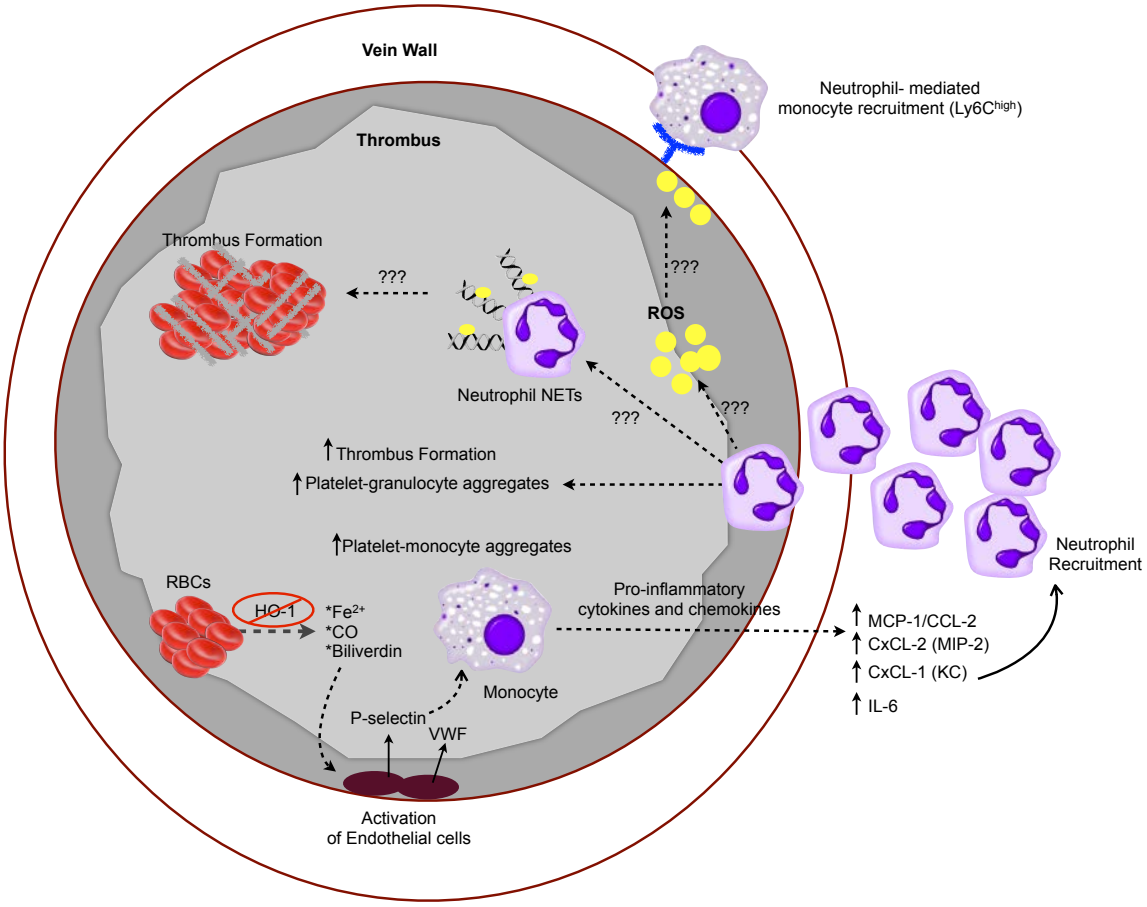

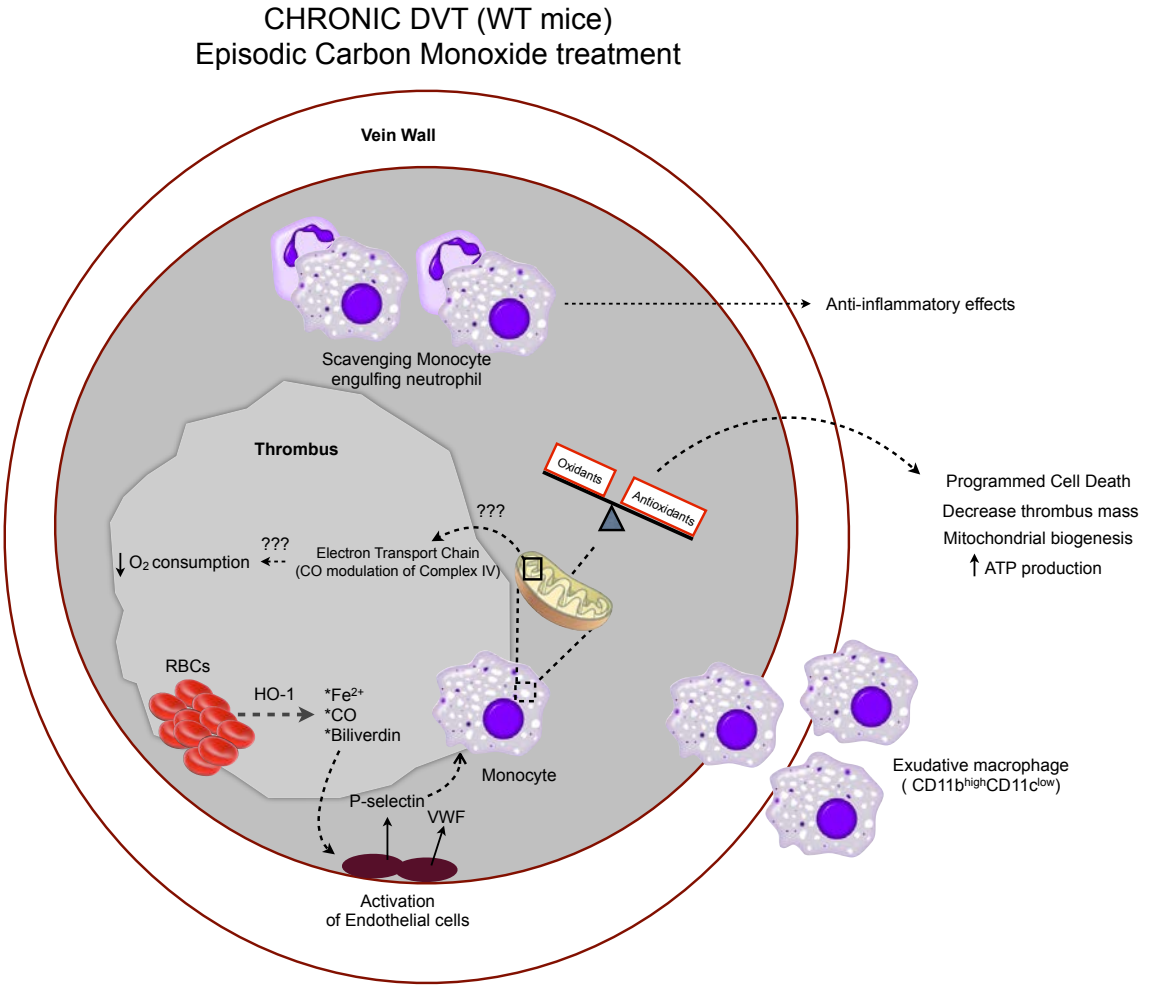

FIGURE III.9 GRAPHICAL REPRESENTATION SUMMARIZING THE MECHANISM(S) POTENTIALLY INVOLVED IN THE ANTI-INFLAMMATORY ACTIVITIES OF HO-1/CO IN ACUTE VS. CHRONIC VENOUS THROMBOSIS

The dynamic and complex balance that exists between thrombosis and inflammation during thrombogenesis plays a pivotal role in the pathogenesis of DVT. Using a well-established and widely employed model of stasis-induced venous thrombosis, we depicted above a proposed hypothesis of HO-1/CO activity after stasis induced DVT in the mouse. During the acute stages (right panel) of inflammation, neutrophils are the predominant cellular responder. The left panel depicts during administration of episodic low dose of carbon monoxide (chronic stages), monocytes increase at the site of

thrombosis and are important in proteolytic digestion and resolution of the thrombus components. This increase of vascular wall thrombogenicity may directly result from the marked upregulation of leukocyte adhesion receptors P-selectin and the induction of prothrombotic von Willebrand factor.

DISCLOSURES

Dr. Pinsky has an equity interest in Proterris, which is developing inhaled CO for clinical use, and potential patent-related royalties from Columbia University.

ACKNOWLEDGEMENTS

This work was supported by: Systems in Integrative Biology predoctoral training grant T32GM008322 (to A.C. Anyanwu); NIH grants HL086676 (to D.J. Pinsky), and the J. Griswold Ruth MD & Margery Hopkins Ruth Professorship (to D.J. Pinsky); and the A. Alfred Taubman Medical Research Institute at the University of Michigan.

NOTES

This manuscript is currently under review.

REFERENCES

1. Heit JA. The Epidemiology of Venous Thromboembolism in the Community. *Arteriosclerosis, Thrombosis, and Vascular Biology* 2008, 28(3): 370-372.

2. Geerts WH, Bergqvist D, Pineo GF, Heit JA, Samama CM, Lassen MR*, et al.* Prevention of venous thromboembolism*: American college of chest physicians evidence-based clinical practice guidelines (8th edition). *CHEST Journal* 2008, 133(6_suppl): 381S-453S.

3. Linkins L-A, Choi PT, Douketis JD. Clinical Impact of Bleeding in Patients Taking Oral Anticoagulant Therapy for Venous ThromboembolismA Meta-Analysis. *Annals of Internal Medicine* 2003, 139(11): 893-900.

4. Smeeth L, Cook C, Thomas S, Hall AJ, Hubbard R, Vallance P. Risk of deep vein thrombosis and pulmonary embolism after acute infection in a community setting. *The Lancet*, 367(9516): 1075-1079.

5. Pinsky DJ, Naka Y, Liao H, Oz MC, Wagner DD, Mayadas TN*, et al.* Hypoxia-induced exocytosis of endothelial cell Weibel-Palade bodies. A mechanism for

rapid neutrophil recruitment after cardiac preservation. *The Journal of Clinical Investigation* 1996, 97(2): 493-500.

6. Lawson CA, Yan SD, Yan SF, Liao H, Zhou YS, Sobel J*, et al.* Monocytes and tissue factor promote thrombosis in a murine model of oxygen deprivation. *The Journal of Clinical Investigation* 1997, 99(7): 1729-1738.

7. Ruggeri ZM. The role of von Willebrand factor in thrombus formation. *Thrombosis Research* 2007, 120, Supplement 1(0): S5-S9.

8. Brill A, Fuchs TA, Chauhan AK, Yang JJ, De Meyer SF, Köllnberger M*, et al.* von Willebrand factor–mediated platelet adhesion is critical for deep vein thrombosis in mouse models. *Blood* 2011, 117(4): 1400-1407.

9. Thanaporn P, Myers DD, Wrobleski SK, Hawley AE, Farris DM, Wakefield TW*, et al.* P-selectin inhibition decreases post-thrombotic vein wall fibrosis in a rat model. *Surgery* 2003, 134(2): 365-371.

10. Myers DD, Hawley AE, Farris DM, Wrobleski SK, Thanaporn P, Schaub RG*, et al.* P-selectin and leukocyte microparticles are associated with venous thrombogenesis. *Journal of Vascular Surgery* 2003, 38(5): 1075-1089.

11. Myers DD Jr SR, Wrobleski SK, Londy FJ 3rd, Fex BA, Chapman AM, Greenfield LJ, Wakefield TW. P-selectin antagonism causes dose-dependent venous thrombosis inhibition. *Thrombosis and Haemostasis* 2001, 85(3): 423-429.

12. Henke PK, DeBrunye LA, Strieter RM, Bromberg JS, Prince M, Kadell AM*, et al.* Viral IL-10 Gene Transfer Decreases Inflammation and Cell Adhesion Molecule Expression in a Rat Model of Venous Thrombosis. *The Journal of Immunology* 2000, 164(4): 2131-2141.

13. Celi A, Pellegrini G, Lorenzet R, De Blasi A, Ready N, Furie BC*, et al.* P-selectin induces the expression of tissue factor on monocytes. *Proceedings of the National Academy of Sciences* 1994, 91(19): 8767-8771.

14. Ryter SW, Alam J, Choi AMK. Heme Oxygenase-1/Carbon Monoxide: From Basic Science to Therapeutic Applications. *Physiological Reviews* 2006, 86(2): 583-650.

15. Willis D, Moore A, Frederick R, Willoughby D. Heme oxygenase: a novel target for the modulation of the inflammatory response. *Nat Med* 1996, 2: 87 - 90.

16. Maines MD. The Heme Oxygenase System: A Regulator of Second Messenger Gases. *Annual Review of Pharmacology and Toxicology* 1997, 37(1): 517-554.

17. Tracz MJ, Juncos JP, Grande JP, Croatt AJ, Ackerman AW, Katusic ZS*, et al.* Induction of Heme Oxygenase-1 is a Beneficial Response in a Murine Model of Venous Thrombosis. *The American Journal of Pathology* 2008, 173(6): 1882-1890.

18. Otterbein LE, Soares MP, Yamashita K, Bach FH. Heme oxygenase-1: unleashing the protective properties of heme. *Trends in Immunology* 2003, 24(8): 449-455.

19. Fujita T, Toda K, Karimova A, Yan S, Naka Y, Yet S*, et al.* Paradoxical rescue from ischemic lung injury by inhaled carbon monoxide driven by derepression of fibrinolysis. *Nat Med* 2001, 7: 598 - 604.

20. Brüne B, Ullrich V. Inhibition of platelet aggregation by carbon monoxide is mediated by activation of guanylate cyclase. *Molecular Pharmacology* 1987, 32(4): 497-504.

21. Gende OA. Carbon monoxide inhibits capacitative calcium entry in human platelets. *Thrombosis Research* 2004, 114(2): 113-119.

22. Durante W. Carbon monoxide and bile pigments: surprising mediators of vascular function. *Vascular Medicine* 2002, 7(3): 195-202.

23. Soares MP UA, Brouard S, Berberat PO, Gunther L, Tobiasch E, Bach FH. Modulation of endothelial cell apoptosis by heme oxygenase-1-derived carbon monoxide. *Antioxid Redox Signal* 2002, 4(2): 321-329.

24. Minamoto K, Harada H, Lama VN, Fedarau MA, Pinsky DJ. Reciprocal regulation of airway rejection by the inducible gas-forming enzymes heme oxygenase and nitric oxide synthase. *The Journal of Experimental Medicine* 2005, 202(2): 283-294.

25. Yet S, Perrella M, Layne M, Hsieh C, Maemura K, Kobzik L*, et al.* Hypoxia induces severe right ventricular dilatation and infarction in heme oxygenase-1 null mice. *J Clin Invest* 1999, 103: R23 - R29.

26. Myers Jr D, Farris D, Hawley A, Wrobleski S, Chapman A, Stoolman L*, et al.* Selectins Influence Thrombosis in a Mouse Model of Experimental Deep Venous Thrombosis. *Journal of Surgical Research* 2002, 108(2): 212-221.

27. Myers Jr DD, Henke PK, Wrobleski SK, Hawley AE, Farris DM, Chapman AM*, et al.* P-selectin inhibition enhances thrombus resolution and decreases vein wall fibrosis in a rat model. *Journal of Vascular Surgery* 2002, 36(5): 928-938.

28. Otterbein L, Bach F, Alam J, Soares M, Tao Lu H, Wysk M*, et al.* Carbon monoxide has anti-inflammatory effects involving the mitogen-activated protein kinase pathway. *Nat Med* 2000, 6: 422 - 428.

29. Lee T, Chau L. Heme oxygenase-1 mediates the anti-inflammatory effect of interleukin-10 in mice. *Nat Med* 2002, 8: 240 - 246.

30. Hancock WW BR, Sayegh MH, Turka LA. Antibody-induced transplant arteriosclerosis is prevented by graft expression of anti-oxidant and anti-apoptotic genes. *Nature Medicine* 1998, 4(12): 1392-1396.

31. Chapman J, Otterbein L, Elias J, Choi A. Carbon monoxide attenuates aeroallergen-induced inflammation in mice. *Am J Physiol Lung Cell Mol Physiol* 2001, 281: L209 - L216.

32. Mishra S, Fujita T, Lama VN, Nam D, Liao H, Okada M*, et al.* Carbon monoxide rescues ischemic lungs by interrupting MAPK-driven expression of early growth

response 1 gene and its downstream target genes. *Proceedings of the National Academy of Sciences of the United States of America* 2006, 103(13): 5191-5196.

33. de Bruijne-Admiraal L, Modderman P, Von dem Borne A, Sonnenberg A. P-selectin mediates Ca(2+)-dependent adhesion of activated platelets to many different types of leukocytes: detection by flow cytometry. *Blood* 1992, 80(1): 134-142.

34. Deatrick KB, Luke CE, Elfline MA, Sood V, Baldwin J, Upchurch Jr GR*, et al.* The effect of matrix metalloproteinase 2 and matrix metalloproteinase 2/9 deletion in experimental post-thrombotic vein wall remodeling. *Journal of Vascular Surgery* (0).

35. Ramacciotti E HA, Farris DM, Ballard NE, Wrobleski SK, Myers DD Jr, Henke PK, Wakefield TW. Leukocyte- and platelet-derived microparticles correlate with thrombus weight and tissue factor activity in an experimental mouse model of venous thrombosis. *Thrombosis and Haemostasis* 2009, 101(4): 748-754.

36. Saha P, Humphries J, Modarai B, Mattock K, Waltham M, Evans CE*, et al.* Leukocytes and the Natural History of Deep Vein Thrombosis: Current Concepts and Future Directions. *Arteriosclerosis, Thrombosis, and Vascular Biology* 2011, 31(3): 506-512.

37. Wakefield TW, Henke PK. The Role of Inflammation in Early and Late Venous Thrombosis: Are There Clinical Implications? *Seminars in Vascular Surgery* 2005, 18(3): 118-129.

38. Henke PK, Varga A, De S, Deatrick CB, Eliason J, Arenberg DA*, et al.* Deep Vein Thrombosis Resolution Is Modulated by Monocyte CXCR2-Mediated Activity in a Mouse Model. *Arteriosclerosis, Thrombosis, and Vascular Biology* 2004, 24(6): 1130-1137.

39. Humphries J MC, Smith A, Waltham M, Poston R, Burnand KG. Monocyte chemotactic protein-1 (MCP-1) accelerates the organization and resolution of venous thrombi. *Journal of Vascular Surgery* 1999, 30(5): 894-899.

40. Ali T, Humphries J, Burnand K, Sawyer B, Bursill C, Channon K*, et al.* Monocyte recruitment in venous thrombus resolution. *Journal of Vascular Surgery* 2006, 43(3): 601-608.

41. Wakefield TW, Myers DD, Henke PK. Mechanisms of Venous Thrombosis and Resolution. *Arteriosclerosis, Thrombosis, and Vascular Biology* 2008, 28(3): 387-391.

42. Myers Jr DD, Henke PK, Bedard PW, Wrobleski SK, Kaila N, Shaw G*, et al.* Treatment with an oral small molecule inhibitor of P selectin (PSI-697) decreases vein wall injury in a rat stenosis model of venous thrombosis. *Journal of Vascular Surgery* 2006, 44(3): 625-632.

43. Wynn TA, Barron L. Macrophages: Master Regulators of Inflammation and Fibrosis. *Semin Liver Dis* 2010, 30(03): 245-257.

44. Peng L ML, Stomel JM, Liu JJ, Sun J, Yet SF, Fay WP. Induction of heme oxygenase-1 expression inhibits platelet-dependent thrombosis. *Antioxid Redox Signal* 2004, 6(4): 729-735.

45. Gasparyan AY AL, Mikhailidis DP, Kitas GD. Mean platelet volume: a link between thrombosis and inflammation? *Curr Pharm Des* 2011, 17(1): 47-58.

46. Wagener FA FE, de Witte T, Abraham NG. Heme induces the expression of adhesion molecules ICAM-1, VCAM-1, and E selectin in vascular endothelial cells. *Proc Soc Exp Biol Med* 1997, 216(3): 456-463.

47. Otterbein LE, Zuckerbraun BS, Haga M, Liu F, Song R, Usheva A*, et al.* Carbon monoxide suppresses arteriosclerotic lesions associated with chronic graft rejection and with balloon injury. *Nat Med* 2003, 9(2): 183-190.

48. Sato K, Balla J, Otterbein L, Smith R, Brouard S, Lin Y*, et al.* Carbon monoxide generated by heme oxygenase-1 suppresses the rejection of mouse-to-rat cardiac transplants. *J Immunol* 2001, 166: 4185 - 4194.

49. Chen B, Guo L, Fan C, Bolisetty S, Joseph R, Wright MM*, et al.* Carbon Monoxide Rescues Heme Oxygenase-1-Deficient Mice from Arterial Thrombosis in Allogeneic Aortic Transplantation. *The American Journal of Pathology* 2009, 175(1): 422-429.

50. Wojcik BM, Wrobleski SK, Hawley AE, Wakefield TW, Myers Jr DD, Diaz JA. Interleukin-6: A Potential Target for Post-Thrombotic Syndrome. *Annals of Vascular Surgery* 2011, 25(2): 229-239.

51. De Maio A TM, Reeves RH. Genetic determinants influencing the response to injury, inflammation, and sepsis. *Shock* 2005, 23(1): 11-17.

52. Merli G, Spyropoulos AC, Caprini JA. Use of Emerging Oral Anticoagulants in Clinical Practice: Translating Results from Clinical Trials to Orthopedic and General Surgical Patient Populations. *Annals of Surgery* 2009, 250(2): 219-228 210.1097/SLA.1090b1013e3181ae1096dbe.

CHAPTER IV

CONCLUSIONS AND FUTURE DIRECTIONS

SUMMARY

The work presented in this thesis explores our evolving understanding of the role of heme oxygenase-1 (HO-1) and carbon monoxide (CO) in pulmonary and cardiovascular disease. All cells catabolize heme using one of the two heme oxygenase (HO), HO-1 or HO-2, which are the inducible and consitutitive isoforms, respectively.[1] The primary focus of this thesis is on heme oxygenase-1 and one of its cytoprotective byproduct carbon monoxide, and its modulation of disease pathologies that have an inflammatory component driven by tissue injury. Several studies have reported that CO independently influences cellular functions in unique and succinct immunological modalities that optimize the ability of the cell to respond to the needs of the tissue. HO-1 is usually activated within hours of exposure to a host of cellular stressors including pathogens, fluctuations in oxygen, endothelial damage, oxidants, growth factors and chemokine mediators.[2] CO generated by HO-1 regulates, either positively or negatively, inter and intracellular networking and communication within the tissue and organ systems, allowing them to respond appropriately to the stressor or changes in environmental cues. The absence of HO-1 gene in mice or humans leads to chronic, multi-organ systemic inflammation, emphasizing the crucial importance of this enzyme

in regulating fundamental physiology and requisite immune response.[3,4] One conundrum that has besieged the field is how HO-1/CO, as a heme-catabolizing enzyme, mediates such potent and broad-reaching salutary effects in contexts ranging from vascular to pulmonary diseases. Thus, the principal goal of this work was to elucidate how HO-1 and its cytoprotective by product CO provide cellular and tissue protection in an inflammatory environment. Carbon monoxide holds a prominent place in the history of the contemporary biological sciences. CO functions similarly to other signaling molecules, such as nitric oxide and hydrogen sulfide, by amplifying a signal intracellularly that leads to changes in cellular function locally. However, CO is unlike other signaling molecules because it propagates effects pericellularly as well as distally to remote cells and tissues through its high diffusivity, its portability using hemoglobin, and its biochemical stability (integrity). CO is perhaps the smallest signaling molecule, it can easily transverse through lipid bilayers and bind to its targets, much like oxygen and carbon dioxide as they are mobilized throughout the body. With such characteristics, CO facilitates the behavior of a matrix of interactions among cell types that, in turn, facilitates rapid responses both to stressors and danger signals.

In chapter II, we developed a novel flow cytometry technique to examine the amount of leucocyte cell populations that trafficked through a developing lung during hyperoxic insult. In addition, the application of pulsatile CO to exert its anti-inflammatory and cytoprotective effects on developing lung. The precise mechanisms by which inflammation inhibits alveolar development are not completely known. However, in this chapter, we begin by exploring the role of heme oxygenase (HO-1) and its

byproduct carbon monoxide (CO), which are thought to be cytoprotective against redox stress, mitigate lung injury and alveolar simplification in hyperoxia-exposed neonatal mice, a model of bronchopulmonary dysplasia (BPD). Furthermore, we tested the requirement of CCL2 for hyperoxia-induced lung injury. Hyperoxia-exposed CCL2 null mice, like CO-treated mice, showed attenuated alveolar simplification and lung inflammatory infiltrate. This work showed for the first time that: 1) brief episodic exposure to low-dose CO significantly mitigates the deleterious effects of hyperoxia on alveolar development; 2) HO-1 deficiency exacerbates hyperoxia-induced lung injury; and 3) CCL2 is required for hyperoxia-induced alveolar simplification. Taken together, this work demonstrated that, in hyperoxia-exposed neonatal mice, inhalation of the HO-1 product CO suppresses CCL2-dependent inflammatory cell trafficking, pro-inflammatory cytokine expression, and alveolar simplification.

HO-1/CO autonomous regulation of leukocytes and inflammation can be paired with monocyte chemoattractant (MCP-1/CCL-2) to suggest a novel therapeutic approach. The work of our lab and others has previously shown that exogenous CO treatment is profoundly protective in hyperoxia induced BPD.[5] The importance of HO-1 during hyperoxia induced lung injury is perhaps best exemplified by observations of the HO-1 deficient mouse[3,6] and the effects of exogenous CO to mimic its HO-1 cytoprotective properties. In chapter II we explored the anti-inflammatory and cytoprotective properties of HO-1/ CO in HO-$1^{-/-}$ and HO-$1^{+/+}$ neonatal animals. Up to this point, only a few studies have examined the role of neutrophils and macrophages in the pathogenesis of neonatal hyperoxic-induced lung injury. In some of the studies, hyperoxia induces

neutrophil influx and hypoalveolarization, which is attenuated by neutralizing antibodies against the neutrophil chemoattractants CXCL1[7] or CXCL2.[8] Neutrophilic inflammation during hyperoxia is also prevented by a selective chemical antagonist of CXCR2.[9] Neutralizing antibodies against MCP-1/CCL2, a monocyte chemoattractant, also decrease lung hypoalveolarization, as well as lung macrophage and neutrophil counts, in hyperoxia-exposed rats.[10] We propose that CO protects against hyperoxia-induced alveolar simplification by blocking macrophage infiltration and activation. In many instances, the exogenous addition of CO can substitute for HO-1 deficency.[11,12] CO preserves cellular and tissue survival *in vivo*, which is likely to reflect the participation of disparate signaling pathways in regulating inflammatory sequelae.

Our studies demonstrate a direct link between CO, the CCL2-dependent control of leukocyte migration into hyperoxic lung tissue, and alveolar growth. Inhibition of inflammatory cell infiltration by either CO or CCL2 gene deletion was associated with the attenuated alveolar simplification. Furthermore, we extend these observations by demonstrating that hyperoxia induces the accumulation of different F4/80-positive macrophage subsets into the lung, specifically $CD11c^{low}$ $CD11b^{high}$ and $CD11c^{high}$ $CD11b^{high}$ cells. Previously, it was shown that, during influenza infection[13] and bleomycin exposure[14], $CD11c^{-}$ $CD11b^{+}$ inflammatory monocytes are recruited to the lung and develop into a $CD11c^{high}$ $CD11b^{+}$ activated macrophage population known as exudative macrophages. On this basis, we speculate that the $CD11c^{low}$ $CD11b^{high}$ cells (our population C) represent inflammatory monocytes, and that $CD11c^{high}$ $CD11b^{high}$ cells (our population B) represent exudative macrophages, a major source of inflammatory

cytokines and chemokines in the lung. This paradigm is somewhat unique for leukocyte trafficking and for the first time provides critical information about the link between HO-1 derived CO and CCL-2, with studies of exogenously administering pulsatile CO in a model of hyperoxia-induced bronchopulmonary dysplasia.

With the techniques employed in this work, we have begun to parse the effects of HO-1/CO modulation of leukocyte trafficking in the neonatal lung. Some major limitations in our present study lie in reconciling the timing of CO treatment. It is also possible that the timing of CO exposure is critical. Specific studies varying this timing may have to be done. In our unpublished study on cardiac preconditioning, two phases of preconditioning are known to exist, early and late (the former does not require de novo protein synthesis, whereas the latter does). Furthermore, It is possible that a longer duration of CO given during either post-hyperoxia or during recovery might result in benefits over and above those shown in the this chapter. Thus we have tried to guard against drawing our conclusions too firmly. It is likely that other mechanisms of CO delivery could be employed to exogenously administer CO in this model such as methylene chloride[15] or carbon monoxide releasing molecules[16]. As arterial pH does not change with the levels of CO, which are used, it is unlikely that inhaled CO causes tissue asphyxia, although at longer episodic exposure and higher concentrations, this remains a possibility. Even though this was not the focus of our study in this chapter, we cannot rule out the possibility that the inducibility of HO-1 might be regulated at the level of post-transcription and/or post-translation processing. In order to verify this hypothesis, we could test the activity of activator protein 1(AP-1), a transcription factor that is an

important regulator of HO-1 transcription in hyperoxia[17]. If there is a lack of AP-1 binding to neonatal lung DNA during hyperoxia, this might partially explain the resistance to HO-1 hyperoxic induction. However, a confounding limitation such as inconsistent mRNA and protein induction will tell us that experiments need to be conducted at the posttranscriptional and posttranslational level in order to understand what proteins regulate the inducibility of HO-1/CO during maturation.

Chapter III takes a different look at the role of HO-1/CO in cardiovascular disease, Venous thromboembolism (VTE) a chronic and multicausal disease.[18] Defined clinically as inappropriate clotting of the blood presenting as either deep vein thrombosis (DVT), pulmonary embolism or both, VTE is estimated to affect approximately 1 in 1000 individuals per year in the U.S. alone. Despite great advancements in the treatment and prevention of VTE in the twentieth century, the burden of this disease is increasing. The inflammatory process is increasingly being recognized as an important mechanism regulating thrombus formation and resolution.[19,20] Platelet activation has recently emerged as a therapeutic target for limiting cardiovascular diseases.[21,22] Identification of new mechanisms, which contribute to thrombus formation and resolution could lead to new insights into its disease pathogenesis and new therapeutic options. With this concept in mind, Chapter III explores the endogenous protection of HO-1 and the application of low therapeutically dose of CO to mitigate leukcosequetsration into the vessel well. In doing so, we employed a long-established and widely used model of venous thrombosis and one based on the ligation of intra-renal inferior vena cava (IVC).[23,24,25,26,27,28]

In chapter III, we highlight the effects of pulsatile low-dose of exogenous CO treatment on stasis-induced venous thrombosis and delineate the role of HO-1 in leukocyte recruitment during acute thrombus formation. In addition, we also examined the effects of endogenous CO production and key inflammatory modulators (p-selectin and vWF), cytokine and chemokine levels and peripheral whole-blood leukocyte-platelet aggregation. The results demonstrated pulsatile CO treatment acutely reduced leukocyte recruitment to the vessel wall post-thrombus induction and endogenous CO production exacerbates the inflammatory response and leukocyte-platelet aggregates. The physiological significance of increased formation of platelet-leukocyte aggregates in the peripheral blood during inflammatory disease still remains uncertain, however, our studies suggest that platelets at the thrombo/inflammatory interface may play an active role in DVT. All together, our findings suggest that intermittent administration of CO over short exposure times would be beneficial and we also demonstrated that the degree of vascular injury also dictated the relative efficacy of CO treatment. We provide evidence that HO-1 deficiency promotes inflammation and results in the increased extravasation of key inflammatory cells and activation of vascular coagulant reactions at the blood/vessel interface 48 hrs post-IVC ligation. Absence of HO-1 further pushes the balance towards a proinflammatory vascular wall phenotype. However, it is important to note that inflammatory response may also vary with the age, gender, and genetic background of the mouse[29], suggested that a number of additional studies would be required to completely understand the effectiveness of CO treatment post IVC ligation. The present studies cannot rule out the possibility that CO would be even more effective in models producing less inflammation or more focal injury.

In any case, it would appear important to examine the effects of CO treatment at early and later time points to fully evaluate HO-1/CO role in acute venous thrombosis. Understanding the complex interplay of vascular injury, stasis and coagulation and how this is modulated by HO-1/CO would lead to new therapies for DVT or other disorders at the nexus of inflammation and platelet aggregation.

The leukocentric focus taken in this chapter was not meant to preclude the idea that HO-1 could only confer protection through the regulation of platelet activation. In fact the answer likely lies somewhere in the middle; a potential synergy may exist between the populations of leukocytes and platelets leading to co-activation and heteraggregation. Ultimately, to address these questions effectively, new molecular tools and genetic mouse models will need to be developed. The classic paradigm of inflammatory cell signaling has primarily focused upon the recruitment and activation of leukocytes, with concomitant release of soluble mediators (cytokines and chemokines) that may amplify and accelerate the inflammatory process during stasis-induced venous thrombosis.

The experiments in this thesis tested whether the HO-1/CO axis regulates inflammatory cell trafficking *in vivo*. Since HO-1/CO is likely to have pleiotrophic effects, the only clear way to dissect the mechanisms that underlie increase leukocyte infiltration and thrombus formation of HO-1 deficient animals is to design *in vitro* experiments that have only one cellular variable at a time. For example, if CO suppresses leukocyte infiltration into the vessel wall *in vivo*, but leukocyte adhesion molecules and transmigration are not affected by the silencing HO-1 in macrophage specific cell line (i.e. RAW264.7), then leukocyte accumulation in the vessel wall may be attributed to the

fact that mechanism other than leukosequestration are also playing a role and could contribute to stasis-induced venous thrombosis. If HO-1/CO regulates inflammatory cell trafficking and the expression of adhesion molecules and chemokines, we could directly test the role of the identified adhesion molecules and chemokines by determining whether the relevant knockout mice are protected from thrombus formation. For example, we could cross adhesion receptor null mice or CXCR2 (the receptor for CXC chemokine neutrophil chemoattractants) null mice with HO-1 null mice. If HO-1/CO mitigates the effect of leukocyte accumulation and thrombigenesis thru the inhibition of PECAM expression, then the expected outcome that may result in the HO-1 null mice may not occur in the double knockout. Similar arguments can also be made for the other adhesion receptors null mice (ICAM-1, VCAM-1, P/E selectin). The majority of these null mice are all commercially available via Jackson laboratories. This does not diminish the value of the current studies, which were critical for demonstrating HO-1/CO is a powerful endogenous protector against venous thrombogenesis, and identifying this field as an area of future investigation.

FUTURE DIRECTIONS

The road towards effective HO-1/CO based therapies to study pulmonary and cardiovascular diseases are fraught with technical challenges and will provide conversation for years to come. Throughout this thesis, I have outlined the possible limitations of our methods and the gaps that remain in our present knowledge. At the point where this research concludes, there are a number of important and exciting questions that remain to be answered.

Macrophages play a crucial role in innate and adaptive immunity in response to oxidative stress and are major mediators of the inflammatory response. During infection, macrophage effectors functions are critical for the elimination of pathogens, however uncontrolled inflammatory responses can induce injury of the tissue environment and must be repressed to allow the process of repair **Figure 1**. During the stages of disease, tissue and cytokine microenvironment induce, *in vivo*, a heterogeneous macrophage population that displays an appropriate inflammatory phenotype.[30] In vitro, two major macrophage populations are characterized. Classically activated (M1) or type I macrophage, induced in particular by IFNγ,[31] display a pro-inflammatory profile whereas alternatively activated (M2) or type II macrophage (AAMϕ), induced by Th-2 cytokines, express anti-inflammatory and tissue repair properties[32] **Figure 2**. In Chapter II, we successfully demonstrated the anti-inflammatory effect of HO-1/CO in neonatal hyperoxia-induce BPD model. One of the exciting projects that has arose from this work

is we found that hyperoxia polarized the population of alveolar macrophages toward an M2 phenotype and that this regimen of intermittent CO administration of hyperoxia-exposed neonatal mice decreased the number of M2 cells. Work in chapter II of this thesis has shown a relationship between exogenous CO administration and alternative activation of key macrophage markers. Yet to this point, we still do not understand what role CO plays in modulating the trafficking of AAMϕ into the lung.

As part of the work for this thesis, I have already begun to investigate the process of leukosequestration in the developing lungs and the mechanism by which CO mitigates lung inflammatory, macrophage type 1 (M1) and type 2 (M2) markers. We found that hyperoxic exposure increased the percentage of M1/M2 macrophages and exogenous administration of CO attenuated this change. In addition to flow cytometric analysis, we also found a significant upregulation in the mRNA levels of canonical M2 markers (CD301b, FIZZ-1, Arg-1, Ym-1) during hyperoxic exposure. Similar modulation of FIZZ-1, Arg-1 and Ym-1 expression was noted following hypoxia-induced pulmonary hypertension [33]. Upregulation of Arg-1 may be of particular physiologic importance. Arg-1 has been shown to contribute to vascular damage and remodeling, and elevated Agr-1 in the lungs of hypoxic mice has been associated with increased severity of pulmonary hypertension [34, 35]. Thus, although both hyperoxia alone and CO alone appear to stimulate M1 to M2 conversion, hyperoxia leads to a faster degradation of macrophage infiltrates, probably due to a higher degree of oxidative stress than that induced by CO alone (**Fig 3-8**). Furthermore, the phagocytic activity of alternatively-activated macrophages may be associated with the clearance of cellular debris, of damaged or dying cells, and of

infiltrating neutrophils, thus resulting in the elimination of several potentially cytotoxic substances [5, 30, 33, 36]. In addition, we also briefly examined the role of HO-1 and alternatively-activated macrophages in this model. We show that hyperoxia exacerbates the expression of M2 markers CD206 and CD301. CCL-22 a macrophage-derived chemokine that induces migration of Th2 lymphocytes through specific receptors CCR4 was significantly increased in the absence of HO-1 during hyperoxia exposure **(Fig 9,10**). CCL-24 a small cytokine that belongs to the CC chemokine family was decreased in the absence of HO-1. CCL24 interacts with chemokine receptor CCR3 to induce chemotaxis in eosinophils. This chemokine is also strongly chemotactic for resting T lymphocyte and slightly chemotactic for neutrophils. Some of the findings in this studies was puzzling, however, it would be of great interest to explore in the future how HO-1/CO modulates the trafficking of AAMϕ into the interstitium of neonatal lung exposed to hyperoxia.

It is tempting to speculate that CO may play a critical role in the switch of a macrophage from an M1 to an M2 state during inflammatory resolution but future ex-vivo studies of expression levels of alternatively-activated macrophage markers are likely to provide insight into weather intermittent CO in the presence of a hyperoxic environment may have a critical function in the switch of a macrophage from an M1 to an M2 state during inflammatory resolution in an acute lung injury.

Another pressing question that arose from this work is the role CO plays in the signaling of mitochondrial reactive oxygen species (ROS) production. Among the earliest

events in cells and tissues exposed to low dose of CO is the rapid production of ROS such as superoxides, H_2O_2 and hydroxyl radicals.[37,38,39,40] Although superoxides anions (O_2^-) and hydrogen peroxide (H_2O_2) are generally considered to be toxic byproducts of respiration, recent evidence suggests that ROS are important regulators of eukaryotic signal transduction regulating biological processes as diverse as immune cell activation and vascular remodeling in mammals.[40] Recent report suggests, the generation of ROS at nondetrimental amounts in response to exogenous administration of low-dose CO might affect cellular respiration eventually resulting in adaption.[41],[42] Mitochondria are the only organelles to provide cells with energy. It has been reported that mitochondrial function is essential for normal growth in pulmonary epithelial-like cells in culture.[43] Compromised mitochondrial oxidative phosphorylation has been implicated in pathogenesis of genetic diseases presenting with developmental and growth restriction of different organs.[44] Clearly, well-functioning mitochondria are needed to convert nutritional substrates into energy to maintain growth and development. **Figure 11** depicts the different cytochromes contained within the mitochondrial respiratory chain ultimately provide electrons to cytochrome c oxidase, which catalyzes electron transfer from cytochrome c to reduced O_2 to H_2O. CO binds to complex IV (cytochrome c interacts with CO by competing with O_2) in the electron transport chain and promotes reduction of respiratory carriers in complex III thereby increasing mitochondrial H_2O_2 production.[45,46] The primary effect of CO on the mitochondria is to retard the rate of electron transport thus enabling electrons to accumulate at complex III.[39,47]

To explore the physiological effects of CO-induced ROS in hyperoxia-induced BPD or stasis-induced venous thrombogenesis, we need to use more precise tools that utilized isolation of mitochondria from neonatal lung or inferior vena cava. Isolation of mitochondria from HO-1 null mice should allow endogenous CO-induced ROS effects to be separated from ROS burst. Mitochondrial isolation could be as an initial technique to selectively compare the morphological differences between a naïve mitochondria isolated from neonatal lung compare to hyperoxia-exposed lung and compared to CO exposed neonatal lung using electron microscopy and complex IV activity assay as measured by spectrophotometric analysis (The follow experiments outlined above can also be applied to isolation of wildtype IVC (absence or presence of CO) compared to HO-1 deficient IVC). Some of the pressing questions that could be answered by using these techniques are as follows: Is CO-induced mitochondrial biogenesis related to the ability of CO to promote further ROS generation or is it related to effects on respiration and the simple need to provide additional ATP for the cells? Or is there a yet to be defined molecular mechanism that drives additional homeostatic cellular response?

As part of this thesis, I have also begun to measure the changes in mitochondrial bioenergetics using XF Cell mitochondrial stress kit. We exposed RAW264.7 cell to CO and normoxia for up to 24 hrs. We measured the changes CO induces upon the oxygen consumption rate (OCR) and extracellular acidification rate (ECAR). Using this technique we were able to measure 4 key parameters of mitochondrial function such as basal respiration, ATP production, spare respiratory capacity and proton leak (**Fig 12**).

Our preliminary data show, CO greatly increased the baseline OCR and reduced the spare respiratory capacity compared to norrnoxia control cells (**Fig 13**). When we analyzed baseline percentage we chose ideal cell density (~100K) for both normoxia and CO exposed RAW264.7 cell (RAW). OCR baseline percentage was 40-50% spare respiratory capacity in normoxia exposed cells, which was significantly reduced in CO exposed cells (**Fig 14**). In addition to OCR measurements, we also measure the ECAR. We injected Oligomycin (ATP Coupler), FCCP (Electron Transport Chain Accelerator), Antimycin A (Mitochondrial Inhibitor A) and Rotenone (Mitochondrial Inhibitor B) – ANTI/ROT at specific time points during the experiments. In **Figure 15 and 16**, we show normoxia and CO exposed cells had the same baseline ECAR. However, once oligomycin (a mitochondrial ATP synthase inhibitor) was injected the ECAR increased, as well as baseline Oligo, FCCP and ANTI/ROT in the CO exposed RAW cells.

Taken together, this preliminary study demonstrated that when measuring the OCR, RAW control cells and RAW CO exposed cells had differential mitochondrial function as determined with the Cell Mito Stress Test at most of the densities tested. Based upon the basal OCR readings, dynamic range of the XF24, and response to drugs, chiefly FCCP, 100,000 cells per well would be the best density to use in future experiments. Raw cells incubated overnight in our *in vitro* CO chamber have increased baseline OCR rates compared to the RAW control cells. In addition, RAW cells exposed to CO have reduced spare respiratory capacity, and OCR rates reached baseline after FCCP injection.

Interestingly, we also show that Oligomycin caused increased ECAR under both conditions with 400k, which is a fivefold increase in RAW cell density with CO exposure. Oligomycin, a mitochondrial ATPase inhibitor, cause a large increase in glycolysis as cells compensate for loss of mitochondrial ATP. Some cells do this quite well, and under hyperoxic conditions, cells can become more glycolytic as well. RAW cells incubated overnight in a CO chamber have similar baseline ECAR rates compared to the RAW control cells, suggesting CO has no effect on baseline ECAR rates. However, RAW cells exposed to CO have an increase in ECAR rates after the administration of the stress test.

It is critical that future experiments focus on HO-1/CO attenuates the amount of oxidants in the cells via an increase in mitochondrial ROS and subsequent cellular signaling events.[39, 47] One possible future experiment could be to isolation the mitochondria from a hyperoxic –exposed neonatal lung or mitochondrial inferior vena cava. This might be technically challenging due to the amount of mice needed to get a sufficient amount of mitochondria for these experiments or lack of reagents that might be needed to assess the integrity of mitochondria. Once the method is established, however, particular attention should be paid to conditioning role of CO by modulating mitochondrial ROS production or metabolic changes following hyperoxia exposure and/or ligation of IVC.

Lastly, many reports have ignored events that occur during CO pretreatment period, instead focusing on the direct effect of CO upon a subsequent stimulus.[48,49,39] The key observation that administration of exogenous CO leading to a transitory burst of ROS would not have been appreciated if investigators continued to think a along the lines that CO is benign in cells and tissues unless there is an inflammatory stimulus present. This rapid increase in ROS likely leads to concomitant induction of antioxidant enzymes and protective genes such that upon the addition of pro-oxidant stimuli, further production of ROS is attenuated. Thus, CO is not acting as an antioxidant molecule; rather, it forces the cell to undergo oxidative conditioning leading to cytoprotective gene expression, which indirectly modulates the ensuing cellular response to the stimulation. While these are valid and important studies, conclusions on mechanisms of CO need to be carefully considered.

In closure, CO is a molecule that has come full circle after being studied for over a century and classified as hazardous. Like other molecules CO has to be re-evaluated, not as a toxic molecule, but rather as a critical signaling molecule akin to nitric oxide. The beneficial effects of CO as an inhaled gas or through the use of CO-releasing molecules have been demonstrated in cell culture and animal models of a number of diseases.[16,5,50,51] As the results of inhaled CO treatment from clinical trials[52] have become available, the utility of this therapy to facilitate pulmonary and cardiovascular diseases will need to be investigated. Taken together, the studies in this thesis has only begun to

scratch surface and hope that in time, further cellular functions can be ascribed to the signaling processes initiated by CO. Our continued understanding of molecular mechanisms of various gaseous mediators and their relationships to one another must be harnessed and translated into clinical therapies.

FIGURES

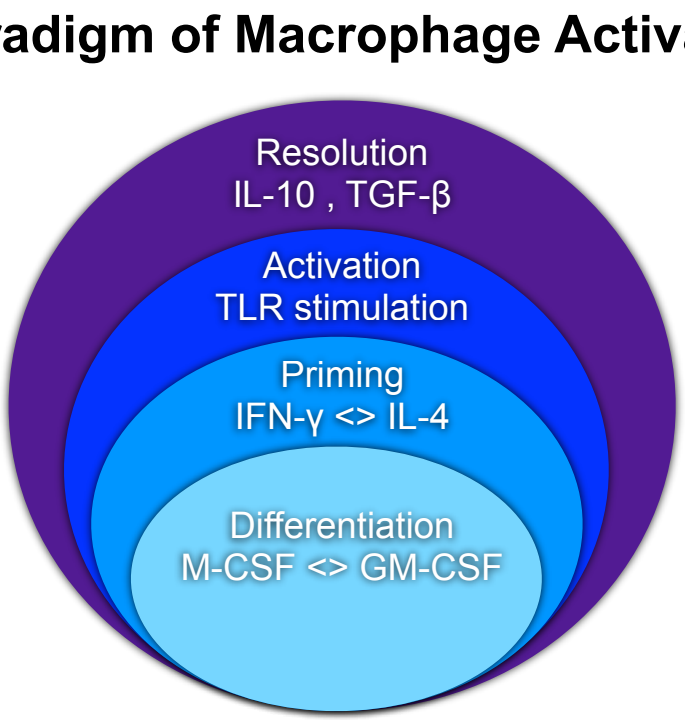

FIGURE IV.1: PARADIGM OF MACROPHAGE ACTIVATION:

Depicted above is a schematic model of macrophage activation modified from Gordon et al. Cell Immunity Review 2010.[53] The first stage, differentiation, depends on the growth factors such as GM-CSF or M-CSF (Macrophage colony-stimulating factor (M-CSF) and granulocyte-macrophage colony-stimulating factor (GM-CSF). The second, priming by IFN-gamma (CAM), IL-4 or IL-13 (AAM) -- switching M1 and M2 phase can occur and the third is a localizing stimulus delivered by a TLR. This stimulus promotes induction of a full complement of classical or alternative activation functions. In the case of AAMs, this may arise in a Th2 cell bias environment. The fourth stage (resolution and repair) is counteracts the negative effects even though the macrophage pro-inflammatory potential

is deactivated, it could undergo functional changes allowing it to clear debris and express repair functions.

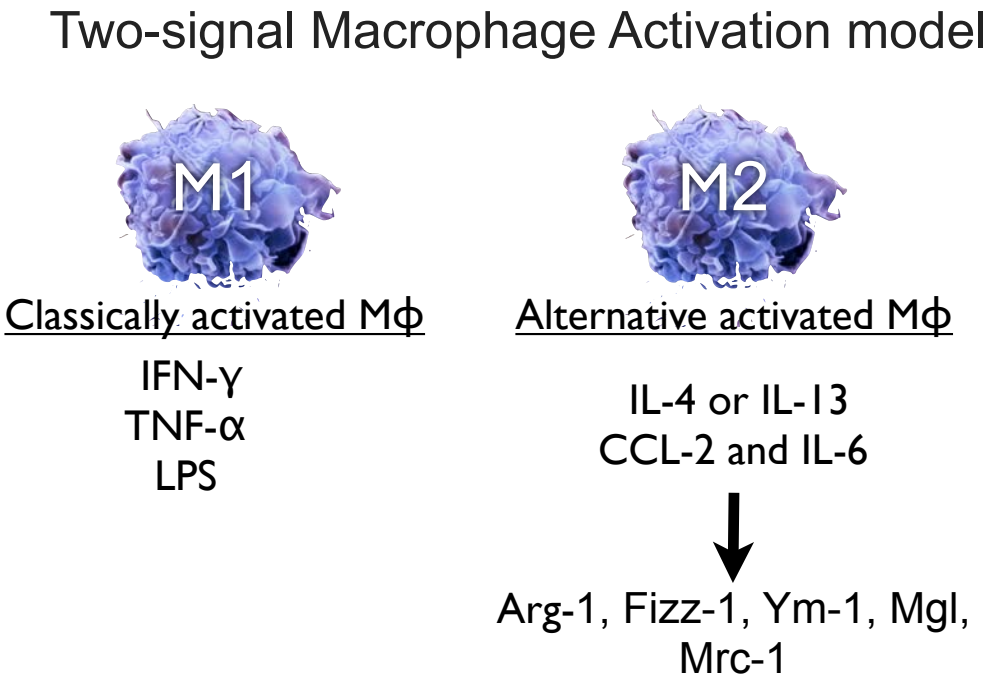

FIGURE IV.2: TWO SIGNAL MACROPHAGE ACTIVATION MODEL:

Classically activated (M1) or type I macrophage, induced in particular by IFNγ display a pro-inflammatory profile whereas alternatively activated (M2) or type II macrophage (AAMϕ), induced by Th-2 cytokines, express anti-inflammatory and tissue repair properties. M2 macrophage have been implicated in the pathogenesis of lung and other disorders via their ability to promote trophic, profibrotic ,and angiogenic function.

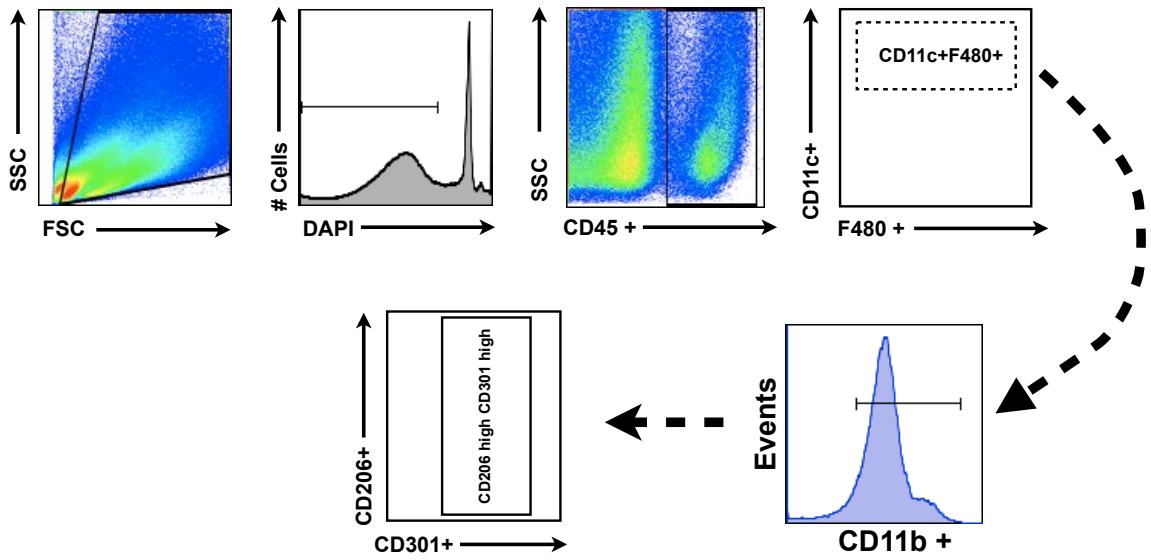

FIGURE IV.3: GATING STRATEGY

Hyperoxia induced lung injury results in the influx of alternatively activated macrophage and pulsatile CO treatment attenuates AAMϕ infiltration. Cells were gated on $CD45^{+}$ and then double positive cells were gated $CD11c^{high}/F4/80^{+}/CD11b+$ then subgated on $CD206^{low}CD301^{+}$ alternative activated macrophages

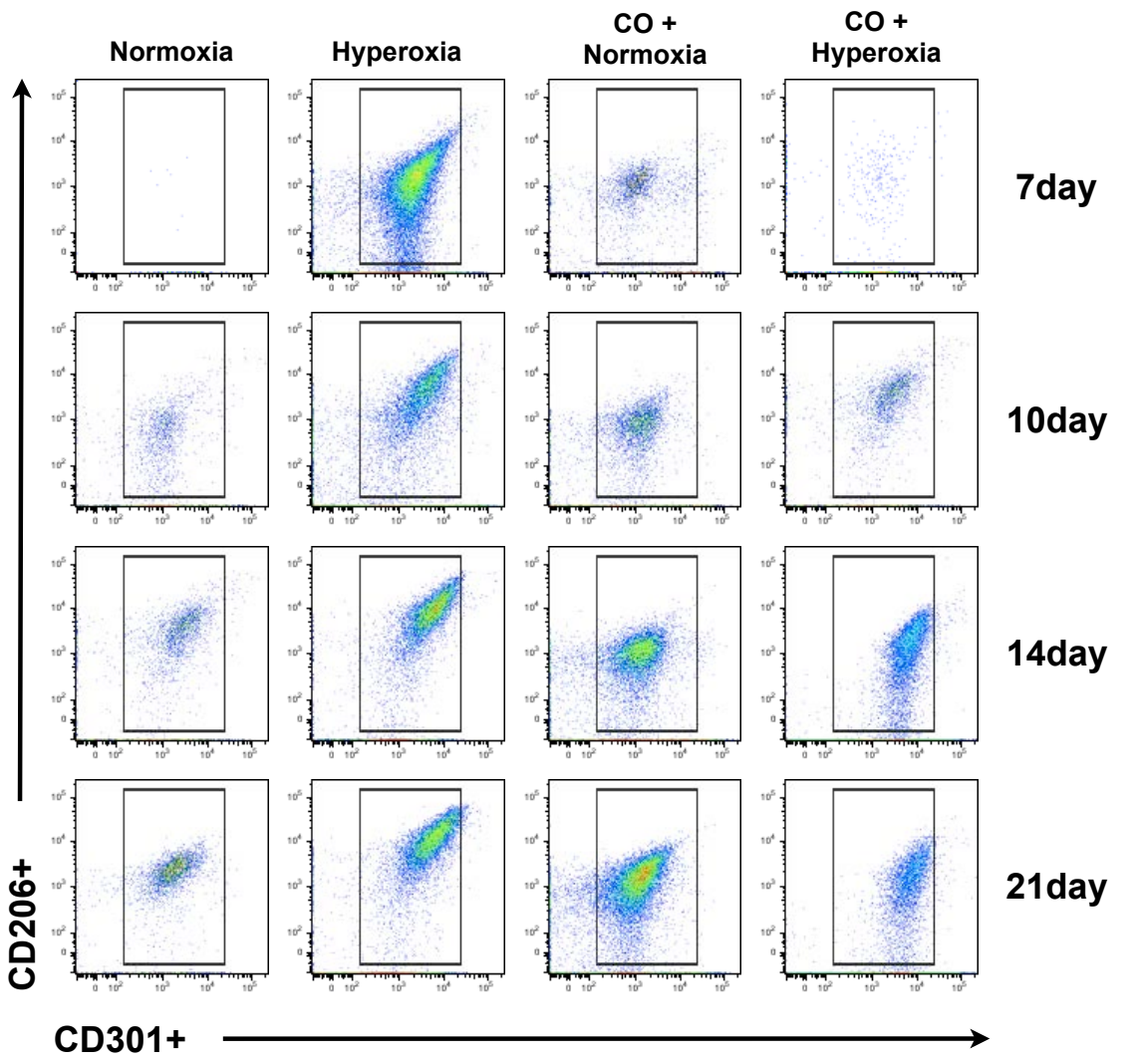

FIGURE IV.4: HYPEROXIA UPREGULATES ALTERNATIVE ACTIVATION OF MACROPHAGES AND CO TREATMENT AMELIORATES M2 MACROPHAGE MARKER EXPRESSION ASSOCIATED WITH HYPEROXIA-INDUCED LUNG INJURY.

M2 expression profile of hyperoxia induced mice show an increase in expression of $CD206^{+}CD301^{+}$ macrophages and CO treatment attenuates infiltration of M2 macrophage into the injured lung from day 7 up to day 21 in wild type animals.

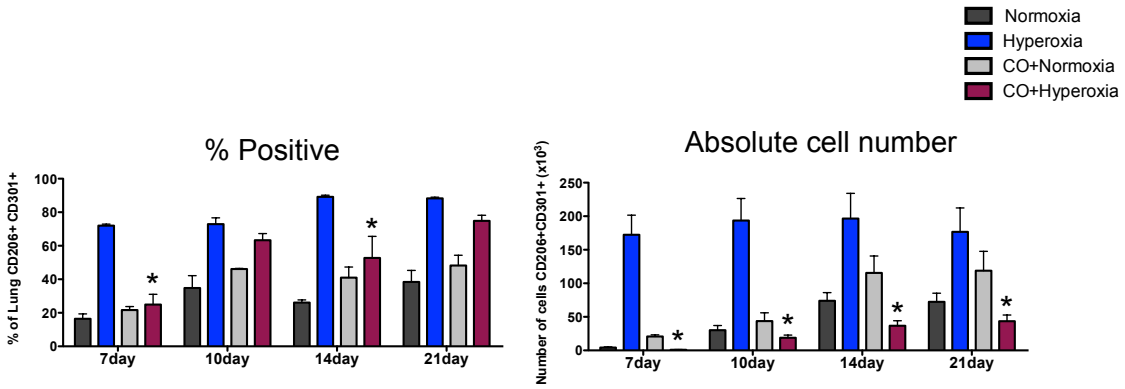

FIGURE IV.5: HYPEROXIA UPREGULATES ALTERNATIVE ACTIVATION OF MACROPHAGES AND CO TREATMENT AMELIORATES M2 MACROPHAGE MARKER EXPRESSION ASSOCIATED WITH HYPEROXIA-INDUCED LUNG INJURY.

Results from percent double positive population and cell number of $CD206^{+}CD301^{+}$ macrophages are shown here. The data are from day 7 up to day 21 from five to eight mice at each time point with two repeats. Numbers represent mean± SEM.* P <0.05 as compared to hyperoxia alone. One-way ANOVA.

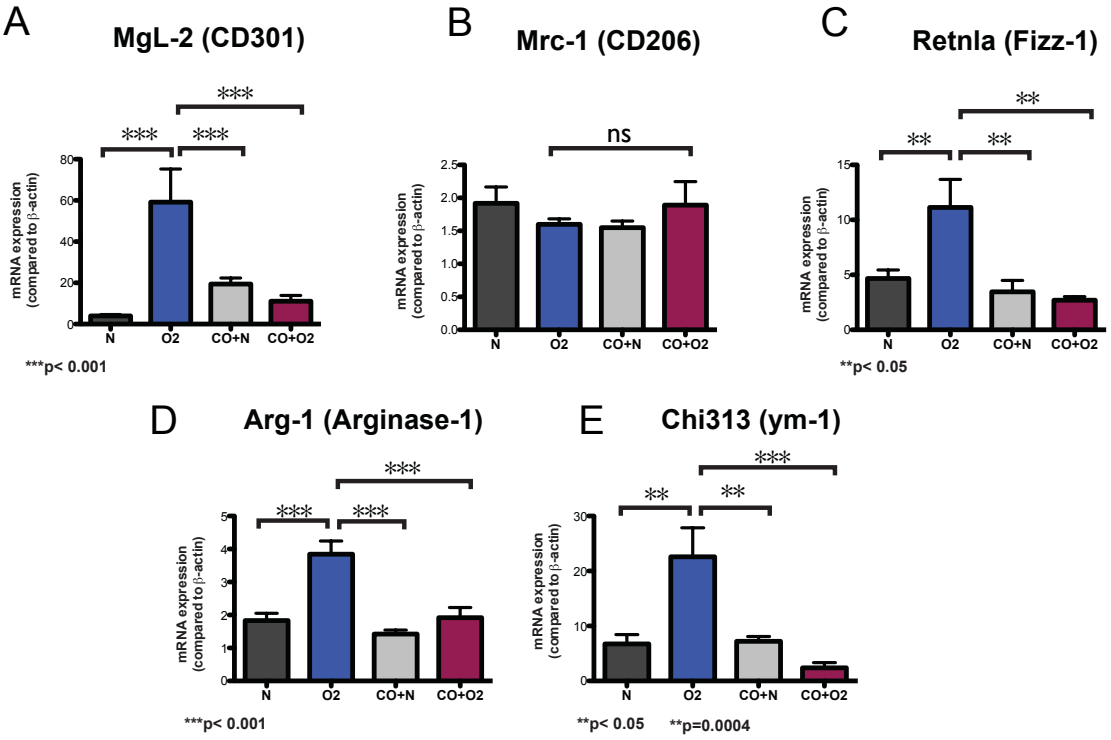

FIGURE IV.6: HYPEROXIA UPREGULATES ALTERNATIVE ACTIVATION OF MACROPHAGES AND CO TREATMENT AMELIORATES M2 MACROPHAGE MARKER EXPRESSION ASSOCIATED WITH HYPEROXIA-INDUCED LUNG INJURY.

(A-E) mRNA was measured by qPCR at 14 day post exposure of hyperoxia and CO treatment. Hyperoxic lung alveolar macrophage mRNA expression show decreased expression of macrophage activation Th2 related cytokine (MgL-2 (CD301), Fizz-1, Arg-1 and Ym-1) 10days post CO administration. (B) The mRNA levels of Mrc-1 (CD206) had no significant decrease after with or without intermittent CO treatment. Numbers represent mean±SD at least n=8-13 mice per group. ** P <0.05; ***P < 0.0001, one way ANOVA.

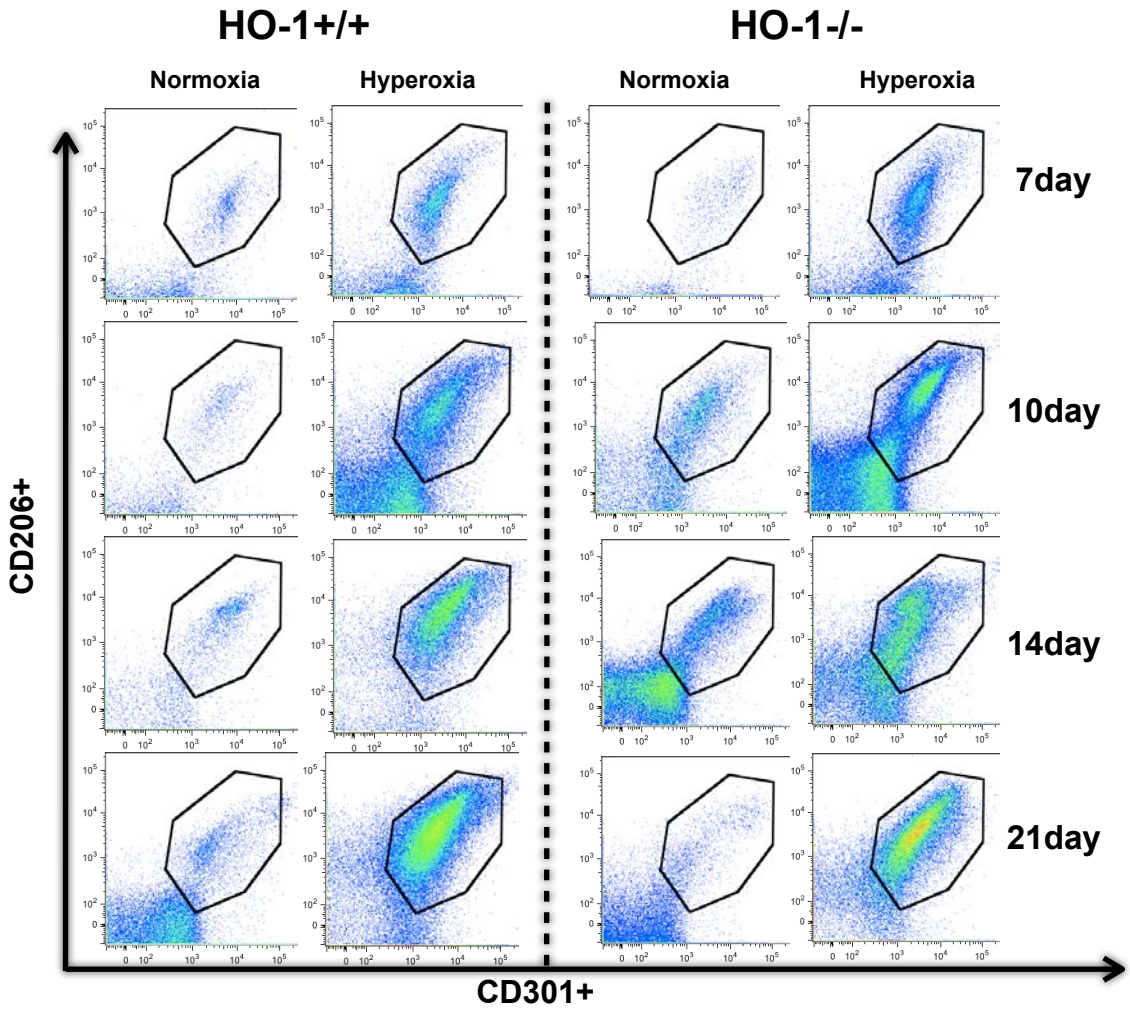

FIGURE IV.7: HYPEROXIA UPREGULATES ALTERNATIVE ACTIVATION OF MACROPHAGES AND HO-1 DEFICIENCY EXACERBATES M2 MACROPHAGE MARKER EXPRESSION ASSOCIATED WITH HYPEROXIA-INDUCED LUNG INJURY.

M2 expression profile of hyperoxia induced mice show an increase in expression of $CD206^{+}CD301^{+}$ macrophages and absence of HO-1 exacerbates the expression of M2 macrophage into the injured lung from day 7 up to day 21 in wild type animals. Cells were subgated from $CD45^{+}/CD11b^{+}$ (data not shown).

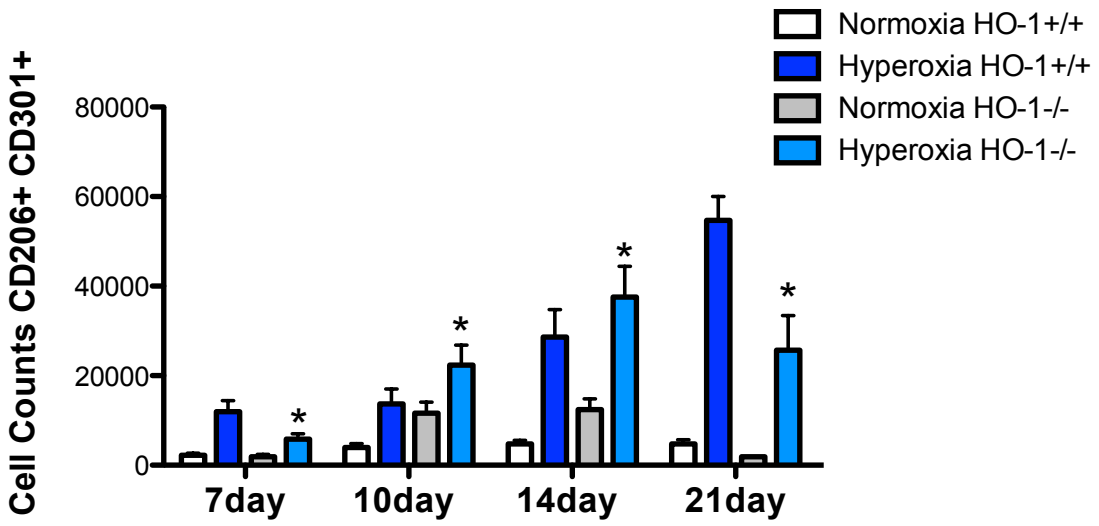

FIGURE IV.8: HYPEROXIA UPREGULATES ALTERNATIVE ACTIVATION OF MACROPHAGES AND HO-1 DEFICIENCY EXACERBATES M2 MACROPHAGE MARKER EXPRESSION ASSOCIATED WITH HYPEROXIA-INDUCED LUNG INJURY.

Results from absolute cell number of $CD206^{+}CD301^{+}$ macrophages are shown here. The data are from day 7 up to day 21 from five to eight mice at each time point with two repeats. Numbers represent mean± SEM.* P <0.05 as compared to hyperoxia alone. One-way ANOVA.

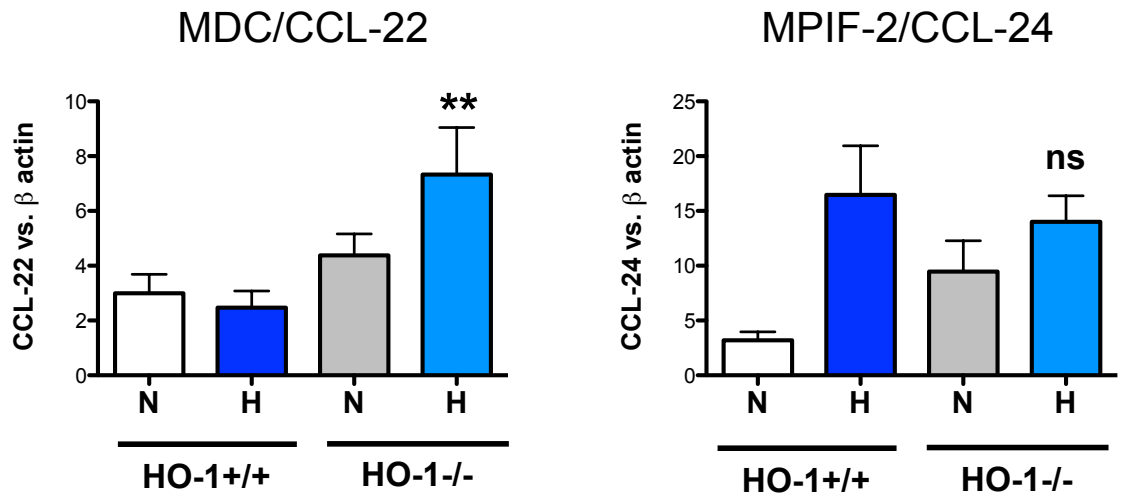

FIGURE IV.9: HYPEROXIA UPREGULATES AAMϕ CHEMOKINE MRNA EXPRESSION.

mRNA was measured by qPCR for CCL-22 and CCL24 at 14 day post exposure of hyperoxia. Hyperoxic lung alveolar macrophage mRNA expression shows increase in expression in CCL22 in HO-$1^{-/-}$ animals compared to HO-$1^{+/+}$ mice. The mRNA levels of MPIF-2 (CCL-24) had no significant increase post hyperoxia exposure in the absence of HO-1. Numbers represent mean ± SEM at least n=4-7 mice per group. ** P <0.05 as compared to HO-$1^{+/+}$ exposed to hyperoxia, one-way ANOVA.

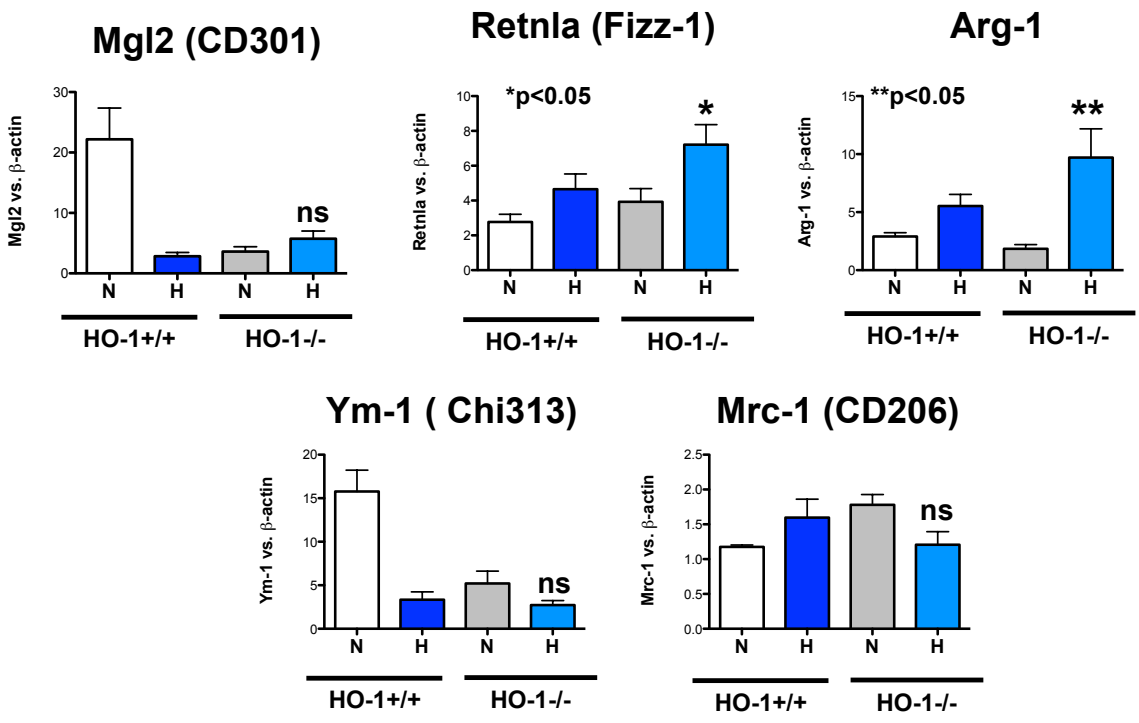

FIGURE IV.10: HYPEROXIA UPREGULATES AAMϕ M2 MACROPHAGE MARKER MRNA EXPRESSION.

mRNA was measured by qPCR at 14 day post exposure of hyperoxia. Hyperoxic lung alveolar macrophage mRNA expression showed a significant increase in Fizz-1 and Arg-1 in the absence of HO-1 compared to wild type. The mRNA levels of Mrc-1 (CD206), Ym-1 (Chi313) and Mrc-1 (CD206) was not significant in the absence of HO-1 compared to wild type. Numbers represent mean ± SEM at least n = 6-14 mice per group. * P <0.05 as compared to HO-$1^{+/+}$ exposed to hyperoxia, one-way ANOVA.

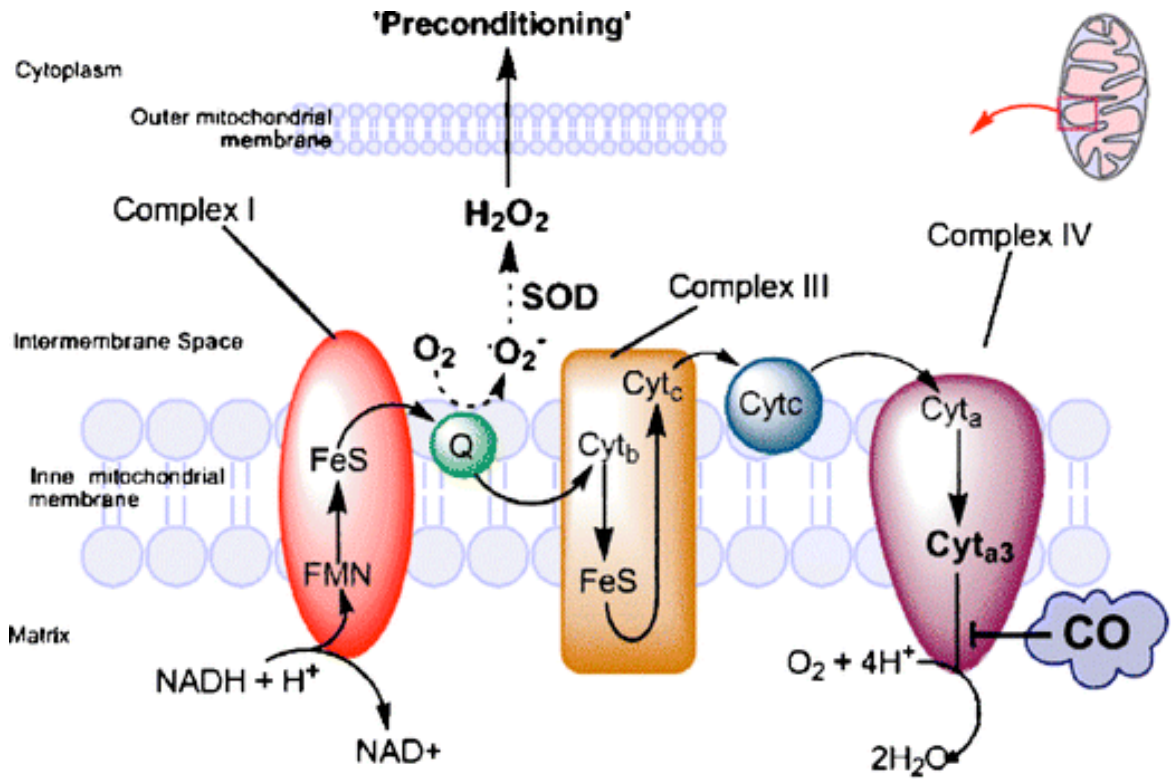

FIGURE IV.11: SCHEME ILLUSTRATING THE EFFECTS OF CARBON MONOXIDE INHIBITION OF THE MITOCHONDRIAL ELECTRON TRANSPORT CHAIN.

CO slows the rate of electron transport (*solid arrows*), enabling electrons to accumulate, including at complex III. As a consequence, the lifetime of the ubisemiquinone state of Coenzyme Q (*Q*) is prolonged which is prone to reduce O2 to superoxide (O_2^-). Superoxide could then be converted enzymatically to other ROS that collectively induce a conditioning response by altering signaling pathways. *FMN* Flavinmononucleotide, *FeS*: iron-sulfur cluster, *Cyt* cytochrome. The area of CO signaling through the mitochondria ROS production is still in its early stages, and the issues of how much CO binding occurs physiologically and what the role of H_2O_2 egress from mitochondria is in cell signaling are not fully understood.

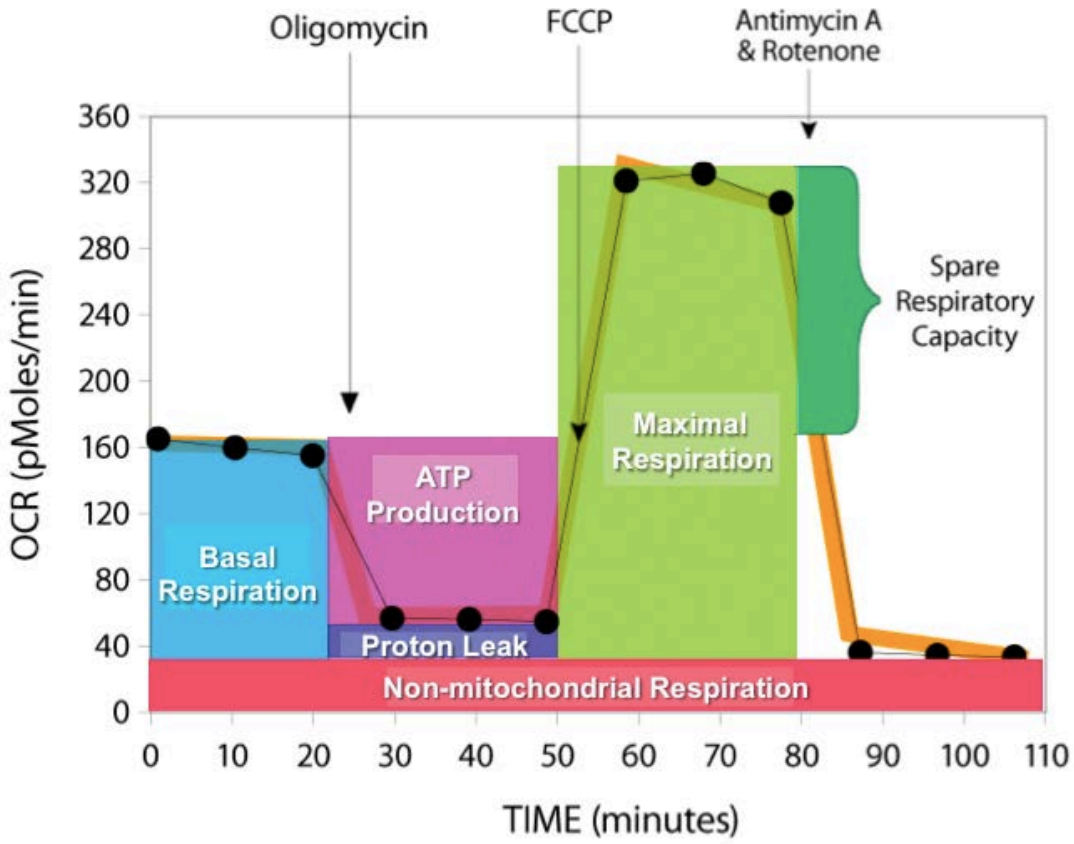

FIGURE IV.12: SCHEMA ILLUSTRATING THE XF CELL MITOCHONDRIA STRESS TEST PROFILE.

The XF Cell Mito Stress Test Kit makes it easy to measure the four key parameters of mitochondrial function in a microplate: basal respiration, ATP production, proton leak, and maximal respiration, revealing critical information not evident in basal metabolism measurements alone. There are 4 different reagents that are important to measure OCR and EACR: Oligomycin (ATP Coupler), FCCP (Electron Transport Chain Accelerator), Antimycin A (Mitochondrial Inhibitor A) and Rotenone (Mitochondrial Inhibitor B).

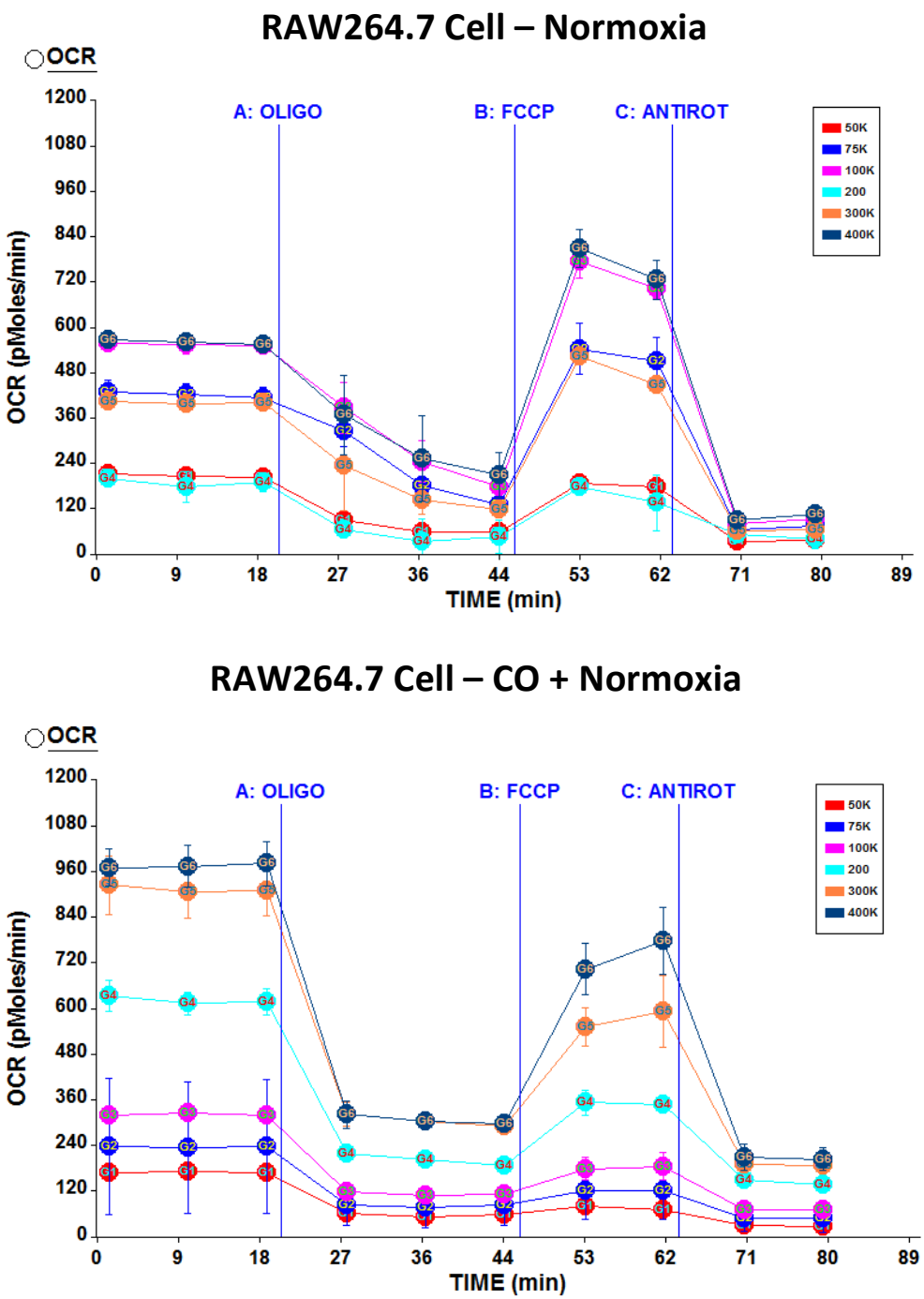

FIGURE IV.13: OCR MEASUREMENTS

. (Top) RAW264.7 cell exposed to normoxia for up to 24hrs. **(Bottom)** RAW264.7 cell exposed to CO + normoxia for up to 24hrs using Cell Mito Stress Test

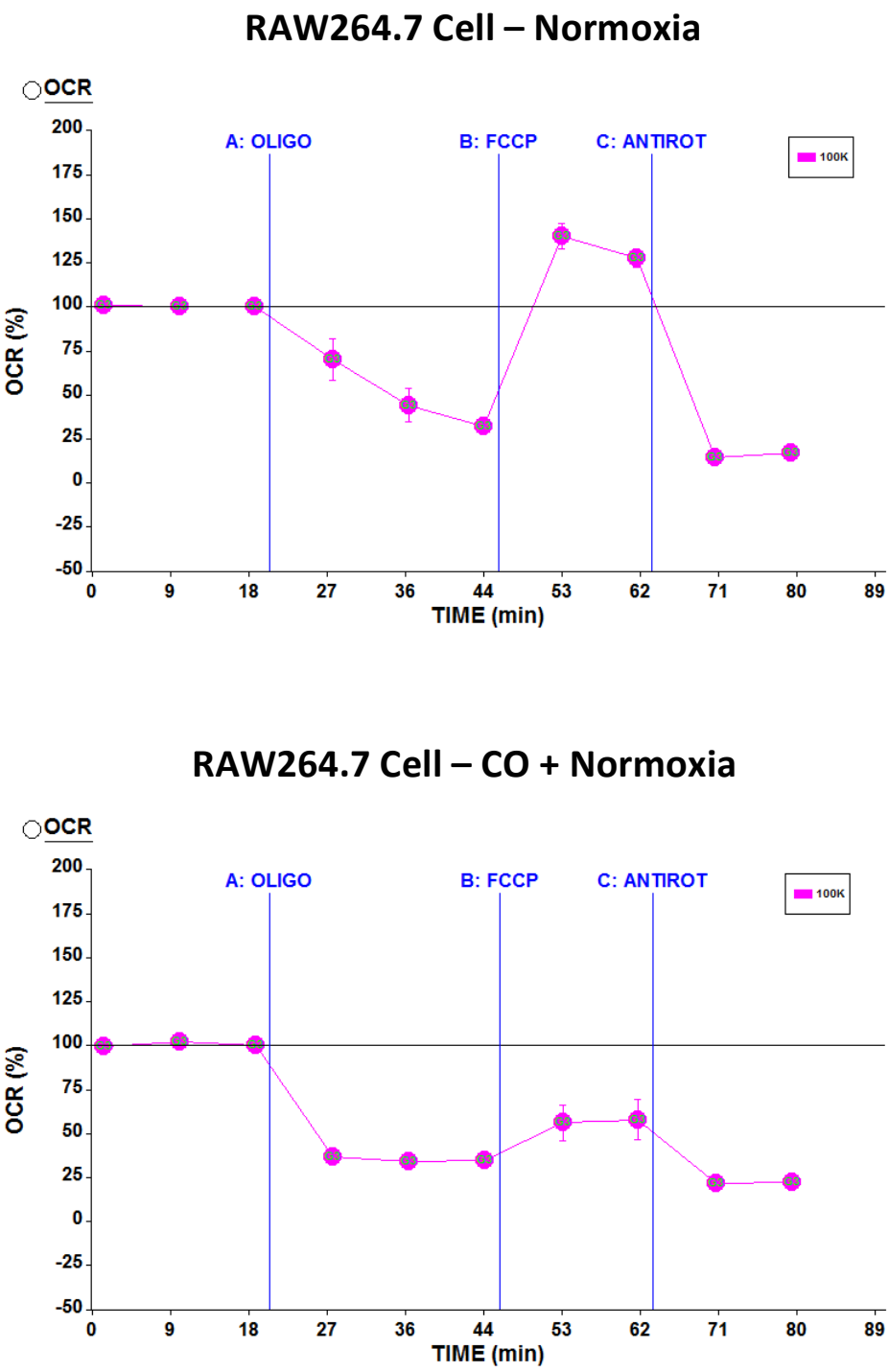

FIGURE IV.14: OCR BASELINE PERCENTAGE CHANGES MEASUREMENTS . (Top) RAW264.7 cell exposed to normoxia for up to 24hrs. **(Bottom)** RAW264.7 cell exposed to CO + normoxia for up to 24hrs using Cell Mito Stress Test.

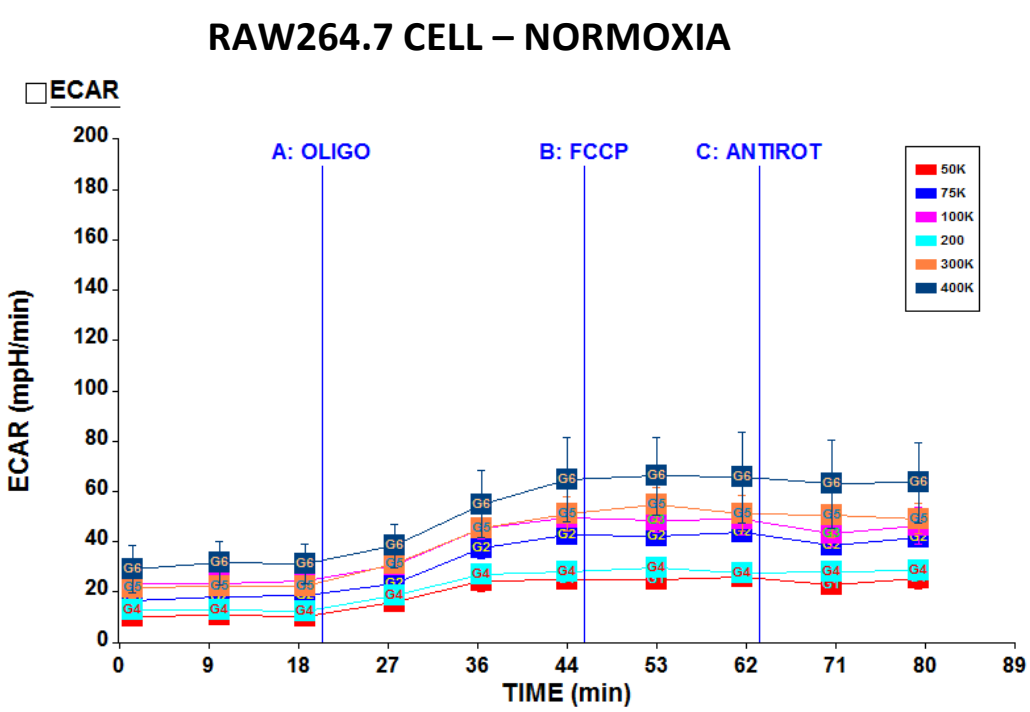

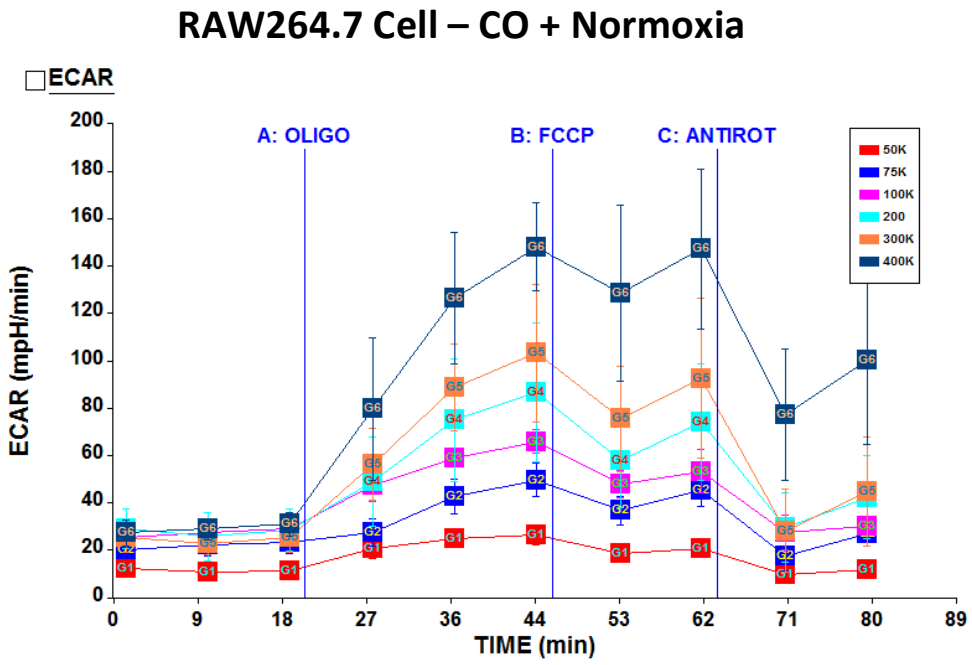

FIGURE IV.15: ECAR MEASUREMENTS

. (Top) RAW264.7 cell exposed to normoxia for up to 24hrs. **(Bottom)** RAW264.7 cell exposed to CO + normoxia for up to 24hrs using Cell Mito Stress Test. There are 4 different reagents that

are important to measure OCR and EACR: Oligomycin (ATP Coupler), FCCP (Electron Transport Chain Accelerator), Antimycin A (Mitochondrial Inhibitor A) and Rotenone (Mitochondrial Inhibitor B).

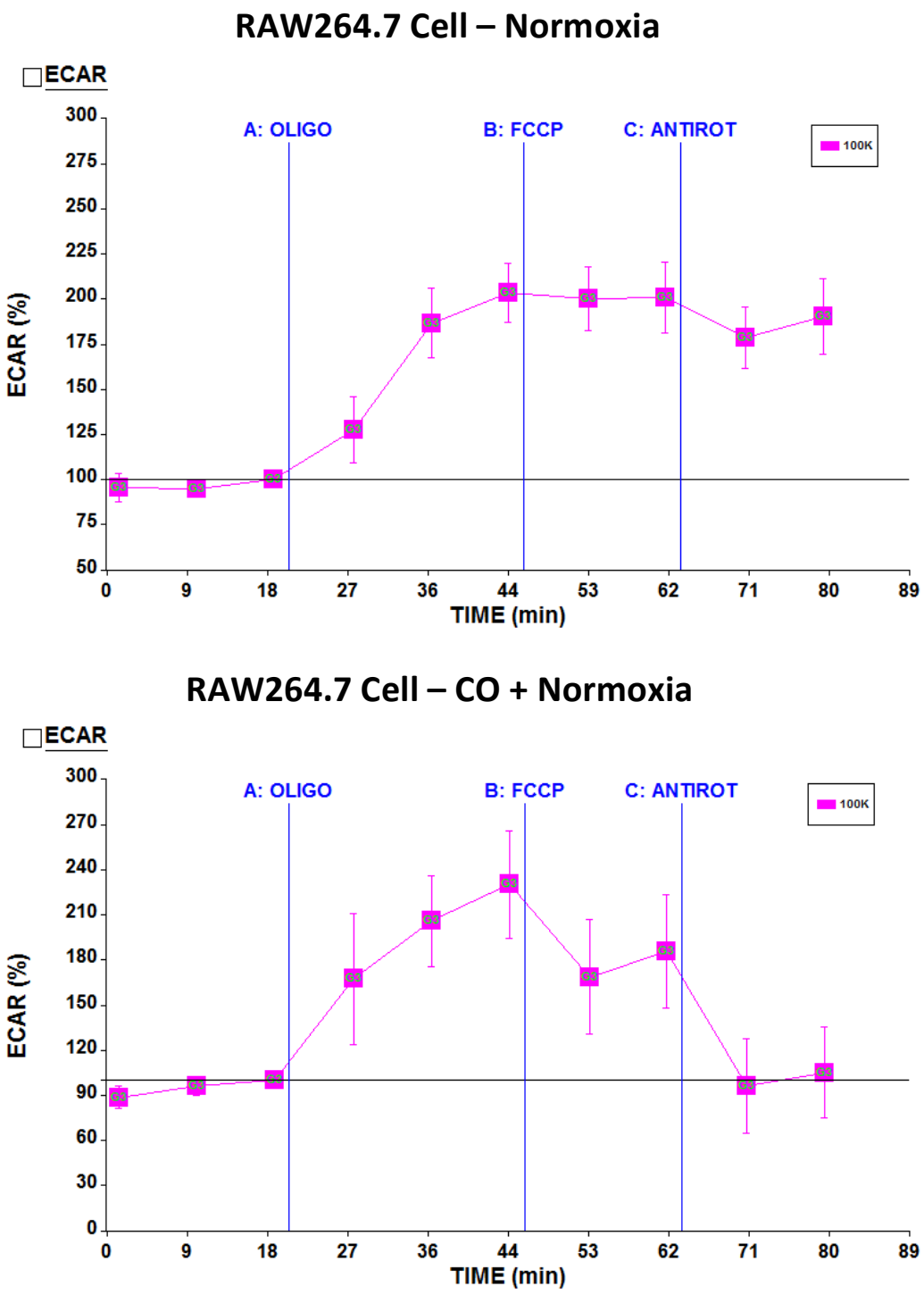

FIGURE IV.16: ECAR MEASUREMENTS

. (Top) RAW264.7 cell exposed to normoxia for up to 24hrs. **(Bottom)** RAW264.7 cell exposed to CO + normoxia for up to 24hrs using Cell Mito Stress Test. There are 4 different reagents that

are important to measure OCR and EACR: Oligomycin (ATP Coupler), FCCP (Electron Transport Chain Accelerator), Antimycin A (Mitochondrial Inhibitor A) and Rotenone (Mitochondrial Inhibitor B).

REFERENCES

1. Maines MD. The Heme Oxygenase System: A Regulator of Second Messenger Gases. *Annual Review of Pharmacology and Toxicology* 1997, **37**(1)**:** 517-554.

2. Ryter SW, Morse D, Choi AMK. Carbon Monoxide and Bilirubin. *American Journal of Respiratory Cell and Molecular Biology* 2007, **36**(2)**:** 175-182.

3. Poss K, Tonegawa S. Heme oxygenase-1 is required for mammalian iron reutilization. *Proc Natl Acad Sci USA* 1997, **94:** 10919 - 10924.

4. Kapturczak MH, Wasserfall C, Brusko T, Campbell-Thompson M, Ellis TM, Atkinson MA*, et al.* Heme Oxygenase-1 Modulates Early Inflammatory Responses: Evidence from the Heme Oxygenase-1-Deficient Mouse. *The American Journal of Pathology* 2004, **165**(3)**:** 1045-1053.

5. Fernandez-Gonzalez A, Alex Mitsialis S, Liu X, Kourembanas S. Vasculoprotective effects of heme oxygenase-1 in a murine model of hyperoxia-induced bronchopulmonary dysplasia. *American Journal of Physiology - Lung Cellular and Molecular Physiology* 2012, **302**(8)**:** L775-L784.

6. Gozzelino R, Jeney V, Soares MP. Mechanisms of Cell Protection by Heme Oxygenase-1. *Annual Review of Pharmacology and Toxicology*, **50**(1)**:** 323-354.

7. Auten RL, Mason SN, Tanaka DT, Welty-Wolf K, Whorton MH. Anti-neutrophil chemokine preserves alveolar development in hyperoxia-exposed newborn rats. *American Journal of Physiology - Lung Cellular and Molecular Physiology* 2001, **281**(2)**:** L336-L344.

8. Deng H, Nicholas Mason S, Auten RL, Jr. Lung Inflammation in Hyperoxia Can Be Prevented By Antichemokine Treatment in Newborn Rats. *Am J Respir Crit Care Med* 2000, **162**(6)**:** 2316-2323.

9. Yi M, Jankov RP, Belcastro R, Humes D, Copland I, Shek S*, et al.* Opposing Effects of 60% Oxygen and Neutrophil Influx on Alveologenesis in the Neonatal Rat. *American Journal of Respiratory and Critical Care Medicine* 2004, **170**(11)**:** 1188-1196.

10. Vozzelli MA, Mason SN, Whorton MH, Auten RL. Antimacrophage chemokine treatment prevents neutrophil and macrophage influx in hyperoxia-exposed newborn rat lung. *American Journal of Physiology - Lung Cellular and Molecular Physiology* 2004, **286**(3)**:** L488-L493.

11. Chung SW, Liu X, Macias AA, Baron RM, Perrella MA. Heme oxygenase-1–derived carbon monoxide enhances the host defense response to microbial sepsis in mice. *The Journal of Clinical Investigation* 2008, **118**(1)**:** 239-247.

12. Otterbein LE MA, Chin BY. Carbon monoxide increases macrophage bacterial clearance through Toll-like receptor (TLR)4 expression. *Cell Mol Biol* 2005, **51**(5)**:** 433-440.

13. Lin KL, Suzuki Y, Nakano H, Ramsburg E, Gunn MD. CCR2+ Monocyte-Derived Dendritic Cells and Exudate Macrophages Produce Influenza-Induced Pulmonary Immune Pathology and Mortality. *The Journal of Immunology* 2008, **180**(4)**:** 2562-2572.

14. Tighe RM, Liang J, Liu N, Jung Y, Jiang D, Gunn MD*, et al.* Recruited Exudative Macrophages Selectively Produce CXCL10 after Noninfectious Lung Injury. *American Journal of Respiratory Cell and Molecular Biology* 2011, **45**(4)**:** 781-788.

15. Bos PMJ, Zeilmaker MJ, van Eijkeren JCH. Application of Physiologically Based Pharmacokinetic Modeling in Setting Acute Exposure Guideline Levels for Methylene Chloride. *Toxicol Sci* 2006, **91**(2)**:** 576-585.

16. Motterlini R, Mann BE, Foresti R. Therapeutic applications of carbon monoxide-releasing molecules. *Expert Opinion on Investigational Drugs* 2005, **14**(11)**:** 1305-1318.

17. Yang G, Madan A, Dennery PA. Maturational differences in hyperoxic AP-1 activation in rat lung. *Am J Physiol Lung Cell Mol Physiol* 2000, **278**(2)**:** L393-398.

18. Kyrle PA, Eichinger S. Deep vein thrombosis. *The Lancet*, **365**(9465)**:** 1163-1174.

19. Rodriguez A, Wojcik B, Wrobleski S, Myers D, Jr., Wakefield T, Diaz J. Statins, inflammation and deep vein thrombosis: a systematic review. *J Thromb Thrombolysis* 2012, **33**(4)**:** 371-382.

20. Saha P, Humphries J, Modarai B, Mattock K, Waltham M, Evans CE*, et al.* Leukocytes and the Natural History of Deep Vein Thrombosis: Current Concepts and Future Directions. *Arteriosclerosis, Thrombosis, and Vascular Biology* 2011, **31**(3)**:** 506-512.

21. Huo Y SA, Forlow SB, Smith DF, Hyman MC, Jung S, Littman DR, Weber C, Ley K. Circulating activated platelets exacerbate atherosclerosis in mice deficient in apolipoprotein E. *Nature Medicine* 2003, **9**(1)**:** 61-67.

22. Massberg S, Brand K, Grüner S, Page S, Müller E, Müller I*, et al.* A Critical Role of Platelet Adhesion in the Initiation of Atherosclerotic Lesion Formation. *The Journal of Experimental Medicine* 2002, **196**(7)**:** 887-896.

23. Wakefield TW, Henke PK. The Role of Inflammation in Early and Late Venous Thrombosis: Are There Clinical Implications? *Seminars in Vascular Surgery* 2005, **18**(3)**:** 118-129.

24. Myers DD WT. Inflammation-dependent thrombosis. *Front Bioscience* 2005, **10:** 2750-2757.

25. Wakefield TW, Myers DD, Henke PK. Mechanisms of Venous Thrombosis and Resolution. *Arteriosclerosis, Thrombosis, and Vascular Biology* 2008, **28**(3)**:** 387-391.

26. Myers Jr D, Farris D, Hawley A, Wrobleski S, Chapman A, Stoolman L*, et al.* Selectins Influence Thrombosis in a Mouse Model of Experimental Deep Venous Thrombosis. *Journal of Surgical Research* 2002, **108**(2)**:** 212-221.

27. Myers Jr DD, Hawley AE, Farris DM, Chapman AM, Wrobleski SK, Henke PK, *et al.* Cellular IL-10 is more effective than viral IL-10 in decreasing venous thrombosis. *Journal of Surgical Research* 2003, **112**(2)**:** 168-174.

28. Myers Jr DD, Rectenwald JE, Bedard PW, Kaila N, Shaw GD, Schaub RG, *et al.* Decreased venous thrombosis with an oral inhibitor of P selectin. *Journal of Vascular Surgery* 2005, **42**(2)**:** 329-336.

29. De Maio A TM, Reeves RH. Genetic determinants influencing the response to injury, inflammation, and sepsis. *Shock* 2005, **23**(1)**:** 11-17.

30. Gordon S, Taylor PR. Monocyte and macrophage heterogeneity. *Nat Rev Immunol* 2005, **5**(12)**:** 953-964.

31. Dalton DK P-MS, Keshav S, Figari IS, Bradley A, Stewart TA. Multiple defects of immune cell function in mice with disrupted interferon-gamma genes. *Science* 1993, **259**(5102)**:** 1739-1742.

32. Gordon S. Alternative activation of macrophages. *Nat Rev Immunol* 2003, **3**(1)**:** 23-35.

33. Vergadi E, Chang MS, Lee C, Liang OD, Liu X, Fernandez-Gonzalez A*, et al.* Early Macrophage Recruitment and Alternative Activation Are Critical for the Later Development of Hypoxia-Induced Pulmonary Hypertension / Clinical Perspective. *Circulation* 2011, **123**(18)**:** 1986-1995.

34. Durante W, Liao L, Reyna SV, Peyton KJ, Schafer AI. Transforming Growth Factor-β1 Stimulates l-Arginine Transport and Metabolism in Vascular Smooth Muscle Cells. *Circulation* 2001, **103**(8)**:** 1121-1127.

35. Jin Y, Calvert TJ, Chen B, Chicoine LG, Joshi M, Bauer JA*, et al.* Mice deficient in Mkp-1 develop more severe pulmonary hypertension and greater lung protein levels of arginase in response to chronic hypoxia. *American Journal of Physiology - Heart and Circulatory Physiology* 2010, **298**(5)**:** H1518-H1528.

36. Otterbein L, Mantell L, Choi A. Carbon monoxide provides protection against hyperoxic lung injury. *Am J Physiol* 1999, **276:** L688 - L694.

37. Bilban M, Bach FH, Otterbein SL, Ifedigbo E, de Costa d'Avila J, Esterbauer H*, et al.* Carbon Monoxide Orchestrates a Protective Response through PPARγ. *Immunity* 2006, **24**(5)**:** 601-610.

38. Chin BY, Jiang G, Wegiel B, Wang HJ, MacDonald T, Zhang XC*, et al.* Hypoxia-inducible factor 1Î± stabilization by carbon monoxide results in cytoprotective preconditioning. *Proceedings of the National Academy of Sciences* 2007, **104**(12)**:** 5109-5114.

39. Veal EA, Day AM, Morgan BA. Hydrogen Peroxide Sensing and Signaling. *Molecular Cell* 2007, **26**(1)**:** 1-14.

40. Geiszt M, Leto TL. The Nox Family of NAD(P)H Oxidases: Host Defense and Beyond. *Journal of Biological Chemistry* 2004, **279**(50)**:** 51715-51718.

41. Boczkowski J, Poderoso JJ, Motterlini R. CO–metal interaction: vital signaling from a lethal gas. *Trends in Biochemical Sciences* 2006, **31**(11)**:** 614-621.

42. Baines CP, Goto M, Downey JM. Oxygen Radicals Released During Ischemic Preconditioning Contribute to Cardioprotection in the Rabbit Myocardium. *Journal of Molecular and Cellular Cardiology* 1997, **29**(1)**:** 207-216.

43. Ahmad S, White CW, Chang L-Y, Schneider BK, Allen CB. Glutamine protects mitochondrial structure and function in oxygen toxicity. *American Journal of Physiology - Lung Cellular and Molecular Physiology* 2001, **280**(4)**:** L779-L791.

44. Morava E, Rodenburg R, Hol F, De Meirleir L, Seneca S, Busch R*, et al.* Mitochondrial dysfunction in Brooks–Wisniewski–Brown syndrome. *American Journal of Medical Genetics Part A* 2006, **140A**(7)**:** 752-756.

45. Zhang X, Shan P, Jiang G, Zhang SS-M, Otterbein LE, Fu X-Y*, et al.* Endothelial STAT3 is essential for the protective effects of HO-1 in oxidant-induced lung injury. *FASEB J* 2006, **20**(12)**:** 2156-2158.

46. Ryter SW, Otterbein LE. Carbon monoxide in biology and medicine. *BioEssays* 2004, **26**(3)**:** 270-280.

47. Stone JR YS. Hydrogen peroxide: a signaling messenger. *Antioxid Redox Signal* 2006, **8**(3-4)**:** 243-270.

48. Taillé C, El-Benna J, Lanone S, Boczkowski J, Motterlini R. Mitochondrial Respiratory Chain and NAD(P)H Oxidase Are Targets for the Antiproliferative Effect of Carbon Monoxide in Human Airway Smooth Muscle. *Journal of Biological Chemistry* 2005, **280**(27)**:** 25350-25360.

49. Otterbein L, Bach F, Alam J, Soares M, Tao Lu H, Wysk M*, et al.* Carbon monoxide has anti-inflammatory effects involving the mitogen-activated protein kinase pathway. *Nat Med* 2000, **6:** 422 - 428.

50. Mishra S, Fujita T, Lama VN, Nam D, Liao H, Okada M*, et al.* Carbon monoxide rescues ischemic lungs by interrupting MAPK-driven expression of early growth response 1 gene and its downstream target genes. *Proceedings of the National Academy of Sciences of the United States of America* 2006, **103**(13)**:** 5191-5196.

51. Minamoto K, Harada H, Lama VN, Fedarau MA, Pinsky DJ. Reciprocal regulation of airway rejection by the inducible gas-forming enzymes heme oxygenase and nitric oxide synthase. *The Journal of Experimental Medicine* 2005, **202**(2)**:** 283-294.

52. Scott JR, Chin BY, Bilban MH, Otterbein LE. Restoring HOmeostasis: is heme oxygenase-1 ready for the clinic? *Trends in Pharmacological Sciences* 2007, **28**(5)**:** 200-205.

53. Gordon S, Martinez FO. Alternative Activation of Macrophages: Mechanism and Functions. *Immunity* 2010, **32**(5)**:** 593-604.

CHAPTER V

ADDENDUM

Inflammatory pathway analysis of the role of CD39 in a murine model of venous thrombogenesis

ABSTRACT

Leukocyte flux is thought to contribute to thrombus formation in deep venous structures under pathologic conditions, but little is known of the driving mechanisms or mechanisms which inhibit venous thrombosis during quiescence. Ectonucleoside tri(di)phosphohydrolase 1 (CD39), an ectoenzyme which catabolizes adenine nucleotides, is embedded on the surface of endothelial cells (EC), leukocytes and platelets. To determine whether CD39 regulates thromboinflammation at the vein/blood interface, mice were subjected to experimental inferior vena cava (IVC) ligation and deep venous thrombus formation examined. Mice homozygous null for the CD39 gene developed significant larger thrombi and more vein wall leukocytes (particularly neutrophils) at 48 hours than wild type mice expressing a normal complement of CD39. Gene expression profiling of CD39 gene-null mice (in comparison to controls) revealed three differentially-expressed inflammatory genes groups (group I, II and III – total of 76 genes) that were significantly upregulated during venous thrombosis and CD39 deletion;

qRT-PCR validation experiments confirmed high expression of 10 of these key inflammatory mediators. From this group, P-selectin and vWF, were chosen for further study due to their proximal involvement with inflammatory and thrombotic events, respectively. Circulating levels of both P-selectin and vWF were strikingly higher following IVC ligation in mice lacking CD39, with a corresponding increment in platelet-leukocyte heteroaggregates. Taken together, these data indicate a cardinal role for CD39 as a mitigator of venous thromboinflammation under conditions of venous stasis.

INTRODUCTION

Deep vein thrombosis (DVT) and its major complication, pulmonary embolism (PE) is the third leading cause of cardiovascular death in the United States. DVT and PE, collectively referred to as venous thromboembolism (VTE) affect > 500,000 individuals and cause up to 180,000 deaths each year in the United States alone.[1, 2, 3] In spite of high disease burden of DVT, much of the underlying etiology and pathophysiology remains unclear. A growing body of evidence supports the paradigm of intertwined roles of inflammation and thrombosis in the pathogenesis of DVT.

In humans, systemic inflammatory conditions such as sepsis, inflammatory bowel disease and rheumatoid arthritis are associated with an increased risk of venous thrombosis.[4] Inflammation in an animal model of DVT drives thrombosis by increasing tissue factor derived from the vessel wall and leukocytes. Inflammation also increases platelet reactivity, fibrinogen synthesis, and decreasing thrombomodulin, thereby increasing thrombosis. Inflammation or hypoxia-driven inflammation increases plasminogen activator inhibitor (PAI-1) by suppressing fibrinolysis. In concert, these changes set out to substantiate accumulated thrombus burden.[5, 6, 7, 8, 9] Early stages of venous thrombosis in animal models are characterized by increased leukocyte recruitment, adhesion and infiltration into the vessel wall.[10, 11, 12] The molecular mechanisms by which thrombosis occurs in DVT have not been fully elucidated. Activation of the vessel wall, vascular tissue factor, disturbed flow, stasis, hypoxia and

activated circulating leukocytes and platelets play significant roles as triggers for thrombus formation.[13, 14, 15, 16, 17, 18, 19]

Selectins, expressed on the surface of endothelial cells (E-selectin and P-selectin) and platelets (P-selectin) have been shown to be important mediators of inflammation and DVT formation.[19, 20] Recent work has shown the role of endothelial, neutrophil, monocyte and platelet cell-cell interactions as facilitators and potentiators of venous thrombus formation and propagation.[19] Though there is some uncertainty as to the role of platelets in thrombosis related to venous stasis, the position of platelets at the thrombosis and inflammatory interface suggested they might play an active role in DVT. von Willebrand Factor (vWF), a multimeric adhesive ligand for platelet (GPIb), serves as a critical endothelial mediator of venous thrombosis by providing binding sites on the luminal surface for leukocyte and platelet adhesion. The observation that thrombi do not form in the absence of vWF in a mouse model of DVT highlights its critical role in venous thrombogeneis.[21, 22] Additionally, diffuse fibrin accumulation serves as a mesh for platelet agglutination. More recently, neutrophil extracellular traps released from activated neutrophils have been implicated as key modulators of venous thrombus propagation, serving as a prothrombotic scaffold and a trap for leukocytes, platelets and red blood cells. In fact, studies in humans with DVT have shown an increase in circulating activated leukocyte-platelet heterodimers.[23] Understanding drivers of, the interaction between innate immune cells and platelets in DVT propagation forms the basis for our work.

Though found in abundance within cells purine nucleotides (ATP, ADP and AMP) are released extracellularly upon injury or death, where they form an extensive cell communication system with central roles in modulating endothelial cell activation, thrombosis, inflammatory cell trafficking and activation, apoptosis and vasoconstriction.[24, 25, 26, 27, 28, 29, 30] Extracellular ATP and ADP metabolism is regulated by an ecto-apyrase (ecto-nucleoside triphosphate diphosphohydrolase-1, CD39), a transmembrane enzyme with a luminal-facing active site, which catalyzes the terminal phosphohydrolysis of ATP and ADP. CD39 thereby plays a critical role in thromboregulation and inflammation. CD39 is located on the surface of endothelial cells, leukocytes and platelets, where it tonically suppresses platelet aggregation by dissipating ADP, the chief agonist for the P2Y12 class of purinergic receptors on the platelet surface.[31, 32] CD39 deficiency causes deleterious outcomes in various models of end-organ injury, such as stroke[33,34], Ischemia reperfusion injury[35] and transplantation as graft survival in xenograft heart transplantation[36] which could be caused by unopposed ATP toxicity. Our previous work demonstrated the protective thromboregulatory function of CD39 in mice [34,37] and in rats[38] with stroke.[37] Through its equally potent ability to dissipate a cloud of ATP released as an injury or danger signal, our group has shown that surface CD39 enables leukocytes to autoregulate their own flux into ischemic tissue.[34] This ectoenzyme therefore has a critical role at the nexus between inflammation and coagulation at the blood/vessel interface.

The objective of this study was to test the hypothesis that CD39 diminishes venous thrombogenesis. To test this hypothesis initially in an agnostic manner, mice ($CD39^{+/+}$ or $CD39^{-/-}$) were subjected to experimental procedure to create venous thrombosis, and gene expression profiling was used to monitor differential gene expression in inferior vena cava post thrombus induction compared to sham-operated control. Comprehensive bioinformatics analyses were used to enrich databases for Gene Ontology and pathway information to provide a deeper insight into candidate genes identified by expression profiling to elucidate inflammatory mechanisms involved during venous thrombogenesis. Using this approach we were able to show CD39 attenuates venous thrombogenesis by down-regulating vWF and soluble (sol) P-selectin expression.

METHODS

Targeted disruption of CD39 and generation of CD39-deficient mice.

The $CD39^{flox/flox}$ mice used in this work were on C57BL/6J background and generated using vector pFlox-Flp-Neo as a backbone for generating a targeting vector with LoxP sites flanking the first exon of CD39 gene. CD39 global knockout mice were generated by crossing the floxed allele to a ubiquitously expressed Cre (EIIA) recombinase promoter. The presence of the EIIA promoter ensured less extraneous genetic material was present in the CD39 global deficient mice. Quantitative RT-PCR analyses confirmed the absence of CD39 mRNA in various adult mouse organs tested **(Figure 1A and B)**. In all experiments reported here, $CD39^{flx/flx}$ littermates were used as controls for $CD39^{-/-}$ mice.

Animals

The control mice used for these experiments were $CD39^{flox/flox}$, designated as $CD39^{+/+}$ mice. Mice which were globally deleted of CD39 utilizing the EIIA cre recombinase deletion strategy, are designated here as $CD39^{-/-}$ mice. All mice, $CD39^{+/+}$ and $CD39^{-/-}$ were back bred at least 8 generations into the C57BL/6J background. For all experiments, $CD39^{+/+}$ and $CD39^{-/-}$ mice were aged-matched, males (8-to-10-weeks-old) weighing 25–30 grams. Animal experiments were approved by and carried out in accordance with the University of Michigan Institutional Animal Care and Use Committee guidelines.

Phenotypic characterization of CD39$^{+/+}$ and CD39$^{-/-}$ mice

Cardiovascular phenotype was assessed by measuring blood pressure and heart rate and by evaluating for baseline differences in overall cardiac function. Blood pressure and heart rate were obtained on acclimatized mice by tail cuff. A minimum of 6 measurements per animal was obtained and averaged. Baseline echocardiographic measurements were obtained in the following manner. Induction of anesthesia was performed in an enclosed container filled with 4-5% isoflurane. After induction, mice were placed on a warming pad to maintain body temperature. 1 – 1.5% isoflurane was supplied via a nose cone to maintain anesthesia. The hair was removed from the upper abdominal and thoracic area with depilatory cream. ECG was monitored via non-invasive resting ECG electrodes. Transthoracic echocardiography was performed in the supine or left lateral position. Two-dimensional, M-mode, Doppler and tissue Doppler echocardiographic images were recorded using a Visual Sonics' Vevo 700 high resolution *in vivo* micro-imaging system.

Analysis of whole-blood hematology profile and platelet aggregometry

Mice were anesthetized with isoflurane (2.5% in 10% oxygen) and blood was drawn by direct cardiac puncture into ethylenediaminetetraacetic acid (EDTA) microtainer tubes or 10% sodium citrate (Becton Dickinson, and Co. Franklyn Lakes, NJ). A complete blood panel was run on 30 μL using the CDC Technologies HEMAVET 950FS® Multispecies Hematology Analyzer (Drew Scientific, Inc. Dallas TX). The hematologic values

evaluated included the white blood cell count, neutrophils, monocytes, lymphocytes, red blood cell count, platelet count, hematocrit, and mean platelet volume. Prothrombin time and partial thromboplastin time were measured by Antech Diagnostics (Irvine, CA). For whole-blood aggregation experiments, murine blood was drawn in heparinized capillary tubes (Fisher Scientific, Pittsburgh PA) from the retro-orbital plexus. Whole-blood was diluted 4-fold with physiologic saline and impedance aggregometry was performed using a Chrono-log 560CA with the Aggro/Link 810 software (Haverton, PA) according to manufacturer's instructions. Whole-blood aggregation was stimulated with 5 μM ADP (Chrono-log).

Mouse model of stasis-induced deep venous thrombosis

The thrombus induced mouse complete stasis model of inferior vena cava thrombosis was used to induce thrombogenesis as previously described[39,20,40,41] by an operator blinded to the genotype of the experimental animal. Eight-to –ten-week- old male mice were anesthetized using inhalational 5-7% isoflurane gas and 100% oxygen mixture, and body temperature was maintained during surgery at 37^{o}C for 45min – one hour thereafter using a temperature –controlled circulating liquid heating pad. After a midline laparotomy to access the inferior vena cava (IVC), the intestines were exteriorized and sterile saline was applied during the entire procedure. Abdominal contents were protected with moist sterile gauze to prevent from drying. A space holder was positioned on the outside of the vessel and fascia surrounding the aorta, and the IVC was approached and all venous side branches were ligated using 7-0 prolene suture (Ethicon, Inc, Somerville, NJ) immediately below the renal veins to obtain complete stasis. After surgery, the intestines were returned to the body cavity, 1.5mL of warm saline was flushed into the peritoneum,

and the abdominal wall and skin closed with 5-0 Vicryl (Ethicon, Inc, Somerville, NJ). Sham-operated experiments consisted of median laparotomy and intestine manipulation without ligation of the IVC. For the initial time course experiment, the thrombus-containing IVC was carefully removed, weighed and the block was measured. Thrombus –containing IVC and IVC of sham-operated mice is widely used in studies of DVT model in mice to characterize the weight and size of the clot.[39,20,40,41] One – seven days after thrombus induction, the entire thrombosed IVC was either 1) weighed in milligrams (mg) to assess the clot weight; 2) placed in 10% formalin for fixation and then 70% ethanol for storage until the time of histological analysis; or 3) thrombus was carefully separated from the IVC wall, snap frozen, and stored at -80^{o}C until used for biochemical analysis.

Thrombus and Inferior vein wall weight measurement

Four-eight hours after surgery, mice from the four experimental groups ($CD39^{+/+}$ sham and IVC-ligated and $CD39^{-/-}$ sham and IVC-ligated), $CD39^{+/+}$ and $CD39^{-/-}$ mice were euthanized, IVC (including contents) was removed, weight and length were measured in milligrams (mg) and centimeter (cm), respectively, and then IVC was carefully stripped from the thrombus and both were weighed independently.

Histological analysis of thrombus-induced IVC/ vein wall morphometric analysis

Post-thrombus induction, thrombus-containing IVC was excised, fixed in 10% formalin overnight at 4^{o}C, then stored in 70% ethanol prior to embedding in paraffin. 5 μm serial cross sections of the thrombus-containing IVC were cut using leica RM2235 microtome.

Tissue sections were stained with hematoxylin and eosin, visualized under light microscopy and images were captured using an Eclipse TE2000-E microscope (Nikon Instruments, Melville, NY 400 x magnifications). MetaMorph image analysis version 7.0r3 software (Molecular Devices, Sunnyvale, CA) was used for morphometric analysis. Morphometric evaluations were made by an experienced pathologist blinded to experimental conditions, using a previously described thrombus surface-organization scoring criteria.[39] Briefly, veins were examined under high-power oil immersion light microscopy (1000x). Five representative high-power fields (HPFs) were chosen from three different section from each animal, positive cells were examined radially around the vein wall, and inflammatory cells (total cells, polymononucleated (PMNs), monocytes/macrophages, or lymphocytes (data not shown)) were identified based on standard histologic criteria.[20] Results from the 5 HPFs were added and mean ± SEM was calculated for each experimental group.

Immunohistochemical localization of P-selectin and von willebrand factor expression

Immunohistochemical analysis of P-selectin and vWF expression was performed on 5 μm sections prepared from formalin fixed, paraffin-embedded thrombus-induced IVC using rabbit polyclonal stained for CD62P (Ab 59738 - Abcam, Cambridge, MA) at 1:200 dilution or vWF (A0082 – Dako, Carpinteria, CA) at 1:250 dilution as a primary antibody. Prior to antibody incubation, thrombus-containing IVC tissues were subjected to 30 minutes of antigen retrieval (10mmol/L citrate buffer, pH6.0, 98^{o}C) and 5 minutes

of serum-free protein block (Cat X0909 Dako). A secondary antibody conjugated to a horseradish peroxidase-labeled polymer (EnVision+, HRP, Rabbit, catalog no. K4003, Dako, Carpinteria, CA) was used according to the manufacturer's instructions to localize sites where the primary antibody had bound. Color development was performed with diaminobenzidine (DAB). Slides were counterstained with hematoxylin, and images acquired with a 400x objective, and analyzed using MetaMorph image analysis software (Molecular Devices, Sunnyvale, CA) on an Eclipse TE2000-E microscope (Nikon instruments Inc).

Ectonucleoside Triphosphate Diphosphohydrolase-1 (ENTDP-1/CD39), P-selectin and VWF plasma protein quantification via enzyme-linked immunosorbent assay

To determine soluble CD39, P-selectin and vWF levels in plasma, blood was collected from thrombus-induced $CD39^{+/+}$ and $CD39^{-/-}$ mice and its respective sham-operated mice via cardiocentesis and placed in tubes containing EDTA as an anticoagulant (Becton Dickinson, and Co. Franklyn Lakes, NJ). Platelet-poor plasma was isolated from whole blood by centrifugation (2000xg, 30minutes and 10,000xg, 10minutes at 4^{o} C for the solP-selectin and CD39 ELISA and at 25^{o} C for vWF AlphaLISA and snap frozen in liquid nitrogen for later analysis. Prior to evaluation, plasma retrieved from the EDTA-treated blood samples was processed according to the manufacturer's instructions in the ELISA kit for sP-selectin (R&D systems Minneapolis, MN). We developed an ELISA based protocol to detect sol CD39 using recombinant CD39 as a standard and anti-CD39 (R&D systems Minneapolis, MN). Plasma vWF antigen levels were determined by AlphaLISA (Perkin Elmer, Waltham, MA) custom designed kit, using a polyclonal anti-human vWF antibody (DAKO, Glostrup, Denmark) conjugated to Alphalisa acceptor

beads and well as biotinylated anti-human vWF antibody (also DAKO) to interact with streptavidin coated donor beads. Mouse plasma was diluted 1:50 in PBS. Twenty µL of diluted plasma was incubated at room temperature with anti-vWF acceptor beads and biotinylated anti-vWF antibody in AlphaLISA buffer (25 mM HEPES, pH 7.4, 1 mg/mL Dextran 500, 0.5% BSA, 0.5% Triton X-100 and 0.05% Proclin-300) for one hour. Steptavidin-coated donor beads were added for a final concentration of 12.5 µg/mL acceptor beads, 5 nM biotinylated antibody and 40 µg/mL donor beads in 60 µL reaction volume. AlphaLISA signals were determined on an EnSpire 2300 Multimode Plate reader (Perkin Elmer), and VWF levels were calculated by comparing signals to a dilution series of C57BL/6J plasma. All vWF levels are reported as a percent of C57BL/6J plasma, which was considered to be 100 U/dL. All mouse samples were assayed at least 3 times and the average CV% of samples was 7.75%.

Assessment of platelet-leukocyte aggregates in whole blood

Following thrombosis induction, mouse blood was collected from the retro-oribital plexus from $CD39^{+/+}$ and $CD39^{-/-}$ mice and its respective sham-operated mice and placed in cold phosphate buffer saline without magnesium or calcium (PBS) at 4^{o} C. FACSlyse buffer (BD Bioscience, Franklin Lake, NJ) was used to lyse erythrocyte contaminants. Total cell counts were assessed by Hemavet hemocytometer (Drew Scientific) and reconfirmed by flow cytometry analysis using PerCPCy5.5-anti mouse CD45 antibody (BD Bioscience, Franklin Lakes, NJ) and absolute count standard beads (BD Bioscience). Viable cells were identified by the absence of DAPI (Molecular Probes, Portland OR) staining. Antibody specificity was verified using an appropriate isotype-labeled antibody (anti–rat IgG2a or anti–rat IgG2b). Nonspecific antibody staining was inhibited using rat-

anti mouse CD16b/CD32 antibody to block the FcγIII/II receptor (BD Bioscience). Total leukocyte analysis of whole blood was performed using APC-anti-mouse CD11b (monocyte/macrophage) and APC-Cy7-anti-mouse Ly6G/Ly-6C (Gr-1-neutrophils) (both from BD Bioscience).

In order to evaluate platelet-leukocyte aggregates, a 6-color flow cytometry assay was developed to analyze platelets binding to neutrophils or monocytes in whole blood. Cells and cell aggregates were purified and identified in four stages. First, the leukocyte population was gated using PerCPCy5.5-conjugated anti-mouse CD45. Second, infiltrating monocyte/macrophages, double positive for staining with APC-conjugated anti-mouse $CD11b^{high}$, and granulocytes, APC-Cy7-conjugated anti-mouse Gr-1. The combinations of rat anti-mouse CD11b-activated protein C, CD45-PerCPCy5.5 and glucocorticoid receptor (GR)-1- APC-Cy7 antibodies and isotype controls (all from BD Bioscience Franklin Lakes, NJ) were used for labeling leukocytes. Neutrophils and monocytes were distinguished from other cells by their size and granularity and by anti-CD11b-activated protein C and anti-GR-1- APC-Cy7 antibody binding. Within the CD11b/CD45 and Gr-1/CD45 positive-double events, the third cell subpopulation was identified using rat anti-mouse CD41 (platelet glycoprotein (GP) IX)- PE antibody to label platelets; the activation of platelets bound to leukocytes was assessed by counting CD62P (P-selectin) – fluorescein isothiocynate (FITC)- positive events. Lastly, activated platelet –monocyte (CD11b-APC/CD41-PE/CD62P-FITC) and activated platelet–neutrophil (GR-1-APC-Cy7/CD41-PE/CD62P-FITC) aggregates were calculated from CD41-PE/CD62P double positive gates. All antibodies were purchased from BD

Bioscience. Platelet- leukocyte aggregates were identified using multispectral BD FACS Canto^{TM} flow, at least 1X10^{5} cells were collected from each sample and analyzed with FlowJo v.9.4.11 (Tree Star, San Carlos, CA).

Microarray-based transcriptional profiling and bioinformatics analysis of microarray data

RNA samples from CD39$^{+/+}$ and CD39$^{-/-}$ mice and their respective sham-operated mice (n=4 per group for biological replicates; Technical replication was achieved by pooling four samples for each of the four groups for analysis) were were used to detect gene expression changes at 48 hrs post – thrombus induction. Total IVC RNA was extracted using the TRIzol reagent (GIBCO BRL) and RNeasy spin (Qiagen) columns following homogenization. Prior to microarray based gene expression profiling total RNA was further purified using RNAeasy reaction cleanup kit (Qiagen). All procedures were based on the manufacturer's RNA amplification protocol. 50 nanogram of total RNA (Ovation PicoSL WTA System V2 P/N 3312) was used to synthesize double-stranded cDNA, according to the NuGen WT-Pico V2 kit protocol. Biotinylated single-stranded cDNA was prepared from 3 μg of cDNA (Encore Biotin Module P/N 4200-12, 4200-60, 4200-A01). Following fragmentation, 3.7 μg of cDNA was hybridized for 20 hr at 48^{o} C on Mouse Gene ST 1.1 strip arrays, using the Affymetrix Gene Atlas system (software version 1.0.4.267; Affymetrix, Inc., Santa Clara,CA). Raw intensity data was processed and exported using Affymetrix Command Console, after scanning with the Affymetrix Gene Atlas system. Subsequent analyses were performed using the R programming environment 2.15.0 (R development core team 2011): a language and environment for statistical computing with the Oligo bioconductor software packages (Bioconductor, Fred

Hutchinson Cancer Research Center, Seattle, WA)[42]

To assess sample quality, we compared the probe intensity distributions across the multiple samples with the expectation that they be similar in shape, location, and scale. We also used degradation plots to assess differences in degradation that might appear as differences in expression. We next calculated the expression values for each gene using a robust multi-array average (RMA)[43] which produced pairwise scatterplots of $\log_2$ whereby converting the perfect match (PM) probe value intensities into $\log^2$ expression values for each sample used quantile normalization and median-polish. (**Figure 4A**). Moreover, the principal component analysis (PCA) was performed using "stats" package in R. When visualizing PCA results, the first 2 principal components (coordinates) are shown z-transformed and give the overall structure of high dimensional data (**Figure 4B**). Having passed all the manufacturer's quality control checkpoints, data was normalized using RMA as mentioned above.[42] Comparisons were made between $CD39^{+/+}$ and $CD39^{-/-}$ mice, and their respective sham-operated mice. Data was filtered using probesets, with a fold change greater than 2 with the added constraint that one of the two samples had an expression value of 2^5 or greater, to remove non-informative genes. Variable genes were plotted as heatmaps with hierarchical clustering using euclidean distance as a distance measure and complete linkage as the clustering method using the "stats" package of R. Fold-changes were visualized with color ranging from red (high expression relative to sham) over white (intermediate expression relative to sham) to blue (low expression relative to sham). Microarray data generated in this study were deposited in Gene Expression Omnibus (GEO) public database.

Molecular interaction networks and functional analysis

Using Ingenuity Pathway Analysis (IPA) tool 9.0 software (Ingenuity Systems Inc. Redwood City, CA), gene ontology achieved identification of cellular functions affected by induction of thrombosis or the deletion of ENTDPase-1/CD39. The "Core Analysis" was used to interpret the large datasets in the context of biological functions, disease processes, and molecular networks. The gene lists containing Affymetrix IDs, fold change, and *P* values, were mapped in the **I**ngenuity **P**athways **K**nowledge **B**ase (IPKB). The focus genes were then used in the network algorithm to generate scored networks, based on the curated list of molecular interactions in IPKB. Pathway and global functional analyses were performed using **I**ngenuity **P**athway **A**nalysis 6.0 (**IPA**; Ingenuity® Systems, www.ingenuity.com). A data set containing gene identifiers and corresponding expression values was uploaded into the application, and each gene identifier was mapped using the IPKB. The IPKB analyses identify the biological functions as well as the pathways from the IPA library that are most significant to the data set. Genes from the data sets associated with biological functions or with a canonical pathway in the IPKB, that met the p-value cutoff of 0.005 were used to build the interactome as described above. Fisher's exact test was used to calculate a *p*-value determining the probability that each biological function and/or canonical pathway assigned to this data set was not due to chance alone.

Validation by quantitative RT-PCR

Differential gene expression identified through microarray analysis was validated via quantitative real-time PCR (qRT-PCR), which was performed using TaqMan probe-based chemistry (Applied Biosystems, Carlsbad, Calif) per manufacturer's instructions, and the ABI Prisim 7500fast sequence detection system (Applied Biosystems, Carlsbad,CA). Briefly, the vein wall was separated from its associated thrombus, placed in a 15 mL conical tube filled with 1.5 mL of TRIzol (Invitrogen, Carlsbad, CA), and homogenized using the standard homogenization protocol. The RNA was cleaned using the RNAeasy reaction cleanup kit (Qiagen Inc, Valencia, Calif) according to the manufacturer's protocol. For this procedure, RNA concentrations were verified using the Nanodrop spectrophotometer (Thermo Fischer Scientific Inc., Wilmington, DE). Reverse transcription of the RNA (500 μg) into cDNA was done using SA Biosciences' RT ^{2} First Strand kit. Real-time PCR was run on the cDNA template according to the manufacturer's protocol for β-actin (housekeeping gene). All the primer used for qRT-PCR was purchased from Invitrogen. Commercially-available mouse primers sequences were derived using validated primer sequences from Affymetrix microarray (Affymetrix, Inc., Santa Clara,CA) were all purchased from Invitrogen. Quantification of inflammatory mediators utilizes the cycle threshold (Ct) for the gene of interest normalized to the housekeeping gene β-actin. Relative mRNA expression is calculated by the formula 2-(Ct target gene-Ct reference gene), and cycle lengths used are within the exponential phase of the polymerase chain reaction. Cycle threshold values were evaluated with the delta CT method to determine increases or decreases in gene expression between the animal groups.

Statistical analysis

All data are represented as mean ± SEM, with the numbers of experiments performed provided in the figure legends. Data are expressed as means ± SE. Differences between statistical groups were evaluated for statistical significance using the Student's *t*-test for unpaired data with Welch's correction. $P < 0.05$ was considered statistically significant. Comparison of results between different groups with more than 2 conditions were compared using a one-way analysis of variance (ANOVA) or a Mann-Whitney U test, as appropriate, using GraphPad Prism 6 software (LaJolla, CA). To discern differences between specific groups, Newman-Keuls test was used. Values were considered significantly different when $P \leq 0.05$

RESULTS

Generation of ectonucleoside tri (di)phosphohydrolase (*cd39)*-deficient mice

To eliminate the *cd39* gene product in mice, a targeting vector was prepared from the 5'portion of the murine *cd39* gene by inserting novel LoxP and Frt sites, and a PKG neomycin resistant cassette in the reverse orientation. By interbreeding homozygote *cd39* $^{flx/flx}$ mice and crossing to a pleiotropic CRE (EIIA) mouse, we were able to successfully excise the *cd39* gene product. No specific abnormalities in development nor reproductive capacity were found in the *cd39* $^{flx/flx}$ and *cd39*$^{-/-}$ mice. Using qRT-PCR we detected *cd39* transcript in mRNA from multiple organs from *cd39* $^{flx/flx}$ *and cd39*$^{-/-}$ mice. As expected, CD39-deficent mice, no *cd39* transcripts were detected **(Fig 1A)**. Not only were *cd39* $^{flx/flx}$ *and cd39*$^{-/-}$ mice phenotypically grossly identical but hemodynamically they were also similar in terms of heart rate and blood

pressure **(Fig 1B, C).** Circulating total leukocyte and subset population cell counts were similar between *cd39* $^{flx/flx}$ and *cd39*$^{-/-}$mice. In keeping with previous published observations, platelet counts were lower in CD39$^{-/-}$ mice compared to *cd39* $^{flx/flx}$ **(Fig. 1 D)**. Both values are nearly within expected normal platelet count range for mice Peripheral blood smears of CD39$^{-/-}$ mice showed reduced platelet number with no megakaryocytes or platelet clumping *(data not shown)*. CD39$^{-/-}$ mice had similar prothrombin and partial thromboplastin time estimates compared to those of *cd39* $^{flx/flx}$ mice (**Fig. 1D**). To further characterize coagulation, whole-blood impedance aggregometry was performed. Consistent with prior published studies, in which globally CD39-deficient mice had significantly impaired platelet aggregation due to platelet desensitization [31]compared to WT mice (**Fig. 2A,B**).

CD39-deficient mice generate significantly more thrombus than wild type mice

Deep venous thrombogenesis was induced in CD39-deficent and WT mice with the use of an IVC ligation stasis (absence of flow) model[20, 39]. In our animal model, thrombus mass measurements give a reliable measurement of DVT formation and resolution. This technique assesses the entire thrombosed vein, and is performed in a standardized fashion. Thrombus weights were evaluated in WT male mice from 1d to 6d after IVC ligation. All 44 WT mice developed a thrombus within 24 hrs post-thrombus induction (**Fig 2C-E**). Forty-eight hours post-thrombus induction, IVCs demonstrated a 50% increase thrombus mass compared to day 4 and 6 in CD39$^{+/+}$ mice (*P= 0.0072*) (**Fig 2C**). Compared to the WT age-matched controls, CD39$^{-/-}$ mice had approximately 47% larger

thrombi, (P = 0.0001), 48 hrs post-thrombogenesis (**Fig 2D**). **Fig 2E** depicts a representative photograph of $CD39^{-/-}$ and $CD39^{+/+}$ thrombi 48 hrs post-thrombogenesis. The data obtained with this model of stasis-induced IVC ligation shows that $CD39^{-/-}$ mice have larger thrombi compared to $CD39^{+/+}$ mice 48 hrs post- thrombogenesis.

Vein wall inflammation is increased in $CD39^{-/-}$ mice 48 hrs post- thrombus induction

When evaluating the vein wall and the thrombus proper, the total inflammatory cells showed a trending increase in $CD39^{-/-}$ thrombi, as compared with $CD39^{+/+}$ mice (**Fig 3**). Hematoxylin and eosin staining of the thrombosed IVC sections qualitatively confirmed that increased leukosequestration in vein wall was present 48 hrs post-thrombogenesis in $CD39^{-/-}$ mice compared to wild-type age-matched counterparts (**Fig 3A-D**). Together with histology and thrombus histomorphological evaluation, a significant increase was observed in neutrophil migration through the vein wall 48 hrs post- thrombus induction in $CD39^{-/-}$ compared to $CD39^{+/+}$ mice, suggesting that the absence of CD39 exaggerates polymorphonuclear neutrophils recruitment into the thrombosed zone (**Fig 3B, D, F**). There was no significant increase in monocyte accumulation in the vein wall 48 hrs post-thrombogenesis in $CD39^{-/-}$ thrombi, as compared with $CD39^{+/+}$ mice (**Fig 3G**). However, there was a significant increase in the vein wall monocyte accumulation at 6 days post-thrombus induction in $CD39^{-/-}$ mice compared to wild type mice (data not shown).

Microarray quality control analysis revealed strong differences in gene expression 48 hr post-thrombus induction in CD39-deficient mice.

To investigate gene expression profiles that are associated with leukosquestration 48 hrs post-thrombrogenesis, mRNA expression in total IVC (from all four groups described above) was profiled using Affymetrix gene chip ST1.1 microarray platform. We used an n=4 biological replicates to run one array strip and employed several quality control parameters prior to analyzing the probeset. **Figure 4A** depicts a histogram showing the distribution of the probes for each chip. One of the underlying assumptions for the normalization procedure was that the probe data all come from the same distribution, with the only differences being the location and scale. Each expression value for each gene used a robust multi-array average.[43] Principal component analysis (PCA) was first performed to examine the correlations among the different experimental variables. The red, green, blue and purple dots represent the overall expression pattern of each IVC sample from $CD39^{+/+}$ sham-operated, $CD39^{+/+}$ IVC-ligated, $CD39^{-/-}$ sham-operated or $CD39^{-/-}$ IVC-ligated mice, respectively (**Fig 4B**). The first component shown in the *x-axis* includes genes with a high degree of variance within the different genotypes ($CD39^{+/+}$ sham and IVC-ligated vs. $CD39^{-/-}$ sham and IVC-ligated). The second component, displayed along the *y-axis*, encompasses genes that also had a high range of variance within the sham and IVC-ligated groups (Sham - $CD39^{+/+}$ and $CD39^{-/-}$ vs. IVC-ligated-$CD39^{+/+}$ and $CD39^{-/-}$). The PCA results indicated that the global expression patterns in IVC of the same experimental mouse groups were similar, whereas those in IVCs of the different mouse groups were different. The PCA analyses also show that the samples within the two experimental variables (genotype, and ligation status), were distinctly separated, indicating that the quality of the microarray data was excellent. As anticipated, when using a Venn diagram to illustrate the number of probe sets common to both sham

and DVT groups. The sham vs. DVT experimental group there were 132 common probe sets **Fig 4C.** Conversely in the $CD39^{+/+}$ IVC-ligated vs. $CD39^{-/-}$ IVC-ligated there were 722 common probe sets **Fig 4D**. Between the four different experimental groups, we identified 854 probe sets as significantly differentially expressed (Fold change -2≥ to ≥2; P≤0.001) in each pairwise comparison (**Fig 4C,D**). Altogether, we observed a considerable increase in the dynamic range of fold differences in microarray data with differences spanning six orders of magnitude.

Hierarchical clustering analysis of differentially expressed genes identified unique groups of highly upregulated inflammatory genes

We hypothesized that induction of thrombosis and the deletion of CD39 will heighten the expression of inflammatory mediators. We also hypothesized that the increase in leukocyte flux seen in the ligated IVCs of $CD39^{-/-}$ mice was due in part to an absence of vascular wall CD39 activity, and possibly the loss of CD39 circulating on the leukocytes. To examine this, an ANOVA was first performed to identify genes that are differentially expressed due to CD39 deficiency or stasis-induced thrombogenesis (**Fig 5A-D**). After ANOVA, 179 inflammatory and immune response genes were found to be highly upregulated during stasis-induced thrombosis and CD39 deficiency were analyzed by hierarchical clustering and visualized as a heatmap (**Fig 5A-B**). We focused our analysis on three groups of genes (group I, II and III = total 76 unique probe sets) that showed a concordant increase in expression in Sham vs. DVT and $CD39^{+/+}$ IVC-ligated vs. $CD39^{-/-}$ IVC-ligated. **Fig 5C and D** depicts the subset of genes that were categorized as groups I,

II, III and visualized as a supervised hierarchical clustering heatmap. By comparing our results from the four different groups, we identified ten differentially expressed genes in common; *Il-6, Nos2, Il-1b, Tnf, Ccl2, Cxcl2, Chi313, Arg1, Selp* and *VWF*. Our data show that *Selp, vWF* and *Il-6* were slightly up-regulated. This finding is concordant with previous studies using varying models of deep vein thrombosis.[44,39,45,46,47,48,21] Interestingly, *Chi313* and *Arg1*, an M2 alternative macrophage marker, was highly upregulated (fold change > 4) during stasis-induced thrombogenesis and also showed a concordant increased in the absence of CD39 (fold change > 5). These experiments showed that CD39 could regulate key inflammatory mediator expression levels during stasis-induced thrombogenesis.

Validation of microarray results by Real-time qRT-PCR of inflammatory mediators and chemokine gene expression profiles 48 hrs post-IVC ligation.

To independently confirm the microarray results, quantitative real-time RT-PCR were performed on samples from $CD39^{+/+}$ and $CD39^{-/-}$ sham operated or IVC-ligated mice 48 hr post IVC ligation that were used in the microarray. The pattern of dysregulation of several genes with prominent proinflammatory functions, as well as several chemokines, presented the first evidence that stasis- induced thrombogenesis might mediate leukosequestration in CD39-deficient mice. The relative expression levels of ten differentially expressed genes identified through the microarray analysis – (*Il-6, Nos2, Il-1b, Tnf, Ccl2, Cxcl2, Chi313, Arg1, Selp* and *vWF)* – were assayed (**Fig 6A-J**). IL-6 and Cxcl2 gene expression were significantly increased ($p<0.001$) during stasis –induced

thrombosis and CD39-deficiency (**Fig 6A,F**), and TNF-α and CCL-2 (M1 polarized inflammatory mediator) and Chi313 and Arg1 (M2 polarized inflammatory mediator) were also significantly increased in $CD39^{-/-}$ mice ($p<0.05$). In addition, during stasis-induced thrombosis, P-selectin and vWF were enhanced by ~4 fold ($p<0.05$) and 6-fold ($p<0.01$), respectively, in the absence of CD39 (**Fig 6I,J**). These findings (P-selectin and vWF gene expression) were then followed up at the protein level by ELISA using plasma from the four different groups described above (**Fig 9A-E**), where similar results were obtained, confirming the microarray findings.

Functional pathway and network analysis affected by stasis induced thrombogenesis and CD39 deficiency

The differential mRNA expression patterns as revealed by the microarray of $CD39^{+/+}$ and $CD39^{-/-}$ sham operated or IVC-ligated mice 48 hr post IVC ligation were analyzed using the Ingenuity System Database, software that includes the Ingenuity Knowledge Base and the Global Molecular Network. These databases integrate published findings on biologically meaningful genetic or molecular gene/gene product interactions and identify functionally related gene networks.

Ingenuity Pathway functional analysis for pathways and diseases revealed many inflammatory and immune response- relevant pathways that were significantly overrepresented in $CD39^{+/+}$ and $CD39^{-/-}$ sham-operated or IVC-ligated mice post-thrombogenesis, including; atherosclerosis signaling; HIF-1α signaling; hypoxia signaling in cardiovascular systems; inhibition of angiogenesis; VEGF signaling; CD40

signaling; IL-12 signaling and the production of macrophages; IL-6; IL-10; IL-8 signaling; iNOS signaling; leukocyte extravasation signaling; NF-κB signaling; p38 MAPK signaling; cytokine mediating communication between immune response; CCR5 signaling in macrophages; chemokine signaling; coagulation system; and eNOS signaling (**Fig 7A**). Each functional pathway or disease category defined by Ingenuity Pathway Analysis includes sublevel functions, thus the data presented in **Figure 7A** represent the most significant sub-level function in each category. Based on the results obtained by Ingenuity canonical pathway analysis, we further investigated the genes involved in leukocyte extravasation signaling in $CD39^{+/+}$ and $CD39^{-/-}$ sham operated or IVC-ligated mice 48 hrs post-thrombogenesis (**Fig 7B-E**). Among the genes that were affected by leukocyte rolling and docking on the endothelial surface of capillaries, PSGL-1 (P-selectin glycoprotein ligand-1) was significantly down-regulated in the sham-operated group (**Fig 7B**). Conversely, during thrombus induction and CD39 deficiency, PSGL-1 was significantly up-regulated (**Fig 7C-E**). This finding is concordant with previous report showing the interaction of P-selectin with PSGL-1 is an exceptionally effective mechanism for mediating leukocyte tethering under flow.[49,50,51] It is interesting to note that, MMP-9 (matrix metalloproteinases-9), located on leukocyte that has transmigrated through a capillary endothelial layer, was also significantly down-regulated under sham conditions. Simultaneously, during thrombogensis and absence of CD39, MMP-9 gene expression levels were significantly up-regulated (**Fig 7B-E**). This finding is complementary to recent work in which deletion of MMP-9 impaired vein wall fibrosis and inflammation in a stasis-induced deep venous thrombosis mouse model.[52]

To further investigate the interaction of *Selp*, *vWF* and other differentially regulated proinflammatory genes with other gene products, pathways, and biological processes, molecular networks were formed in Ingenuity Pathway Analysis using functional relationships between genes products based on known connections in the literature. These networks include genes that are biologically relevant to the pathway but not identified in the microarray. **Figure 7A-D** represents the IPA-generated molecular networks assembled from diffentially-expressed genes in $CD39^{+/+}$ and $CD39^{-/-}$ sham-operated or IVC-ligated mice 48 hrs post-thrombogenesis. Each network was identified based on a numerical rank score according to the degree of relevance of the network to the molecules in the significant genes list and based on the hypergeometric distribution calculated as –log (Fisher's exact test result). A score greater than two indicates a ≥99% confidence that a focused gene network was not generated by chance alone IPA. In these network illustrations, genes or gene products are represented as nodes, and the biological relationship between two nodes is represented as an edge (line). All edges are supported by at least one published reference. Focus genes are denoted by red symbols for upregulated genes and green symbols indicate downregulated genes. Grey and open symbols are intermediate molecules, placed in the network by the Ingenuity software and shown in the literature to interact with genes in this dataset. Symbols representing the functional categories of the molecules are listed in the legend (**Fig 7F-I**). These GMN findings showed in the sham-operated group the interaction between *Selp*, *vWF* and other differentially regulated proinflammatory genes caused an upregulation in *Selp* and down-regulation of *vWF* and the proinflammatory cytokine group (**Fig 7F**). In contrast, thrombus induction and CD39-deficiency caused *Selp* and *vWF* to be slightly up-

regulated, and proinflammatory cytokines to be moderately down-regulated (**Fig 7G, I**).

Vein wall P-selectin and vWF was increased in CD39-null mice 48 hr post-thrombus induction

P-selectin and vWF have previously been shown to be involved in facilitating the initial rolling and recruitment of leukocytes during thrombosis.[39,45,21] In addition, previous studies have suggested a link between inflammation and DVT[7,53], yet the precise role that CD39, P-selectin, and vWF plays in leuckosequestration during thrombogenesis has not been explored. To discern the localization of P-selectin and vWF in CD39 null mice via immunohistochemical analysis, we stained tissue sections from $CD39^{+/+}$ and $CD39^{-/-}$ sham operated or IVC-ligated mice 48 hrs post-thrombogenesis (**Fig 8A-H**), with an antibody that recognize murine P-selectin and vWF. Immunohistological examinations reveal an increase in expression of P-selectin and vWF in CD39 null mice 48 hrs post-thrombus induction (**Fig 8D-H**). Interestingly, there were a large number of inflammatory cells recruited to the thrombus milieu that were stained with P-selectin antibody in $CD39^{-/-}$ IVC-ligated, compared to $CD39^{+/+}$ IVC-ligated thrombus induced group (**Fig 8B, D**). Furthermore, the increased staining of vWF was significantly greater on the endothelium in CD39-deficient mice compared to their wild type counterparts (**Fig 8F, H**).

Circulating P-selectin and VWF was significantly enhanced in CD39-deficient mice 48 hr post-thrombus induction

Soluble P-selectin is an established biomarker for deep venous thrombosis as confirmed in both patients[54,55] and mice that have deep venous thrombosis[56,57], vWF-null mice are

protected from DVT.[21] To determine whether soluble P-selectin and vWF play a role in modulating the leuckosequestration in CD39-deficient animals post-thrombosis, a series of time course experiments was performed in $CD39^{+/+}$ IVC-ligated animals. ELISA analysis show at 48 hr soluble CD39 was significantly higher compared to the other time-points (**Fig 9A**). Conversely, soluble P-selectin and vWF were increased at 48 hr, however, were not significantly differed compared to the other time-points (**Fig 9 B, C**). In a separate set of experiments, traditional ELISA and alphaELISA assays[58] were used to examine circulating levels of P-selectin and vWF (respectively) in $CD39^{+/+}$ and $CD39^{-/-}$ sham-operated or IVC-ligated mice 48 hrs post-thrombus-induction. Data demonstrated that both soluble P-selectin and soluble VWF were significantly higher in $CD39^{-/-}$ IVC-ligated mice compared to $CD39^{+/+}$ IVC-ligated animals soluble P-selectin (**Fig 9D, E**).

CD39 regulates platelet-leukocyte trafficking and aggregation 48 hrs post-thrombus induction

P-selectin on activated platelets is a major mediator of adhesion to leukocytes.[59] Utilizing flow cytometry to quantify platelet-leukocyte aggregation, we analyzed $CD39^{+/+}$ and $CD39^{-/-}$ sham operated or IVC-ligated mice 48 hrs post-thrombus -induction mouse peripheral blood was assessed by 6-color flow cytometry. Antibody against CD45 and CD11b characterized the monocyte subpopulation ($CD45^{hi}/CD11b^{+}$) and CD45 and Gr-1 characterized the neutrophil subpopulation ($CD45^{hi}/Gr\text{-}1^{+}$) were gated respectively and subsequently sub-gated into two distinct groups; Platelet - monocyte heteroaggregates ($CD45^{hi}/CD11b^{+}/CD41^{hi}/CD62P^{hi}$) and Platelet – granulocyte (neutrophil)

heteroaggregates ($CD45^{hi}/Gr\text{-}1^{+}/CD41^{hi}/CD62P^{hi}$). Although we were not able to detect platelet-monocyte aggregates in all mice studied, in four of nine mice we were able to detect them. In these mice, platelet-monocyte aggregates of IVC ligated CD39-deficient mice were more abundant compared to $CD39^{+/+}$ IVC-ligated mice 48 hrs post-IVC ligation (76.3 ± 12.3 vs. 52.6 ± 10.2 $p<0.001$ n=3-4). Conversely, Platelet – granulocyte heteroaggregates demonstrated 42% more total aggregates in CD39 null mice as compared with CD39 wild type (13.7%) 48 hrs post-thrombus-induction (**Fig 10A, B**). In addition to examining representative platelet-leukocyte aggregate dotplots, we calculated the absolute levels of recruited platelet-leukocytes populations in mice in which we detected them. Absolute numbers of both platelet-monocyte and platelet – granulocyte hetroaggregates were significantly increased 48 hrs post-thrombogenesis in CD39-deficient animals as compared to their wild type counterparts (**Fig 10C, D**). These data show for the first time that CD39 regulates leukosequestration and attenuates venous thrombogenesis by down-regulating soluble vWF and soluble P-selectin expression in a mouse model of DVT.

DISCUSSION

As links between local thrombosis and inflammation are likely to serve as underpinnings for the development and propagation of a DVT, we proposed to examine a potentially relevant molecular mechanism. Although there are a number of intersection points in the nexus between coagulation and inflammation, one in particular stands out as being particularly important. CD39, an ectoapyrase expressed on endothelium and leukocyte subpopulation[60], rapidly metabolizes ATP to ADP and AMP, which are released by platelets and other activated cells, inhibiting platelet recruitment into an evolving thrombus. In this current study, our laboratory successfully engineered a globally deficient CD39 mouse using the Cre EIIA system. We sought to determine the role of CD39 in DVT by employing a mouse model of venous thrombosis in which we ligated the inferior vena cava. Our data reveal for the first time that CD39 plays a critical role in mitigating venous thrombogenesis by squelching inflammatory and coagulant reactions at the blood/vessel interface.

Our current studies show that CD39 plays an important, protective role in the recruitment of inflammatory vascular mediators to the vessel wall post thrombus induction. The $CD39^{-/-}$ mice engineered by our group had an apparently normal phenotype at baseline, with the exception of platelet hyporeactivity, as previously reported.[31]

Several investigators have reported a bidirectional relationship that exists between thrombosis and inflammation[39,20,40,41]. To test this relationship, we used a long-

established and widely employed model of infra-renal inferior vena cava venous thrombosis.[39,20] We studied the effects of deletion of CD39 on thrombus formation in IVC-ligated mice at baseline and 48 hrs post IVC-ligation. Deletion of CD39 was associated with significantly increased thrombus size, with less neovascularization and fibrosis, despite increases in vein wall leukocyte accumulation. Prior studies have demonstrated that clot size is an index of thrombogenesis following ligation of the IVC.[48,20] Moreover, the increase in thrombus cellularity in CD39-deficient mice was consistent with other experimental models.[44,61,48] From these findings, we conclude that deficiency of CD39 impairs the process of thrombosis, which might be associated with complex interplay of factors that are likely not simply related to coagulation but also related to inflammatory changes.

To further examine the possible contribution of CD39 to DVT pathogenesis, we compared vein wall leukocyte influx in $CD39^{+/+}$ mice and CD39 null mice after IVC-ligation. Our data showed in CD39-knockout mice, leukosequestration was increased and the vein wall appeared larger than $CD39^{+/+}$ mice. Consistent with other models of thrombosis, we observed that neutrophils constitute the predominant leukocyte subset recruited to the site of DVT at 48 hrs[46,45, 61]. This may, through formation of neutrophil extracellular traps, contribute to venous thrombogenesis.[62,63,64,65] Further, in contrast, monocyte/macrophage recruitment was not significantly increased (at 48 hrs), suggesting that monocyte/macrophage might play a lesser role in early thrombosis and inflammation, but more of a later role in thrombus resolution. Although CD39 expression is recognized

on certain leukocyte populations (B cells, monocytes, neutrophils; refs.[60,66] the present investigation suggests that CD39 apyrase is an important mechanistic link between neutrophil-driven venous inflammation and venous thrombogenesis.

To comprehensively understand how CD39 plays a role in thrombogenesis, especially related to leukocyte influx, the IVC was subjected to ligation in order to identify differentially expressed inflammatory genes, utilizing microarray technology. Microarray analysis is a powerful tool for identifying gene expression patterns that are reflective of the response to absence of CD39 during thrombogenesis, and can be informative of mechanisms of action.[67] Using this technology, we have investigated whether CD39 modulates inflammatory pathways during thrombus induction. Though high-throughput data obtained from microarray analysis may be generally of high variability, low reproducibility and contain non-specific noise[68], this effect can be ameliorated using comprehensive text mining and bioinformatics approaches. Examples of such approaches include Gene Ontology (GO) analysis, DAVID pathway analysis, Short Time-series Expression Miner (STEM) cluster analysis, Dynamic Gene Network analysis, and Ingenuity Pathway Analysis (IPA). We chose GO and IPA as they are effective method to enrich the most relevant DVT-responsive genes, the biology of leukocyte recruitment to the vein wall of thrombosed IVCs.

Affymetrix microarray analyses demonstrate that 132 genes were affected by IVC-ligation, and 722 genes were affected by CD39-deficiency and IVC-ligation, with a fold change $-2 \geq FC \geq 2$. Principal component analysis revealed the microarray data were of

excellent quality (**Fig 4B**). We pooled four samples for each of the four groups for analysis, and examined all groups at the 48 hr time point (this was the time point with the highest thrombus weight in CD39 null mice (**Fig 2**) and highest CD39 expression (**Fig 9A**). One of our initial goals was to identify the inflammatory genes that regulate CD39-mediated leukocyte trafficking after thrombosis. We used the R statistical programing environment to generate hierarchical clustered heat maps of differentially expressed inflammatory genes identified from integrated results of GO analysis of the four experimental groups ($CD39^{+/+}$ sham and DVT, $CD39^{-/-}$ sham and DVT). 179 inflammatory and immune response genes were found to be highly upregulated during stasis-induced thrombosis and CD39 deficiency (Fig 5A-B). Futhermore, our analysis identified three groups of genes (groups I, II and III = total 76 unique probe sets) that show a concordant increase in expression in sham vs. DVT, and $CD39^{+/+}$ IVC-ligated vs. $CD39^{-/-}$ IVC-ligated mice. The three groups were visualized as a supervised hierarchical clustering heatmap. We confirmed the presence of a few of the previously reported inflammatory/coagulant genes (*Il-6, Selp, vWF and Ccl2)* [47,48,21,44] , and extend this list to a least 6 transcripts significantly expressed above the background during IVC-ligation that have known roles in coagulation and leukosequestration. In addition, *Il-1β, Tnf* (classical M1-polarized macrophage marker), *Chi313, and Arg1* (M2-polarized macrophage marker), were upregulated during stasis-induced thrombogenesis and also showed a concordant increased in the absence of CD39.

M1 macrophages are classically activated proinflammatory macrophages, whereas M2 macrophages are alternatively activated non-inflammatory macrophages. An increase in the ratio of M2 to M1 macrophage would lead to a reduced inflammatory response.[69] As

there appears to be more than one type of alternative activation state[70], it is important to note that our data lead to the conclusion that thrombosis activates alternative macrophage response markers but does not exclude the possibility that there will be distinct differences from the M2 states induced in other models of thrombosis. Although this hypothesis remains to be tested, further analysis is needed to gain a better understanding of the biological role of these alternative activation M2 markers in other thrombogenic models of DVT.

In an effort to better understand the dynamic biological interactions of differentially regulated inflammatory genes, 76 unique datasets representing genes with altered expression profiles derived from our microarray analysis were imported into the Ingenuity Pathway Analysis Tool. The list of differentially expressed genes analyzed by IPA revealed 19 significant networks affected by CD39-deficiency and IVC-ligation (**Fig 7A**). Of the networks, leukocyte extravasation signaling was chosen from the pathway identified in IPA analysis for closer examination. Leukocyte extravasation signaling is of interest to our study because it encompasses genes that are regulated during thrombosis and inflammation.[71] The classic paradigm of leukocyte extravasation has focused upon recruitment and activation of leukocytes. PSGL-1 (P-selectin glycoprotein ligand-1) has been shown to play an important role in leukocyte rolling, adhesion and transmigration at the site of inflammation and thrombus generation.[72,45] In our study, we show in that PSGL-1 was significantly down-regulated in the sham-operated group (**Fig 7B**). Conversely, during thrombus induction and CD39 deficiency, PSGL-1 was profoundly up-regulated (**Fig 7C-E**) compared to IVC-ligated $CD39^{+/+}$ group. The observation that most of the genes involved in both leukocyte adhesion and transmigration were activated

during IVC-ligation and CD39 deletion implies that CD39 plays a direct role in the regulation of leukocyte migration into the vascular wall during the propagation of thrombosis. This postulation is consistent with that of our previous studies in ischemic tissues.[34] It is also interesting to note that, MMP-9 (matrix metalloproteinases-9), located on leukocyte that has transmigrated through the capillary endothelial layer, was also significantly down-regulated under sham conditions. Simultaneously, during thrombogenesis and absence of CD39, MMP-9 gene expression levels were signifcanly up-regulated (**Fig 7B-E**). This finding is complementary to recent work in which deletion of MMP-9 impaired vein wall fibrosis and inflammation in a IVC-ligation mouse model deep venous thrombosis.[52,73] Consistent with our qRT-PCR analysis, we show in the sham-operated group that the interaction between *Selp*, *vWF* and other differentially-regulated proinflammatory genes caused an upregulation in *Selp* and down-regulation of *vWF* and downregulation of the proinflammatory cytokine (**Fig 7A**). In contrast, IVC-ligation and CD39-deficiency caused *Selp* and *vWF* to be slightly up-regulated (1.4 fold), and proinflammatory cytokines to be moderately down-regulated (by 4 fold) (**Fig 7F-G**). This suggests that *Selp* and *vWF* may play an important role in leukocyte rolling and tethering on the endothelium during IVC-ligation, even in the absence of CD39. Taken together, we demonstrated gene expression profiles of acute venous-thrombosed CD39-deficient mice by microarray assay, integrated with a multi-step bioinformatics strategy to understand the dynamic interactions that occured during luekosequestration and thrombogenseis. Our results indicate immune response genes play a critical role in thrombogenesis in the absence of CD39. The analysis performed in the IPA platform provide basic information for the association of key inflammatory mediators during

thrombus induction, which provided our laboratory with an initial step for better deciphering the molecular mechanisms involved in the protective role of CD39 during acute venous thrombosis.

This *in silico* analysis has a couple of limitations. First, our 76 differentially expressed inflammatory genes and the follow up pathway/network analyses were conducted based on computational strategies. Although informative, this approach generally requires extensive experimental validation. Therefore, further validation of specific novel genes using more samples is needed. Second, the pathway crosstalk analysis was based on the scores measured by Jaccard Coefficient (*JC*) and Overlap Coefficient (*OC*). In this study, we selected the pathway pairs empirically, that is, those ranked in the top 10%. *P* values from a statistic test would be better applied to select significant crosstalk.

To take our *in silico* experiment a step further, we validated some key findings based on the results obtained. Our *in silico* analysis identified *Selp* and *vWF* as key modulators of thrombogensis in our CD39 deletion model. This integrated experimental and theoretical approach yielded several key insights and suggested three new experiments that required extensive experimental validation. To discern the localization of P-selectin and vWF in CD39 null mice via immunohistochemical analysis, we stained tissue sections from $CD39^{+/+}$ and $CD39^{-/-}$ sham operated or IVC-ligated mice 48 hrs post-tIVC-ligation. We showed an increase in expression of P-selectin and vWF in CD39 null mice 48 hrs post-thrombus induction (**Fig 8D-H**). Concordant with our *in silico* findings we also show a

large number of inflammatory cells recruited to the thrombus that were stained with anti-P-selectin antibody in $CD39^{-/-}$ IVC-ligated mice compared to $CD39^{+/+}$ IVC-ligated thrombus induced group (**Fig 8B, D**). This suggests that some of the anti-inflammatory properties of CD39 may play a role in increasing stores of vein wall P-selectin and activating vWF in the endothelium during thrombosis.

To further examine the possible contribution of CD39 to DVT pathogenesis, we analyzed the circulating levels P-selectin and vWF from $CD39^{+/+}$ and $CD39^{-/-}$ sham-operated or IVC-ligated mice 48 hrs post-IVC-ligation. Concordant with our IVC date, we showed an increase in soluble P-selectin and VWF in the plasma of $CD39^{-/-}$ mice. It is interesting to speculate how CD39 efficiency resulted in increased plasma vWF. CD39-deficiency could produce slower clearance of vWF and other vascular modulators from the circulation and, thus, elevated vWF levels. Alternatively, vWF multimers activate platelets, which in turn may activate the endothelium. Previously, our laboratory[34,74,75] as well as that of others, has shown that hypoxia alone is sufficient to trigger thrombosis at the blood wall interface, by triggered release of von Willebrand Factor (vWF) and P-selectin from endothelium. Absent CD39, especially after IVC-ligation, increased inflammation of the vascular wall, could have the same effect

Circulating blood leukocytes in DVT, particularly monocyte/macrophage and neutrophils[39,20,40,41], display an activated phenotype that may predispose them to endothelial adhesion and amplification of vascular inflammation and vaso-occlusion. Thrombotic processes associated with enhanced platelet activation and the formation of platelet-

leukocyte aggregates have been observed in several models of inflammation.[76,77] CD39 has been shown by our group[37] and others [31] to be an important mechanism driving platelet-mediated platelet recruitment, through release of ADP and activation of the P2Y12 receptors. This can be terminally disrupted through enzymatic ADP dissipation by CD39. Our work in this area showed that an engineered soluble form of CD39 can prevent platelet aggregation in a cuvette following introduction of any of a number of platelet activation agonists, such as ADP, sodium arachidonate (which leads to thromboxane generation), or collagen. In our current study, we employed a 5-color flow cytometry of cell markers to simultaneously analyze platelet binding to neutrophils and monocytes in whole blood. The analysis of platelet- leukocyte aggregates revealed more platelets bound to monocytes than to neutrophils in the absence of CD39. Although, this finding was seen in 4 out of the 9 mice we examined, these observations may provide some evidence that platelets play a role in enhancing leukocyte activation during thrombogenesis in CD39-deficient mice. The physiological significance of increased formation of platelet-leukocyte aggregates in the peripheral blood during inflammatory disease still remains uncertain, however, our studies suggest that platelets at the thrombo/inflammatory interface may play an active role in DVT.

In conclusion, these studies are the first to demonstrate a direct link between vascular ectoenzyme (CD39) and DVT. We provide evidence that CD39 deficiency promotes inflammation and results in the increased extravasation of key inflammatory cells and activation of vascular coagulant reactions at the blood/vessel interface 48 hrs post-IVC ligation. Our present study also demonstrates through gene expression profiling with bioinformatics analysis that complicated inflammatory networks are activated following

creation of a DVT. Absence of CD39 further pushes the balance towards a proinflammatory vascular wall phenotype. Understanding the complex interplay of vascular injury, stasis and coagulation and how this is modulated by a naturally protective vascular ectoenzyme would lead to new therapies for DVT or other disorders at the nexus of inflammation and coagulation.

FIGURES

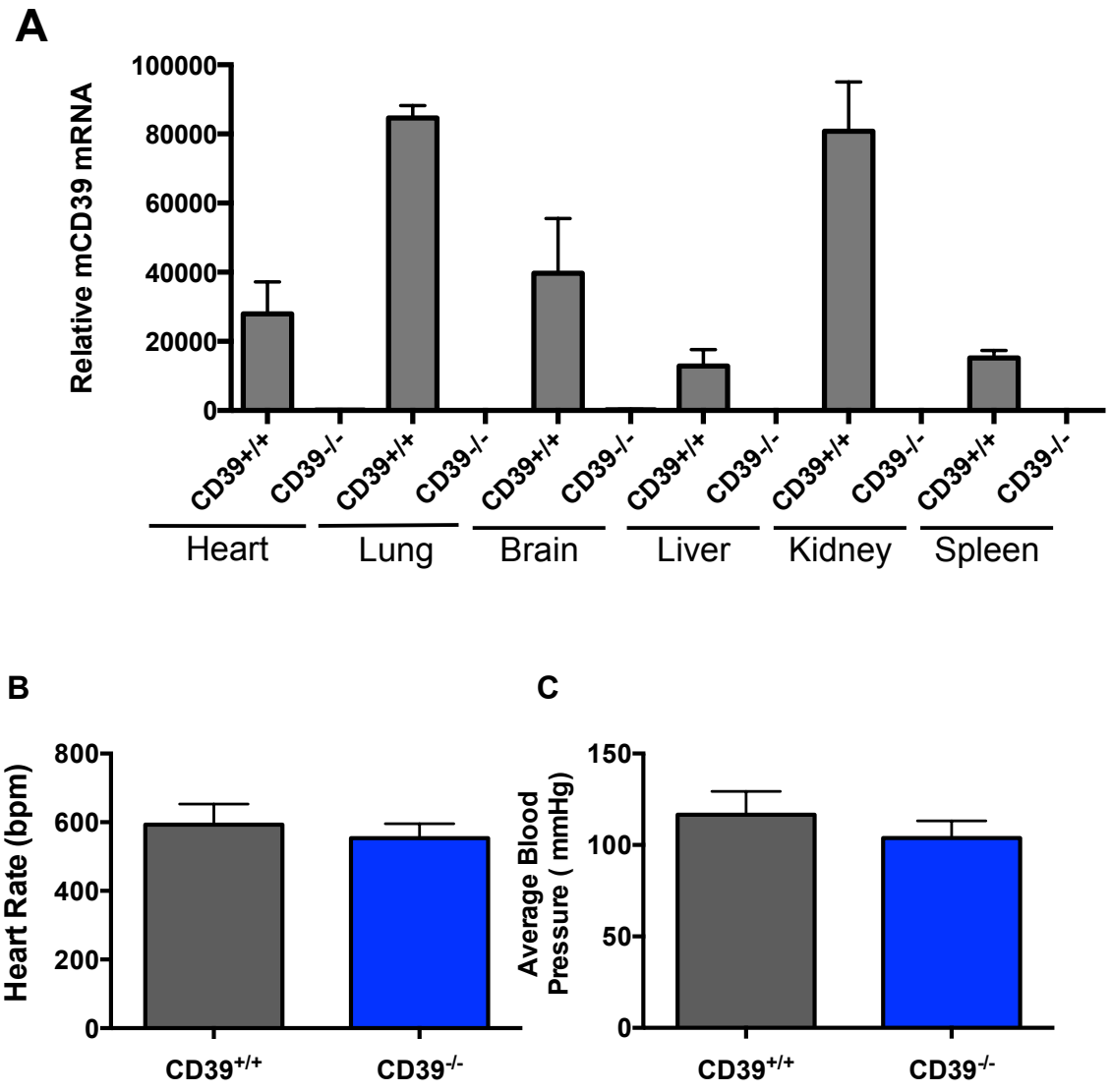
A
Relative mCD39 mRNA
100000
80000
60000
40000
20000
0
CD39+/+
CD39-/-
Heart
Lung
Brain
Liver
Kidney
Spleen
B
Heart Rate (bpm)
800
600
400
200
0
CD39+/+
CD39-/-
C
Average Blood Pressure (mmHg)
150
100
50
0
CD39+/+
CD39-/-

D

Genotype	CD39$^{+/+}$	CD39$^{-/-}$	*p* value
Total WBC (K/uL)	3.485 ± 0.51	4.317 ± 0.48	0.2669
Neutrophils (K/uL)	0.7775 ± 0.13	0.6871 ± 0.06	0.5519
Lymphocytes (K/uL)	2.588 ± 0.42	3.537 ± 0.42	0.1495
Monocytes (K/uL)	0.0925 ± 0.01	0.07857 ± 0.01	0.2613
Platelets (K/uL)	509.0 ± 109.7	132.2 ± 10.83	*0.0407
Hemoglobin (g/dL)	11.63 ± 0.76	11.87 ± 0.31	0.7782
RBC (M/uL)	8.075 ± 0.71	8.654 ± 0.25	0.4841
PT (sec)	8.133 ± 0.067	8.067 ± 0.089	0.5813
aPTT (sec)	33.30 ± 1.644	30.13 ± 1.244	0.1994

FIGURE V.1: TARGETING OF THE CD39 GENE BY HOMOLOGOUS CRE RECOMBINATION

(A QRT-PCR analysis of 1.5µg of mRNA from various adult mouse tissues (specified on blots, with sample genotype) (n = 3) **(B)** No heart rate differences were observed between *cd39*$^{+/+}$ and *cd39*$^{-/-}$ cohorts in average heart rate or **(C)** BP (n=4 per group). Comparisons between groups were performed via independent samples t test **(D)** Hematological profile of CD39$^{flx/flx}$ and CD39$^{-/-}$ mice. Circulating blood cell and coagulation parameter measurements of CD39$^{flx/flx}$ (n = 4) and CD39$^{-/-}$ (n = 5 to 7) mice. P = non-significant for statistical comparisons between all groups except platelets. Data are shown as means ±SD. *$P < 0.05$, **$P < 0.001$, ***$P < 0.0001$

A Platelet Aggregation of $CD39^{+/+}$ vs. $CD39^{-/-}$

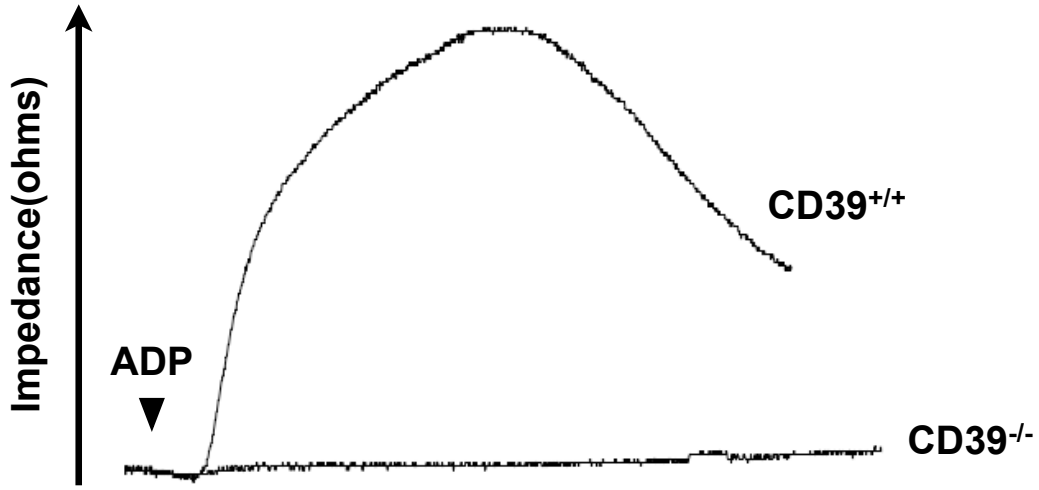

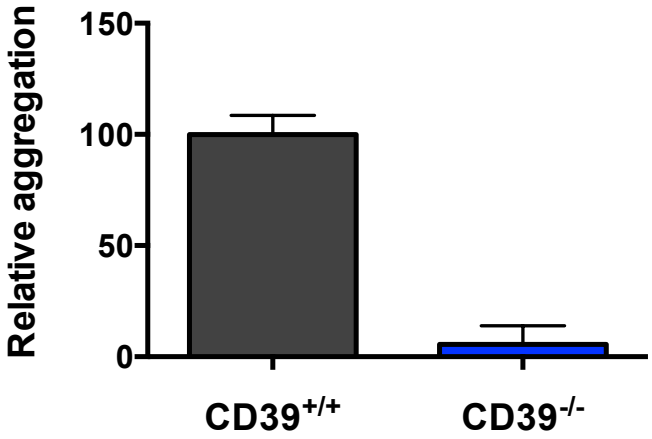

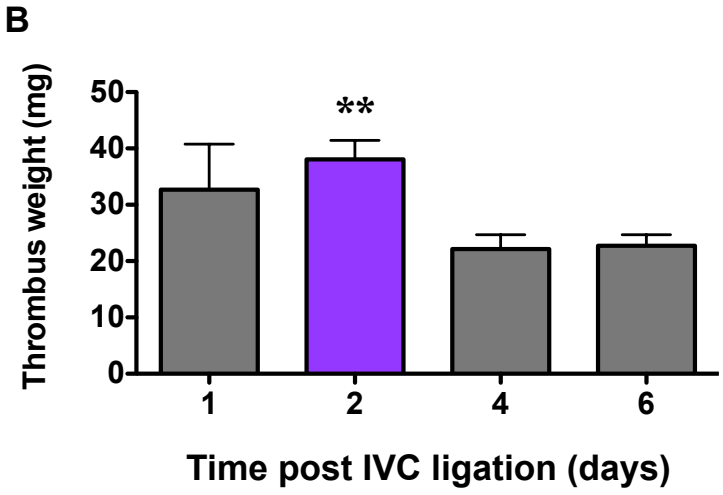
B
Thrombus weight (mg)
50
40
30
20
10
0
**
1
2
4
6
Time post IVC ligation (days)

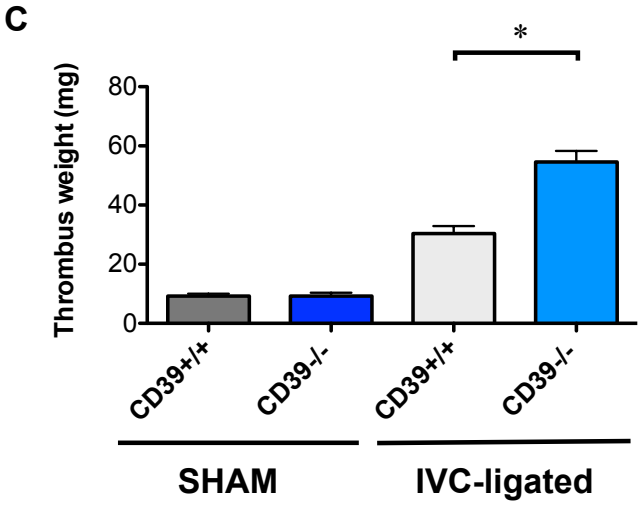
C
*
Thrombus weight (mg)
80
60
40
20
0
CD39+/+
CD39-/-
CD39+/+
CD39-/-
SHAM
IVC-ligated

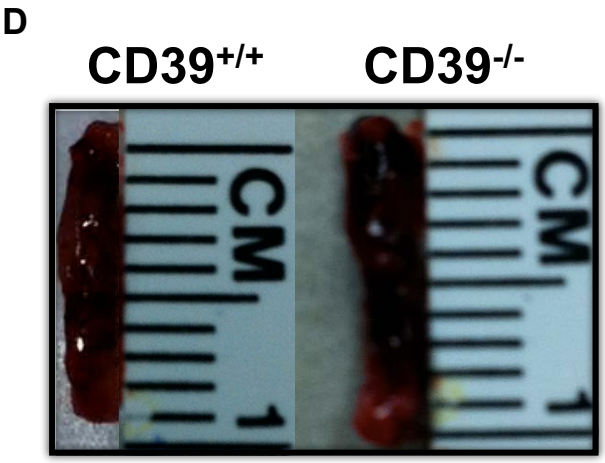

FIGURE V.2: CHARACTERIZATION OF THROMBUS WEIGHT IN CD39$^{+/+}$ AND CD39$^{-/-}$ MICE 48 HR POST STASIS-INDUCED THROMBOGENESIS.

(A) Whole-blood aggregometry with 5 μM ADP stimulation was performed on WT and CD39$^{-/-}$ mice (n = 4 per group). Representative whole-blood platelet aggregation profiles of WT and CD39$^{-/-}$ mice (n = 4 per group). Quantification of relative platelet aggregation profiles (n = 4 per group). **(B)** Inferior vena cava (IVC) stasis-induced venous thrombosis in CD39$^{+/+}$ mice was induced. Thrombus weight was measured in CD39$^{+/+}$ mice at 1-6 days following IVC ligation (All mice CD39 $^{flox/flox}$ designated as CD39$^{+/+}$): 1d, n = 6; 2d, n = 20; 4d, n = 8; 6d, n = 10). **(C)** Thrombus weight in sham-operated and stasis-induced venous thrombogenesis in CD39$^{+/+}$ and CD39$^{-/-}$ mice at 48 hours. Sham: CD39$^{+/+}$, n = 8; CD39$^{-/-}$ n = 8. IVC-ligated: CD39$^{+/+}$, n = 15; CD39$^{-/-}$ n = 8. **(D)** Representative photographs of stasis-induced venous thrombosis of CD39$^{+/+}$ and CD39$^{-/-}$ mice at 48 hours post ligation. Data are shown as means ±SD. *P < 0.05, **P < 0.001, ***P < 0.0001

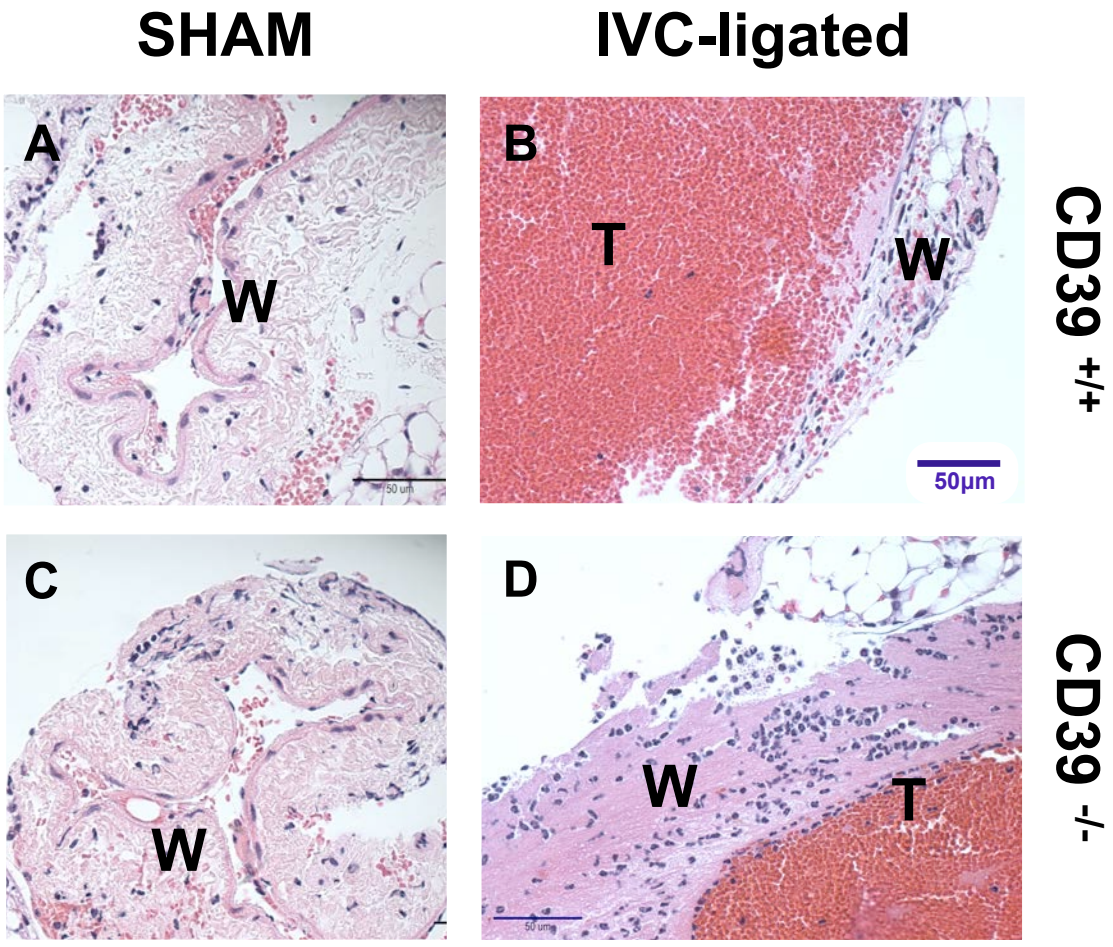
SHAM
IVC-ligated
A
W
B
T
W
50µm
CD39 +/+
C
W
D
W
T
CD39 -/-

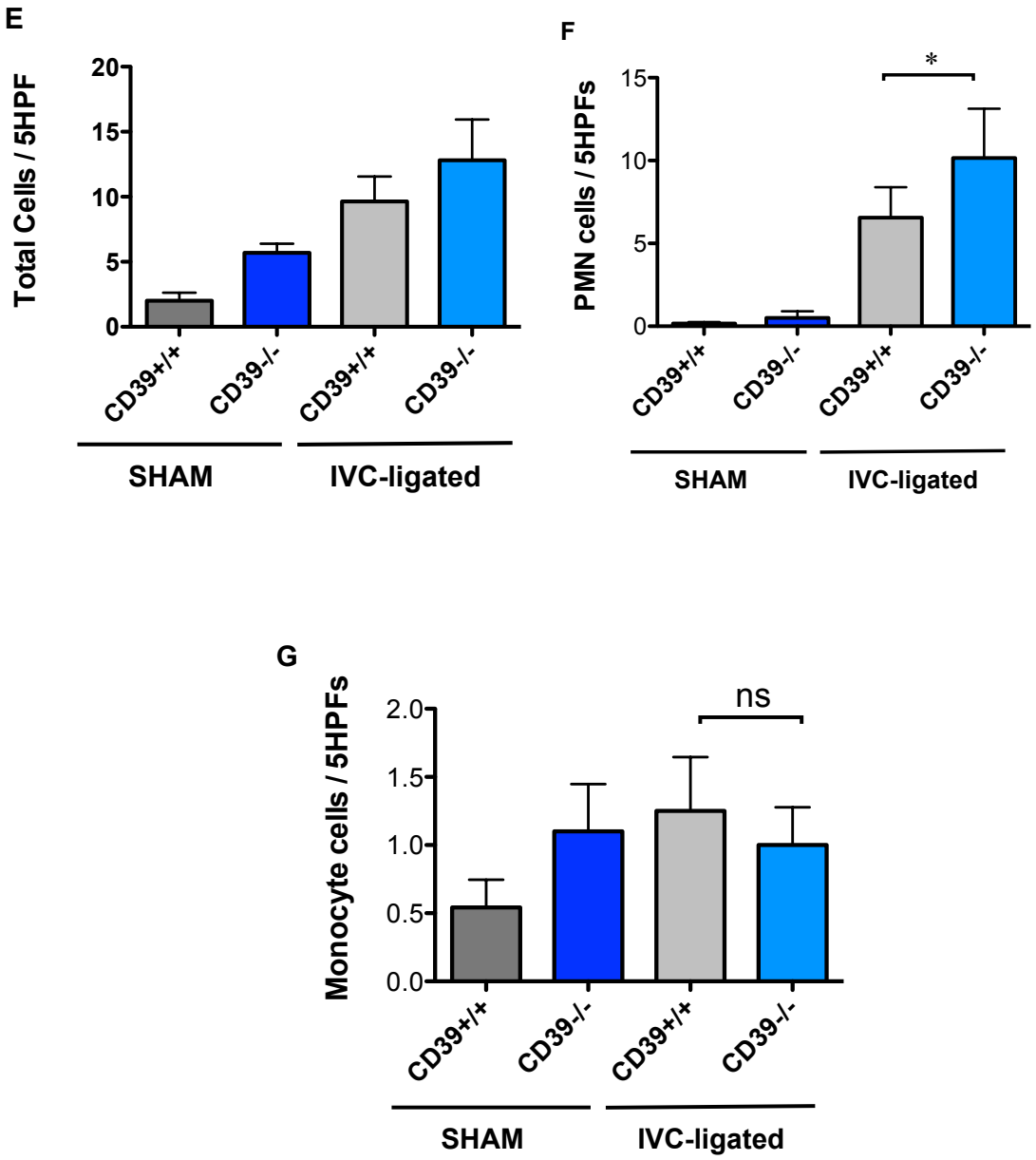

FIGURE V.3: HISTOLOGICAL ANALYSIS AND INFLAMMATORY CELL COUNTS OF THE THROMBUS-CONTAINING IVC 48H POST IVC LIGATION IN $CD39^{+/+}$ AND $CD39^{-/-}$ MICE.

(A-D) Hematoxylin and eosin stained inferior vena cava section of 48 hr sham operated (**A and C**) and thrombosed IVC (B and D) of $CD39^{+/+}$ and $CD39^{-/-}$ mice. (**B**) Compared $CD39^{+/+}$ mice (**D**) due to inflammatory infiltrate, relative acellularity, and extracelluar

matrix deposition (magnification = original x400). T = thrombus W= vein Wall. **(E-G)** Morphometric evaluation of inflammatory cell counts of five high-powered field in the vein wall of $CD39^{+/+}$ and $CD39^{-/-}$ mice 48 hr post IVC ligation and sham-operated controls. Total inflammatory cell **(E),** Polymorphonuclear cells (neutrophils) **(F)** and Monocytes **(G)** (n = 3-5 all groups). Data are shown as means ±SD. $*P < 0.05$, $**P < 0.001$, $***P < 0.0001$

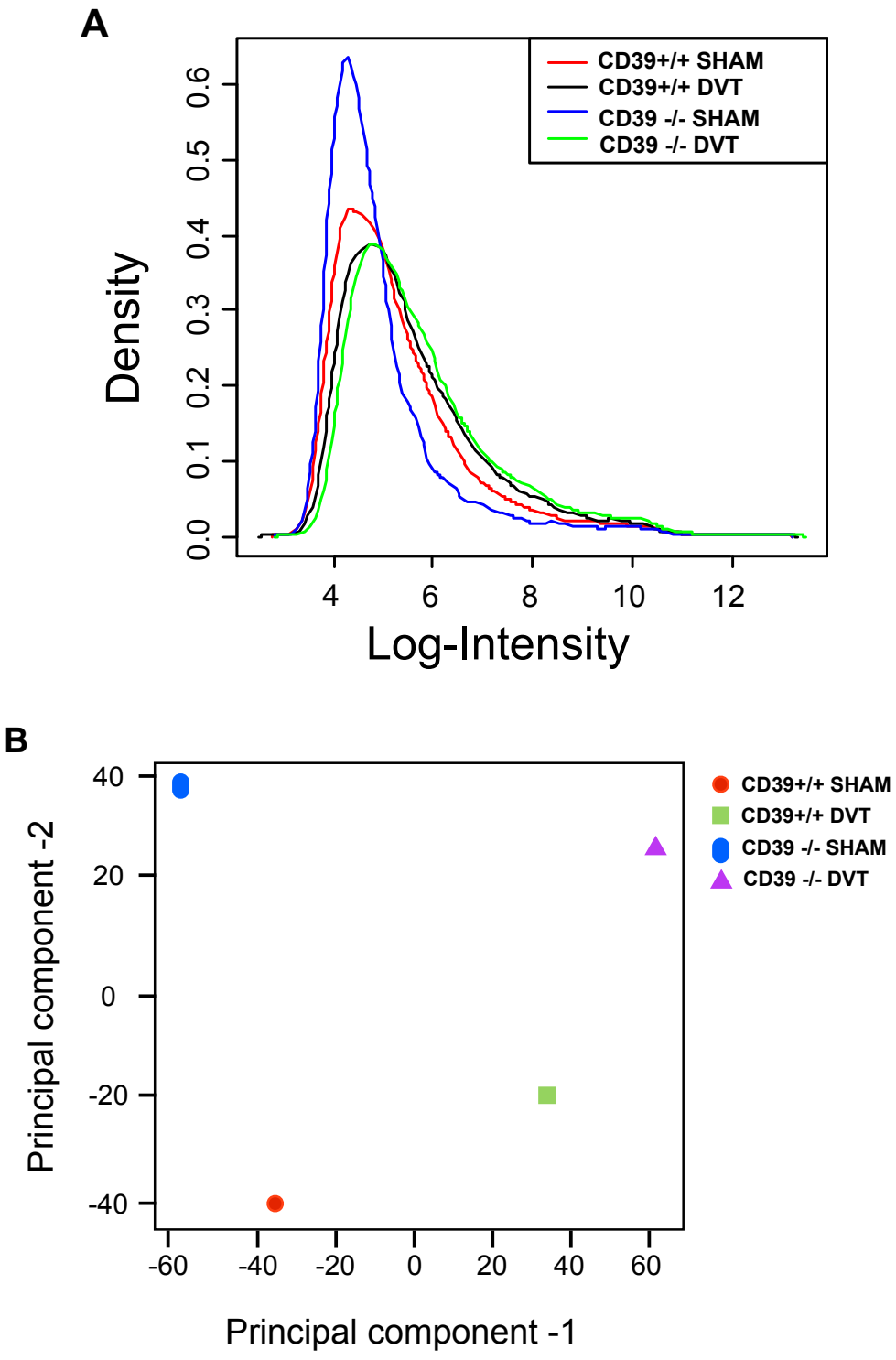
A
CD39+/+ SHAM
CD39+/+ DVT
CD39 -/- SHAM
CD39 -/- DVT
Density
0.0
0.1
0.2
0.3
0.4
0.5
0.6
4
6
8
10
12
Log-Intensity
B
CD39+/+ SHAM
CD39+/+ DVT
CD39 -/- SHAM
CD39 -/- DVT
Principal component -2
40
20
0
-20
-40
-60
-40
-20
0
20
40
60
Principal component -1

C

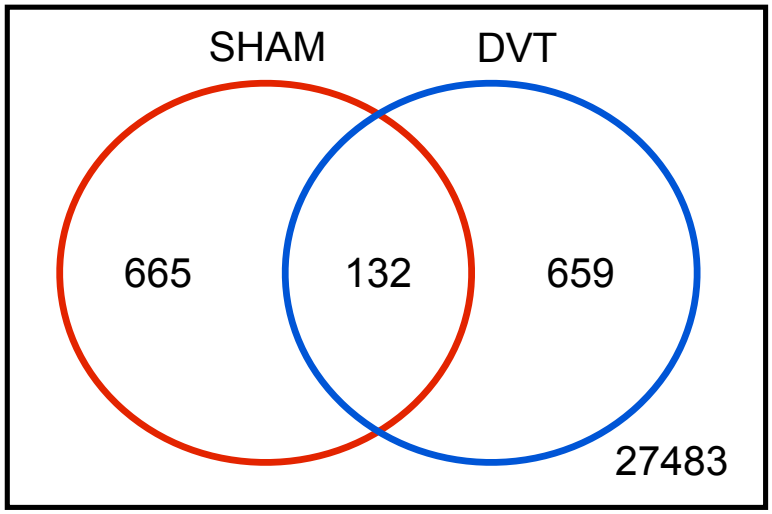

D

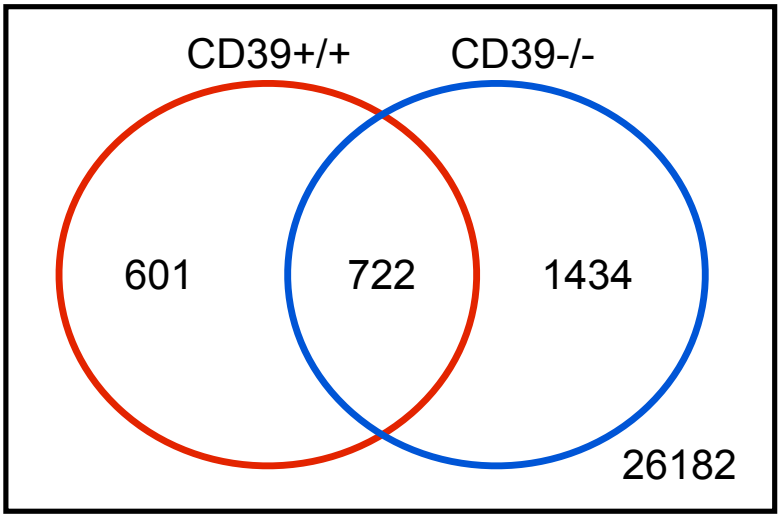

FIGURE V.4: MICROARRAY QUALITY CONTROL ANALYSIS OF CD39$^{+/+}$ AND CD39$^{-/-}$ MICE 48 HR POST-IVC-LIGATION.

(A) Quality control plots of CD39$^{+/+}$ and CD39$^{-/-}$ sham operated or IVC-ligated mice 48 hr post IVC ligation depicts the distribution of the probes for each chip: with Agilent 2001 Bioanalyzer to ensure that each samples prepared for microarray hybrization meet the Affymetrix guidelines. All samples came from the same distribution with only difference being the location and scale based the normalization procedure. Each expression value for each gene used a robust multi-array average *(Irizarry et al. 2003)*. **(B)** Principle component analysis (PCA) of CD39$^{+/+}$ and CD39$^{-/-}$ mice 48 hr post-thrombus induction. Red, blue (CD39$^{+/+}$ and CD39$^{-/-}$ sham-operated mice) green and purple (CD39$^{+/+}$ and CD39$^{-/-}$ IVC-ligated mice) dots represent linear combinations of the expression data, including relative expression value and variance of the 28,939 probe sets in IVC from each experimental group. The PCA software examined two component of genes in different samples for those similar or different expression profiles. The first component shown in the *x-axis*, includes genes with a high degree of variance within the different strains (CD39$^{+/+}$ sham and IVC-ligated vs. CD39$^{-/-}$ sham and IVC-ligated). The second component, displayed in the *y-axis*, encompasses genes that also had a high range of variance within the sham and thrombus inducted group (Sham - CD39$^{+/+}$ and CD39$^{-/-}$ vs. IVC-ligated- CD39$^{+/+}$ and CD39$^{-/-}$). **(C, D)** Venn diagrams illustrating the number of probe sets identified as significantly differentially expressed (Fold change ≥2; P≤0.001) in each pairwise comparison. **(C)** CD39$^{+/+}$ sham vs. CD39$^{-/-}$ sham; CD39$^{+/+}$ IVC-ligated vs. CD39$^{-/-}$ IVC-ligated and common and unique genes between each group **(D)** CD39$^{+/+}$ sham vs. CD39$^{+/+}$ IVC-ligated; CD39$^{-/-}$ sham vs. CD39$^{-/-}$ IVC-ligated group and common and unique genes between each group.

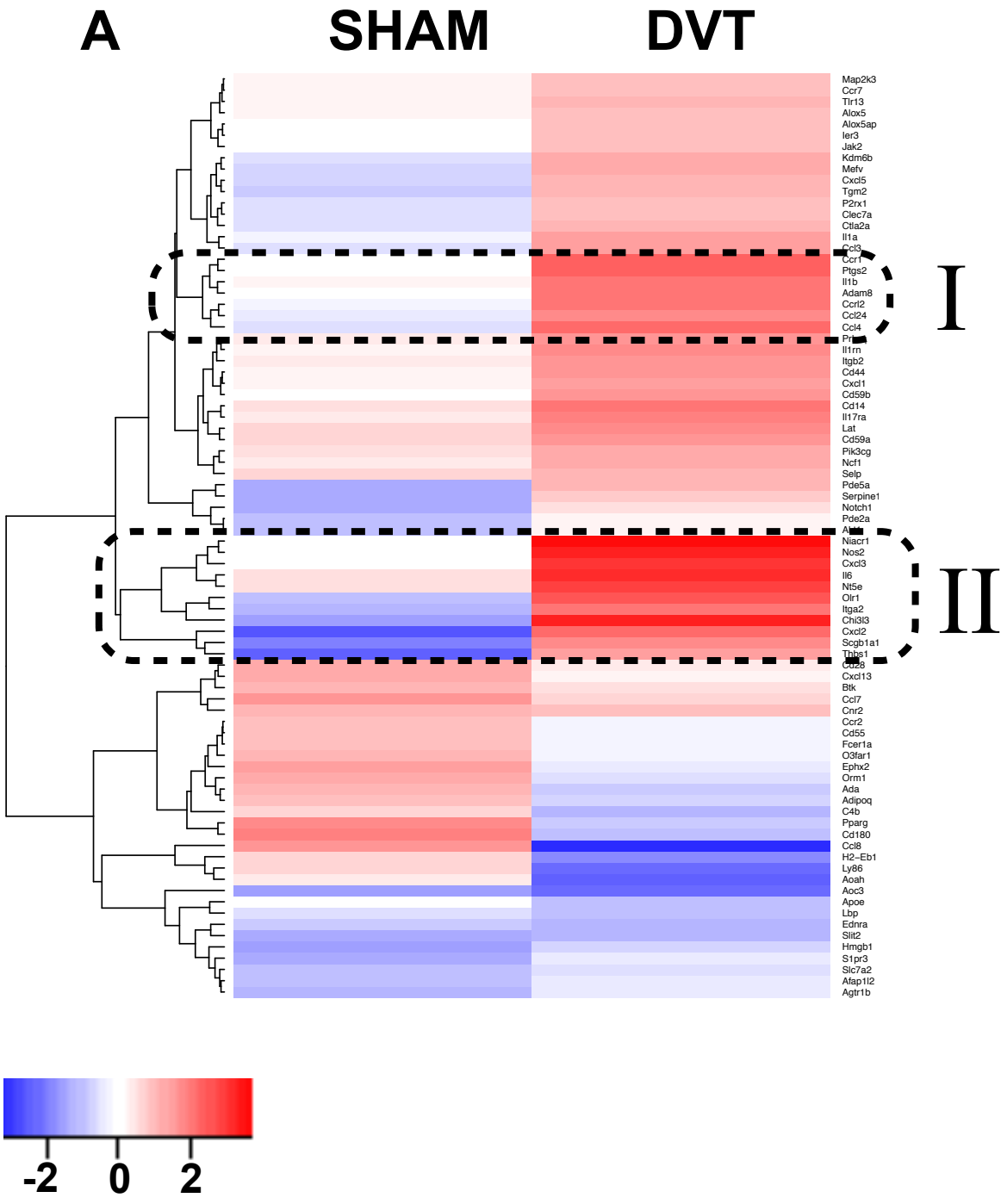
A
SHAM
DVT
I
II
Map2k3
Ccr7
Tlr13
Alox5
Alox5ap
Ier3
Jak2
Kdm6b
Mefv
Cxcl5
Tgm2
P2rx1
Clec7a
Ctla2a
Il1a
Ccl3
Ccr1
Ptgs2
Il1b
Adam8
Ccrl2
Ccl24
Ccl4
Il1rn
Itgb2
Cd44
Cxcl1
Cd59b
Cd14
Il17ra
Lat
Cd59a
Pik3cg
Ncf1
Selp
Pde5a
Serpine1
Notch1
Pde2a
Niacr1
Nos2
Cxcl3
Il6
Nt5e
Olr1
Itga2
Chi3l3
Cxcl2
Scgb1a1
Thbs1
Cxcl13
Btk
Ccl7
Cnr2
Ccr2
Cd55
Fcer1a
O3far1
Ephx2
Orm1
Ada
Adipoq
C4b
Pparg
Cd180
Ccl8
H2-Eb1
Ly86
Aoah
Aoc3
Apoe
Lbp
Ednra
Slit2
Hmgb1
S1pr3
Slc7a2
Afap1l2
Agtr1b
-2
0
2

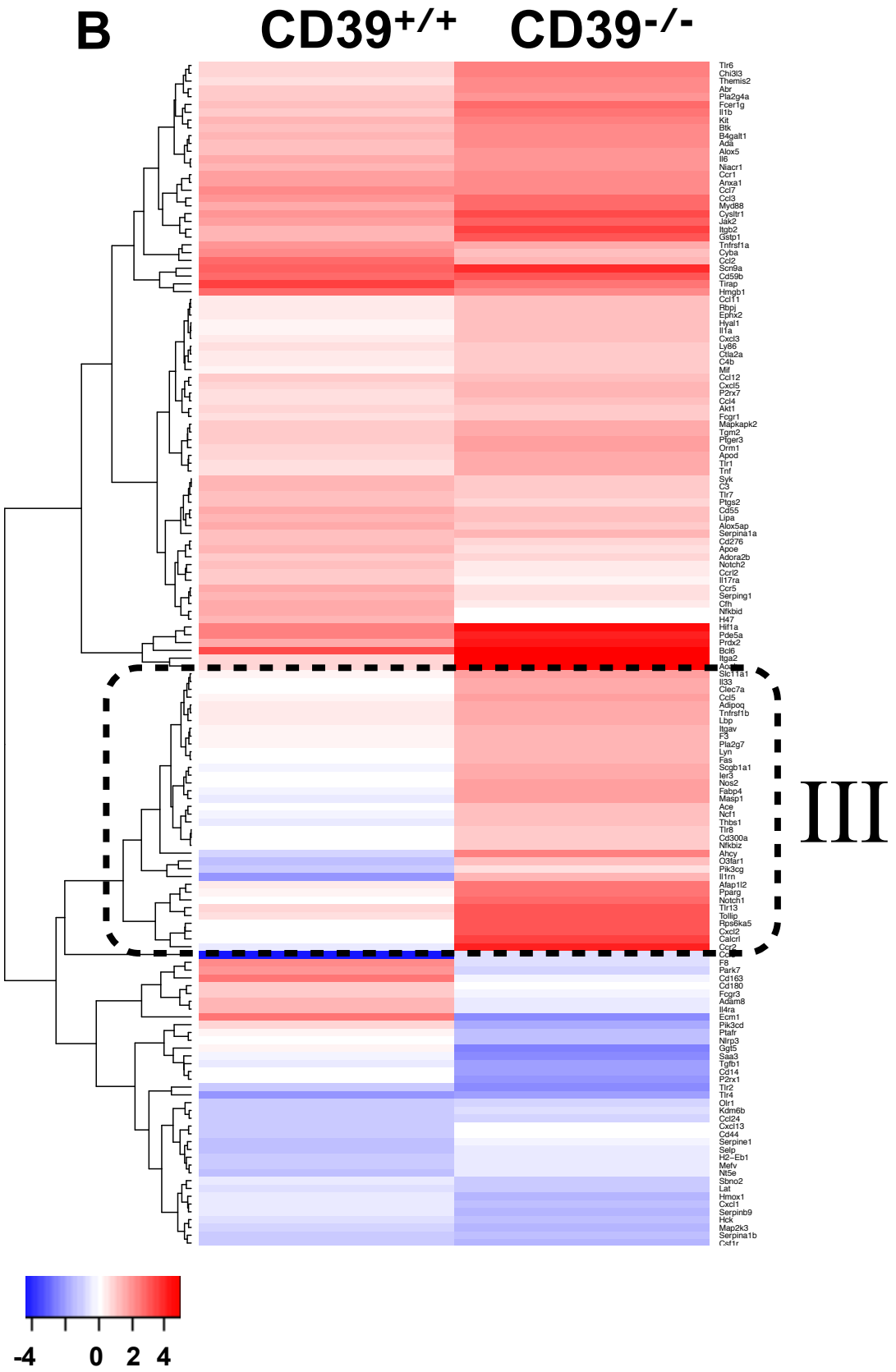
B
CD39+/+
CD39-/-
III
-4
0
2
4

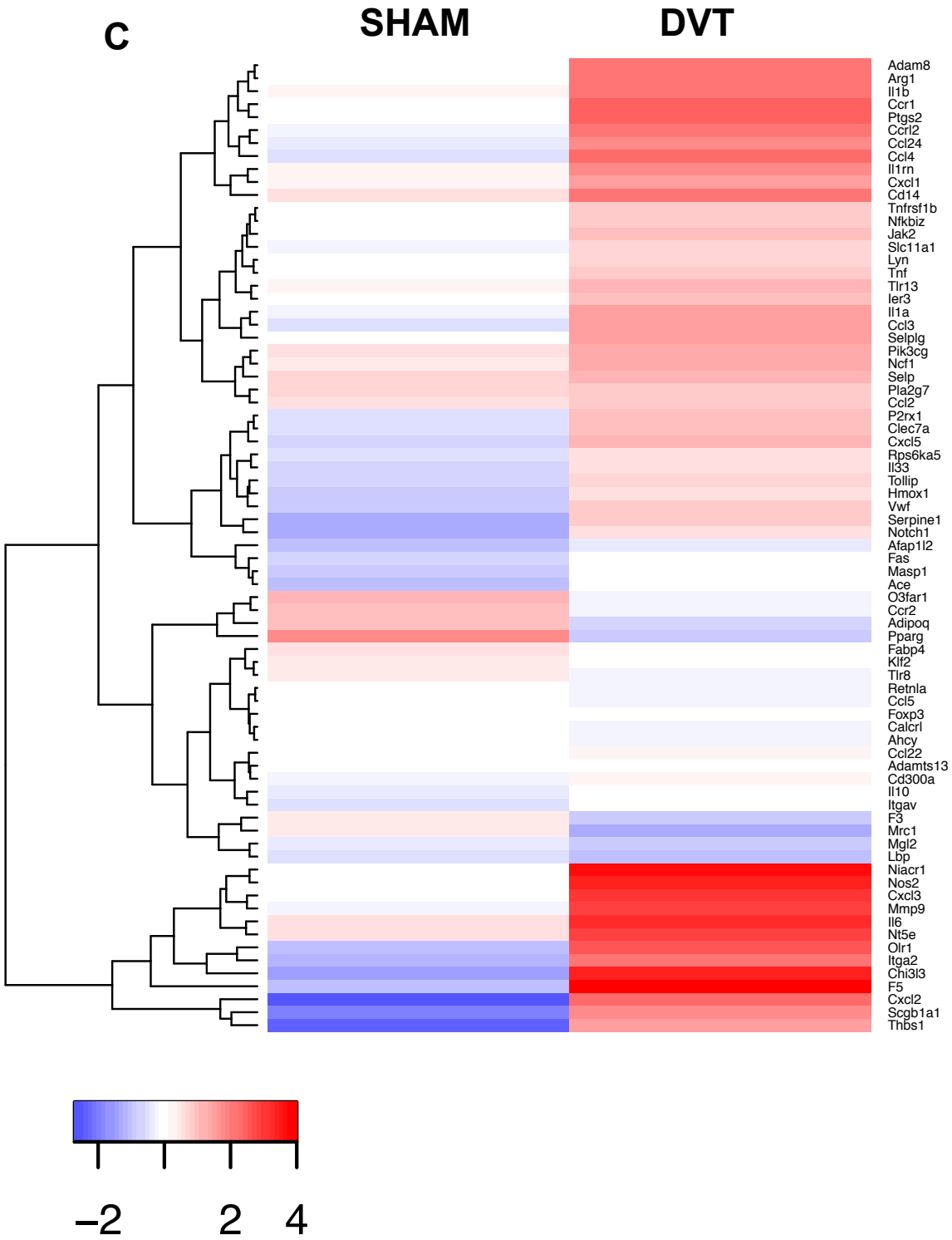
C
SHAM
DVT
Adam8
Arg1
Il1b
Ccr1
Ptgs2
Ccrl2
Ccl24
Ccl4
Il1rn
Cxcl1
Cd14
Tnfrsf1b
Nfkbiz
Jak2
Slc11a1
Lyn
Tnf
Tlr13
Ier3
Il1a
Ccl3
Selplg
Pik3cg
Ncf1
Selp
Pla2g7
Ccl2
P2rx1
Clec7a
Cxcl5
Rps6ka5
Il33
Tollip
Hmox1
Vwf
Serpine1
Notch1
Afap1l2
Fas
Masp1
Ace
O3far1
Ccr2
Adipoq
Pparg
Fabp4
Klf2
Tlr8
Retnla
Ccl5
Foxp3
Calcrl
Ahcy
Ccl22
Adamts13
Cd300a
Il10
Itgav
F3
Mrc1
Mgl2
Lbp
Niacr1
Nos2
Cxcl3
Mmp9
Il6
Nt5e
Olr1
Itga2
Chi3l3
F5
Cxcl2
Scgb1a1
Thbs1
−2
2
4

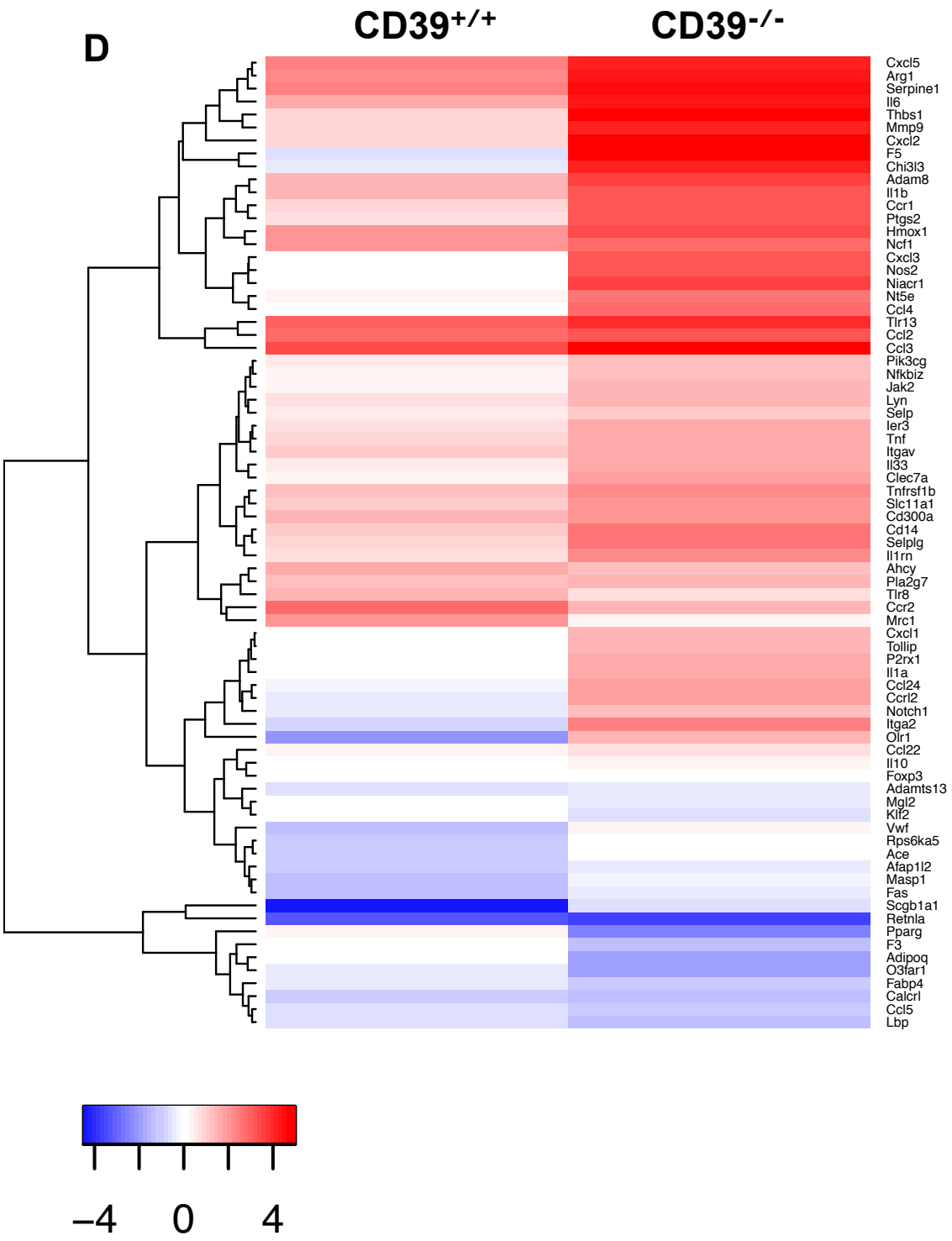
D
CD39+/+
CD39-/-
Cxcl5
Arg1
Serpine1
Il6
Thbs1
Mmp9
Cxcl2
F5
Chi3l3
Adam8
Il1b
Ccr1
Ptgs2
Hmox1
Ncf1
Cxcl3
Nos2
Niacr1
Nt5e
Ccl4
Tlr13
Ccl2
Ccl3
Pik3cg
Nfkbiz
Jak2
Lyn
Selp
Ier3
Tnf
Itgav
Il33
Clec7a
Tnfrsf1b
Slc11a1
Cd300a
Cd14
Selplg
Il1rn
Ahcy
Pla2g7
Tlr8
Ccr2
Mrc1
Cxcl1
Tollip
P2rx1
Il1a
Ccl24
Ccrl2
Notch1
Itga2
Olr1
Ccl22
Il10
Foxp3
Adamts13
Mgl2
Klf2
Vwf
Rps6ka5
Ace
Afap1l2
Masp1
Fas
Scgb1a1
Retnla
Pparg
F3
Adipoq
O3far1
Fabp4
Calcrl
Ccl5
Lbp
−4
0
4

FIGURE V.5: HIERARCHICAL CLUSTERING OF DIFFERENTIALLY EXPRESSED INFLAMMATORY GENES RELATED TO $CD39^{+/+}$ AND $CD39^{-/-}$ MICE 48 HR POST-IVC-LIGATION.

(A-D) Genes involved in inflammation and immune response were analyzed. ANOVA was first performed to identify genes that are differentially expressed due to CD39 deficiency or stasis-induced thrombogenesis. Each lane represents the expression profile of inflammatory genes of two mice **(A)** Differentially expressed genes between sham ($CD39^{+/+}$ sham compared to $CD39^{-/-}$ sham) and DVT ($CD39^{+/+}$ IVC-ligated compared to $CD39^{-/-}$ IVC-ligated), **(B)** $CD39^{+/+}$ ($CD39^{+/+}$ IVC-ligated compared to $CD39^{+/+}$ sham) and $CD39^{-/-}$ ($CD39^{-/-}$ IVC-ligated compared to $CD39^{-/-}$ sham) groups were visualized as heatmaps for microarray analysis. Red and blue colors indicate up and down – regulated expression levels, respectively. White color indicates no change in expression levels. Inflammatory genes highly upregulated during stasis-induced thrombosis and $CD39^{-/-}$ deficiency were categorized as group I, II, III and supervised hierarchical clustering of 76 unique probe sets were visualized as a heatmap using oligo package of bioconductor implemented in the R statistical environment **(C, D).**

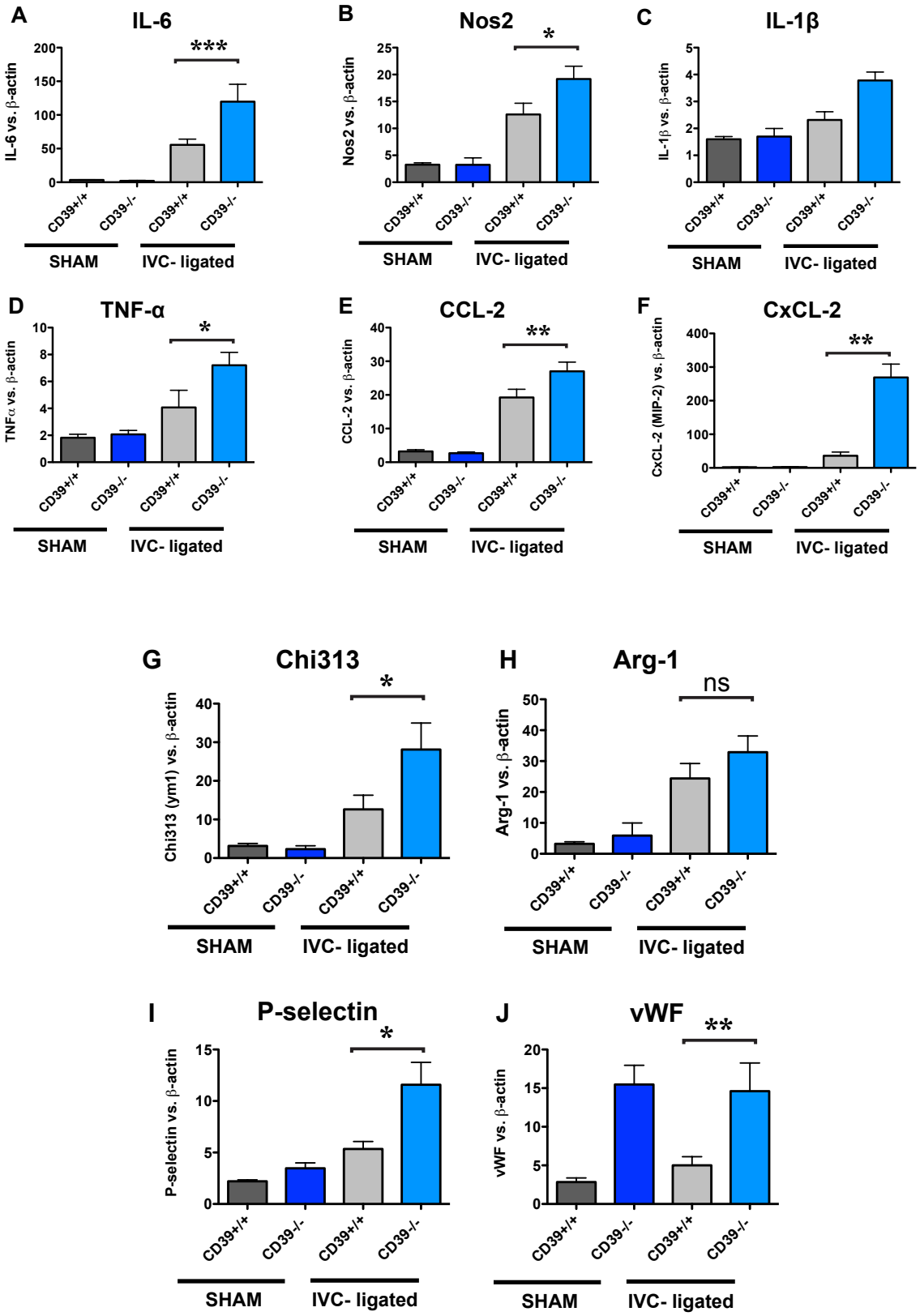
A
IL-6
IL-6 vs. β-actin
***
B
Nos2
Nos2 vs. β-actin
*
C
IL-1β
IL-1β vs. β-actin
D
TNF-α
TNFα vs. β-actin
*
E
CCL-2
CCL-2 vs. β-actin
**
F
CxCL-2
CxCL-2 (MIP-2) vs. β-actin
**
G
Chi313
Chi313 (ym1) vs. β-actin
*
H
Arg-1
Arg-1 vs. β-actin
ns
I
P-selectin
P-selectin vs. β-actin
*
J
vWF
vWF vs. β-actin
**
CD39+/+
CD39-/-
SHAM
IVC- ligated

FIGURE V.6: VALIDATION OF MICROARRAY RESULTS VIA QUANTITATIVE RT-PCR ANALYSIS OF $CD39^{+/+}$ AND $CD39^{-/-}$ MICE 48 HR POST-IVC-LIGATION.

(A-J) Gene expression of proinflammatory mediators and chemokines were analyzed in $CD39^{+/+}$ and $CD39^{-/-}$ 48 hr post IVC ligation, selected on the basis of the output of the microarray studies, and were assessed during qRT-PCR. Fold changes were normalized to β-actin. Results are shown as the mean ± SD of at least six independent experiments. Data are shown as means ±SD. $*P < 0.05$, $**P < 0.001$, $***P < 0.0001$

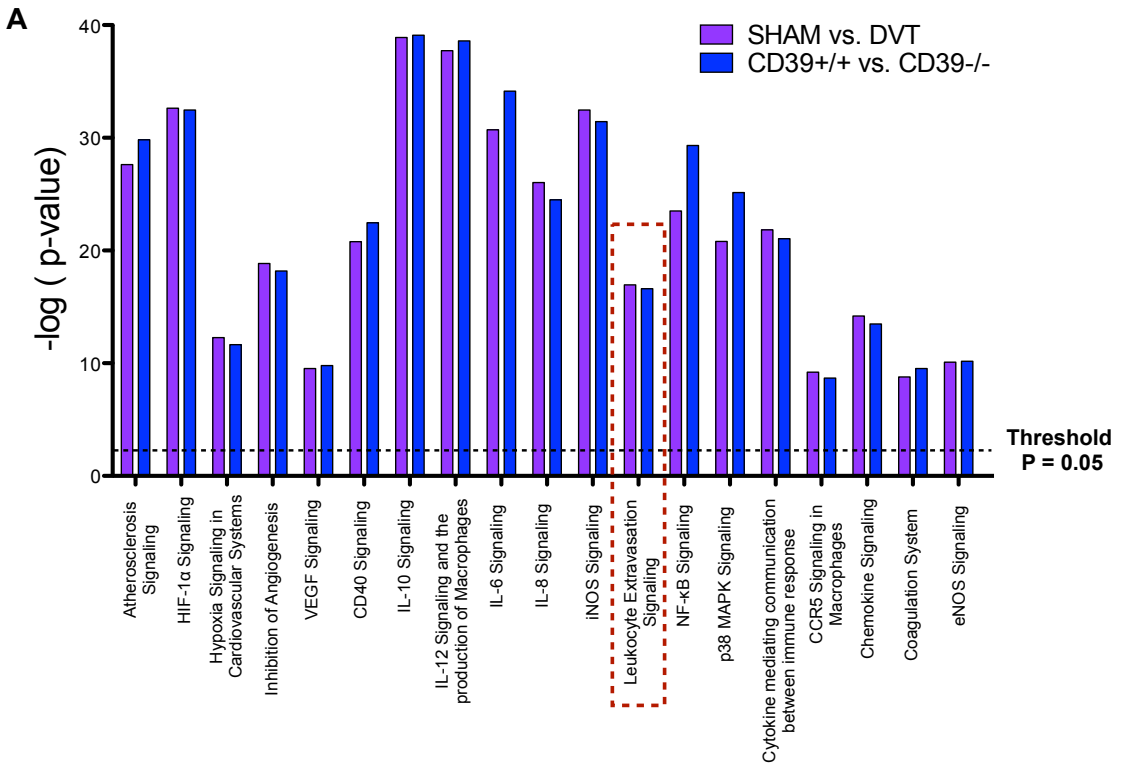
A
SHAM vs. DVT
CD39+/+ vs. CD39-/-
-log (p-value)
40
30
20
10
0
Threshold
P = 0.05
Atherosclerosis Signaling
HIF-1α Signaling
Hypoxia Signaling in Cardiovascular Systems
Inhibition of Angiogenesis
VEGF Signaling
CD40 Signaling
IL-10 Signaling
IL-12 Signaling and the production of Macrophages
IL-6 Signaling
IL-8 Signaling
iNOS Signaling
Leukocyte Extravasation Signaling
NF-κB Signaling
p38 MAPK Signaling
Cytokine mediating communication between immune response
CCR5 Signaling in Macrophages
Chemokine Signaling
Coagulation System
eNOS Signaling

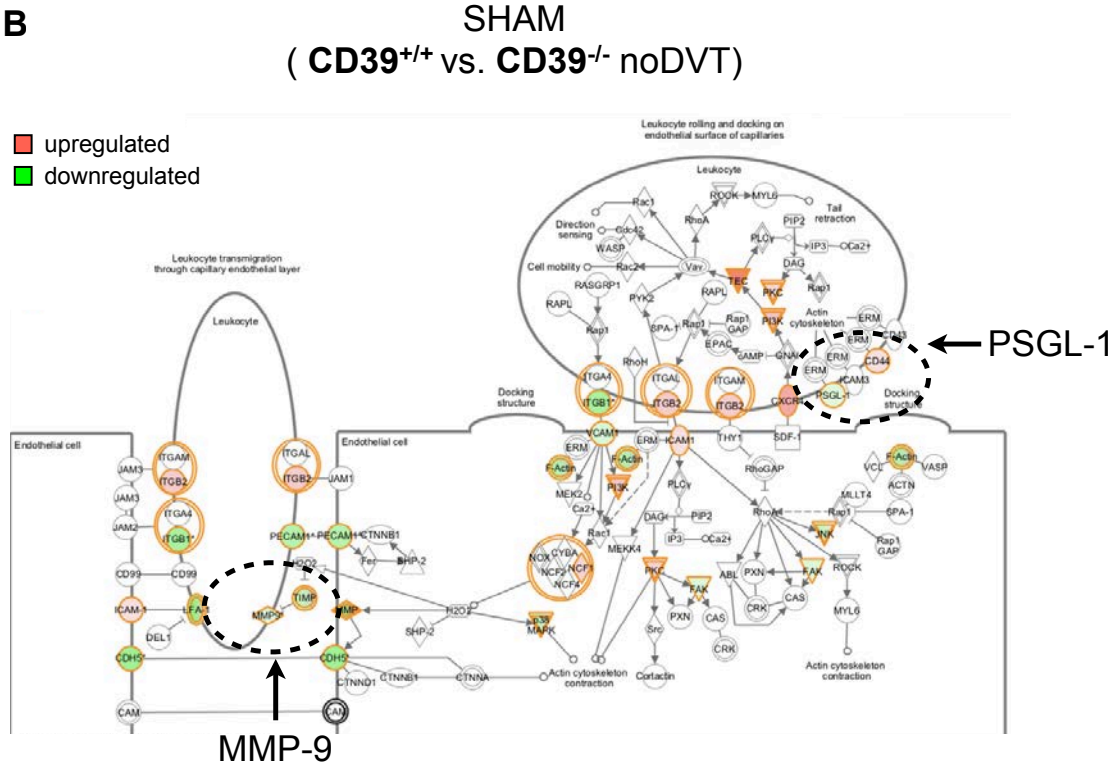
B
SHAM
(CD39+/+ vs. CD39-/- noDVT)
upregulated
downregulated
PSGL-1
MMP-9
Leukocyte rolling and docking on endothelial surface of capillaries
Leukocyte transmigration through capillary endothelial layer
Leukocyte
Endothelial cell
Docking structure
Actin cytoskeleton contraction

C

DVT
(**CD39$^{+/+}$** vs. **CD39$^{-/-}$** DVT)

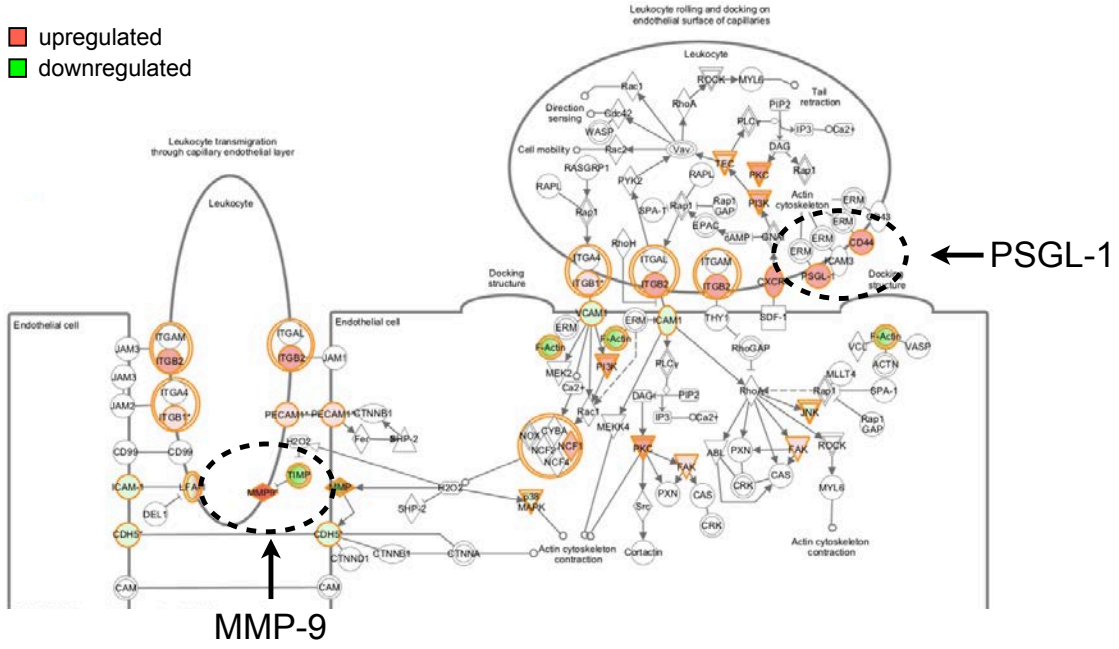

D

CD39$^{+/+}$
(noDVT vs.DVT)

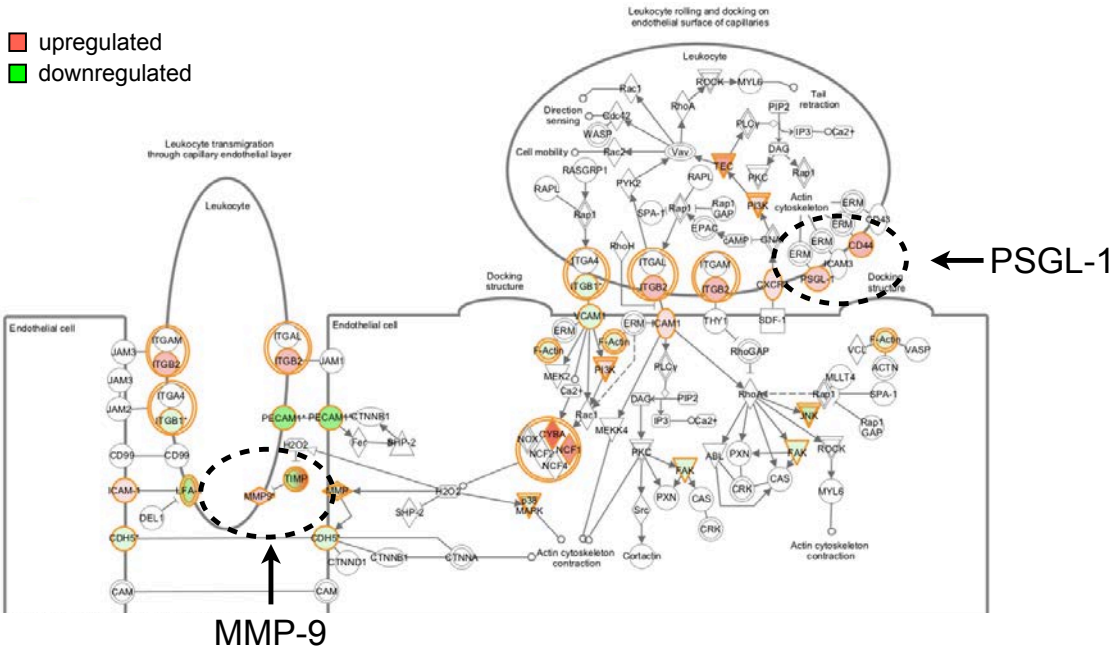

E

CD39$^{-/-}$
(noDVT vs.DVT)

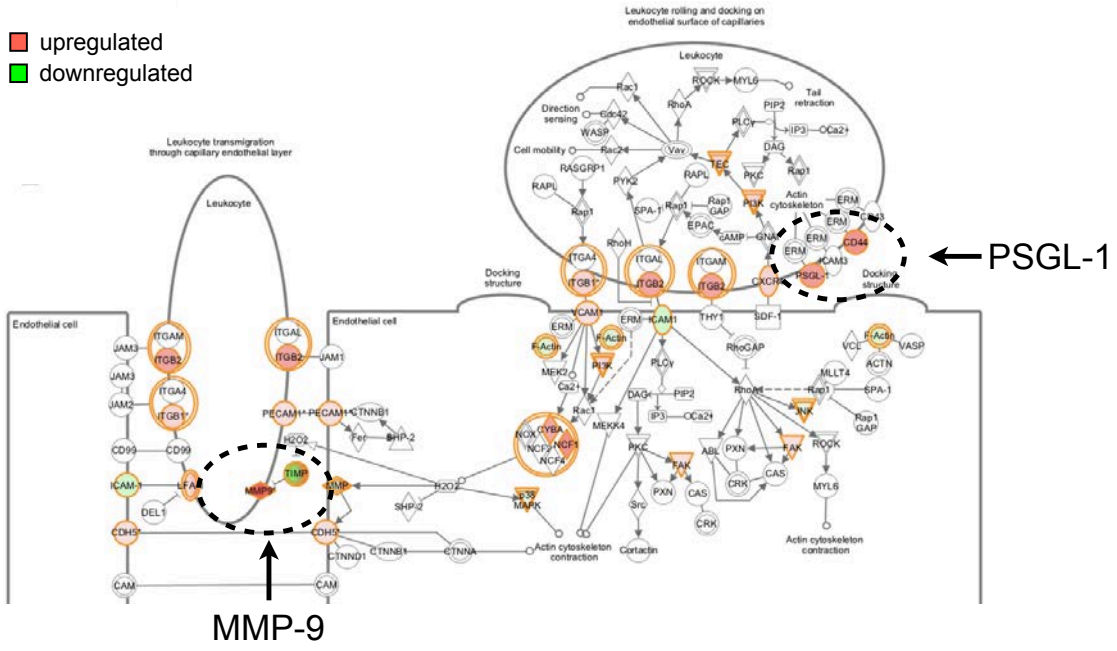

F **SHAM**
(CD39+/+ vs. CD39-/- noDVT)

G **DVT**
(CD39+/+ vs. CD39-/- DVT)

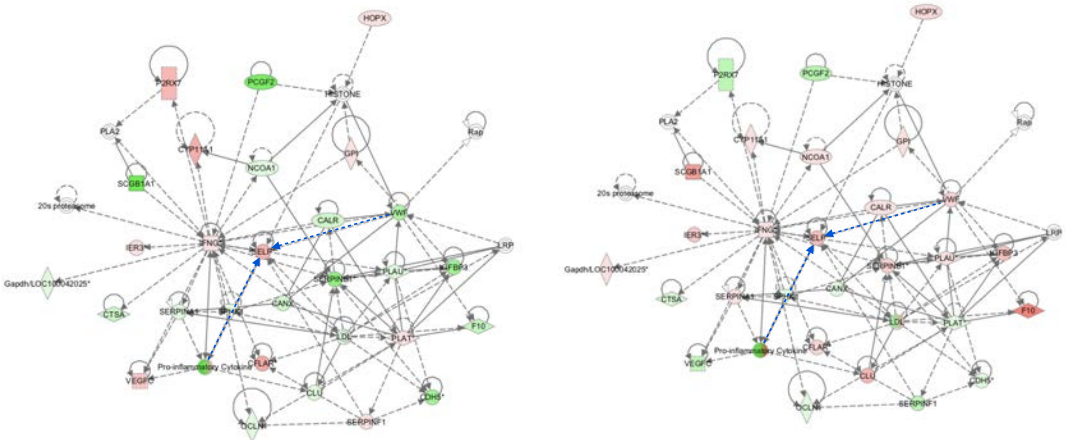

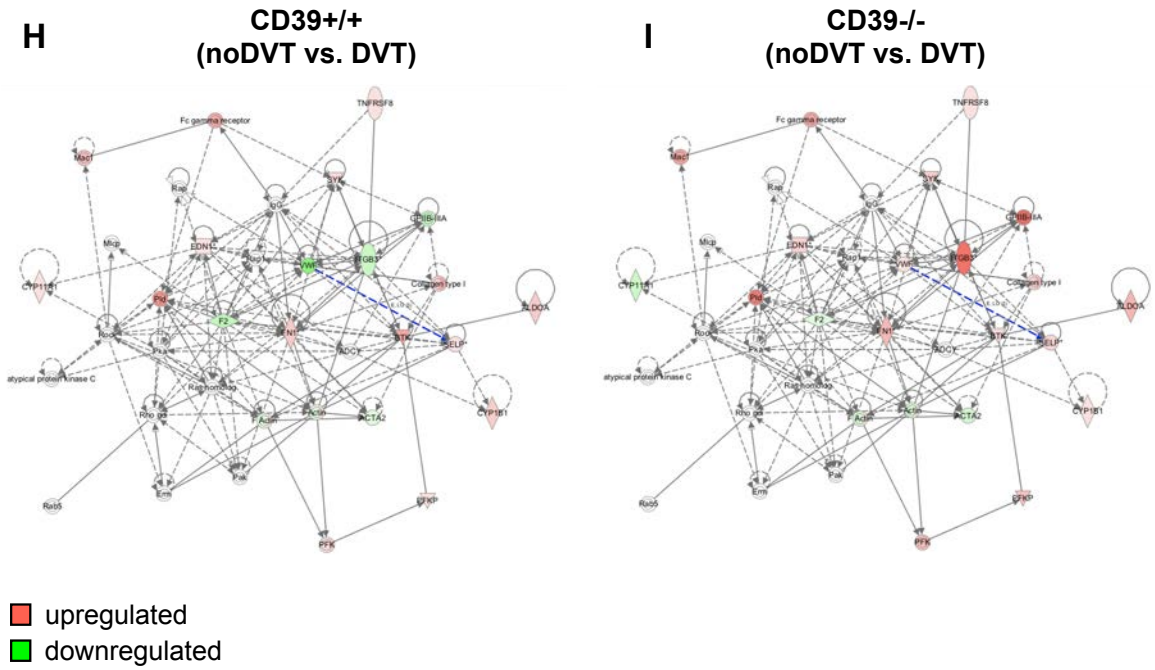

FIGURE V.7: IPA GENERATED MOLECULAR NETWORK PATHWAY ANALYSIS OF CD39$^{+/+}$ AND CD39$^{-/-}$ MICE 48 HR POST-IVC-LIGATION.

The demonstrated network/pathway diagrams are taken from IPA analysis of the microarray data based on upregulated genes and visualized using the network analysis tool. **(A)** Integrated gene network analysis reveals strong differences in gene expression of CD39$^{+/+}$ and CD39$^{-/-}$ mice 48 hrs post-IVC-ligation. Cellular functions identified by IPA as being affected by IVC induced thrombosis or CD39 deficiency are illustrated with bar graphs based on the levels of –log (p-value), the higher the levels the more significant of the effect. White bars indicate functions affected by IVC-ligaton, whereas the black bars denote those affected by CD39-deficiency and IVC-ligation. 4 independent biological replicates for each arrayed group were performed. **(B-E)** Leukocyte extravasion pathway identified by IPA. **B,** represents the subnetwork of the CD39$^{+/+}$

sham vs. $CD39^{-/-}$ sham pathway **C,** represents the subnetwork of the $CD39^{+/+}$ IVC-ligated vs. $CD39^{-/-}$ IVC-ligated pathway **D,** $CD39^{+/+}$ sham vs. $CD39^{+/+}$ IVC-ligated pathway and **E,** $CD39^{-/-}$ sham vs. $CD39^{-/-}$ IVC-ligated pathway. Color nodes: genes that changed significantly in $CD39^{+/+}$ and $CD39^{-/-}$ mice 48 hrs post-thrombus induction with a fold change >2. Red: upregulation; green: downregulation. The diagram was modified from Ingenuity Pathway Analysis (Ingenuity® Systems). **(F-I)** Key inflammatory gene co-expression network analysis. **F,** represents the subnetwork of the $CD39^{+/+}$ sham vs. $CD39^{-/-}$ sham pathway **G,** represents the subnetwork of the $CD39^{+/+}$ IVC-ligated vs. $CD39^{-/-}$ IVC-ligated pathway **H,** $CD39^{+/+}$ sham vs. $CD39^{+/+}$ IVC-ligated pathway and **I,** $CD39^{-/-}$ sham vs. $CD39^{-/-}$ IVC-ligated pathway. In this visualization, genes/proteins (nodes) are shown as circles, and the interactions between these nodes are shown as lines (edges). Nodes are colored according to the degree of dysregulation from highly up regulated (red), highly down regulated (green) and baseline (white). The networks were generated through the use of Ingenuity Pathways Analysis (Ingenuity® Systems, www.ingenuity.com).

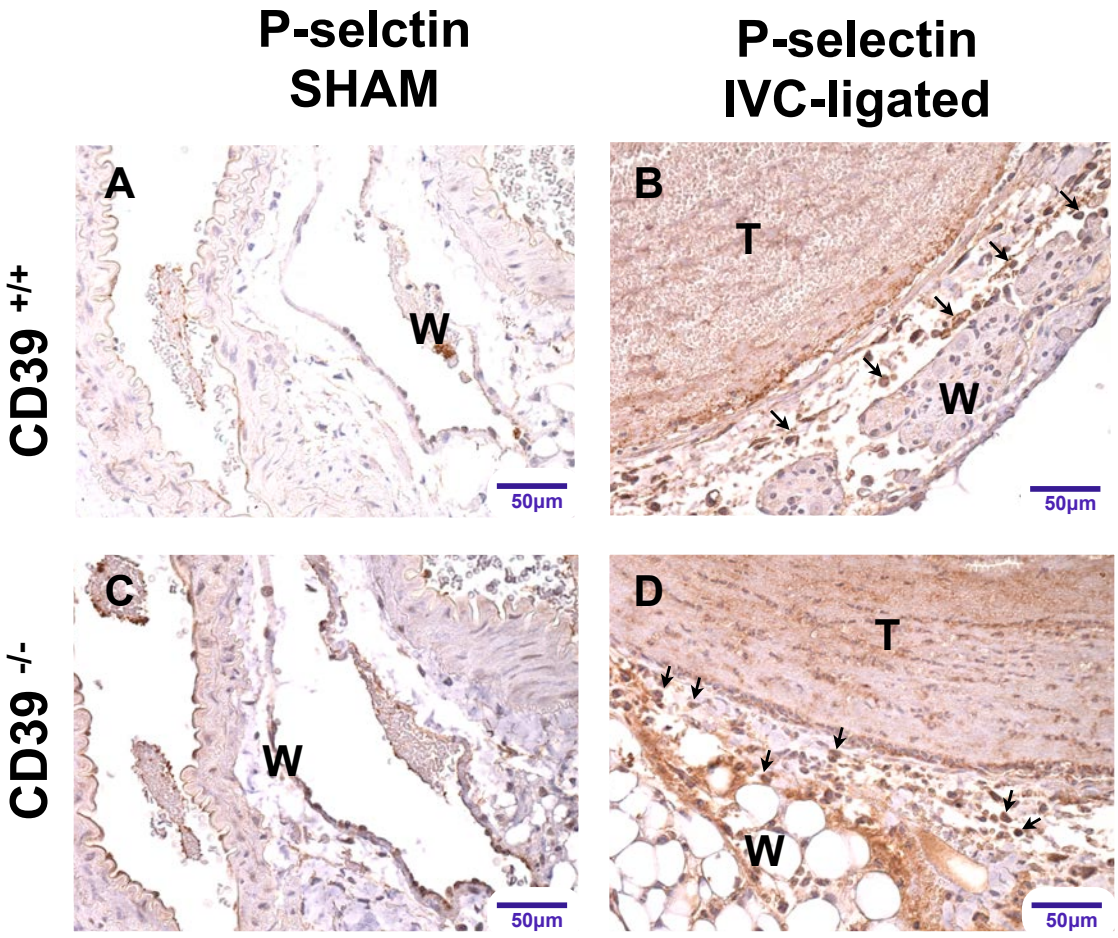
P-selctin
SHAM
P-selectin
IVC-ligated
CD39 +/+
CD39 -/-
A
B
C
D
T
W
50µm

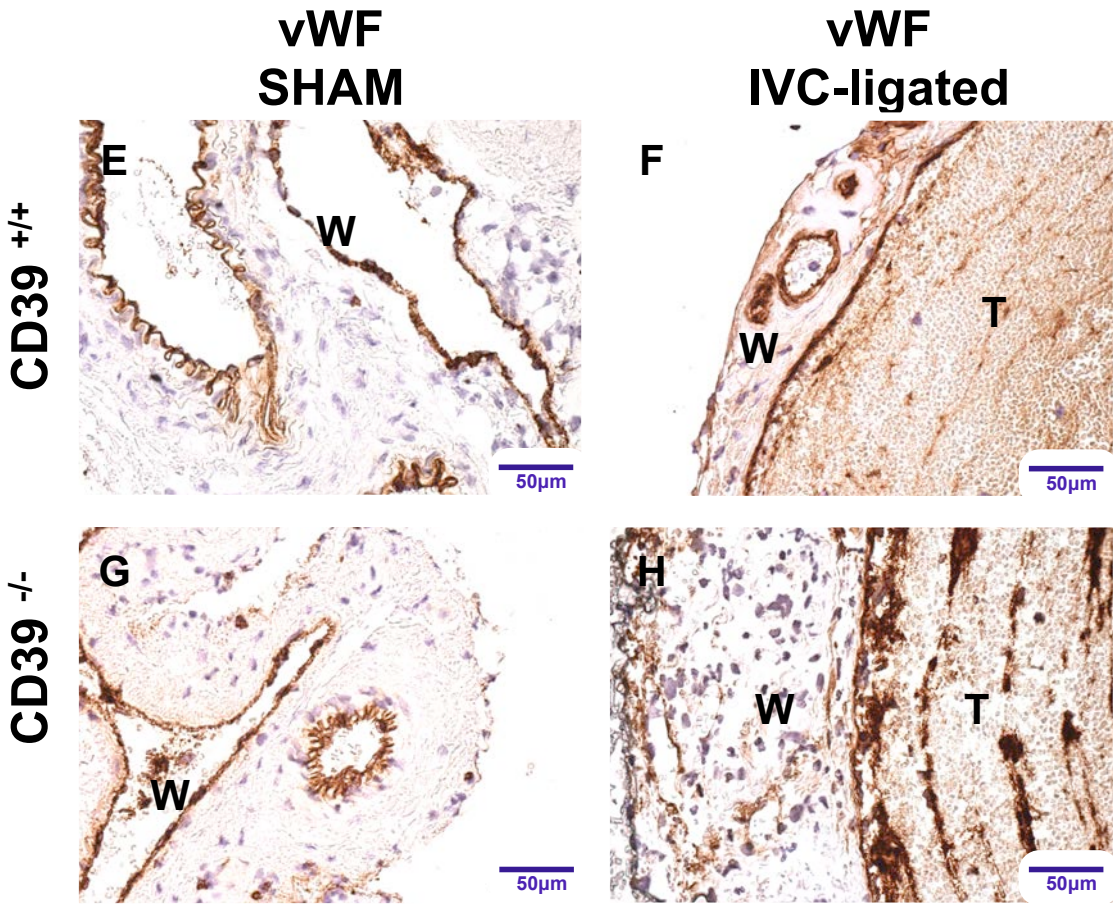

FIGURE V.8: LOCALIZATION OF VEIN WALL P-SELECTIN AND VON WILLEBRAND (VWF) FACTOR PROTEIN BY IMMUNOHISTOCHEMISTRY 48H POST-IVC LIGATION.

(A, E) High power view of the IVC in the sham-operated $CD39^{+/+}$ mouse (x 400). (**B, F**) High power view of the IVC in the $CD39^{+/+}$ IVC-ligated mouse (x 400). (**C, G)** High power view of the IVC in the sham-operated $CD39^{-/-}$ mouse (x 400). **(D, H)** High power view of the IVC in the $CD39^{-/-}$ IVC-ligated mouse (x 400). Cells expressing P-selectin and vWF appear dark brown in color (indicated by dark arrows). P-selectin and vWF are

expressed in the endothelial cells of vena cava of the $CD39^{+/+}$ and $CD39^{-/-}$ sham-operated mice. T = thrombus W= vein Wall

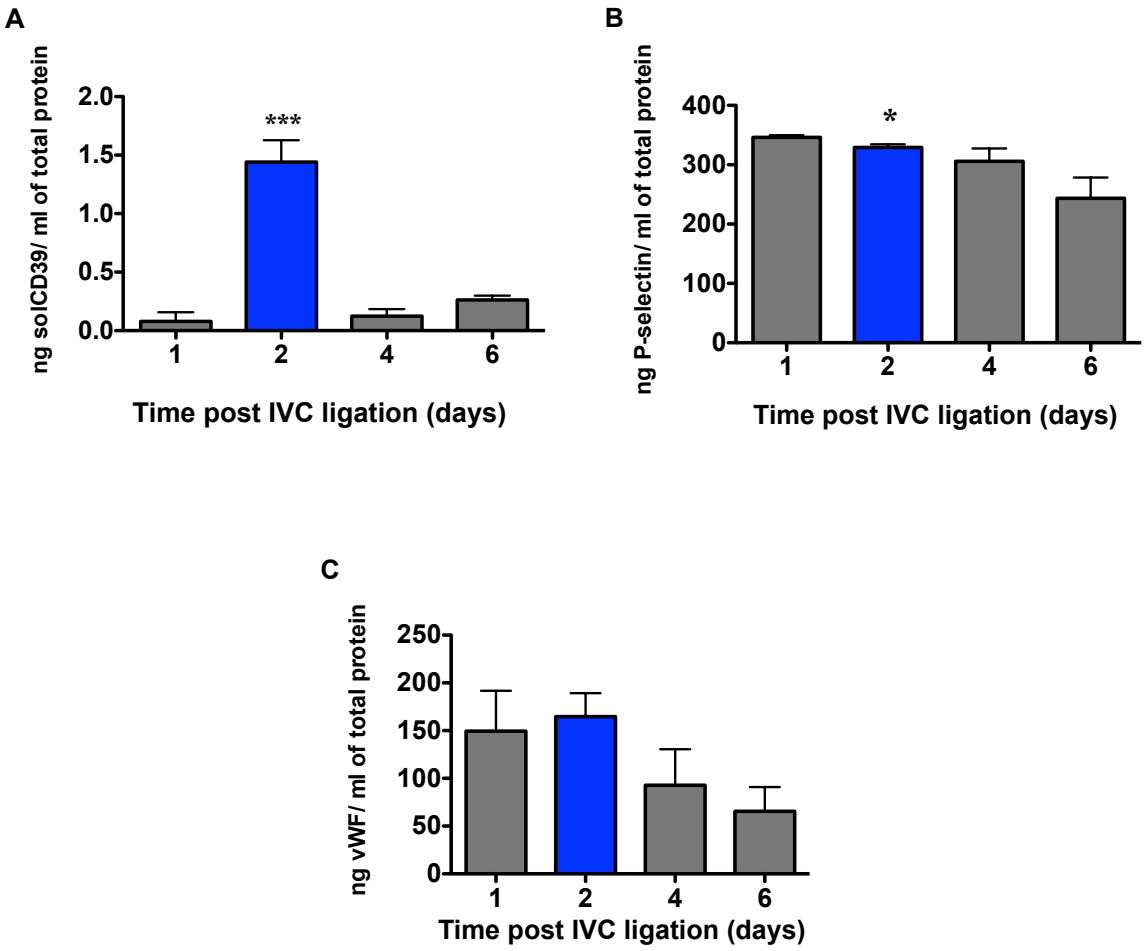
A
ng solCD39/ ml of total protein
2.0
1.5
1.0
0.5
0.0
***
1
2
4
6
Time post IVC ligation (days)
B
ng P-selectin/ ml of total protein
400
300
200
100
0
*
1
2
4
6
Time post IVC ligation (days)
C
ng vWF/ ml of total protein
250
200
150
100
50
0
1
2
4
6
Time post IVC ligation (days)
D
ng P-selectin/ ml of total protein
150
100
50
0
*
CD39+/+
CD39-/-
CD39+/+
CD39-/-
SHAM
IVC-ligated
E
ng vwF/ ml of total protein
300
200
100
0
*
CD39+/+
CD39-/-
CD39+/+
CD39-/-
SHAM
IVC-ligated

FIGURE V.9: EXPRESSION OF SOLUBLE (SOL) CD39, P-SELECTIN AND VWF PLASMA PROTEIN FOLLOWING LIGATION OF THE IVC.

(A-C) $CD39^{+/+}$ mice bred on C57BL/6J background were IVC-ligated for the indicated time and whole blood plasma protein from retro-orbital plexus were isolated. ELISA was used to detect the time course of expression of soluble CD39, P-selectin and vWF (1d, n = 3; 2d, n = 3-4; 4d, n = 3; 6d, n = 3-6). D and E show solP-selectin and vWF 48 hrs post IVC-ligation. Plasma P-selectin and VWF expression obtained from $CD39^{+/+}$ and $CD39^{-/-}$ sham operated or IVC-ligated mice 48 hrs post thrombus induction were determined by ELISA. N= 8-10 total animals in the sham-operated and IVC-ligated groups. Data are shown as means ±SD. $*P < 0.05$, $**P < 0.001$, $***P < 0.0001$

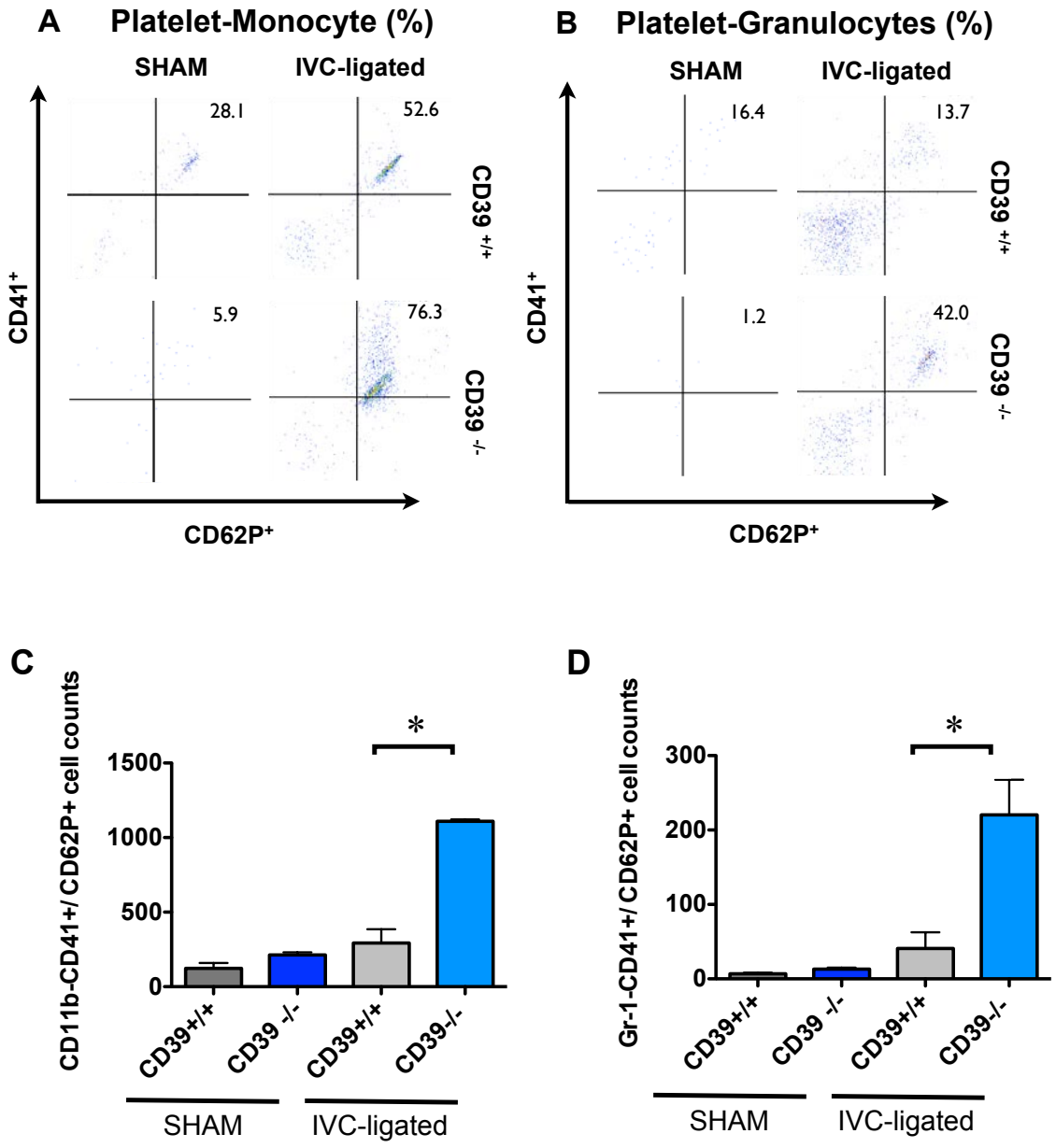

FIGURE V.10 : WHOLE-BLOOD ANALYSIS OF CIRCULATING LEUKOCYTE PLATELET AGGREGATES 48 HRS POST- IVC-LIGATION.

(A, B) Representative fluorescence-activated cell sorter analysis of whole-blood platelet-granulocyte (neutrophils – Gr-1^{+}) and platelet-monocyte (CD11b^{+}) aggregates in CD39$^{+/+}$ and CD39$^{-/-}$ sham operated or IVC-ligated mice 48 hrs post-IVC-ligation. Platelets and leukocytes were recognized by their forward and side-scatter characteristics. DAPI-

negative cells were subgated, and gated on forward and side-scatter $CD45^+$ leukocytes, neutrophils and monocytes (data not shown). The percentage of neutrophils and monocytes found in heteroaggregates with P-selectin ($CD62P^+$) and platelets ($CD41^+$) is greater in $CD39^{-/-}$ compared to $CD39^{+/+}$ IVC-ligated mice. (**C, D)** Quantitative cell count analysis of Gr-1 and CD11b-$CD41^{+/}CD62P^+$ cells in $CD39^{+/+}$ and $CD39^{-/-}$ sham operated or IVC-ligated mice 48 hrs post IVC-ligation. Data are shown as means ±SD. $*P < 0.05$, $**P < 0.001$, $***P < 0.0001$

SUPPLEMENTAL FIGURES:

TABLE V.1: GO TERMS OVERREPRESENTATION ANALYSIS

Gene Ontology analysis revealed several over-represented biological themes due to the absence of CD39 and thrombogenesis.

	$CD39^{+/+}$ IVC-Ligated		$CD39^{-/-}$ IVC-Ligated	
GO term (BP)	**p Value**	**Odds Ratio**	**p Value**	**Odds Ratio**
Inflammatory response	0	3.0919848	0	4.5591088
leukocyte activation	0.0000001	2.452202	0.0000001	2.5226555
immune effector process	0.0000003	2.6932053	NS	NS
immune response	0.0000012	2.3690353	0.0000316	3.5084034
localization	0.0000032	1.4141233	0	1.9533259
response to organic substance	0.0000041	1.6591012	0.0000027	2.1912359
response to external stimulus	0.0000044	1.8369236	0	1.5110622
leukocyte proliferation	0.000006	3.1977548	0.0000626	6.5309609
receptor-mediated endocytosis	0.0000074	3.5290737	NS	NS
cell adhesion	0.000008	1.8401734	0	2.6257471
cell chemotaxis	0.0000106	3.3220069	0	4.4292611
regulation of biological quality	0.0000151	1.4989794	0.0000254	6.5309609
regulation of homeostatic process	0.0000189	2.6576885	0.0000047	1.632204
lymphocyte proliferation	0.0000207	3.0622135	0.0000962	2.4891514
cytokine secretion	0.0000223	5.2194175	0.0000016	2.9122982
positive regulation of immune system process	0.0000226	2.1807008	0.0000018	4.5775438
neutrophil chemotaxis	0.0000277	6.0820413	0.0000023	7.1624033
adaptive immune response	0.000035	3.0982175	NS	NS
leukocyte migration	0.0000372	2.8543756	NS	NS
B cell mediated immunity	0.0000443	4.4375121	NS	NS
collagen metabolic process	0.000054	5.4724806	NS	NS
T cell activation	0.0000575	2.3943687	NS	NS
transport	0.0000636	1.3748109	NS	NS
locomotion	0.000083	1.6107195	NS	NS
myeloid leukocyte mediated immunity	0.0000837	5.6421426	0.0000007	8.5973825
bone remodeling	0.0000996	4.9737491	NS	NS

GO terms with the highest p value and odds ratios that were related to inflammatory cell trafficking are represented

ACKNOWLEDGEMENTS

This work was supported by: Systems in Integrative Biology predoctoral training grant T32GM008322 (to A.C. Anyanwu); NIH grants HL086676 (to D.J. Pinsky) and the J. Griswold Ruth MD & Margery Hopkins Ruth Professorship (to D.J. Pinsky); and the A. Alfred Taubman

NOTES

This manuscript is currently being reviewed.

REFERENCES

1. Silverstein MD, Heit JA, Mohr DN, Petterson TM, O'Fallon WM, Melton LJ, 3rd. Trends in the incidence of deep vein thrombosis and pulmonary embolism: a 25-year population-based study. *Arch Intern Med* 1998, **158**(6)**:** 585-593.

2. Bureau. USC. Monthly populations estimates for the United States: April 1, 2010 to December 1, 2012. Population Estimates 2012 [cited 2012 December 31, 2012]Available from: http://www.census.gov/popest/data/national/totals/2012/index.html

3. Yusuf HR, Tsai J, Atrash HK, Boulet S, Gross SD. *Venous thromboembolism in adult hospitalizations-United States, 2007-2009*. U.S. Dept. of Health and Human Services, Centers for Disease Control and Prevention: Atlanta, Ga, 2012.

4. Ocak G, Vossen CY, Verduijn M, Dekker FW, Rosendaal FR, Cannegieter SC*, et al.* Risk of venous thrombosis in patients with major illnesses: Results from the MEGA study. *J Thromb Haemost* 2012.

5. Alberio L, Safa O, Clemetson KJ, Esmon CT, Dale GL. Surface expression and functional characterization of alpha-granule factor V in human platelets: effects of

ionophore A23187, thrombin, collagen, and convulxin. *Blood* 2000, **95**(5)**:** 1694-1702.

6. Baxi S, Crandall DL, Meier TR, Wrobleski S, Hawley A, Farris D*, et al.* Dose-dependent thrombus resolution due to oral plaminogen activator inhibitor (PAI)-I inhibition with tiplaxtinin in a rat stenosis model of venous thrombosis. *Thromb Haemostasis* 2008, **99**(4)**:** 749-758.

7. Day SM, Reeve JL, Pedersen B, Farris DM, Myers DD, Im M*, et al.* Macrovascular thrombosis is driven by tissue factor derived primarily from the blood vessel wall. *Blood* 2005, **105**(1)**:** 192-198.

8. Esmon CT. Inflammation and thrombosis. *J Thromb Haemost* 2003, **1**(7)**:** 1343-1348.

9. Taylor FB, Chang A, Esmon CT, Dangelo A, Viganodangelo S, Blick KE. Protein-C Prevents the Coaggulopathic and Lethal Effects of Escherichia-Coli Infusion in the Baboon. *J Clin Invest* 1987, **79**(3)**:** 918-925.

10. Schaub RG, Simmons CA, Koets MH, Romano PJ, 2nd, Stewart GJ. Early events in the formation of a venous thrombus following local trauma and stasis. *Lab Invest* 1984, **51**(2)**:** 218-224.

11. Stewart GJ, Ritchie WGM, Lynch PR. Venous Endothelial Damage Produced by Massive Sticking and Emigration of Leukocytes. *Am J Pathol* 1974, **74**(3)**:** 507-532.

12. Wakefield TW, Strieter RM, Prince MR, Downing LJ, Greenfield LJ. Pathogenesis of venous thrombosis: a new insight. *Cardiovasc Surg* 1997, **5**(1)**:** 6-15.

13. Acker T, Fandrey J, Acker H. The good, the bad and the ugly in oxygen-sensing: ROS, cytochromes and prolyl-hydroxylases. *Cardiovasc Res* 2006, **71**(2)**:** 195-207.

14. Bovill EG, van der Vliet A. Venous valvular stasis-associated hypoxia and thrombosis: what is the link? *Annu Rev Physiol* 2011, **73:** 527-545.

15. Diaz JA, Obi AT, Myers DD, Jr., Wrobleski SK, Henke PK, Mackman N*, et al.* Critical review of mouse models of venous thrombosis. *Arterioscler Thromb Vasc Biol* 2012, **32**(3)**:** 556-562.

16. Lopez JA, Kearon C, Lee AY. Deep venous thrombosis. *Hematology Am Soc Hematol Educ Program* 2004**:** 439-456.

17. Mackman N. Mouse Models, Risk Factors, and Treatments of Venous Thrombosis. *Arterioscl Throm Vas* 2012, **32**(3)**:** 554-555.

18. Manly DA, Boles J, Mackman N. Role of Tissue Factor in Venous Thrombosis. *Annu Rev Physiol* 2011, **73:** 515-525.

19. von Bruhl ML, Stark K, Steinhart A, Chandraratne S, Konrad I, Lorenz M*, et al.* Monocytes, neutrophils, and platelets cooperate to initiate and propagate venous thrombosis in mice in vivo. *J Exp Med* 2012, **209**(4)**:** 819-835.

20. Myers D, Farris D, Hawley A, Wrobleski S, Chapman A, Stoolman L*, et al.* Selectins influence thrombosis in a mouse model of experimental deep venous thrombosis. *J Surg Res* 2002, **108**(2)**:** 212-221.

21. Brill A, Fuchs TA, Chauhan AK, Yang JJ, De Meyer SF, Kollnberger M*, et al.* von Willebrand factor-mediated platelet adhesion is critical for deep vein thrombosis in mouse models. *Blood* 2011, **117**(4)**:** 1400-1407.

22. Pendu R, Terraube V, Christophe OD, Gahmberg CG, de Groot PG, Lenting PJ*, et al.* P-selectin glycoprotein ligand 1 and beta2-integrins cooperate in the

adhesion of leukocytes to von Willebrand factor. *Blood* 2006, **108**(12)**:** 3746-3752.

23. Chirinos JA, Heresi GA, Velasquez H, Jy W, Jimenez JJ, Ahn E*, et al.* Elevation of endothelial microparticles, platelets, and leukocyte activation in patients with venous thromboembolism. *Journal of the American College of Cardiology* 2005, **45**(9)**:** 1467-1471.

24. Burnstock G. Dual Control of Local Blood-Flow by Purines. *Ann Ny Acad Sci* 1990, **603:** 31-45.

25. Chen Y, Corriden R, Inoue Y, Yip L, Hashiguchi N, Zinkernagel A*, et al.* ATP release guides neutrophil chemotaxis via P2Y2 and A3 receptors. *Science* 2006, **314**(5806)**:** 1792-1795.

26. Freyer DR, Boxer LA, Axtell RA, Todd RF. Stimulation of Human Neutrophil Adhesive Properties by Adenine-Nucleotides. *J Immunol* 1988, **141**(2)**:** 580-586.

27. Linden J. Cell biology. Purinergic chemotaxis. *Science* 2006, **314**(5806)**:** 1689-1690.

28. Vischer UM, Wollheim CB. Purine nucleotides induce regulated secretion of von Willebrand factor: involvement of cytosolic Ca2+ and cyclic adenosine monophosphate-dependent signaling in endothelial exocytosis. *Blood* 1998, **91**(1)**:** 118-127.

29. von Albertini M, Palmetshofer A, Kaczmarek E, Koziak K, Stroka D, Grey ST*, et al.* Extracellular ATP and ADP activate transcription factor NF-kappa B and induce endothelial cell apoptosis. *Biochem Bioph Res Co* 1998, **248**(3)**:** 822-829.

30. Zimmermann H. Nucleotides and cd39: principal modulatory players in hemostasis and thrombosis. *Nature Medicine* 1999, **5**(9)**:** 987-988.

31. Enjyoji K, Sevigny J, Lin Y, Frenette PS, Christie PD, Esch JSA*, et al.* Targeted disruption of cd39/ATP diphosphohydrolase results in disordered hemostasis and thromboregulation. *Nature Medicine* 1999, **5**(9)**:** 1010-1017.

32. Marcus AJ, Broekman MJ, Drosopoulos JHF, Islam N, Alyonycheva TN, Safier LB*, et al.* The endothelial cell ecto-ADPase responsible for inhibition of platelet function is CD39. *J Clin Invest* 1997, **99**(6)**:** 1351-1360.

33. Petrovic-Djergovic D, Hyman MC, Ray JJ, Bouis D, Visovatti SH, Hayasaki T*, et al.* Tissue-Resident Ecto-5′ Nucleotidase (CD73) Regulates Leukocyte

Trafficking in the Ischemic Brain. *The Journal of Immunology* 2012, **188**(5)**:** 2387-2398.

34. Hyman MC, Petrovic-Djergovic D, Visovatti SH, Liao H, Yanamadala S, Bouis D*, et al.* Self-regulation of inflammatory cell trafficking in mice by the leukocyte surface apyrase CD39. *Journal of Clinical Investigation* 2009, **119**(5)**:** 1136-1149.

35. Lau CL, Zhao Y, Kim J, Kron IL, Sharma A, Yang Z*, et al.* Enhanced fibrinolysis protects against lung ischemia–reperfusion injury. *The Journal of Thoracic and Cardiovascular Surgery* 2009, **137**(5)**:** 1241-1248.

36. Imai M, Takigami K, Guckelberger O, Lin Y, Sevigny J, Kaczmarek E*, et al.* CD39/vascular ATP diphosphohydrolase modulates xenograft survival. *Transplantation Proceedings* 2000, **32**(5)**:** 969.

37. Pinsky DJ, Broekman MJ, Peschon JJ, Stocking KL, Fujita T, Ramasamy R*, et al.* Elucidation of the thromboregulatory role of CD39/ectoapyrase in the ischemic brain. *The Journal of Clinical Investigation* 2002, **109**(8)**:** 1031-1040.

38. Belayev L, Khoutorova L, Deisher TA, Belayev A, Busto R, Zhang Y*, et al.* Neuroprotective Effect of SolCD39, a Novel Platelet Aggregation Inhibitor, on Transient Middle Cerebral Artery Occlusion in Rats. *Stroke* 2003, **34**(3)**:** 758-763.

39. Myers Jr DD, Henke PK, Wrobleski SK, Hawley AE, Farris DM, Chapman AM*, et al.* P-selectin inhibition enhances thrombus resolution and decreases vein wall fibrosis in a rat model. *Journal of Vascular Surgery* 2002, **36**(5)**:** 928-938.

40. Myers Jr DD, Hawley AE, Farris DM, Chapman AM, Wrobleski SK, Henke PK*, et al.* Cellular IL-10 is more effective than viral IL-10 in decreasing venous thrombosis. *Journal of Surgical Research* 2003, **112**(2)**:** 168-174.

41. Myers Jr DD, Rectenwald JE, Bedard PW, Kaila N, Shaw GD, Schaub RG*, et al.* Decreased venous thrombosis with an oral inhibitor of P selectin. *Journal of Vascular Surgery* 2005, **42**(2)**:** 329-336.

42. Gentleman R, Carey V, Bates D, Bolstad B, Dettling M, Dudoit S*, et al.* Bioconductor: open software development for computational biology and bioinformatics. *Genome Biology* 2004, **5**(10)**:** R80.

43. Irizarry RA, et. al. Use of Mixture Models in a Microarray-Based Screening Procedure for Detecting Differentially Represented Yeast Mutants

. *Statistical Applications in Genetics and Molecular Biology* 2003, **2**(1)**:** 1544-6115.

44. Henke PK, Pearce CG, Moaveni DM, Moore AJ, Lynch EM, Longo C*, et al.* Targeted Deletion of CCR2 Impairs Deep Vein Thombosis Resolution in a Mouse Model. *The Journal of Immunology* 2006, **177**(5)**:** 3388-3397.

45. Myers DD, Hawley AE, Farris DM, Wrobleski SK, Thanaporn P, Schaub RG*, et al.* P-selectin and leukocyte microparticles are associated with venous thrombogenesis. *Journal of Vascular Surgery* 2003, **38**(5)**:** 1075-1089.

46. Thanaporn P, Myers DD, Wrobleski SK, Hawley AE, Farris DM, Wakefield TW*, et al.* P-selectin inhibition decreases post-thrombotic vein wall fibrosis in a rat model. *Surgery* 2003, **134**(2)**:** 365-371.

47. Wojcik BM, Wrobleski SK, Hawley AE, Wakefield TW, Myers Jr DD, Diaz JA. Interleukin-6: A Potential Target for Post-Thrombotic Syndrome. *Annals of Vascular Surgery* 2011, **25**(2)**:** 229-239.

48. Culmer DL, Diaz JA, Hawley AE, Jackson TO, Shuster KA, Sigler RE*, et al.* Circulating and vein wall P-selectin promote venous thrombogenesis during aging in a rodent model. *Thrombosis Research* 2013, **131**(1)**:** 42-48.

49. Xia L, Sperandio M, Yago T, McDaniel JM, Cummings RD, Pearson-White S*, et al.* P-selectin glycoprotein ligand-1–deficient mice have impaired leukocyte

tethering to E-selectin under flow. *The Journal of Clinical Investigation* 2002, **109**(7)**:** 939-950.

50. McEver RP. P-selectin and PSGL-1: exploiting connections between inflammation and venous thrombosis. *Thrombosis and Haemostasis* 2002, **87**(3)**:** 364-365.

51. McEver RP. Adhesive Interactions of Leukocytes, Platelets, and the Vessel Wall during Hemostasis and Inflammation. *Thrombosis and Haemostasis* 2001, **86**(3)**:** 728-938.

52. Deatrick KB, Luke CE, Elfline MA, Sood V, Baldwin J, Upchurch Jr GR*, et al.* The effect of matrix metalloproteinase 2 and matrix metalloproteinase 2/9 deletion in experimental post-thrombotic vein wall remodeling. *Journal of Vascular Surgery* (0).

53. Roumen-Klappe EM, Janssen MCH, Van Rossum J, Holewijn S, Van Bokhoven MMJA, Kaasjager K*, et al.* Inflammation in deep vein thrombosis and the development of post-thrombotic syndrome: a prospective study. *Journal of Thrombosis and Haemostasis* 2009, **7**(4)**:** 582-587.

54. John E. Rectenwald DDM, Jr, Angela E. Hawley, Christopher Longo, Peter K. Henke,, Kenneth E. Guire AHS, Thomas W. Wakefield. D-dimer, P-selectin, and microparticles: Novel markers to predict deep venous thrombosis A pilot study. *Thrombosis and Haemostasis* 2005, **94**(6)**:** 1116-1344.

55. Ramacciotti E, Blackburn S, Hawley AE, Vandy F, Ballard-Lipka N, Stabler C*, et al.* Evaluation of Soluble P-Selectin as a Marker for the Diagnosis of Deep Venous Thrombosis. *Clinical and Applied Thrombosis/Hemostasis* 2011, **17**(4)**:** 425-431.

56. Diaz JA, et. al. Thrombogenesis with continuous blood flow in the inferior vena cava

A novel mouse model. *Thrombosis and Haemostasis* 2010, **104**(2)**:** 366-375.

57. Diaz JA, Wrobleski SK, Hawley AE, Lucchesi BR, Wakefield TW, Myers JDD. Electrolytic Inferior Vena Cava Model (EIM) of Venous Thrombosis. 2011(53)**:** e2737.

58. Desch KC, Ozel AB, Siemieniak D, Kalish Y, Shavit JA, Thornburg CD*, et al.* Linkage analysis identifies a locus for plasma von Willebrand factor undetected by genome-wide association. *Proceedings of the National Academy of Sciences* 2013, **110**(2)**:** 588-593.

59. de Bruijne-Admiraal L, Modderman P, Von dem Borne A, Sonnenberg A. P-selectin mediates Ca(2+)-dependent adhesion of activated platelets to many different types of leukocytes: detection by flow cytometry. *Blood* 1992, **80**(1)**:** 134-142.

60. Pulte ED, Broekman MJ, Olson KE, Drosopoulos JHF, Kizer JR, Islam N*, et al.* CD39/NTPDase-1 activity and expression in normal leukocytes. *Thrombosis Research* 2007, **121**(3)**:** 309-317.

61. Brill A, Fuchs TA, Chauhan AK, Yang JJ, De Meyer SF, Köllnberger M*, et al.* von Willebrand factor–mediated platelet adhesion is critical for deep vein thrombosis in mouse models. *Blood* 2011, **117**(4)**:** 1400-1407.

62. Ward PA. Recruitment of inflammatory cells into lung: Roles of cytokines, adhesion molecules, and complement. *Journal of Laboratory and Clinical Medicine* 1997, **129**(4)**:** 400-404.

63. Fuchs TA, Brill A, Duerschmied D, Schatzberg D, Monestier M, Myers DD*, et al.* Extracellular DNA traps promote thrombosis. *Proceedings of the National Academy of Sciences* 2010, **107**(36)**:** 15880-15885.

64. Massberg S GL, von Bruehl ML, Manukyan D, Pfeiler S, Goosmann C, Brinkmann V, Lorenz M, Bidzhekov K, Khandagale AB, Konrad I, Kennerknecht E, Reges K, Holdenrieder S, Braun S, Reinhardt C, Spannagl M, Preissner KT, Engelmann B. Reciprocal coupling of coagulation and innate immunity via neutrophil serine proteases. *Nature Medicine* 2010, **16**(8)**:** 887-896.

65. Ammollo CT, Semeraro F, Xu J, Esmon NL, Esmon CT. Extracellular histones increase plasma thrombin generation by impairing thrombomodulin-dependent protein C activation. *Journal of Thrombosis and Haemostasis* 2011, **9**(9)**:** 1795-1803.

66. Koziak K SJ, Robson SC, Siegel JB, Kaczmarek E. Analysis of CD39/ATP diphosphohydrolase (ATPDase) expression in endothelial cells, platelets and leukocytes. *Thrombosis and Haemostasis* 1999, **82**(5)**:** 1538-1544.

67. Zhang J, Yang Y, Wang Y, Zhang J, Wang Z, Yin M*, et al.* Identification of Hub Genes Related to the Recovery Phase of Irradiation Injury by Microarray and Integrated Gene Network Analysis. *PLoS ONE* 2011, **6**(9)**:** e24680.

68. von Mering C BP. Teamed up for transcription. *Nature* 2002, **417**(6891)**:** 797-798.

69. Zderic T, Hamilton M. Identification of hemostatic genes expressed in human and rat leg muscles and a novel gene (LPP1/PAP2A) suppressed during prolonged physical inactivity (sitting). *Lipids in Health and Disease* 2012, **11**(1)**:** 137.

70. Mosser DM, Edwards JP. Exploring the full spectrum of macrophage activation. *Nat Rev Immunol* 2008, **8**(12)**:** 958-969.

71. Chauhan AK, Kisucka J, Brill A, Walsh MT, Scheiflinger F, Wagner DD. ADAMTS13: a new link between thrombosis and inflammation. *The Journal of Experimental Medicine* 2008, **205**(9)**:** 2065-2074.

72. Ramacciotti E, Myers Jr DD, Wrobleski SK, Deatrick KB, Londy FJ, Rectenwald JE*, et al.* P-selectin/ PSGL-1 Inhibitors versus enoxaparin in the resolution of venous thrombosis: A meta-analysis. *Thrombosis Research* 2010, **125**(4)**:** e138-e142.

73. Zhang YB LW, Yao LQ, Zhao XL, Wang B, Li HK, Ning Y, Song E, Zhang XX. Expression changes and roles of matrix metalloproteinases in a rat model of traumatic deep vein thrombosis. *Chin J Traumatol* 2010, **13**(3)**:** 188-192.

74. Pinsky DJ, Naka Y, Liao H, Oz MC, Wagner DD, Mayadas TN*, et al.* Hypoxia-induced exocytosis of endothelial cell Weibel-Palade bodies. A mechanism for

rapid neutrophil recruitment after cardiac preservation. *The Journal of Clinical Investigation* 1996, **97**(2)**:** 493-500.

75. Pinsky DJ, Liao H, Lawson CA, Yan SF, Chen J, Carmeliet P*, et al.* Coordinated induction of plasminogen activator inhibitor-1 (PAI-1) and inhibition of plasminogen activator gene expression by hypoxia promotes pulmonary vascular fibrin deposition. *The Journal of Clinical Investigation* 1998, **102**(5)**:** 919-928.

76. May AE, Langer H, Seizer P, Bigalke B, Lindemann S, Gawaz M. Platelet-Leukocyte Interactions in Inflammation and Atherothrombosis. *Semin Thromb Hemost* 2007, **33**(02)**:** 123-127.

77. Zarbock A, Polanowska-Grabowska RK, Ley K. Platelet-neutrophil-interactions: Linking hemostasis and inflammation. *Blood Reviews* 2007, **21**(2)**:** 99-111.